HARMONISED METHOD TO VALIDATE THE IMPACT RESISTANCE PERFORMANCE OF COMPOSITE PASSENGER RAILWAY CARBODIES

ASIM ÖNDER

A THESIS SUBMITTED FOR THE DEGREE OF

DOCTOR OF PHILOSOPHY

SCHOOL OF MECHANICAL AND SYSTEMS ENGINEERING

NEWCASTLE UNIVERSITY

OCTOBER 2017

ABSTRACT

The pursuit to become a better and more efficient transportation mode and the need of renovation has led the railway industry to search for new technologies. An example to such reform is the ongoing efforts to implement new lightweight materials into the railway vehicles as primary load bearing structures, which can help to reduce energy consumption, maintenance costs, and to increase passenger and line capacity. Composite materials are promising candidates in this respect and this thesis addresses a railway specific risk namely flying object strike, which requires attention when composites are in use especially in high speed rail operation, consequently providing detailed analysis on impact behaviour of composite materials for rail specific applications.

This thesis shows for the first time an approach to harmonise and unify different railway standards into a single method for small object strike against composite rail vehicles. The original and essential contribution of this study is a cost effective and practical method for the rail industry that removes the necessity of high velocity impact experiments. Quasi-static punch tests (QSPT) were carried out with glass fibre reinforced laminates and foam core sandwich materials incorporating such laminates. It has been shown that the failure modes experienced in a high velocity impact can be mimicked via QSPT method. A numerical model was developed and was validated with QSPT experiments. Following, the numerical model was used to perform high-velocity impact simulations in a velocity range that is relevant with rail service while considering the strain rate effects. Lastly, various standards for impact risks against railway vehicles were investigated from proposed methodology perspective, and discussed whether they can be harmonized into the presented assessment method.

The results showed that the proposed methodology has considerable potential to be preferred over costly high velocity impact experiments. The analysis of the energy transfer characteristics, contact forces, impact velocity change of the projectile, and structural damage showed that the proposed method can be used alone instead of various existing standards, providing a significant reduction in sample size as well as avoiding the costly high-velocity impact experiments, hence resulting in substantial cost savings.

Dedicated to my family and friends.

ACKNOWLEDGEMENTS

The financial support of Anadolu University of Turkey and Council of Higher Education of Turkey are greatly acknowledged and appreciated.

CONTENTS

LIST OF FIGURES

LIST OF TABLES

LIST OF ABBREVIATIONS

BVID	*Barely visible impact damage*	**FE**	*Finite element*
CAI	*Compression after impact*	**FEA**	*Finite element analysis*
CDM	*Continuum damage mechanics*	**FEM**	*Finite element method*
CF	*Circular flat (punch)*	**FRP**	*Fibre reinforced plastic*
CF	*Contact force*	**GFRP**	*Glass fibre reinforced plastic*
CFL	*Courant-Friedrichs-Levy condition*	**H**	*Hemispherical (punch)*
CFRP	*Carbon fibre reinforced plastic*	**H & G**	*Haque and Gillespie penetration model*
CLT	*Classical laminate theory*	**HSR**	*High speed rail (operation)*
CP	*Cross-ply*	**HST**	*High speed train*
CSM	*Chopped strand mat*	**HVI**	*High velocity impact*
DCB	*Double cantilever beam*	**HYVI**	*Hyper velocity impact*
EOS	*Equation of state*	**IE**	*Internal energy*

ILSS	*Inter laminar shear stress*	**PVC**	*Polyvinylchloride*
IVI	*Intermediate velocity impact*	**PW**	*Plain weave*
KE	*Kinetic energy*	**QS-PST**	*Quasi static punch shear test*
L & J	*Lambert and Jonas penetration model*	**QSPT**	*Quasi static punch test*
LVI	*Low velocity impact*	**SBS**	*Short beam shear (test)*
LVID	*Large visible impact damage*	**SPR**	*Span to punch ratio*
OOP	*Out of plane*	**STB**	*Steel ball*
PEI	*Polyetherimide*	**STND**	*Standard*
PES	*Polyethersulfone*	**SW**	*Satin weave*
PET	*Polyethylenterephtalate*	**UD**	*Unidirectional*
PMI	*Polymethacrylimide*	**VEL**	*Velocity*
PU	*Polyurethane*	**WP**	*Work package*

Chapter 1. Introduction

1.1 Background

A transportation system that carries large number of passengers or amounts of freight must be reliable and safe. In the early times of the railway industry, conventional materials like wood and steel were used for rail vehicle construction that could meet the structural requirements achieved by the technology of that era. However, while providing the necessary durability, these materials were disadvantageous in terms of high energy consumption, demanding traction-braking systems, and damage/wear of wheel/rail because of their heavy weight. When compared with a lighter vehicle, a heavier vehicle will consume more energy/fuel, consequently increasing costs in operation. Increased energy/fuel consumption also implies a likelihood of higher CO_2 emissions at some point in the energy supply chain (Robinson et al. 2012). In addition, wheel or rail damage caused by heavy mass can result in line closures, leading to huge losses for companies. Therefore, rail vehicles incorporating light-weight materials such as composites can be capable of boosting the efficiency of the system in many different aspects.

The past decades have seen the rapid development of composite materials in many areas like aviation/aerospace, offshore-marine applications, automotive, defence, and wind energy. It is particularly important for the aerospace sector to use lightweight materials since the main challenge is against gravity in the first place. As a result, specific knowledge is obviously more advanced for this sector. Although not used as widely as the other sectors, railway vehicles have included parts made of composites for many years, for example, vehicle doors, seats, tables, and inner panels (Batchelor & Wilson 1984). However, using composite materials for main structural components in rail vehicles remains a challenge.

One of the main obstacles in the implementation of lightweight composite materials in the railway sector is mainly the lack of structural standards and certification procedures in view of their specific applications. Existing structural standards are only applicable for metallic materials. However, metals are isotropic materials, so they have the same mechanical properties in all directions, while this is not the case for composites materials where the mechanical properties are tailored to meet specific loading requirements. Key load paths can be secured through aligning the reinforcing fibres along the loading direction while unnecessary weight can be reduced in other directions, creating “lighter” designs compared to metals. This allows designers to create weight optimised designs. Consequently, it is necessary for new standards

applicable to composite materials for railway applications to be put in place, if the potential benefits of the composite materials are to be realised. To address this issue, the European Commission funded project – REFRESCO – investigated the applicability of lightweight materials, with the aim to create a regulatory framework for the use of new structural materials such as laminated and sandwich composites.

The REFRESCO project had dedicated activities which analysed the compatibility of lightweight materials with respect to specific requirements such as structural requirements (static and fatigue loading), crashworthiness (energy absorption), fire-noise-electromagnetic compatibility, joint and manufacturing, prognostic and health management (damage/failure), and lastly reparability and maintainability. Before these activities could take place, a benchmarking study was carried out on material solutions applicable to the railway sector, and a gap analysis study for existing rail standards in order to identify the short comings. The results of the study revealed that most of the railway standards are applicable when the composites are introduced in carbody shells. The exceptions were EN12663 – Structural requirements of railway vehicle bodies, EN15227 – Crashworthiness requirements of railway vehicle bodies, EN50121 – Electromagnetic compatibility, and EN15273 – Gauges, which need adaptation or modification. Among these standards, EN12663 defines the admissible proof loads a rail vehicle carbody can withstand in various loading conditions. This is the most relevant standard to this thesis although importantly, it lacks information on evaluation criteria for object impact.

Impacts from small objects are especially important for high-speed train (HST) lines, where the aerodynamic forces generated by either an individual train or two passing trains coupled with mechanical/natural influences become strong enough to make objects airborne. Airborne objects can contact with infrastructure or rolling stock and cause damage. The closest solid object around the track – a piece of ballast – is influenced primarily, hence this phenomenon is called “flying ballast damage” in most cases. However, sometimes ice piled up under the rail vehicle or around the bogie could fall and results in hard ice or ballast projection as well (also known as snow/ice falling). Consequently, ballast flight damage is a concerning phenomenon for HST operation and is classified as a highly probable phenomenon (50% chance) (REFRESCO WP7-D7.2 2014).

Although EN12663 does not provide an assessment for this phenomenon, to the best of author’s knowledge, there are other various national standards that identify specific object impact requirements for carbodies, for example, British railway group standard GM/RT2100, European standard EN 15152 - Front windscreens for train cabs, French national standards NF-

F07-101 and NF-F15-818, and UIC (Union Internationale des Chemins de fer - International Union of Railways) standard for windscreens. These safety standards identify the potential threats against different parts of carbodies such as front ends, roof areas, windscreens, and body side windows. Even though the aforementioned standards provide assessment and guidelines to deal with railway specific impact threats, the problem still remains as there is no harmony between most of these methods and the requirements are case specific. Therefore, a more flexible and unifying assessment method is needed.

Furthermore, a convenient assessment method on impact risks against carbody shells should be established if composite materials are to be considered as main structural elements. This necessity arises as a result of the rather sensitive nature of these materials to impacts, and the complex response of laminated composites to impact type loading, e.g. delamination – more commonly known as barely visible impact damage (BVID) – which is difficult to detect although it is an important type of failure which leads to unstable structural integrity.

1.2 Purpose and objectives

This thesis proposes a methodology for the assessment of flying object impact against composite rail vehicle carbodies, and evaluates it by performing a comparison with various national and international impact resistance requirements in order to determine whether the proposed concept can be applied. One important aspect of this work is that while existing standards are case specific, the research carried out here is innovative in that it proposes and creates a harmonised test. Harmonisation here means to draw the considered standards to a common ground, by proposing a method that produces similar outcomes as each of the individual standard does. That being said, the essence of this methodology is to remove the necessity of high-velocity impact experiments which are used to measure penetration resistance of composite materials when they are used in railway vehicles. These experiments are expensive therefore removing the need for high velocity experiments would result in significant cost savings during a composite rail vehicle's development stage.

The proposed method leads to the following research questions:

- To what extent is the new methodology a reliable representation of the assessment of an object strike?
- Which parameter is the most reliable for assessment?
- What are the challenges of the proposed method?

As a result of these questions, the objectives of the evaluation are:

- Determination of important impact parameters,
- To analyse the extent of visible and invisible material failure,
- To provide relevant numerical modelling guides,
- To harmonize various impact related standards into one test,
- To create a simpler method for assessing flying object strike for composite materials in railway vehicles.

1.3 Scope of the thesis

This thesis addresses small object impact risks on rail vehicles which is an issue that needs particular attention in HST operation. An experimental testing method is presented and respective numerical models are validated in static and dynamic loadings. Quasi-static punch tests (QSPT) were carried out with E-glass fibre reinforced laminates and foam core sandwich materials with such laminates, and the material data obtained by these experiments were used in finite element (FE) numerical models to simulate intermediate-to-high velocity impact loading scenarios. Strain rate effects were considered as well. The motivation of preferring E-glass fibre reinforced laminates and foam core sandwich materials is based on the fact that they are cost effective and suitable for rail vehicle applications. Taking into account the vehicle operation environment, conditions of specific threats, and the specifications of impact risk requirement standards, this thesis focuses mainly on the impact of small objects travelling at high velocities. It is beyond the scope of this thesis to examine large object – low velocity impacts which can be distinguished by global structural response.

1.4 Contribution

The significant and pioneering aspect of this research is in the attempt to create a single harmonised method which can be used for various different railway intrinsic small object impact resistance requirements. Another important contribution of this thesis to the railway industry is to present a well-documented source of railway specific impact risks and relevant analysis methods. The design and qualification of composite structures for specific applications is costly and time consuming. Given the fact that there is an increasing demand for the use of composites in the rail industry and that they are proven candidates for main structural elements in rail vehicles, it is believed that this research will prove to be a useful reference especially in

the design and qualification process, and in particular for the rapid and cost effective approach on assessing flying object strikes.

1.5 Thesis structure

This thesis is composed of seven chapters. Chapter One gives the background and the purpose of the research, while Chapter Two reviews the existing composite applications in railway vehicles, and the previous research on impact response of composites while including the basic definitions and characteristics of composite materials. Chapter Three identifies the impact risks to rail vehicle carbodies, and the requirements from various national and international standards perspective. Chapter Four provides the explanation and presentation of the proposed methodology of this thesis which will be evaluated through relevant railway standards in Chapter Six. Chapter Five will investigate the experimental and numerical work that has been implemented in this research. Lastly, Chapter Seven will finalize the thesis with general conclusions and the recommendations for future research.

Chapter 2. Review of the state-of-the-art of impact research on composites

The use of composite materials as primary load bearing structures is relatively new. That is to say, considering a rail vehicle carbody which is operated in an environment with diverse conditions and risks, the literature available in this area of interest is limited. Introducing new materials into the rail industry as main structural elements requires complete understanding of the capabilities and the potentials of these materials. As well as having many advantageous properties over conventional materials, composites have their own different intrinsic characteristics which make them difficult to use without having an in-depth analysis of their behaviour. This is especially relevant for impact loading in which the response and assessment of composites can become quite complex, not only due to the various number of failure modes and interactions between the constituents, but also due to the potential for rapid occurrence of the event itself. Therefore, a literature review on the subject is needed to demonstrate a sufficient level of knowledge.

2.1 Laminated composite materials: A brief introduction on basics

Composite materials can be formed by combining different materials that are complementary to each other. The essence of this concept is nothing new - inserting straws into mud and forming bricks to construct houses is one of the most primitive examples. However, the progress to date is absolutely magnificent - high performance composite materials are widely (up to 50%) used in production of the cutting edge aviation structures such as Airbus A350 and Boeing 787, and most recently the application of carbon fibre reinforced plastic (CFRP) leaf spring in efWING train bogie (Kawasaki 2015) in the railway industry (Figure 1).

Figure 1 Kawasaki efWING carbon fibre laminate leaf spring for bogie application (Kawasaki 2015)

It is possible to generate numerous types of new material combinations as long as they are not incompatible with each other and the final product serves the main purpose of having better

quality material that could perform better than either of the components alone. Figure 2 shows the engineering materials and how different types of composite materials can be formed. All three major groups of engineering materials – metals, plastics, and ceramics – can be used to form new composite materials to be used in any desired application. The focus of this thesis will be on fibre reinforced plastic (FRP) composites. The major material groups above have been used for a long time and thoroughly investigated over the years, thus their properties and behaviours are known quite well. Although this situation is not exactly the same for composites, there has been great effort to identify their characteristics and properties (Tsai & Melo 2015). Endless number of configurations can be manufactured according to the needs of the user, but the challenge in implementation is mainly the anisotropic nature of composite materials.

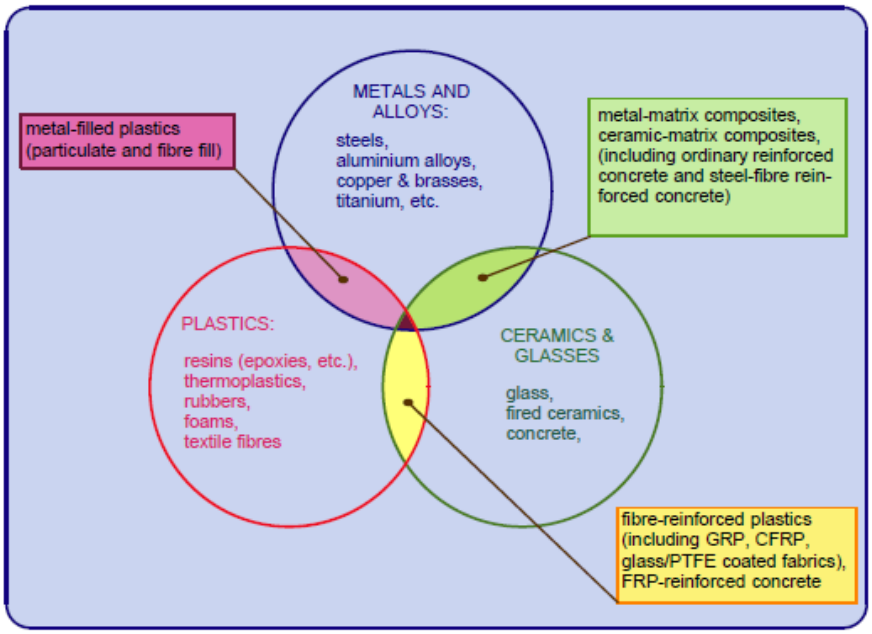

Figure 2 Possible type of constituents from numerous other materials to form a composite material (Harris 1999)

The main advantages of composites are their high strength-to-weight and stiffness-to-weight ratios which allow them to be used for lightweight purposes. In Figure 3 we can see that the composites such as carbon fibre reinforced plastics are located at the top right corner, indicating their higher specific strength and stiffness values, which results in to be preferred over metallic materials for lightweight applications (Ashby 2011). But they also have superior properties over conventional materials, such as:

- Fatigue life,
- Corrosion resistance,

- Wear resistance,
- Thermal insulation and conductivity,
- Acoustic insulation,
- Temperature dependent behaviour,
- Easier 3D shaping and attractiveness.

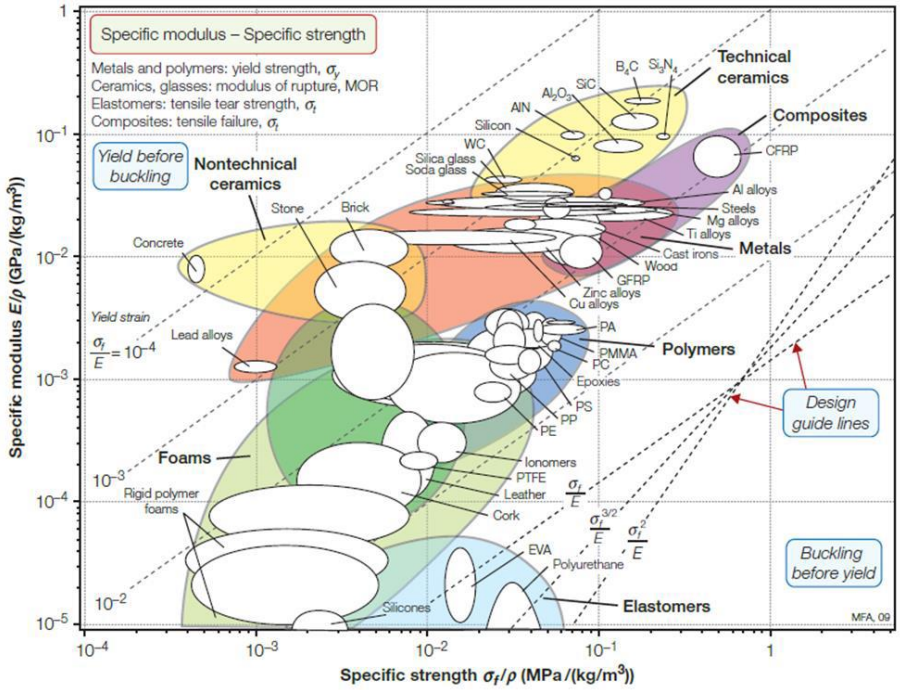

Figure 3 Specific modulus and specific strength of engineering materials (Ashby 2011)

2.1.1 Basic terminology: constituents, structures, and configurations

Composite materials basically consist of two phases which are called fibre (reinforcing) and matrix. This section will describe each of them briefly along with some of the basic terminology.

Fibre Phase

Fibres – or reinforcements – are the main load bearers of a fibre reinforced composite material. Fibres can be described geometrically as thin long tubes, very small (micron or nano scale) in diameter, very long in length compared to their diameter (cm-mm scale), and they can be distributed inside the material as continuously aligned, oriented at an angle, or randomly distributed as short chopped fibres (e.g. chopped strand mat (CSM)). Fibres themselves usually have quite high tensile moduli (70-800 GPa) and strength values (1000-7000 MPa) (Reid, Zhou, et al. 2000). The reason is directly related with their geometry, which results the micro structure

to be aligned in fibre axis, and the presence of fewer defects compared to the bulk material of the same type.

There are many types of reinforcing fibres such as aluminium, titanium, steel, boron, aramid and graphite, but the most common used types used today in railway industry are glass and carbon fibres. The percentages of carbon and glass fibre use in various industrial applications are shown in Figure 4, in which the rail industry is considered in transport and civil engineering.

Although carbon fibres are superior to glass fibres in terms of mechanical properties, impact or damage tolerance of pure carbon composite products can be low or very poor due to their brittle nature. On the other hand, glass fibres are very cheap, making them cost effective, and they are less brittle compared to carbon fibres, and have higher strains to failure. Glass fibre reinforced composites also have higher impact strength compared to carbon counterparts (Reid, Zhou, et al. 2000).

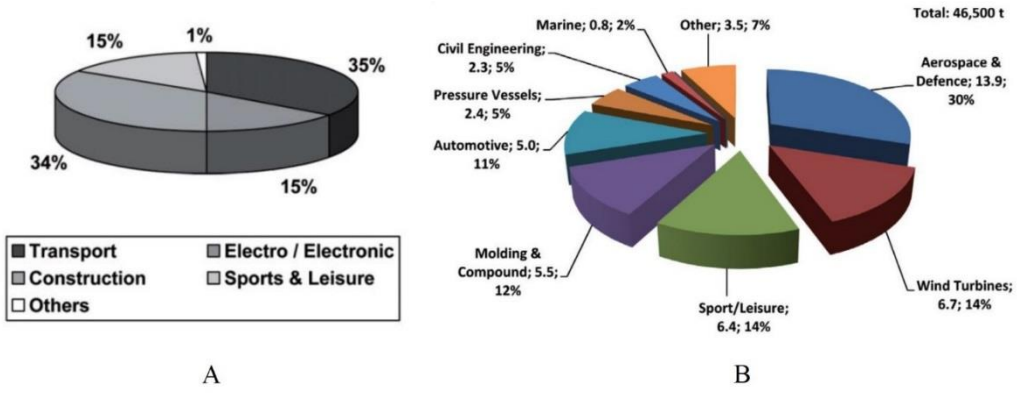

Figure 4 Fibre production: A) glass reinforced fibre production in Europe for different application industries in 2013 (Holmes 2014a), B) global carbon fibre demand by application in thousand tonnes in 2013 (Holmes 2014b)

Matrix Phase

Matrix phase of a composite material fulfils the duty of keeping the fibres in place, alignment of the fibres in desired direction, covering and protecting them from outside effects, and transferring forces to and across the fibres. Although matrix phase has generally lower mechanical properties compared to the fibre phase, without the matrix phase properly supporting them, no gain can be obtained by the high mechanical properties of the fibres. One of the most important functions of matrix phase is to transfer the loads between fibres in case if fibres are broken.

Polymer based matrix materials for composite systems can be divided into two categories: thermoset and thermoplastic polymers, and are usually called resins. Thermoset matrix materials generally have higher strength compared to thermoplastics, but they are generally also more brittle. Thermoset resins, once hardened, cannot be reheated and melted to a different shape unlike thermoplastics which could be reheated and reshaped. Because of this irreversibility, thermosets are difficult to recycle. The most commonly used matrix materials in railway industry applications are epoxy, polyester, vinylester, acrylic and phenolic resins (Figure 5). Among these resin systems, polyester resin dominates the others, while phenolic resin is a more appropriate choice if strict fire and smoke performance is required.

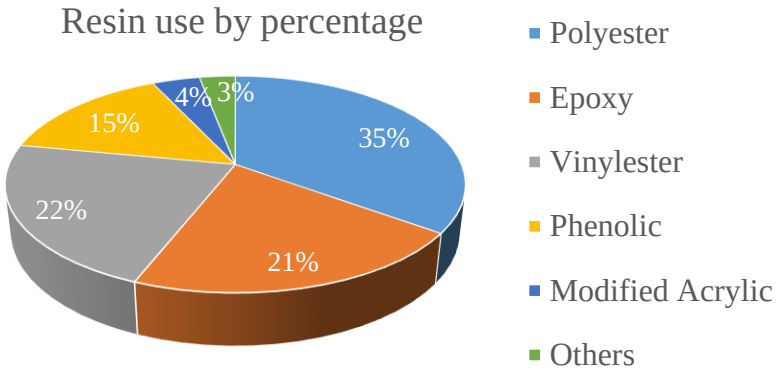

Figure 5 Type of resin systems used in rail vehicle applications (reproduced from (Robinson 2000))

The type of composites with potential for application in the rail vehicle carbody are called fibre reinforced laminated plastics. ***Laminated*** composites consist of many ***laminae*** which can be accounted as the most basic element, and is a thin layer of fibre and matrix combination. A lamina/laminate can be named according to the position of the fibres inside such as ***unidirectional (UD)***, ***angle-ply***, or ***woven (fabric)*** lamina/laminate. Each lamina can be laid up in different ***orientation*** – the angle of lamina inside a laminate; such as [0°], [90°], [-45°] etc. The order of the laminae to form a laminated structure is called ***stacking sequence***, and it can be shown in the form of $[(x^{o}/\, y^{o}/\, z^{o}/\ldots)_{n}]_{s}$. In this notation *x*, *y*, *z* are fibre orientation angles, *n* is the number of repetition of group of layers inside the bracket, and *s* means that the group inside the square bracket is symmetric to the mid-plane of the laminated structure. Some examples are shown in Figure 6.

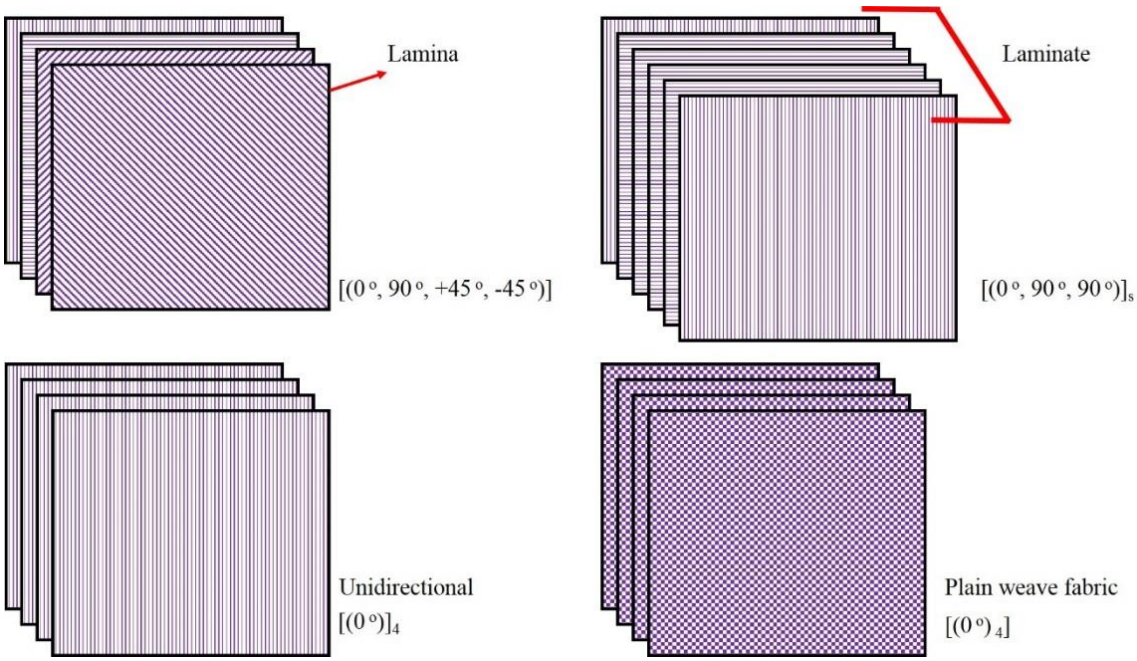

Figure 6 Examples of different laminate configurations

Weaving: Weaving term refers to the fibre architecture of fabric plies. Various types of fabric weaving can be seen in Figure 7. These architectures can influence the physical and characteristic behaviour of the final product. The threads perpendicular to each other are named as warp and weft.

Facesheet (face, skin, face layer): Facesheet is the term that is used to identify the top and bottom layers of sandwich structures. Most of the time the facesheets are in form of laminated composites.

Core (insert): Core term refers to the material inserted in between the facesheets of a sandwich structure. More detail was given in sandwich composite materials section (Section 2.2).

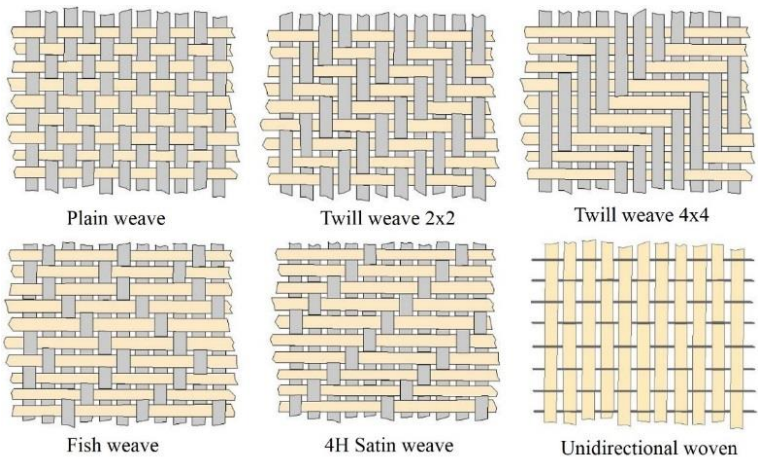

Figure 7 Different weaving architectures (Fibermax composites 2016)

2.1.2 Mechanics

Most conventional materials such as steel, are homogeneous – which means that they have uniform properties throughout, and they are isotropic – which means their properties are independent of the material directions (coordinate system) (Jones 1999). On the contrary, composite materials are known for their heterogeneous internal structure and their anisotropy. However, this doesn't mean that every composite material is anisotropic and heterogeneous; the degree of anisotropy depends on the number of symmetry axes in the material/structure.

At this point, the generalized Hooke's Law will be shown for anisotropic materials to describe the stress-strain relationship. According to the Hooke's law, the relation between stress and strains can be shown as:

$\sigma_{ij} = C_{ij}\varepsilon_j$ i, j=1,2,…,6

$\varepsilon_i = S_{ij}\sigma_j$ i, j=1,2,…,6

where

σ_{ij} : is the stress component,

C_{ij} : is the stiffness matrix,

ε_j : is the strain component,

S_{ij} : is the compliance matrix.

For a material that has no symmetry plane (triclinic material), there are 36 constants that completely describe it. However, since the stiffness matrix of this type of material is symmetric, it holds 21 independent constants. The same procedure also applies for the compliance matrix which is the inverse of stiffness matrix. This means:

$S_{ij} = S_{ji}$, $C_{ij} = C_{ji}$

$$\begin{bmatrix} C_{11} & C_{12} & C_{13} & C_{14} & C_{15} & C_{16} \\ C_{21} & C_{22} & C_{23} & C_{24} & C_{25} & C_{26} \\ C_{31} & C_{32} & C_{33} & C_{34} & C_{35} & C_{36} \\ C_{41} & C_{42} & C_{43} & C_{44} & C_{45} & C_{46} \\ C_{51} & C_{52} & C_{53} & C_{54} & C_{55} & C_{56} \\ C_{61} & C_{62} & C_{63} & C_{64} & C_{65} & C_{66} \end{bmatrix}$$: Stiffness matrix of a triclinic material

$$\begin{bmatrix} S_{11} & S_{12} & S_{13} & S_{14} & S_{15} & S_{16} \\ S_{21} & S_{22} & S_{23} & S_{24} & S_{25} & S_{26} \\ S_{31} & S_{32} & S_{33} & S_{34} & S_{35} & S_{36} \\ S_{41} & S_{42} & S_{43} & S_{44} & S_{45} & S_{46} \\ S_{51} & S_{52} & S_{53} & S_{54} & S_{55} & S_{56} \\ S_{61} & S_{62} & S_{63} & S_{64} & S_{65} & S_{66} \end{bmatrix}$$: Compliance matrix of a triclinic material

The red coloured components of stiffness and compliance matrix defines the line of symmetry inside the matrix (not for material coordinate system).

When there exist additional symmetry axes in the material, the number of the independent constant decreases consequently. For example, if the 1-2 plane is the only symmetry plane, then the number of the independent constants to identify the material drops down to 13, viz. describing a monoclinic material.

$$\begin{bmatrix} C_{11} & C_{12} & C_{13} & 0 & 0 & C_{16} \\ C_{21} & C_{22} & C_{23} & 0 & 0 & C_{26} \\ C_{31} & C_{32} & C_{33} & 0 & 0 & C_{36} \\ 0 & 0 & 0 & C_{44} & C_{45} & 0 \\ 0 & 0 & 0 & C_{54} & C_{55} & 0 \\ C_{61} & C_{62} & C_{63} & 0 & 0 & C_{66} \end{bmatrix}$$ Monoclinic material

If there are three orthogonal symmetry axes present in the material, then this means an orthotropic material with 9 independent constants, which is also a basic stiffness definition for composite material behaviour.

$$\begin{bmatrix} C_{11} & C_{12} & C_{13} & 0 & 0 & 0 \\ C_{21} & C_{22} & C_{23} & 0 & 0 & 0 \\ C_{31} & C_{32} & C_{33} & 0 & 0 & 0 \\ 0 & 0 & 0 & C_{44} & 0 & 0 \\ 0 & 0 & 0 & 0 & C_{55} & 0 \\ 0 & 0 & 0 & 0 & 0 & C_{66} \end{bmatrix}$$ Orthotropic material

Likewise, if at every point of a material there is one plane in which the mechanical properties are equal in every direction, then this type of anisotropy is called transversely isotropy (Jones 1999), and this type of symmetry is used for mostly unidirectional composites and anisotropic fibres to identify their elastic constants.

$$\begin{bmatrix} C_{11} & C_{12} & C_{12} & 0 & 0 & 0 \\ C_{21} & C_{22} & C_{23} & 0 & 0 & 0 \\ C_{21} & C_{32} & C_{22} & 0 & 0 & 0 \\ 0 & 0 & 0 & \frac{C_{22}-C_{23}}{2} & 0 & 0 \\ 0 & 0 & 0 & 0 & C_{66} & 0 \\ 0 & 0 & 0 & 0 & 0 & C_{66} \end{bmatrix}$$ Transversely isotropic material

Finally, in case of infinite number of symmetry planes, this material type is called isotropic material, which has 2 independent material constants that defines it.

$$\begin{bmatrix} C_{11} & C_{12} & C_{12} & 0 & 0 & 0 \\ C_{21} & C_{22} & C_{12} & 0 & 0 & 0 \\ C_{21} & C_{21} & C_{11} & 0 & 0 & 0 \\ 0 & 0 & 0 & \frac{C_{11}-C_{12}}{2} & 0 & 0 \\ 0 & 0 & 0 & 0 & \frac{C_{11}-C_{12}}{2} & 0 \\ 0 & 0 & 0 & 0 & 0 & \frac{C_{11}-C_{12}}{2} \end{bmatrix}$$ Isotropic material

From this basic demonstration of Hooke's law, it can be understood that the basic difficulty behind dealing with composite materials is the need for more material parameters. Following this demonstration, the engineering constant of composites can be generalised as Elasticity (Young's) modulus (E), Poisson's ratio (v), and shear modulus (G), and of course additional parameters to identify the complete behaviour of the material. Most of the time orthotropic anisotropy is of concern for practical composites, therefore the following shows the compliance matrix of an orthotropic material in which the engineering constants are shown explicitly:

$$[S_{ij}] = \begin{bmatrix} \frac{1}{E_1} & -\frac{v_{21}}{E_2} & -\frac{v_{31}}{E_3} & 0 & 0 & 0 \\ -\frac{v_{12}}{E_1} & \frac{1}{E_2} & -\frac{v_{32}}{E_3} & 0 & 0 & 0 \\ -\frac{v_{13}}{E_1} & -\frac{v_{23}}{E_2} & \frac{1}{E_3} & 0 & 0 & 0 \\ 0 & 0 & 0 & \frac{1}{G_{23}} & 0 & 0 \\ 0 & 0 & 0 & 0 & \frac{1}{G_{31}} & 0 \\ 0 & 0 & 0 & 0 & 0 & \frac{1}{G_{12}} \end{bmatrix}$$

Where

E_1, E_2, E_3 : Young's moduli in 1-2-3 material directions,

$v_{ij} = -\frac{\varepsilon_j}{\varepsilon_i}$: Poisson's ratio (i, j=1, 2, 3),

G_{23}, G_{31}, G_{12} : Shear moduli in 23, 31, and 12 material planes.

Characterisation of FRP composites

Mechanical testing of laminated composites can become daunting and complicated process. Since they exhibit dissimilar behaviour for every direction in their own coordinate system, additional testing is required. Most common techniques used for characterisation of composite materials can be classified as follows:

- Tensile and Compression testing – for determination of in-plane or through thickness properties,
- 3 and 4 Point bending test (3P-4P) – for flexural properties,
- Double cantilever beam (DCB) and short beam shear (SBS) tests – for crack energy release and inter-laminar properties,

Table 1 shows the standardized methods to characterise the mechanical properties of laminated composite materials with ISO and ASTM standards.

Property name	***Relevant testing method***	
	ASTM	**ISO-EN**
Tensile Modulus (E)	D 3039	527-1 to 5
Poisson's ratio (ν)	D 3039	527-1 to 5
Shear Modulus (G)	D 5379	14129
In-plane tensile Strength (S_T)	D 3039	527-1 to 5
Out-of-plane tensile strength (S_{T3})	D 6415	-
Compressive Strength (S_C)	D 3410 / D 695	14126
Fibre crush strength (S_{FC})	-	-
Fibre shear strength (S_{FS})	D 732	-
Flexural Strength	D 7264	14125

Table 1 Characterization methods with ASTM and ISO standards

2.1.3 Failure modes

Composite materials may exhibit various failure modes depending on many factors such as fibre and matrix characteristics, fibre-matrix interface, type of loading (static, dynamic, or fatigue), boundary conditions, and material configuration (thickness, ply orientation, laminated/sandwich structure). The failure modes can be listed below as:

- Fibre breakage and fracture,
- Fibre rupture and pull out,
- Fibre kinking,
- Matrix cracking,
- Delamination/de-bonding,

- Indentation.

These damage modes may be exhibited in consequence of tensile, shear, flexural or compressive loadings and they can contribute to one another, after the initial elastic response (Figure 8). For example, a matrix crack can propagate to the interface between plies and can lead to delamination – de-bonding of the adjacent plies, which is an important damage mode that greatly affects the strength and stiffness of the structure especially in compression mode. Fibre rupture might lead to fibre pull out, arising from the insufficient interface strength between fibre and matrix.

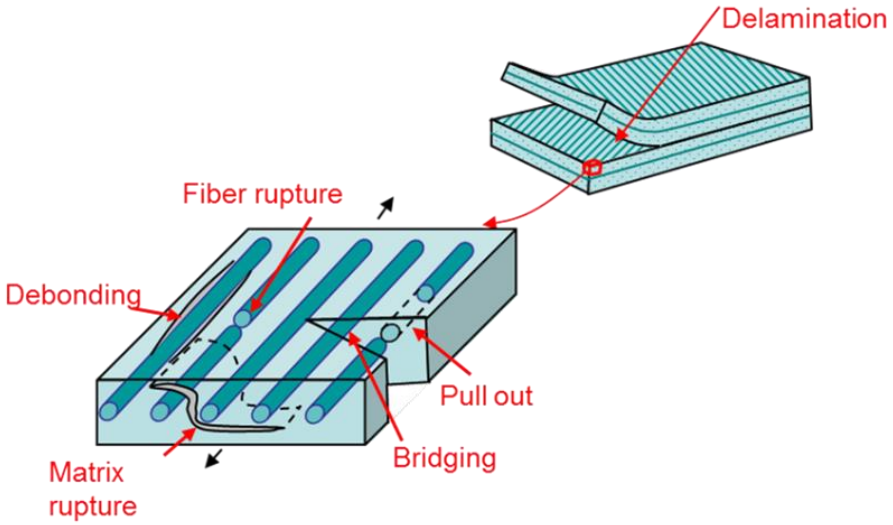

Figure 8 Composite material failure modes (URL-1 2016)

Loading type can also have considerable influence on failure modes. At low velocity impacts matrix cracking induced by flexural stress, and delamination are important modes, while in high velocity impacts more shear based failure modes are dominant such as fibre shear and plug formation.

Figure 9 shows an example of boundary condition effect on failure behaviour. In the left figure, the failure occurs at the impacted face due to the high concentration of contact force between the laminate and the impactor, viz. matrix cracks due to compression failure. These cracks then lead to delamination failure in later stages in case of insufficient bond strength. In the right figure, even though it is same type of loading, the tensile stresses at the reverse side of the structure lead to matrix cracks and later delamination. Therefore, when the structure is supported by a rigid background the contact stresses are more important, while bending/membrane stresses are critical if the structure is supported from its sides.

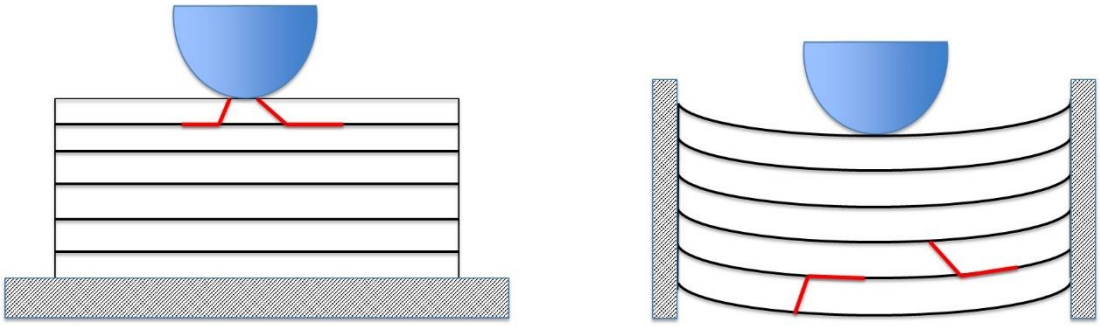

Figure 9 Effect of boundary condition on failure. Red lines are representative of matrix cracks (not to scale)

2.2 Sandwich composite materials

Section 2.1 explained that the main reason to introduce laminated composites into many engineering fields was to achieve higher structural performance and light-weighting at the same time. Sandwich composite materials are the result of this continuing innovation. While the layered concept remains the same, the improved properties are achieved with the introduction of a relatively less dense but much thicker core (insert) material. Basically, a sandwich material consists of thin face layers (also called facesheet or skin) bonded to the top and bottom of the thick core by an adhesive layer. Although the faces are thin and therefore act like a membrane, their high elasticity modulus allows them to carry tensile/compression forces and bending moments. On the other hand the less dense and less stiff thick core carries shear forces and also supports the face layers against buckling. Figure 10 shows the improvement achieved in flexural stiffness and strength in a sandwich material with respect to core thickness (hence with respect to weight), as well as the stress and strain distribution.

From the rail industry perspective, clearly the light-weight designs achieved by the introduction of sandwich materials primarily helps to keep the vertical loads on the rails and the bogie axles inside the allowable limits. However, it is not the only benefit of sandwich structures for the rolling stock. It is possible and practical to include numerous different requirements for a rail carbody in single type structure such as thermal and acoustic isolation, and limited vibration (Wennberg 2013). Novel structural designs proved that sandwich composites are capable of absorbing greater amounts of crash kinetic energy compared to aluminium designs in

crashworthiness applications of rail vehicles (Carruthers 1995; Carruthers et al. 1998; Robinson et al. 2012).

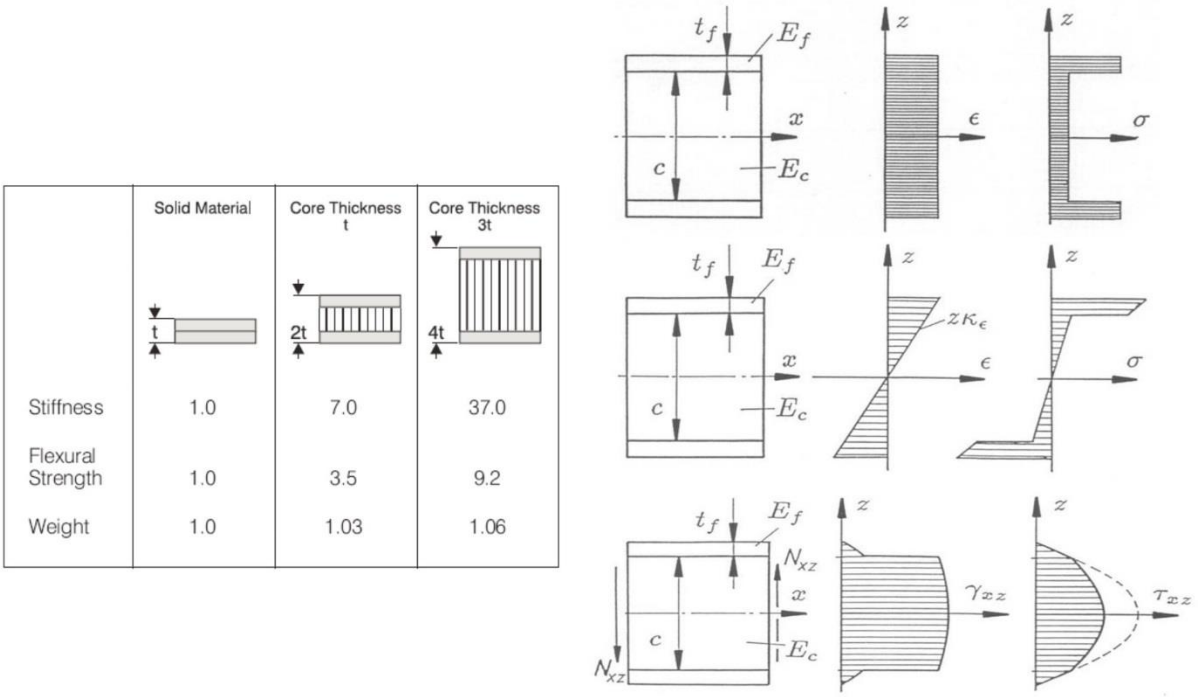

Figure 10 Improved properties in stiffness and flexural strength achieved by sandwich concept (t=2tf) (left), and stress and strain distribution in a sandwich composite material (right) (Starlinger 2013)

Furthermore, the flexibility in manufacture allows sandwich materials to be shaped into complex 3D parts. This is increasingly important considering the public demand for more appealing and stylish structure designs and the aerodynamic characteristics of the HST front sections which consists of lots of smooth curvatures.

Another advantage is that the assembly methods for these type of materials such as adhesive joints enable to reduce the assembly labour and costs. However, one of the weak points of sandwich composites is their lower performance against impact loading. The main reason of this low performance is due to the design of relatively thinner facesheets. It is indeed possible to manufacture thicker facesheet sandwich structures but the design will most likely compromise the lightweight advantage which opposes the primary design philosophy.

2.2.1 Core materials

Core materials in sandwich structures have been in use and are suitable for the railway vehicle applications. While the focus will be on foam cores, basic introductions and examples will be

provided for other possible core structures. Most known core materials for engineering sandwich structures can be classified as honeycombs, foams, balsa wood, and lattice/corrugated cores.

A core element can be manufactured from various materials (metal, plastic, even paper) and can be built either by using a single type or the combination of many types. A good example can be seen in Figure 11, where polymer foam core and corrugated fibre-reinforced plastic laminate were used together. The same way of construction was even extended to honeycomb-like core structure as in the middle example.

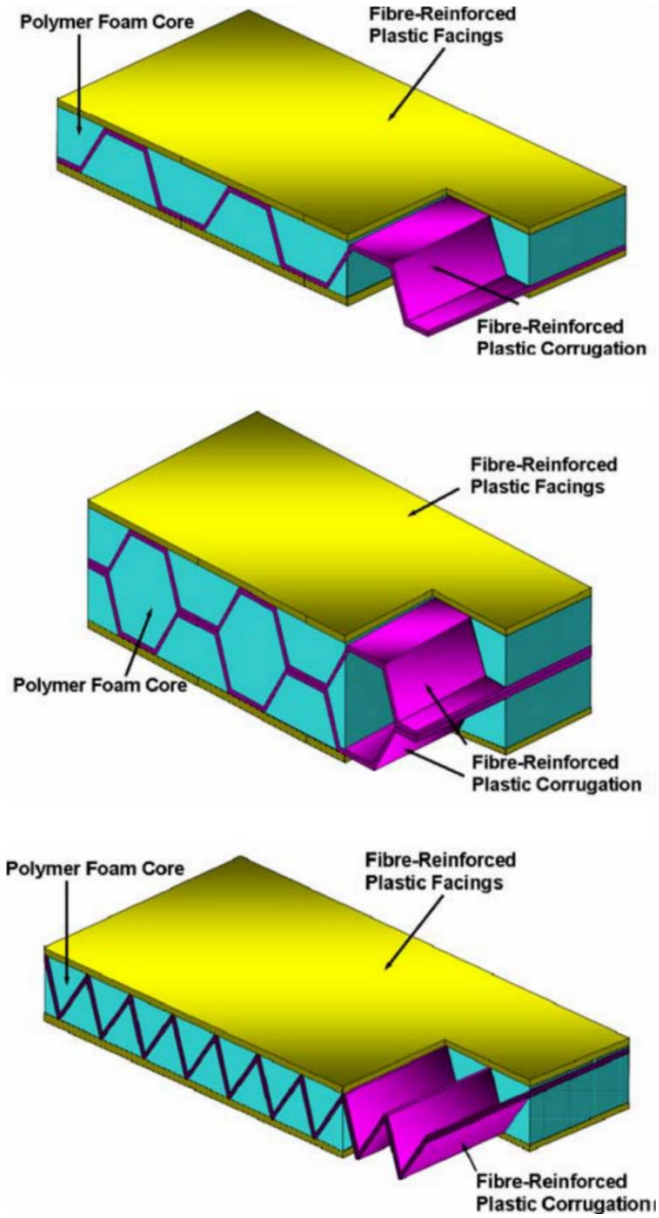

Figure 11 Examples of different sandwich material core constructions (Zangani et al. 2007)

Foam cores

Polymer foam materials have been in use as structural, safety, or comfort elements in many different engineering field for more than 30 years. Especially the automotive industry has extensive applications of such materials for example in seats, roofs, and bumpers. More recently the aviation vehicles benefit from foam materials through sandwich constructions.

From a manufacturing perspective, a foam can be described as the expansion of a base material such as metal or polymer with additive chemicals. This expansion process results in a microcellular – or porous – structure which is formed by the cell walls and struts (Figure 12).

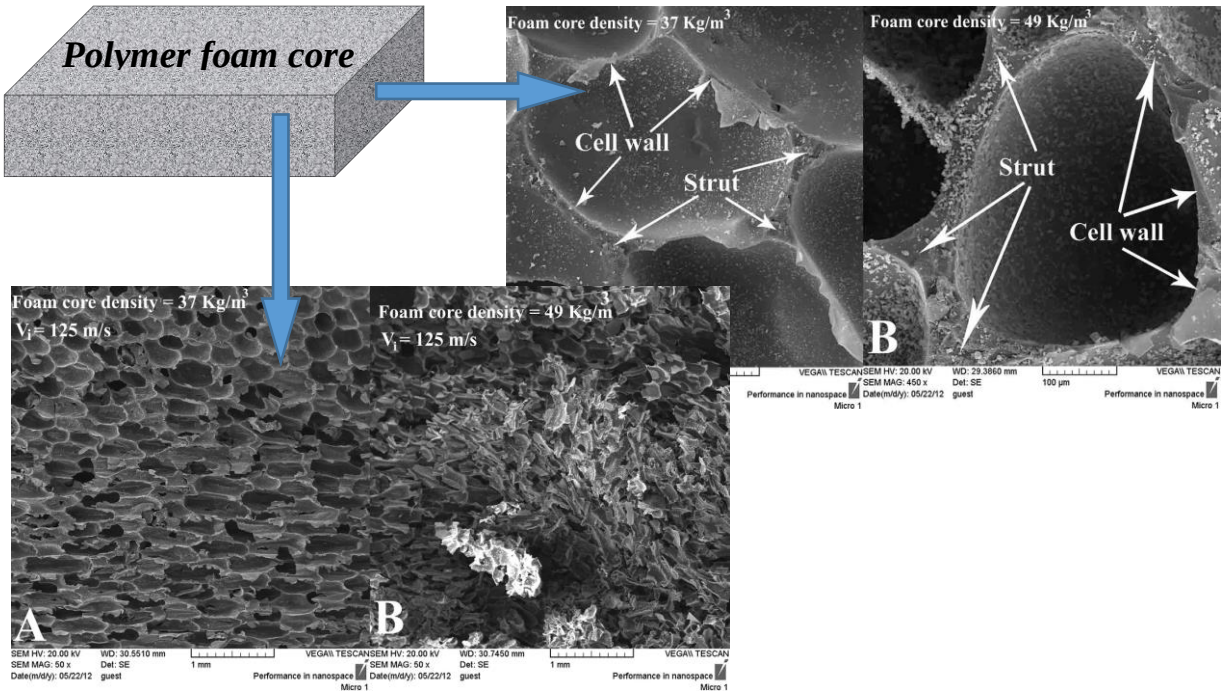

Figure 12 Scanning electron microscope (SEM) figures of a polymer foam core showing the porous morphology, cell wall, and struts (Nasirzadeh & Sabet 2014)

Depending on the porous morphology foams can be categorized into closed cell and open cell foams. Open cell foams allow the air inside the cells escape easily while under compression. However, in closed cell foams, compression results in increase of the air pressure inside the cells thus applying stress to the cell walls, eventually breaking the cell walls in case of insufficient wall strength. This rupture of cell walls indicates the plastic deformation. Most of the foams are known to exhibit great amount of elasticity before plastic deformation. Foams can be manufactured with either rigid or flexible characteristics. Recovery of previous form can either be rapid or slow, but is quicker with flexible foams. Rigid foams on the other hand show very little recovery and they fail in crush mode. Polymer foams are also named based on the

polymer composition such as PVC (polyvinylchloride), PU (polyurethane), PEI (polyetherimide), PES (polyethersulfone), PET (polyethylenterephtalate), etc.

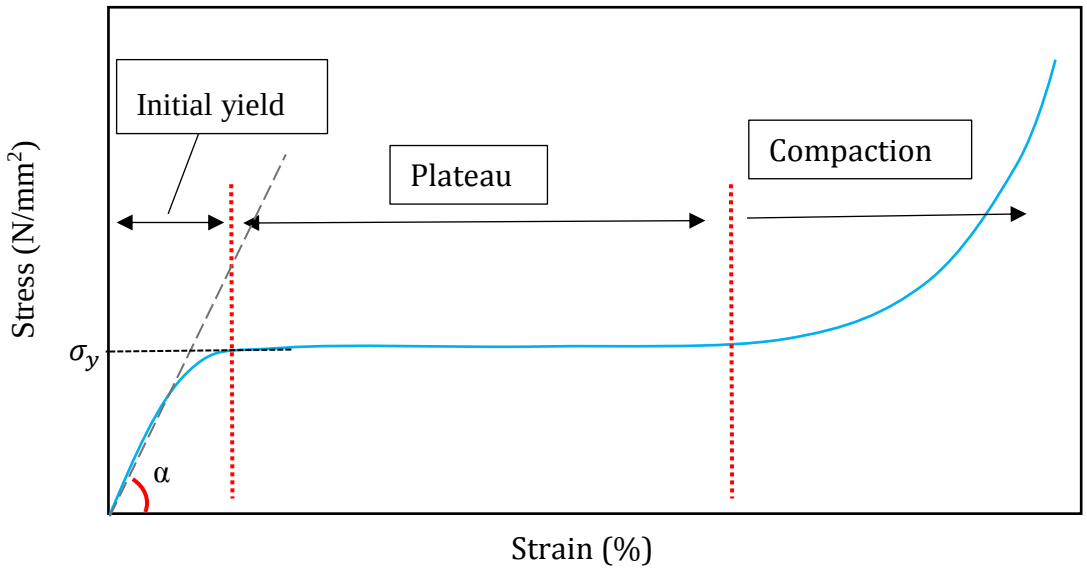

Figure 13 Typical behaviour of foams under unidirectional compression. Three distinct area can be observed: initial yield, plateau, and compaction

Figure 13 shows the unidirectional compression behaviour of a typical polymer foam. In most foams, three regions can be observed: initial yield, plateau, and compaction. Up to yield stress (σ_y), linear elastic stress-strain is observed as the cell walls exhibit elastic buckling. Cell walls starts to rupture at yield stress and the elasticity modulus of the foam starts to degrade (Flores-Johnson et al. 2008). This sequential collapse continues during the plateau region where the stress change is very little or almost zero. Compaction region starts after all the affected cell walls are broken, leading to stress increases with respect to increasing strain. This region is basically the crushing of the airless remaining material. Since during the plateau region phase the air inside the cells escape, the density of the foam material increases during the last two regimes.

This characteristic makes foam material advantageous against impact loadings. Porous materials are extremely effective in attenuating shocks and mitigating impact pressures. The material compacts to its solid density at relatively low stress levels, but, because the volume change is relatively large, a large amount of energy is irreversibly absorbed thereby attenuating shocks by lengthening the wave in time and reducing it in amplitude as more material is compacted.

Honeycomb cores

Another widely used type of core material in sandwich structures is the honeycomb core. As with foam cores, honeycomb cores can be manufactured by different materials such as GFRP/CFRP, aramid, aluminium, etc. (Figure 14).

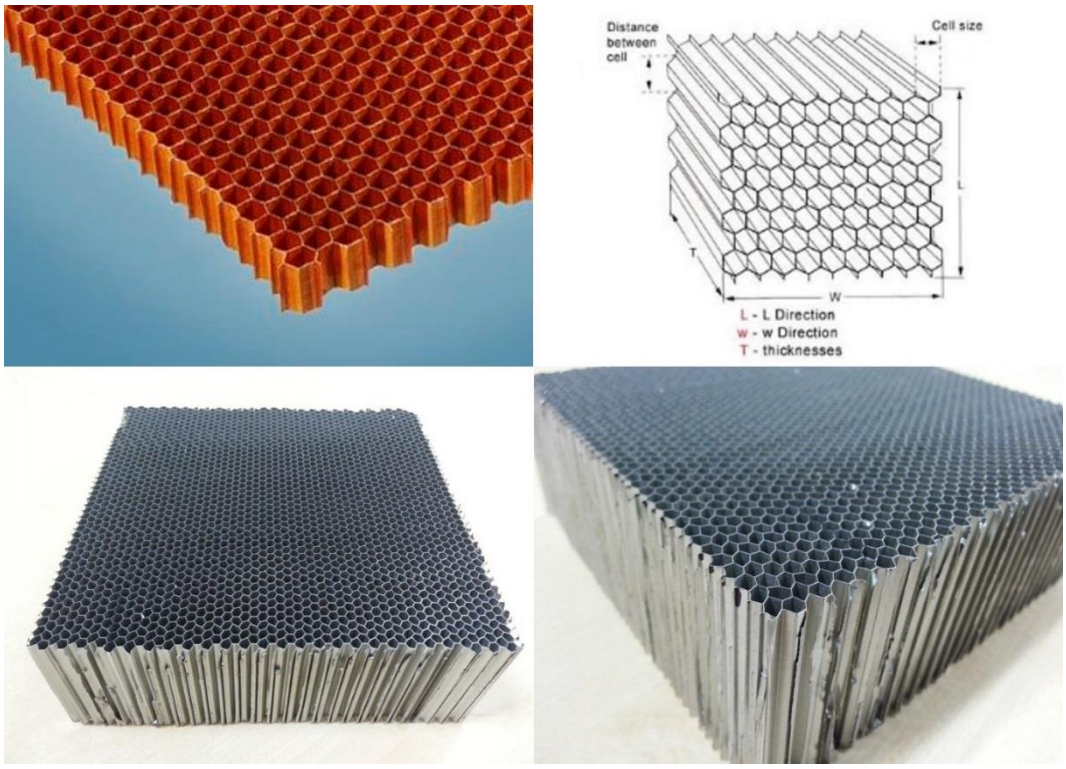

Figure 14 Examples of honeycomb cores. Clockwise from top left: aramid honeycomb, geometry of honeycomb core, aluminium honeycombs

Although aluminium honeycomb sandwich composites are structurally efficient, some drawbacks exist. Unlike most of the foam cores, honeycomb cores have orthotropic nature arisen from the cell shape and geometry. Their susceptibility to long term moisture exposure which leads to corrosion, degradation of the adhesive bonds, and extensive face sheet de-bonding is one of the drawbacks (Nguyen et al. 2005). In addition, the contact between the core and the facesheet is not entirely continuous, which results in rather weak interface strength.

Balsa wood cores

Balsa wood is another structural core material used with fibre reinforced facesheets. It is widely used especially in marine applications such as boat hulls. Although in macroscopic scale it looks like continuous fibrous structure, it can be seen in Figure 15 that in microscopic scale it has actually a closed cell natural honeycomb structure. Balsa wood has generally low density (40-

340 kg/m^3) which makes it attractive for lightweight applications. Some other examples of balsa core use are wind turbine blades, boat decks, surfboards, and luxury car floor pans.

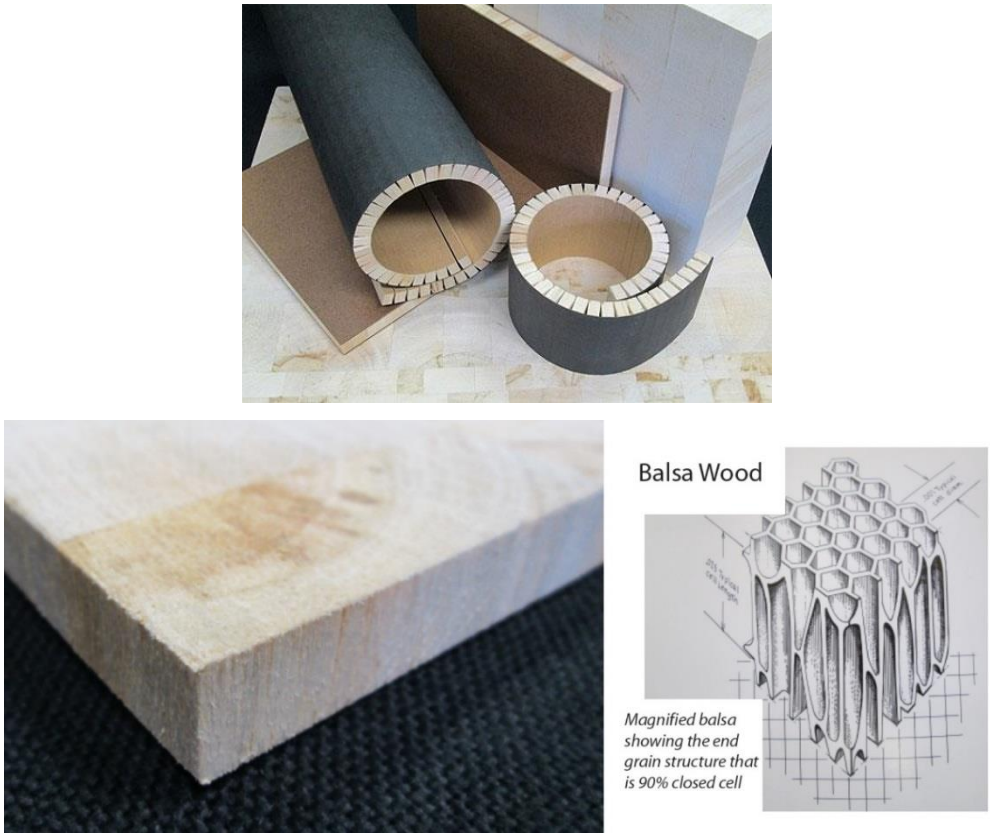

Figure 15 Balsa core in various designs (URL-2 2016)

2.2.2 Failure modes

Similarly to laminated composites, sandwich composites exhibit many different failure modes. However, since there is an additional material in the system with considerably weaker mechanical properties, new type of failure modes can be observed consequently. Petras and Sutcliff created a map of such failure modes for glass fibre skin/Nomex honeycomb core sandwich materials together with the failure criteria (Figure 16) (Petras & Sutcliff 1999). The failure modes seen in the figure were considered in their study. Face yielding (Figure 16 (a)) was described as the result of insufficient in-plane strength of the skin material. The cause of intra-cell dimpling (Figure 16 (b)) was identified as the insufficient bond strength between the core and the skin, leading to local buckling at the unsupported parts by the honeycomb core. Another buckling mode was the face wrinkling (Figure 16 (c)) which can further result in either core crush or skin de-bonding. Failure modes mentioned up to this point generally are the result of in-plane compression loading. The out-of-plane stress variation caused by shear or bending

loads can initiate core shear failure mode (Figure 16 (d)), while out-of-plane local compression loads lead to local indentation (Figure 16 (e)) when the through thickness strength of the core is exceeded. The predictions by the failure map was successful for the in-plane modes (Figure 16 (a), (b), (c)) but not for the core shear and local indentation. This was possibly due to the model's dependency to the Classical Laminate Theory (CLT) which doesn't consider the out-of-plane properties.

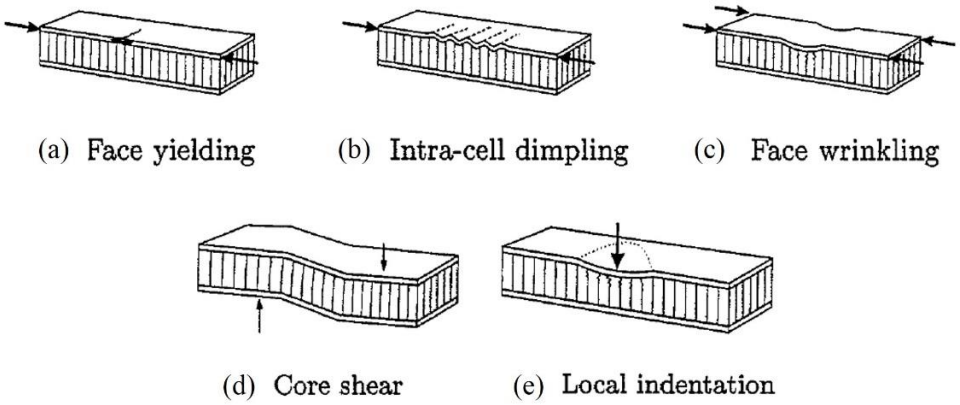

Figure 16 Failure modes of a sandwich beam (Petras & Sutcliff 1999)

Another failure map was created recently by Rajaneesh and co-workers for GFRP skin PVC foam core sandwich plates (Rajaneesh et al. 2014a). Clamped circular sandwich plate was subjected to bending by a flat punch, and stiffness and failure loads were analysed mathematically.

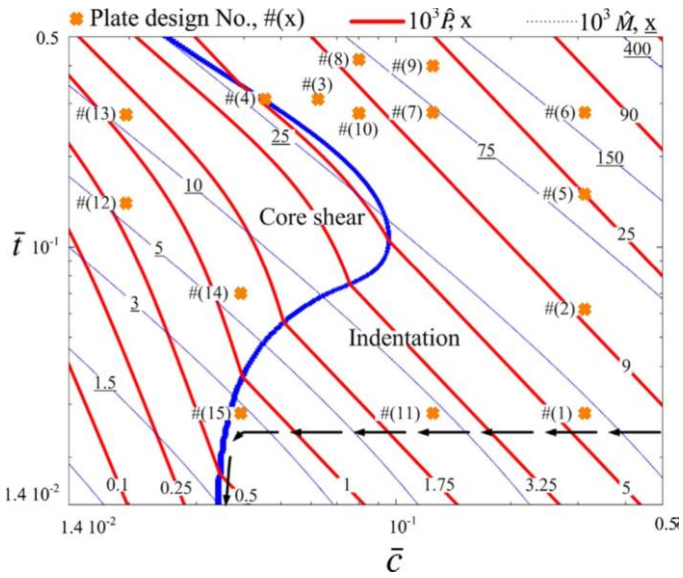

Figure 17 Failure mode map of GFRP/PVC foam core sandwich material (Rajaneesh et al. 2014a)

The main competing failure modes were considered as core indentation, core shear, and face failure. Different sandwich designs based on face and core thickness were assessed by analytical models, experimental measurements, and finite element simulations. Based on the assessment results, failure mode map (Figure 17) was generated with respect to non-dimensional parameters (i.e. strength ($\bar{\sigma}, \bar{\tau}$), stiffness ($\bar{E}, \bar{G}$), loading ($\bar{R}$)). The failure loads for each mode were in good agreement with both analytical and numerical analysis, and it was stated that the failure mode map could be used for lightweight design purposes for the given material configuration.

2.3 Existing research on composites in railway vehicles

Most running rail vehicle car bodies today consist mainly of steel and aluminium. Differential and integral constructions are available with developments in the aluminium manufacturing techniques, like welding or extruded profiles. In addition to these two construction techniques, hybrid constructions, like lattice and body shell designs have been developed over the last few years. However, for conventional as well as hybrid construction, consistent lightweight design is essential for a significant weight reduction (König et al. 2009).

Composite materials, due to their superior mechanical properties over conventional materials, have been applied in a wide range of applications. Fibre-reinforced resin-matrix composite materials that have high strength-to-weight and stiffness-to-weight ratios have become important in weight sensitive applications such as aircraft and space vehicles (Jones 1999). Recently, the demands for the composites are increasing in the railway industry because they are capable of meeting the customer's needs and requirements for the reduction of weight, production costs, and number of parts. Batchelor and Wilson reported the use of glass reinforced plastics (GRP) in different applications in the railway industry such as various areas of the vehicle and overhead structures (Batchelor & Wilson 1984). They presented various case studies of cab fronts, seats, carriage doors, freight applications and pantographs. The authors stated that the freight business was affected less than the passenger business mostly due to the relative importance of weight in freight trains. They concluded that increasing the use of these materials would result in an increase in competitiveness in future. In the railway industry, vehicle parts such as the front cab/cab ends (e.g. UK's Intercity 125 and the Italian ETR 500), lightweight panels like the roof, floor and sidewalls, and interior fittings such as window trim surrounds, toilet modules and vestibule panels can all be built using composite materials. In

addition, full body shells, fairings, valances, bogies, and pantographs can be made (Robinson 2000).

Robinson and co-workers created a lightweight rail vehicle driver's cab made of composite sandwich materials (Robinson et al. 2012). They presented the new design (Figure 18) and validation process according to the European structural safety and crashworthiness standards. The authors were inspired by Bombardier's previous SPACIUM design and used different materials for different parts of the vehicle as shown in Figure 19: foam cores wrapped in glass fibre reinforced polymer (GFRP) at the lower buffer regions for reinforcement, and aluminium honeycomb construction at the buffer-level energy absorbers. As a result, more than a 50% weight saving was achieved at the buffer absorbers compared to the inspired design. The work was simulated with FEM software and validated with the quasi-static axial compression test and the new design was found to be satisfactory.

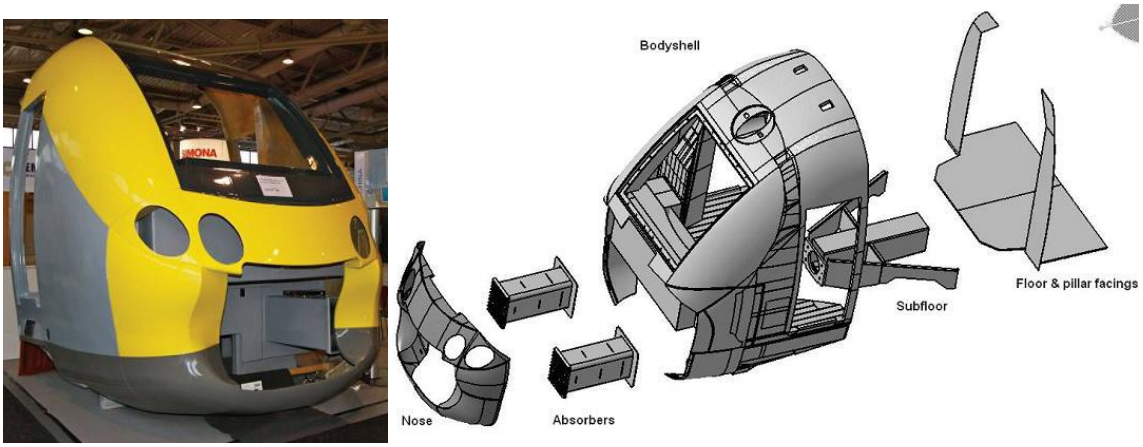

Figure 18 Lightweight D-CAB design (Robinson et al. 2012)

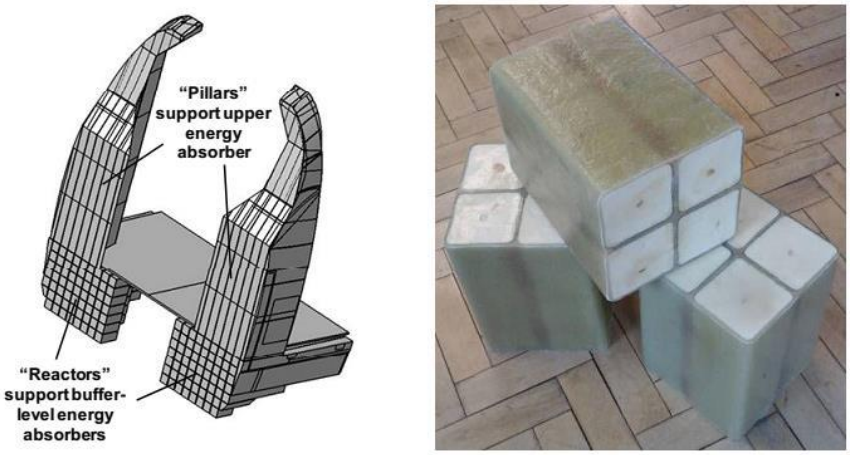

Figure 19 Foam cores wrapped in glass fibre reinforced polymer (GFRP) (Robinson et al. 2012)

Zinno and co-workers investigated a multi scale approach for the design of composite sandwich structure for the roof of a railway vehicle with experimental, theoretical and numerical studies (Zinno et al. 2010). In their detailed study, the authors considered two types of reinforcements (glass and carbon fabric), and two type of core materials, i.e. phenolic honeycomb (Nomex) and polymer foam. Extensive characterisation tests were performed in addition to the theoretical predictions, and the results were validated via numerical analysis. The use of carbon and glass prepreg bonded to Nomex core allowed approximately 50% of weight reduction for the roof panel. After the coupon level validation, the authors analysed as well the joint and sub-component performance of the structure shown in Figure 20 to see whether the structure was capable of meeting the EN 12663 requirements, which did meet indeed. In conclusion, the authors proved that combination of experimental and numerical program is highly beneficial in design phase of composites to replace conventional materials in rail vehicles.

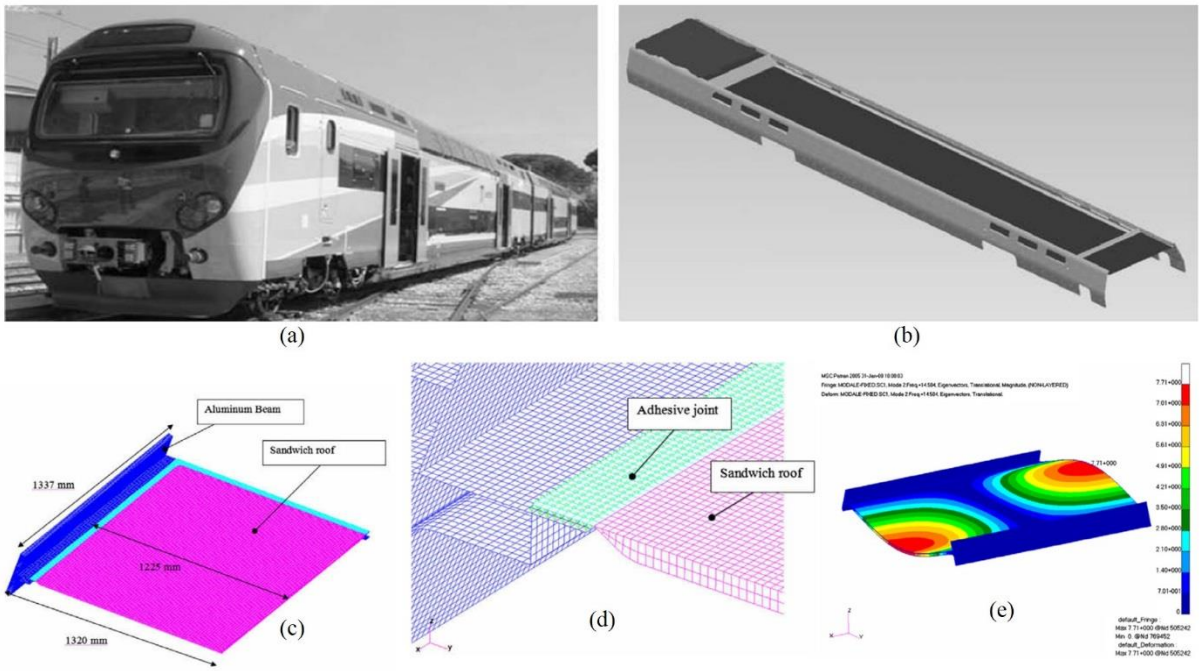

Figure 20 Design of a sandwich composite roof structure of a train: a) rail vehicle, b) roof model, c) sub-component, d) joint configuration, e) Numerical analysis of elastic deformation (Zinno et al. 2010)

Belingardi et al. performed impact, static and quasi-static tests on both face sheets, foam material, and sandwich structures, and illustrated the results of material characterisation program for glass fibre composite/foam sandwich structure for a high-speed train front shield (Belingardi et al. 2003). The composite shield is meant to provide protection from impacting against an obstacle and it is subjected to bending loads, therefore the testing program mainly

considered bending resistance. They reported that the structural response of the sandwich is affected greatly by the strength properties of the core material, and they obtained improved dynamic impact resistance by adding a net of resin walls within the foam (Figure 21). This addition however changed the failure mode of the sandwich samples from foam collapse to foam shear. The authors observed no strain rate effects inside the testing range, however no attempt was made to justify and connect this relationship with high-speed train operation and relevant strain rates in a crash event.

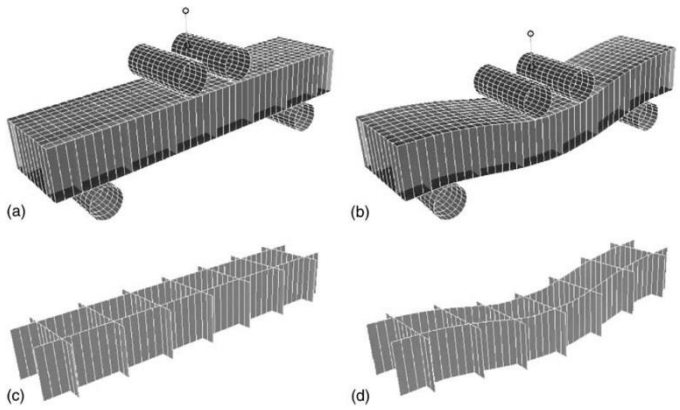

Figure 21 Addition of resin wall to the sandwich samples. (a) and (b): complete sandwich structure subjected to 4-point bending prior to and during testing. (c) and (d): the resin wall - undeformed and deformed state, respectively (Belingardi et al. 2003)

Kim and Chung studied the low energy absorption performance of carbon epoxy fabric laminates designed for Korean tilting train (Kim & Chung 2007). Fabric plates were subjected to 2.4 J, 2.7J, and 4.2 J impact by a drop tower test equipment with a hemispherical tip. The laminates were found to show slightly different mechanical properties in fill (0° fibre orientation in a fabric) and warp (90° fibre orientation in a fabric) directions, and therefore three stacking sequence were studied. Even though each configuration responded similarly, it was found that $[fill]_8$ laminate absorbed the most amount of energy, whereas $[fill_2/warp_2]_s$ laminate absorbed the least. Based on this finding, the authors suggested to take into account the impact resistance before manufacturing the train body shell.

Seo et al. presented the concept of a hybrid body shell for the Korean tilting train TTX and developed a prototype model (Seo et al. 2008). Rationale behind this approach was to obtain a lighter rail vehicle which, at the same time, should be more stable at curves given the fact that tilting technology requires lower centre of gravity. The one-piece hybrid body shell was produced by using mould manufacturing style, combining carbon fibre/aluminium honeycomb

sandwich structure with steel inner frames (Figure 22). This structure was later connected to the steel under frame of the vehicle to form the whole body, consequently achieving 28% weight reduction. Considered manufacturing method was found more convenient compared to the previous design as well. Finally, the structure was verified by static, fatigue strength and fire safety testing.

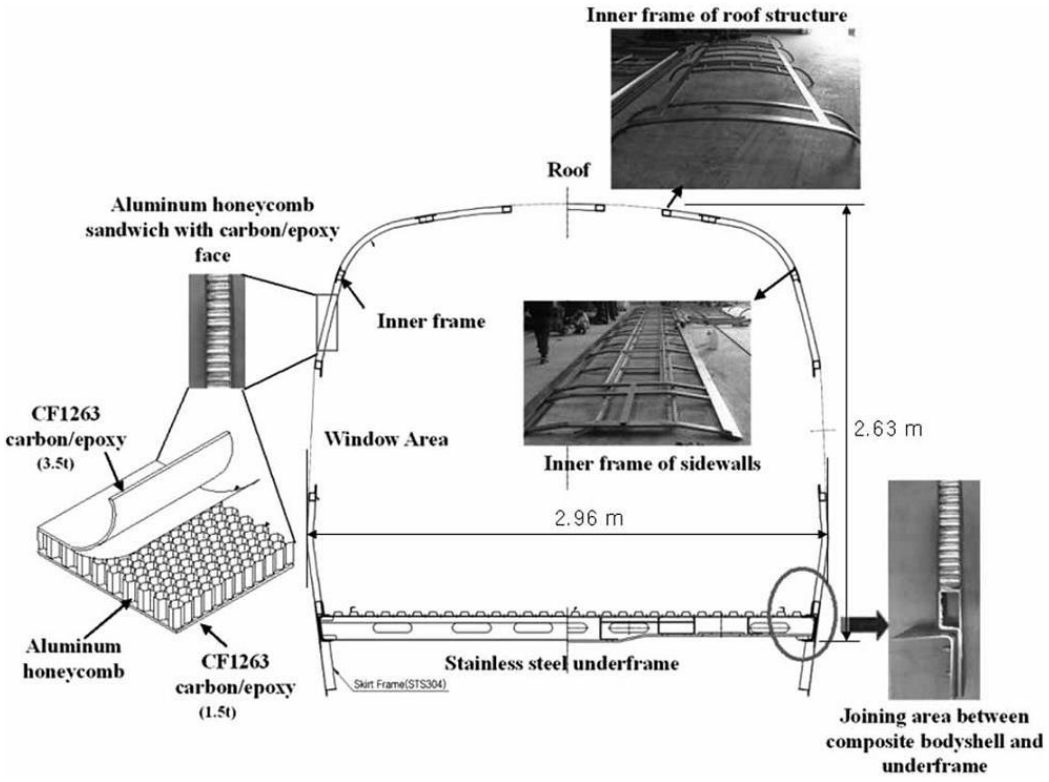

Figure 22 One-piece hybrid car body section detail (Seo et al. 2008)

Harte et al. carried out the optimisation of design parameters associated with composite sandwich body shell walls of light rail vehicles (LRV) (Harte et al. 2004). The body shell of the rail vehicle in question consisted of glass/epoxy – PU foam sandwich composite supported on a steel stiffener frame. The authors used convex linearization method (CONLIN), modified diagonal quadratic approximation (MDQA) and generalised Conlin method (GCM) algorithms, and found MDQA algorithm to be the most efficient for the optimisation of wall ply thickness (to reduce overall weight) and geometric shapes for areas such as doors and window openings (to reduce stressed areas). In another optimisation study, Hudson et al. investigated weight – cost related optimisation for rail vehicle composite sandwich floor panels by using ant colony optimisation (ACO) (Hudson et al. 2010). They performed the optimisation for three different setups: low mass, low cost, and intermediate design. Facing thickness, facing material, core material and timber support spacing (transverse and longitudinal) were included in the

optimisation method. In conclusion, they observed that low cost design was the most advantageous choice with a 37% mass reduction and 40% cost reduction. They obtained more weight savings in the low mass design and intermediate design by 53% and 40% respectively, however these designs resulted in a 93% and 13% cost increase, respectively.

At DLR - Institute of Composite Structures and Adaptive Systems (DLR 2012), carbon fibre reinforced composite car body designs were being developed, aiming at significant weight reduction and increasing cost savings for overall efficiency increase. DLR's Next Generation Train (NGT) (Figure 23) has the main objectives of increasing driving speed by 25% to 400 km/h in compliance with existing safety standards as well as reducing the specific energy consumption by 50%.

Figure 23 DLR's Next Generation Train – NGT (DLR 2012)

The NGT is composed of three differently designed modules according to specific demands: vehicle end sections are designed in accordance with the crash requirements given in DIN EN 15227 thus serving as crash absorbers; the running gear modules, which enclose the passenger module in the longitudinal direction, are made of a light alloy framework ideally suited to carry and to distribute the axle loads to the adjacent sections; and last but not least the passenger section which is especially suited for a composite sandwich design to achieve a significant

weight reduction of the whole vehicle. As a result, a weight reduction of up to 30% can be achieved compared to an all-metal design.

A successful attempt to create a radical new crashworthy composite cab for UK passenger rolling stock was accomplished by Ingleton (Ingleton 2005). This extensive and detailed work included critical standard requirements, collapse mechanisms, maintenance, repair and joint configuration. By using collapse and energy cells in the primary module and collapse tubes in the secondary module, the author was able to conclude and demonstrate that fibre reinforced composite materials could undoubtedly be used as structural safety elements in rolling stock.

Shin and Hahn studied the structural properties of graphite/epoxy composite materials following the use of ageing effects such as ultraviolet radiation, temperature and humidity, and analysed its integrity for hybrid railway carriage structures (Shin & Hahn 2005). A suitable ageing option was selected for the test facility by taking into account Korean weather activities; light/dark durations and temperatures, 85% humidity, water sprays and irradiance. The authors tested the specimens for their stiffness and strength properties at 0, 500, 1000, 1500 and 2000 hours. The effects of ageing were observed much more on strength properties than stiffness. They also reported unexpected increase in the transverse tensile stiffness over time, and determined that it was a direct result of post-curing of epoxy resin due to exposure to temperature and xenon arc. When they analysed the stress and deflection values of the hybrid vehicle after exposure to the ageing effects, it was seen that all the stress values were in the permissible levels. However, maximum deflection values of the aluminium underframe in all steps exceeded the permissible levels. As a conclusion, composite materials exposed to ageing effects were found satisfactory in terms of design requirements, however, emphasis was put on for further evaluation of integrity.

Another study of composite applications in Korean Tilting Train TTX was presented by Kim et al. (Kim, Lee, et al. 2007). The composite one-piece body was produced by a hand lay-up method in a mould (Figure 24), inserting an aluminium honeycomb core and mild steel inner reinforcing frame between the inner and outer carbon/epoxy faces, and applying vacuum bagging where necessary. A large autoclave, 30 meters in length and 5 meters in diameter, was specifically built for this purpose. The authors performed static tests such as vertical, compression, torsion, and 3-point support tests (Figure 25) and the new body achieved the design requirements by showing a maximum stress of 12.2% of the strength of carbon/epoxy, while providing 39% weight reduction in upper body construction.

Figure 24 Manufacturing process of Korean TTX train (Kim, Lee, et al. 2007)

A further investigation of static deformation behaviour of TTX composite carbody was carried out by Kim et al. (Kim, Jeong, et al. 2007) and the vertical and horizontal deformations were found similar to a Japan Rail East E653 train.

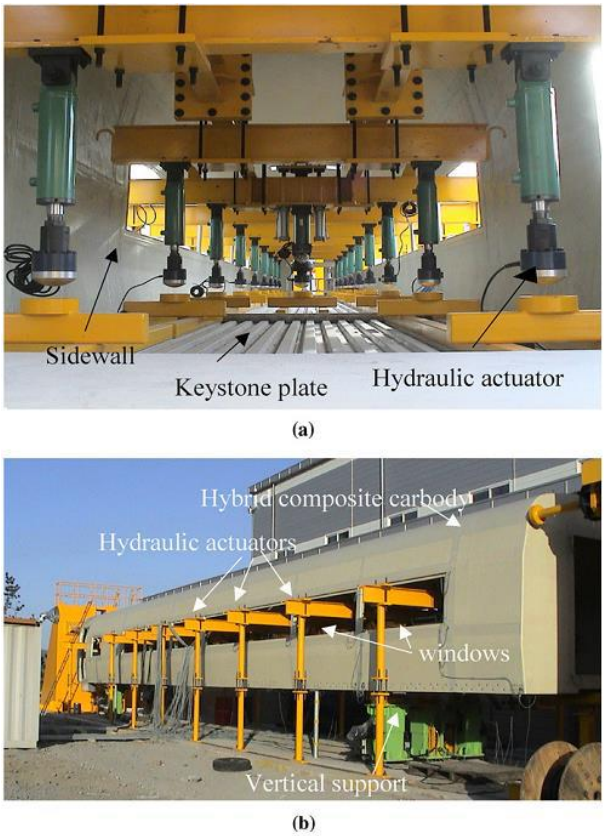

Figure 25 Testing of TTX train: (a) vertical load actuators, (b) test set-up (Kim, Lee, et al. 2007)

A fast and reliable two-dimensional method to predict mechanical response of GFRP-steel bolted joints for the railway industry was proposed by Catalanotti et al. (Catalanotti et al. 2011).

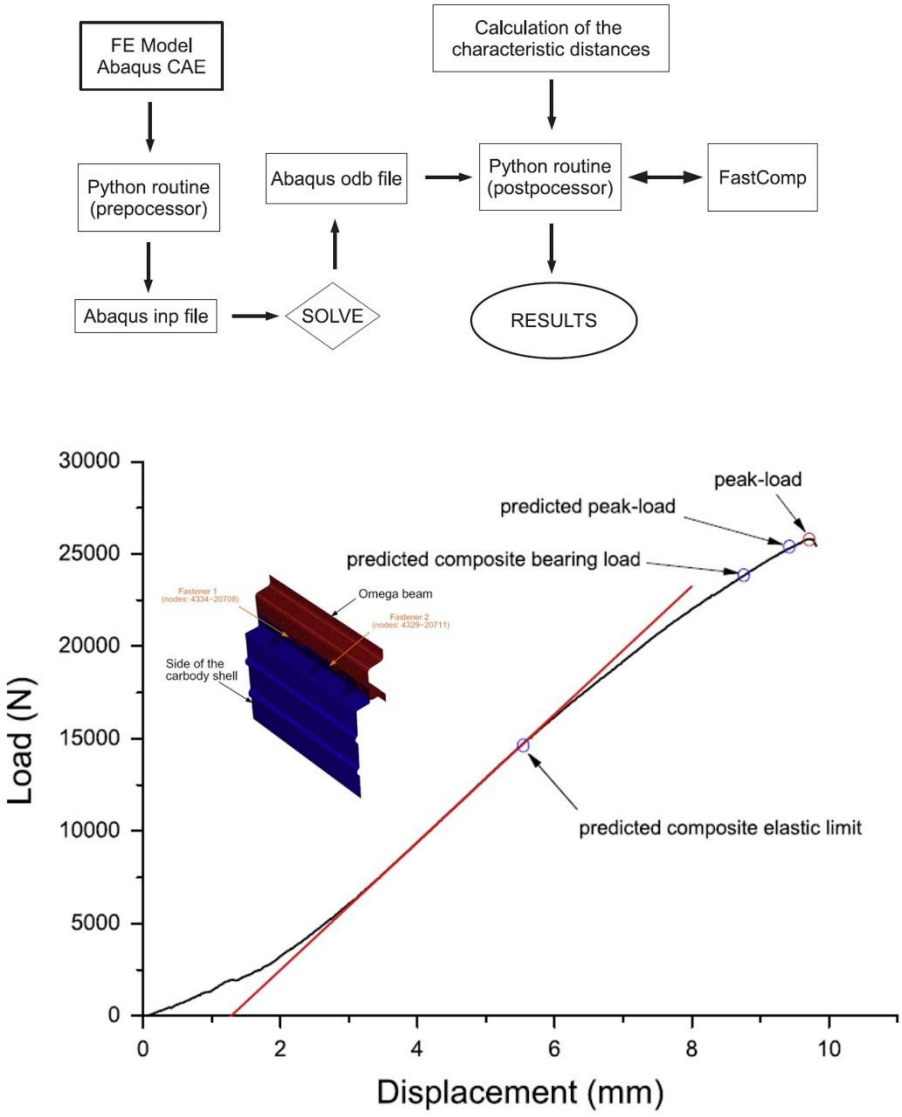

Figure 26 Multi-material bolted joint prediction method (top), and its correlation between the experiments (bottom) (Catalanotti et al. 2011)

The authors analysed the stress and strength states at and around the bolt hole in the composite joint by using the previously proposed method by Camanho and Lambert (Camanho & Lambert 2006). This allowed to obtain the elastic region and the strength of the composite bolted joint. Combining it with the bolt strength, Abaqus numerical model and Python routine was used to execute the proposed methodology (Figure 26 (top)). An industrial case study was investigated by using the proposed method to design composite-steel bolted joints. As Figure 26 (bottom) shows, the prediction of the first non-linearity in the loading which is accepted as the elastic limit of the composite was predicted very well by the proposed method. It was concluded that

the methodology could benefit the railway industry as being a fast, reliable, and easy to use method.

In a doctoral study, Wennberg analysed the requirements of a futuristic high speed composite railway vehicle body from strength, thermal insulation, fire safety, and sound transmission perspectives, and presented the results of the optimisation and multi-functionality research (Wennberg 2013). The author observed that using a multi-functionality approach and increased design complexity better revealed the full benefits of the design, e.g. reduced carbody wall thickness allowed to increase the passenger capacity in 2+3 configuration instead of 2+2, or allowed to increase the seat comfort with larger seats while maintaining 2+2 configuration. This finding could be extremely important for countries such as UK which has strict infrastructure and vehicle dimensional limits that hinders the capacity improvement. In addition to this benefit, he reported that up to 60% of weight savings is achievable when using carbon fibre as a load carrying structure. According to author's analysis and in parallel with the literature, great cost savings can be achievable in maintenance, manufacturing, and service situations, even though the raw materials are more expensive compared to conventional materials.

2.3.1 Findings

The literature review indicates that the initiative of implementing structural composites to railway vehicles began in early to mid-90's, and shows that currently it is a growing research area. The scope of the previous studies range from full scale body to sub-structure investigations which evidently were successfully implemented. Innovative and efficient designs of complete carbody shells or front cabs have proven the benefits of such applications mainly for countering weight concerns as well as its positive reflection to overall vehicle performance such as energy absorption for passive safety, sound, vibration, and thermal control for passenger comfort. Futuristic and concept studies have exposed the potentials of composite body shells for countering the capacity increase limitations caused by the strict infrastructure/rail gauge length.

However, very scarce amount of attention was given to date to the object strike against composite rail carbodies. No more than a few studies investigating the composite designs in rail vehicles addressed the impact risks. These studies were described in detail in Section 3.2 because of the relevance of their content. Therefore, it is certain that more research is strongly required to explore this specific field of interest. In addition, considering the composite applications in the railway industry is relatively a recent progression, new and practical methods

are required for a rapid transition to new lightweight structures, which this research attempted to accomplish.

2.4 Literature review: Impact loading response of laminated composites

Impact loading can be categorised depending on the velocity of the impactor. Different velocity ranges were defined by various researchers: low velocity impact (LVI) occurs in 1-10 m/s range, intermediate velocity impact (IVI) in 10-50 m/s, high velocity impact (HVI) between 50-1000m/s, and finally hyper velocity impact (HYVI) occurs above 1000m/s velocities (Abrate 2011). It was identified by some researchers that 20 m/s is a reasonable transition velocity from low to high velocity impact (Cantwell & Morton 1989; Cartié & Irving 2002). A point to consider in this classification is also that the mass and size of the projectile in these categories are generally distinctive. That is to say, the low and intermediate velocity impact takes into account objects with heavy mass or large geometry such as working tools or debris (hundreds of grams or kilogram levels), while high and hyper velocity impacts focuses on light mass and small geometry objects such as ammunition and space micro meteorite (up to tens of grams level). Accordingly, the response of the structure varies in each impact time scale. In simple terms, high and hyper velocity impact unfold so quickly that only the impacted portion of the structure could respond, leading to localised damage. On the contrary, in low or intermediate velocity impact there would be enough time to transfer the loads to and away from the vicinity of impact so that more global response could be exhibited. In the scope of this thesis the main interest was on small and light object strike travelling at intermediate to high velocities.

Many factors can affect an FRP composite's behaviour against impact type loadings. Fibre type, fibre architecture, staking sequence, fibre orientation angle, and thickness are some of them, along with impact parameters such as kinetic energy, impact velocity, and projectile properties. The literature review has shown that a great deal of effort has been made during the past 40 years on impact of composites. In general, studies investigated the effects of stacking sequence, laminate thickness, impactor nose shape, incident velocities, and mathematical and numerical modelling of various impact conditions through commercial software. This section presents the most relevant past research individually, makes connections where necessary, and summarises the notable findings at the end.

Abrate presented two extensive reviews of the early impact research on composites that has been carried out between 1970's and early 90's (Abrate 1991; Abrate 1994). These reviews included the essentials of impact mechanics and how the early composites respond to varying

types of impact loading. Both reviews put forth the results of experimental and analytical techniques, impact damage, damage prediction, and residual properties after impact ,while the latter review revealed the increasing interest in ballistic impact and the wave/stress propagation effects. As Abrate stated, it was almost clear that the fundamentals of impact on composites were well understood (even by then), however the then remaining challenge of impact damage prediction has also been succcesfully overcome lately with the improvement of numerical models implemented in finite element software which will be shown in the next sections.

Another early review on impact of composites was presented by Cantwell and Morton in order to identify the important parameters (Cantwell & Morton 1991). Techniques to investigate various impact loading were presented and then focus was given to the individual influence of the constituents to the overall resistane performance of composites. Strain energy absorbing capacity (higher strain to failure) was addressed as the most important parameter. In general, both the fiber and matrix were found to play crucial role. Specifically, it was reported that the surface treatment of fibre surface can be accounted more like an optional requirement since it influences the penetration resistance and residual properties. For multidirectional laminates, stacking sequence should be considered carefully, while unidirectional configurations should be avoided if the impact events are likely in the intended application.

In their extensive research, Mines and co-workers investigated static and ballistic perforation behaviour of glass fibre laminated composites of varying thickness (6, 12, and 24 ply) and architectures (woven, z-stitched, through-thickness z-stitched) (Mines et al. 1999). Laminates were subjected to the impact of three different impactors (flat, conical, hemispherical) with two massess (6, 12 g) and energy partition analysis were performed to discuss the dominating mode of failure for each material. The authors generated a parameter called dynamic enhancement factor (ϕ_p) which is the ratio of high-velocity perforation energy to static perforation energy, and found that this parameter was the highest for flat ended projectile even though some scatter was observed for the thinnest laminates (Figure 27). It was found that all the considered reinforcement architectures behaved similarly. Energy partition analysis revealed that local energy dissipation modes were dominant for 6 ply laminates, while delamination dominated the energy absorption for 12 and 24 ply laminates.

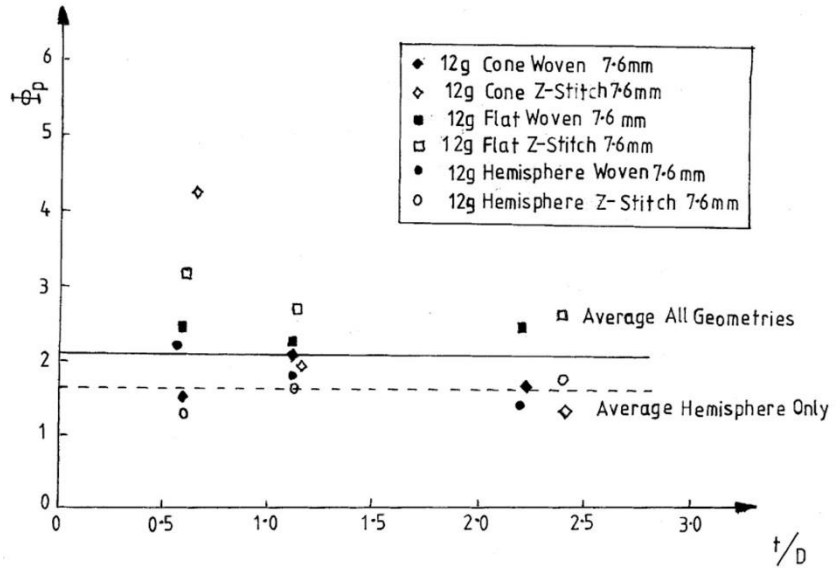

Figure 27 Dynamic enhancement factor parameter with respect to laminate thickness (Mines et al. 1999)

Zhou and Davies performed static perforation and low-velocity impact tests with woven roving glass/polyester laminates and investigated the energy absorption, strain rate effect, damage progression and thickness effect (Zhou & Davies 1994). In contrast to many researchers at that time, they considered thicker laminates, i.e. 10 mm and 25 mm. The dynamic tests showed that energy absorption increases as the thickness of the laminates increase, and strain rate effect caused by low-velocity impact resulted in 36% and 22% increase in maximum failure load for 10 mm and 25 mm laminates respectively (Figure 28). However, this effect had no influence on the damaged area. Authors concluded that use of impact force, incident kinetic energy history, damage force and kinetic energy maps are quite useful to characterize impact behaviour of glass fibre laminates.

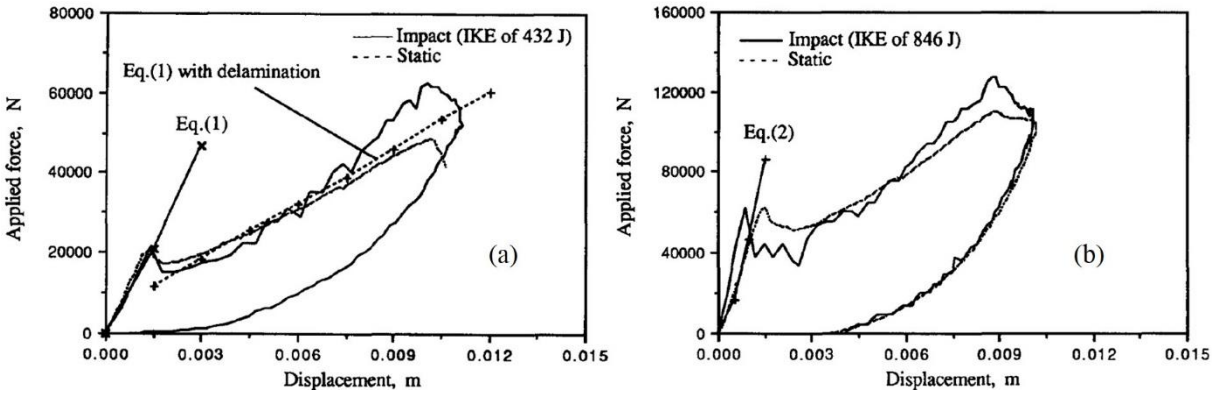

Figure 28 Static and dynamic impact comparison for (a) 10 mm and (b) 25 mm thick laminates showing the strain rate effect (Zhou & Davies 1994)

Gellert et al. experimentally investigated the thickness dependency of glass fibre reinforced composites at ballistic impact levels by using three different impactors with two different sizes (Gellert et al. 2000). They derived simple formulations for the work done by indentation by implementing the formulations of work of tension, fracture and bending. Consequently, this analysis helped to create a definition for thin targets, of which exhibits failure by dishing rather than indentation. Authors recommended that the thickness of the laminate should be maximised in order to have an effective ballistic protection, stating that energy absorption is more significant at indentation phase.

Cheeseman and Bogetti reported a review of the factors affecting the ballistic performance of fabric and compliant (armour-grade) composite laminates (Cheeseman & Bogetti 2003). Dominant factors such as yarn material properties, yarn interactions, projectile shape and velocity, and number of layers were investigated as well as the less influencing factors such as friction, far-field boundary conditions and fabric structure. Authors presented the results of many researchers which has both supporting and contradicting findings. In general, evidence suggests that the performance of fibre reinforced laminates depends on an interactive system rather than a couple of controlling elements.

Sabet and co-workers studied the different type of fibre reinforcement architectures under high velocity impact loading by a conical projectile (Sabet et al. 2011). The architectures considered were all glass based fibres namely the chopped strand mat (CSM), plain weave (PW), satin weave (SW), unidirectional (UD), and cross-ply unidirectional (CP). Laminates of such configurations were manufactured as two different thicknesses (3 mm and 6 mm) by using plies of 300-400 gr/m^2 areal density, and were subjected to gas gun impact loading in 80-160 m/s velocity range. Of all the tested samples, fully penetrated ones exhibited same failure shape irrespective of thickness, which was the cone shape at reverse side arisen from the conical tip of the projectile. General conclusion was made towards the use of plain weave architecture followed by cross-ply unidirectional for better performance in terms of energy absorption as Figure 29 (left) shows. Although the difference wasn't significant between other configurations, satin weave architecture provided the best specific energy absorption (energy per mass) (Figure 29 (right)).

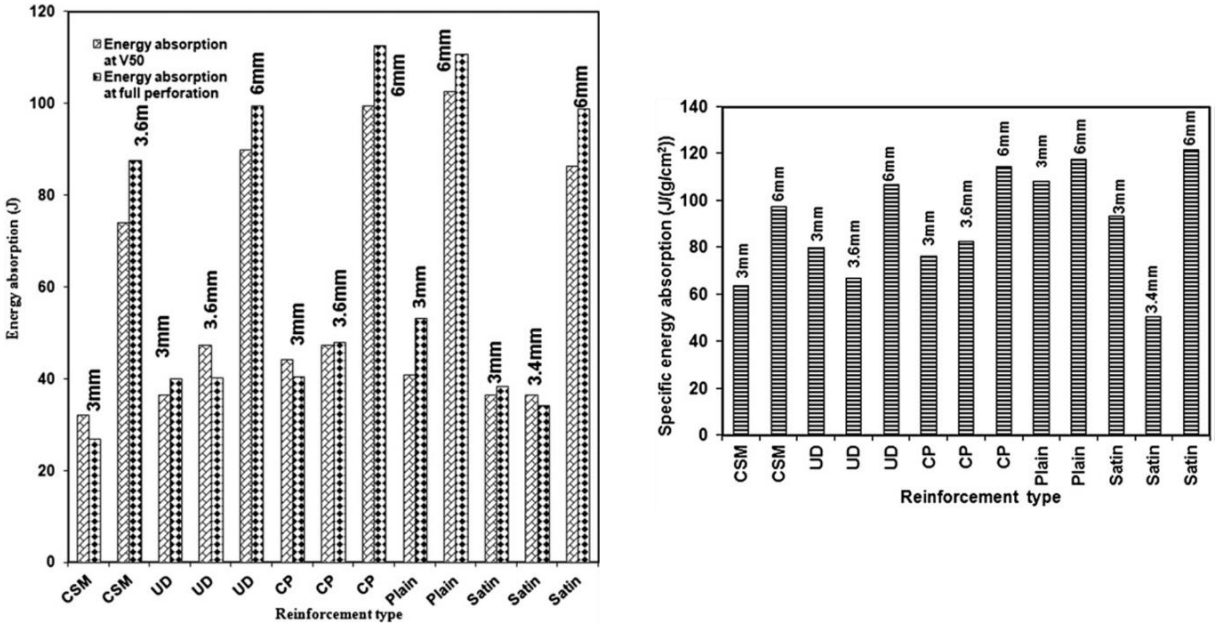

Figure 29 Energy absorption at ballistic limit and full penetration (left), specific energy absorption (right) (Sabet et al. 2011)

Hosur et al. investigated the performance of stitched and unstitched carbon/epoxy fabrics under ballistic impact loading (Hosur et al. 2004). Plain and satin weave fabrics were used to manufacture the laminates with a low cost VARIM technique (vacuum assisted resin infusion moulding). Three thicknesses were considered for unstitched laminates whereas it was two for stitched laminates which also had two different stitch grid (12.7 mm and 25.4 mm grid). The authors carried out non-destructive ultrasonic technique to create failure maps of impacted laminates and found out that stitching resulted in change of the reverse face failure mode. It was observed that stitched laminates performed worse than unstitched ones in terms of ballistic limit velocity which was explained as the localisation of the energy dissipation. Since reverse face tensile failure was suppressed by the stitch failure, the projectile forced the laminates to fail in shear, which resulted in lower ballistic limit velocities. In general, it was concluded that laminates with stitching performed poorly compared to unstitched counterparts against ballistic impact loading (Figure 30).

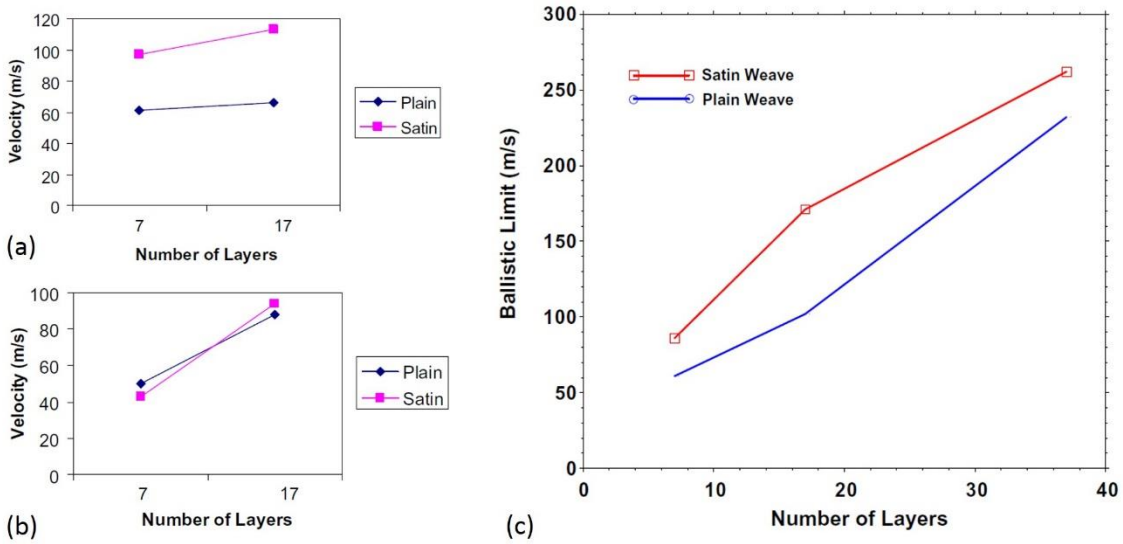

Figure 30 Ballistic limit for stitched laminates: (a) 12.7 mm grid, (b) 25.4 mm grid, and ballistic limit for unstitched laminates (c) (Hosur et al. 2004)

Larsson carried out mechanical testing and damage tolerance analysis of unidirectional stitched carbon fibre reinforced laminates in low and high velocity impact loading conditions (Larsson 1997). Stating a possible method to improve the interlaminar fracture toughness of similar composites was to enhance the matrix material, the author compared the findings of the testing program with brittle epoxy, toughened epoxy, and toughened thermoplastic matrix (polyetheretherketone - PEEK). Test program included longitudinal and through-thickness tensile testing, double-cantilever beam testing (for G_{IC} fracture toughness), low-velocity, and high velocity impact testing. This extensive program revealed that stitching was not effective, causing the tensile properties to drop by 20-25%. On the contrary, significant improvement was achieved in interlaminar fracture toughness (10 times greater than unstitched laminates) and impact delamination energy (more than 20 times greater). Compression after impact (CAI) strength of the stitched laminates were found better than brittle and toughened epoxy, and a little poorer than PEEK matrix laminates, while ballistic damage tolerance was 50% better than brittle epoxy laminate and was equal to PEEK matrix laminate. It was concluded that stitching was proved as a worthy method to increase the damage tolerance of unidirectional laminates.

In an excellent review, Kim and Sham presented the fracture mechanisms in laminated composites and their relationship to impact loading and damage tolerance of woven fabric laminates (Kim & Sham 2000). Focusing mainly on the delamination behaviour and the effect of mode I G_{IC} and mode II G_{IIC} fracture toughness on the impact resistance of reinforced laminates, the authors reported the effect of fibre surface treatment on toughness parameters as

well. Crack initiation and propagation mechanisms were clearly explained which were different between unidirectional, cross-ply, and woven fabric laminates. For low energy impact loading, it has been found that mode II fracture toughness values were much greater than mode I, and fibre surface treatment has considerable effect on impact damage resistance and tolerance of woven fabric composites. Conclusions made as follows: woven fabric laminates generally have better toughness properties compared to unidirectional and angle-ply counterparts, mode II G_{IIC} fracture toughness is almost independent of inter-ply angle, woven fabric laminates are weaker in terms of maximum load bearing capacity, however, they exhibit smaller damage area, are more ductile and have higher residual compression after impact strength which is much desired for industrial applications.

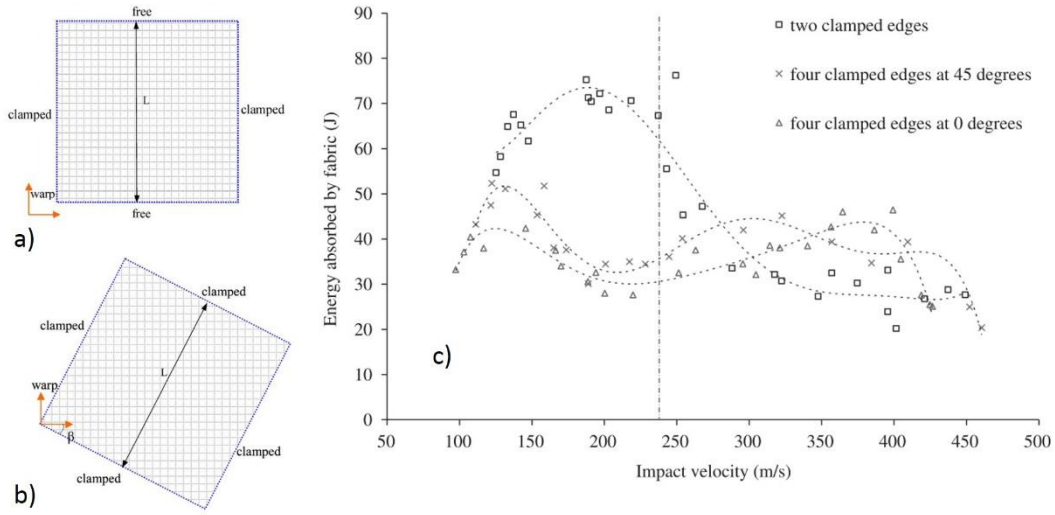

Figure 31 Different boundary conditions (a and b) and their effects on ballistic energy absorption (c) (Zeng et al. 2005)

Zeng et al. investigated the boundary condition effect on the ballistic performance of armour type square fabrics (Zeng et al. 2005). Three conditions were considered, i.e. clamped in all edges, clamped from two edges, and clamped at four edges with the edges 45° to the yarn direction (Figure 31a, b). High velocity experiments were carried out at and above ballistic limit of the fabrics. It was found that the two-edge clamping resulted in more energy absorption due to the free movement of unconstrained edges, making the fabric less tense (Figure 31c). It was also observed that clamping the fabric by 45° angle to the yarns improved the energy absorption capability of the fabric (Figure 31c). Even though it was an interesting study, the implication of such approach may not be suitable for every need. Furthermore, it is well known that the role

of matrix material (which was not considered in the study) is also crucial on energy dissipation against high velocity impacts.

Naik and Shrirao presented an analytical model which predicts the ballistic limit, contact duration at ballistic limit, and the energy absorbed by various failure mechanisms for E-glass/epoxy and T300 carbon/epoxy composite laminates (Naik & Shrirao 2004). This model requires dynamic material property input, and target and projectile geometrical input. The authors first introduced the major deformations that occurs in a typical ballistic event such as the cone formation at the back face, shear plugging, deformations in the secondary yarns which are not in direct contact with the projectile, and primary yarns right under the projectile contact surface. They generated time interval equations based on elastic/plastic strains of a single yarn, then integrated this formula to the whole woven fabric composite. Stating that shear plug formation was not observed in glass fibre reinforced composites (which is not entirely true since thicker targets may exhibit predominant shear plugging), they observed that shear plugging dominated the carbon-based composite, while primary yarn tensile failure was predominant energy absorber for glass based composite. They achieved generally good agreement with the previous ballistic experiments in terms of ballistic limit velocity and predicted primary damage area.

In subsequent two interrelated studies, Naik and co-workers carried out analytical and parametric studies of ballistic impact on E-glass/epoxy laminates (Naik et al. 2006; Naik & Doshi 2008). Formulations of the analytical method which based on wave theory was presented in the former, and parametric ballistic comparisons were made in the latter. Comparison included different incident velocities, impactor residual velocities, contact duration, target thickness, and projectile properties such as mass and diameter. As opposed to other researchers such as (Chan et al. 2007), they reported that energy absorbed by delamination was not significant (Figure 32). This comparison suggests that even though both studies used epoxy resin, the response of the structure to a specific loading could be different. This is one of the drawback of composite materials: even one simple or small change in the configuration or component might affect a certain characteristic(s) slightly or greatly. Therefore, specific needs must be dealt with relevant specific approaches.

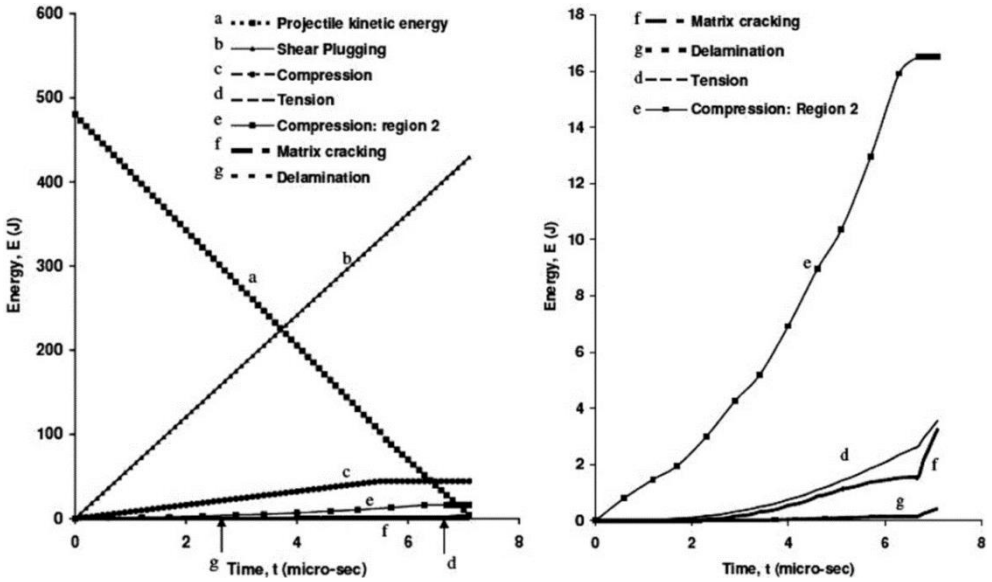

Figure 32 Energy absorption by different mechanisms for woven fabric E-glass/epoxy laminate (Naik & Doshi 2008)

Yen pointed out that there was a need for new material model as the previous reported material models were not providing accurate results, and developed a progressive failure model for non-linear behaviour of composites for ballistic impact (Yen 2002).

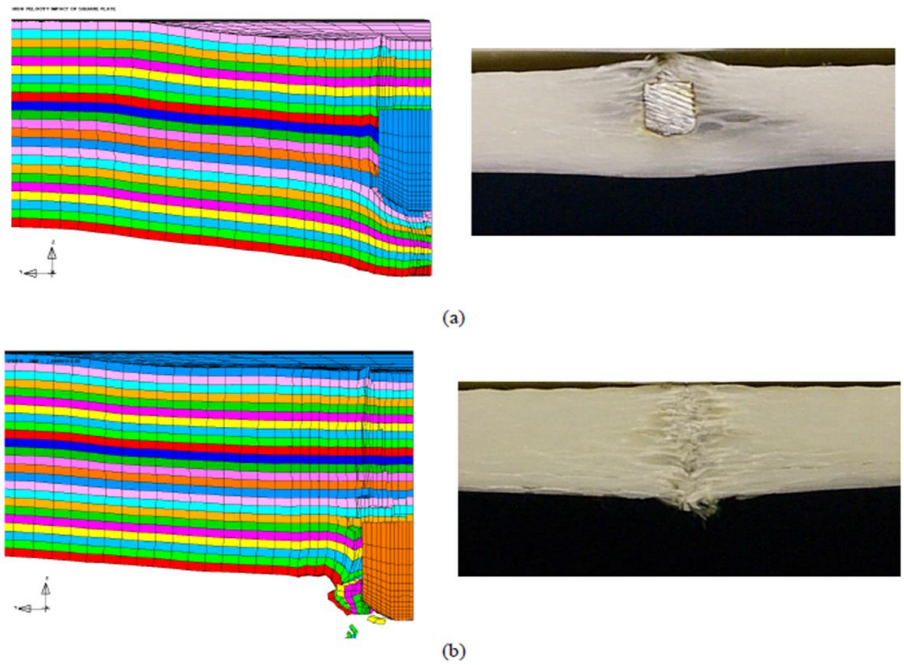

Figure 33 Comparison of progressive damage between FE model and experiment showing strong similarity (Yen 2002)

Based on Hashin's failure criteria and Continuum Damage Mechanics (CDM) approach previously presented by Matzenmiller (Matzenmiller et al. 1995), the author then presented the

rate dependant damage progression criteria which was missing in previous material models. The author performed the simulations for two different ballistic scenarios on S2-glass/Epoxy composites and it was observed that fibre related damage and delamination phenomena can be successfully represented by the new model (Figure 33). However, it was stated that more experimental work should be done further to get more precise correlation, especially for delamination and strain rate effects. Presented material model was then implemented to FE software Ls-Dyna.

In a further work, Yen extended the previous model to include unidirectional configuration and validation with the then newly obtained material data (Yen 2012). As a result, improved results were obtained by more detailed investigation of strain rate effect parameters represented in individual principal material directions (Figure 34).

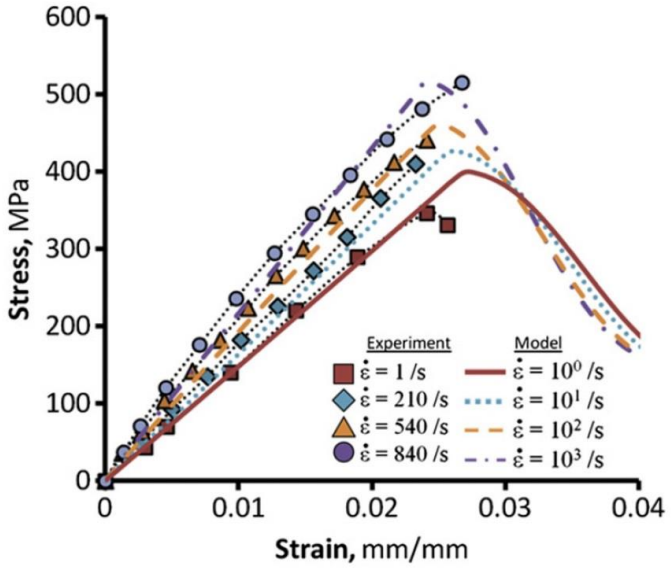

Figure 34 Effect of strain rate on axial stress-strain data from the numerical model and experiments (Yen 2012)

Xin and Wen proposed another progressive material model to capture the impact damage of laminated FRPs (Xin & Wen 2015), which is quite similar to Yen's model (Yen 2012). The difference was the adaptation of the stress-displacement relation instead of stress-strain based on fracture energy approach, and the addition of parameter L_c. Interestingly, the stress-displacement relation reduced the mesh dependency of the numerical model as shown in Figure 35 (left). Various published low velocity and ballistic impact cases were performed with the proposed method and the results were satisfying (Figure 35 (right)).

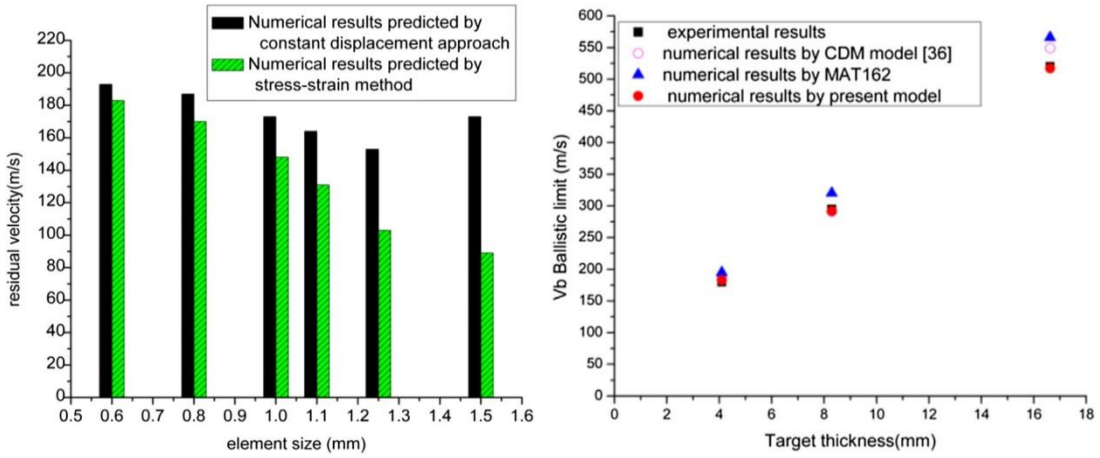

Figure 35 Effect of stress-displacement approach on residual velocity (left) showing the mesh dependency was reduced, and accuracy of the presented model (right) (Xin & Wen 2015)

Chan et al. performed high velocity impact tests on carbon fibre laminate composite material samples to research the ballistic impact limits considering the effect of stacking sequence, and attempted to predict the same levels by developing a progressive damage model in Ls-Dyna software (Chan et al. 2007). Seven samples with different ply orientation were tested and compared with the numerical models. Experimental results showed that ballistic limit velocities of the samples didn't vary greatly. The authors concluded that the S_{RT} factor used in the material model was capable of modifying required strength parameters of materials during the simulation, leading to negligible changes in strain rate, which also in turn permitting the use of static material properties for dynamic impact event. This finding suggests that strain rate effects of carbon fibre laminates are not as influential as it is for glass fibre counterparts. It was also seen that the delamination failure was crucial for the amount of absorbed energy of these types of materials.

By using Ls-Dyna explicit dynamics solver, Gama and Gillespie simulated the high velocity impact behaviours of thick section glass fibre composites (Gama & Gillespie 2011). After observing the numerical and experimental results, they concluded that there are two distinct phases in ballistic penetration, i.e. short time phase – shock compression, and long-time phase – penetration. They observed significant variation between simulations and experiments in terms of ballistic limit velocity, and proposed that post-damage softening parameters, strain rate parameters, and erosion strain parameters have a reasonable effect on penetration event. Seven different rate effect sets: combination of strength, shear modulus and through-thickness modulus were simulated to obtain matching results with ballistic experiment and to see the best correlating rate effect set. Simulation results showed that "increased shear and transverse

moduli, and material strengths" and "increase in all strength and moduli" property sets gave excellent results. Successful numerical model was applied to laminates with two different thicknesses and excellent agreement was obtained with the experimental data shown in Figure 36 which means the incremental strain rate effect was viable for this material system.

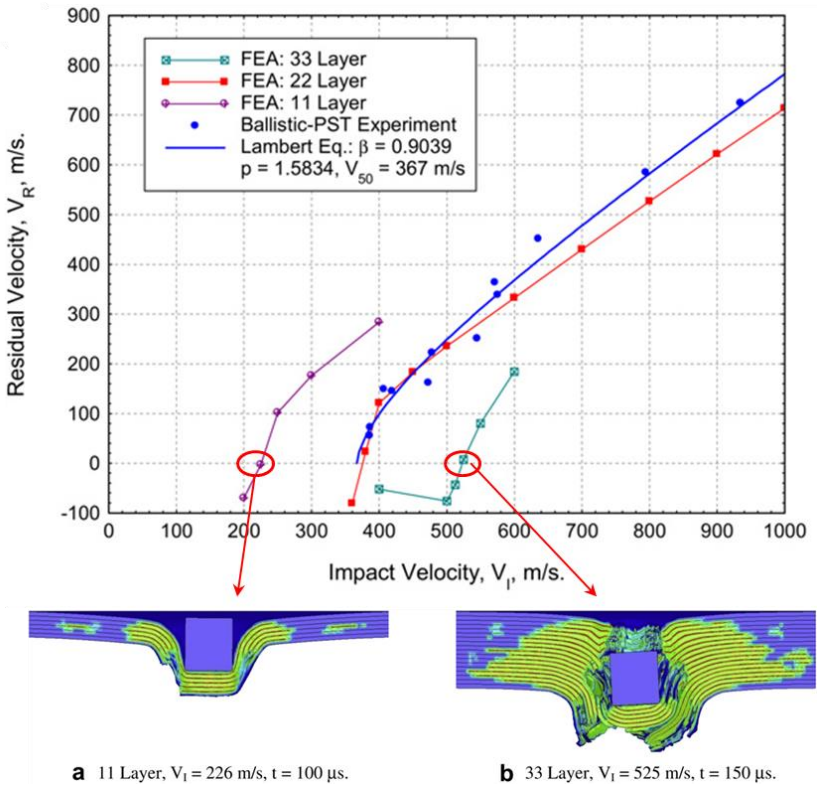

Figure 36 Comparison of FE model for 11 layer and 33 layer laminates showing that developed model captured the ballistic limit accurately (Gama & Gillespie 2011)

Jordan et al. produced an extensive material property table for E-glass/phenolic composite laminates for numerical purposes (Jordan et al. 2014). Previously conducting impact experiments (Jordan et al. 2013) with three different test fixtures (low-velocity impact, depth of penetration, and ballistic test) with different velocities and conditions, they obtained material model parameters by carrying out parametric simulations to match the experimental data. Figure 37 (right) showing such example in which the FE model predicted the depth of penetration accurately. Validation with separate ballistic experiments revealed the excellent correlation between LS-dyna simulations while using MAT_162 material model (Figure 37 left).

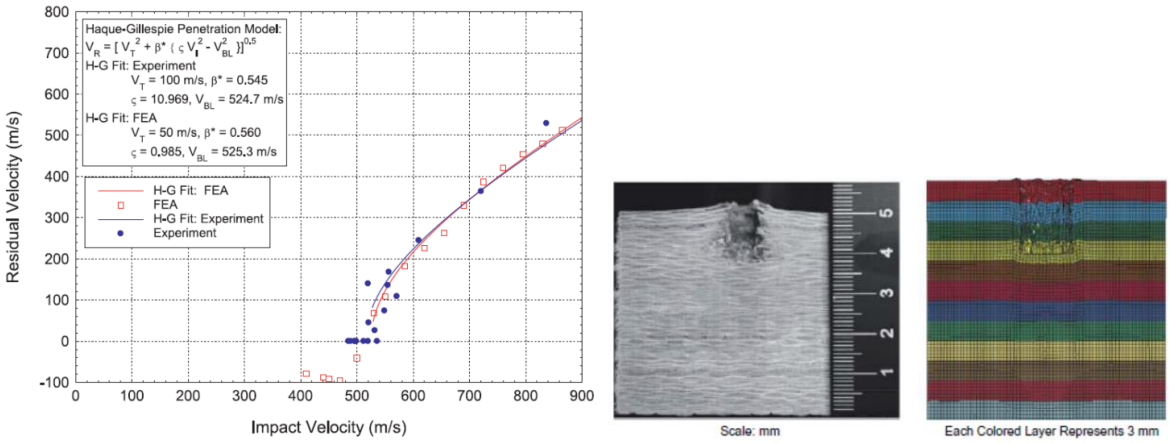

Figure 37 Numerical model validation of high-velocity impact on E-glass/phenolic laminates (left) and the correlation of depth of penetration experiment and simulation (right) (Jordan et al. 2014)

Antonucci et al. embedded fibre optic Bragg sensors (FBG) inside composite laminates to detect indentation induced deformations during quasi-static test (Antonucci et al. 2014). The sensor was able to capture the non-linear behaviour of load-displacement curve. However, the strain values were found to be strongly affected by the change of the original position of sensors due to the manufacturing. This shows that embedded sensors for monitoring the impact damage analysis in-service is not a reliable method yet.

Monti and co-workers used carbon nano-fillers (CNFs) with unsaturated polyester resin and glass fibre to evaluate the laminate's electrical properties for health monitoring purposes (Monti et al. 2011). In order to obtain appropriate level of viscosity from the resin-CNF mixture, CNF content was held below 1wt%, while investigating 0.5wt% and 1wt% concentrations. Preliminary results showed that 1wt% gave stronger and more defined data and therefore focus was given on this configuration. Flexural and impact tests (Figure 38) were carried out while variation percentage in electrical resistance was observed at the same time. As it can certainly be seen from the figure that electrical resistance coincides with the loading pattern of the samples, indicating that cracks accumulated during loading increases the electrical resistance of the composite by disrupting the current flow through CNFs, which were also supported by the scanning electron microscopy images. In conclusion, using CNFs was proven a promising health monitoring approach for composites that are electrically poor conductors.

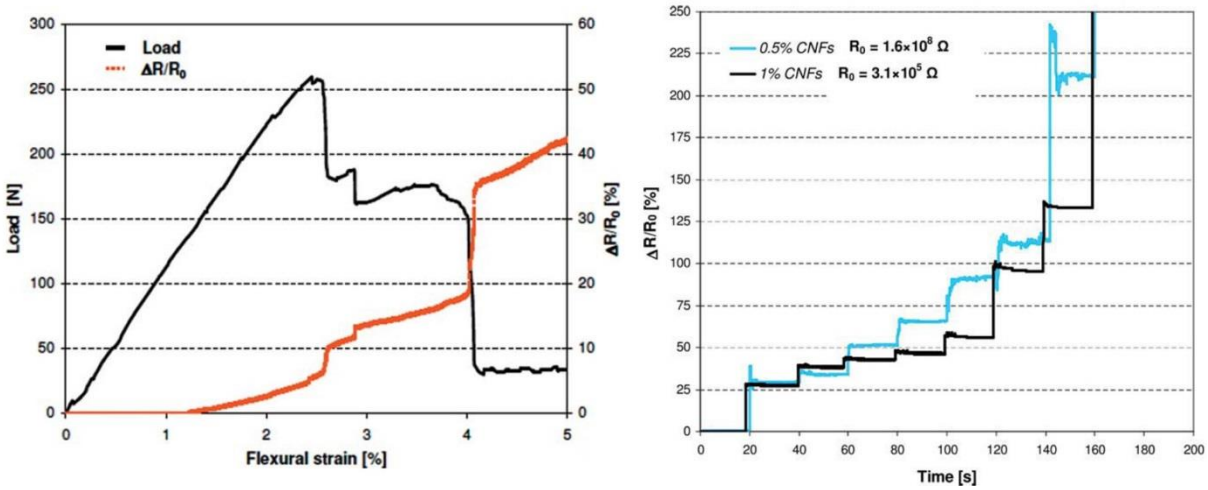

Figure 38 Change in electrical resistance in GFRP samples: (left) 3-point bending test, (right) repeated impact test (Monti et al. 2011)

2.4.1 Quasi-static punch testing

In order to understand how the impact energy is dissipated and transferred to the material, the efforts of previous research have revealed an advantageous finding. The damage mechanisms under high velocity impact event show similar patterns with the quasi-static punch shear tests (QS-PST) under the same boundary conditions. The advantage in this case clearly is the ability to analyse the energy dissipation in a more static environment with QS-PST process. The following section reviews the application of quasi-static punch tests available in the literature.

Lee and Sun investigated the damage behaviour of graphite/epoxy laminates under high velocity impact loading (Lee & Sun 1993). The authors showed that when all the boundary conditions are the same, there was a similarity of damage in graphite/epoxy laminates between dynamic perforation and static punch. Identifying the leading damage modes as delamination and plug formation in a static event, they detailed the penetration process in three stages: pre-delamination, post-delamination before plugging, and post-plugging. One of the important remarks was the use of displacement levels of the punch as failure criteria in simulations since force levels seemed to be affected greatly from damping and time step size (time step size is the incremental change in time for which the governing equations are being solved), making it difficult to use. In conclusion, with the evidence of decent agreement between experiments and computational results (computational algorithm was presented as in Figure 39), static penetration models were found useful to predict ballistic response of graphite/epoxy targets without the necessity of dynamic testing.

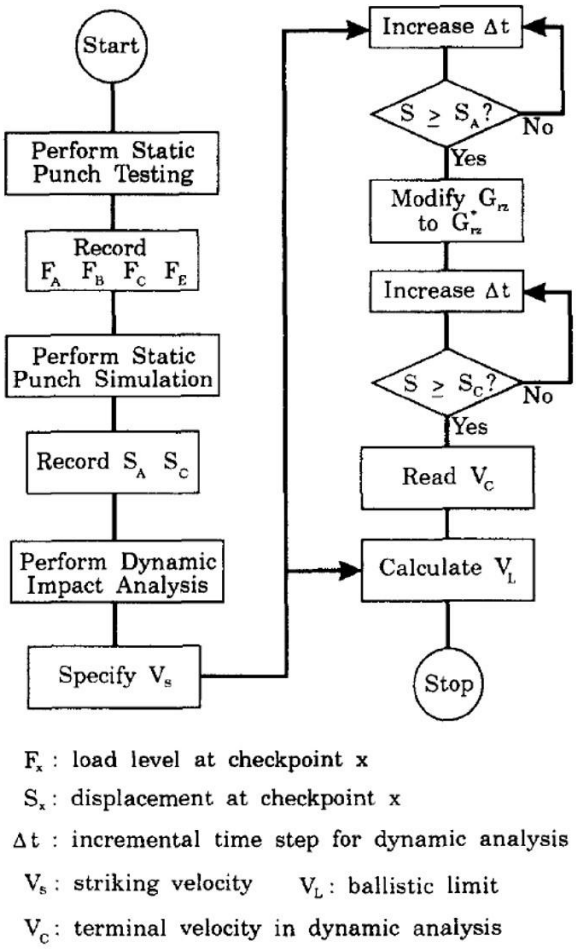

Figure 39 Computational modelling carried out by Lee and Sun (Lee & Sun 1993)

Sun and Potti (Potti & Sun 1996) generated an approach for capturing the failure behaviour of composite laminates under high velocity impact loading. Performing quasi-static punch and high velocity impact tests on graphite-epoxy laminates with two sizes of special fixtures, it has been seen that energy consumed by specimens in dynamic penetration was higher than the static penetration. High velocity impact tests also showed that damage was local and it was not highly influenced by the specimen size for the same thickness. Dynamic model showed good agreement with experiments when it was used in combination with load-displacement data from quasi-static tests and critical deflection criterion. The authors stated that failure initiation load and plug formation load was approximately the same for span-to-punch ratios (SPR) of 3 and 5 for graphite-epoxy laminated composite. However, this type of behaviour can be different for glass-fibre laminates as it can be seen from the work of Gama (Gama & Gillespie 2008); that the loads might be different when the SPR decreases from 4 to 1.

Potti and Sun, in addition to their previous research (Potti & Sun 1996), investigated the delamination damage for different impact velocities (Potti & Sun 1997). This time the dynamic

model included critical shear strain as a criterion to predict the delaminated area. It was stated that the area of the delamination can be assessed in two categories, i.e. below and above the ballistic limit. For the impact velocities below the ballistic limit, delamination length increases with increased speed, but decreases with the increasing impact velocity if it is above the ballistic limit velocity (Figure 40).

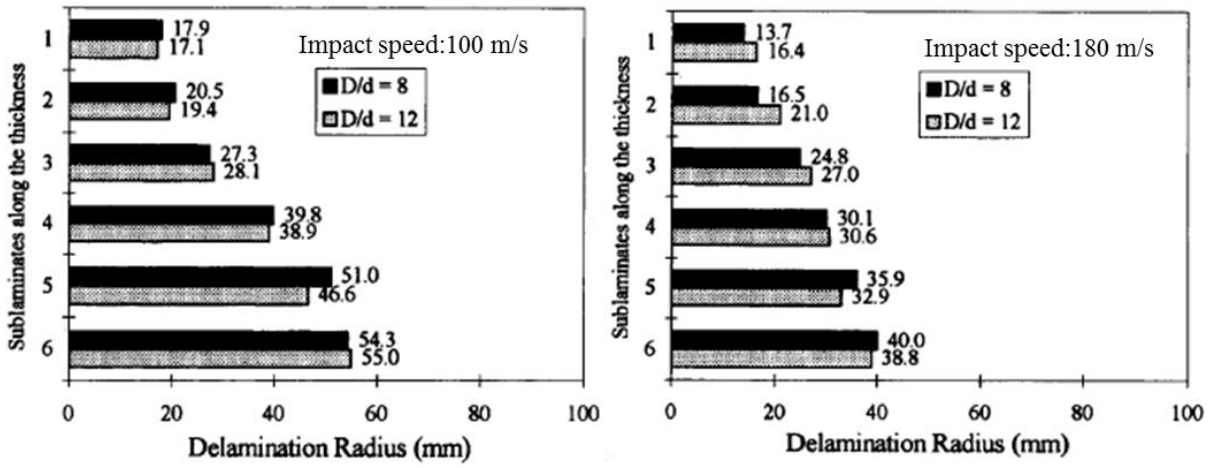

Figure 40 Change in delamination length with respect to impact speed (Potti & Sun 1997)

Goldsmith et al. carried out ballistic and quasi-static experiments with a sharp point conical striker impacting on woven carbon/epoxy laminates with varying thicknesses (Goldsmith et al. 1995), and generated a prediction model based on the energy balance and case specific damage mechanisms such as petal bending (Figure 41). This model was successful for predicting the ballistic limit of the laminates. The perforation energies of thin laminates were also predicted with reasonable accuracy, however, it was not the case for thicker laminates. They concluded that the static perforation energy is always less than the dynamic for the same thickness, but their finding for 6.6mm thick laminates was against this conclusion.

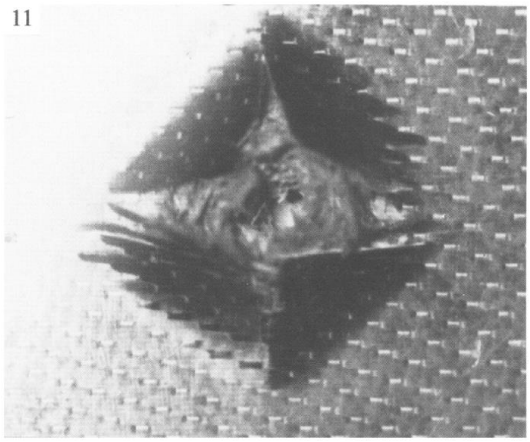

Figure 41 Petal bending failure type in woven carbon/epoxy laminate (Goldsmith et al. 1995)

Xiao et al. analysed the damage sequence in laminated S-2 glass/SC-15 epoxy composites by quasi-static punch shear tests, which were performed for two different span-to-punch ratios and six different thicknesses (Xiao et al. 2007).

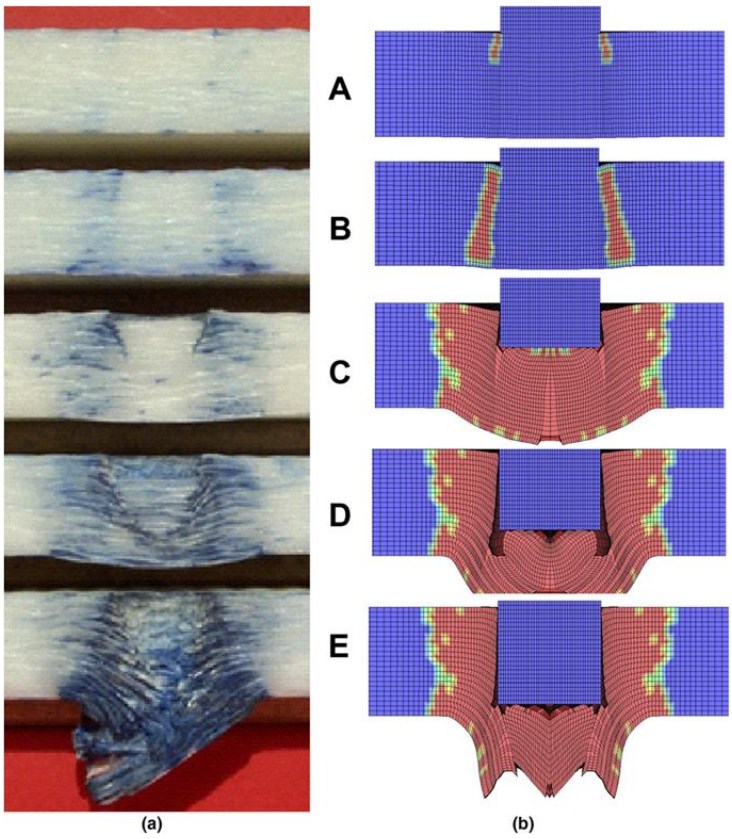

Figure 42 Comparison of fibre tensile/shear and delamination failure at different displacement levels under quasi-static loading; (a) experiment, (b) simulation (Xiao et al. 2007)

They distinguished the behaviours of thin and thick laminate, by identifying a non-dimensional parameter to categorize thickness, and stated that delamination is more obvious in thick laminates while thin laminates undergo membrane tension. The authors investigated the effects of various damage parameters of the material model MAT_162 of Ls-Dyna, which enables a progressive damage simulation of laminates, and selected the best values for each parameter for more accurate simulation. As a result, they achieved a strong similarities in terms of failure types, size, and sequence between experiments and simulations (Figure 42). The authors defined the damage progression of the plain weave material under punch shear loading as delamination forming, delamination progression, fibre compression and shear, and lastly fibre tension and shear failure.

Gama and Gillespie developed an influential methodology for calculating the ballistic limit of glass fibre laminated composite plates by using quasi-static punch shear testing (QS-PST)

(Gama & Gillespie 2008). By determining the dominant damage modes during a ballistic impact first, they attempted to correlate the energy absorbing mechanisms with quasi-static testing. Mentioning that mechanisms of ballistic limit penetration (the partial penetration of samples) can be better represented by quasi-static approach, they stated that damage mechanisms were a function of span-to-punch (SPR) ratio. The authors penetrated the samples and analysed the sequence of the failure modes and the energy partition during impact event. Lastly, they created a curve that can envelope the load-displacement histories for various span-to-punch ratio tests alone (Figure 43) which allows to predict penetration energy, and achieved good agreement with actual ballistic test results.

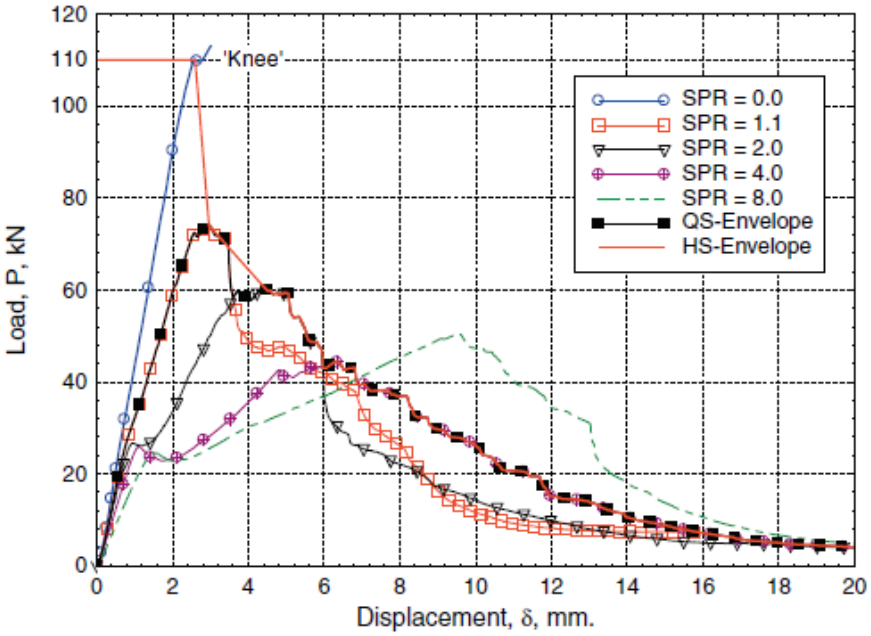

Figure 43 HS-Envelope (hydrostatic) curve obtained by quasi-static punch tests at various SPR ratios (Gama & Gillespie 2008)

The QS-PST and HS (hydrostatic) envelope concepts are quite interesting and obviously practical findings. However, Erkendirci and Haque showed that it may not be applicable to other material systems without modifications. Erkendirci and Haque carried out quasi-static punch shear tests on S-2 Glass/SC-15, S-2 Glass/HDPE (high density polyethylene) and E-Glass/HDPE composite laminates with different thicknesses in order to compare their penetration resistance by using methodology developed before (Erkendirci & (Gama) Haque 2012). It was observed that when using HDPE resin, the force-displacement behaviour was very different compared to SC15 epoxy resin system. Maximum load appeared to have a decreasing behaviour with increased span-to-punch diameter ratio (SPR) for SC15 resin but for HDPE

system it almost remained constant with the increasing SPR values. Author stated that the reason for this behaviour was the lower transverse shear stiffness of HDPE system. Obtaining different load-displacement behaviour for HDPE system led the authors to identify new definitions for penetration resistance: non-linear penetration stiffness (NL-PS) (Figure 44), which allowed them to present average penetration resistance force (APRF) graphs. By transforming previous data into NL-PS, they observed that the resistance behaviours became similar for all material types and APRF graphs represented the materials ability to dissipate energy for quasi-static punch shear loadings.

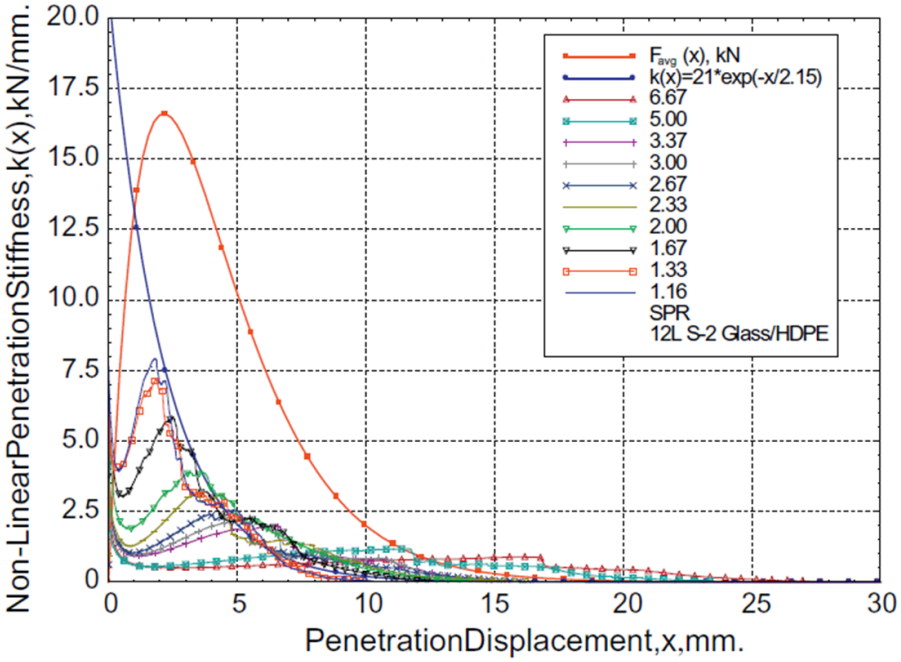

Figure 44 Non-linear penetration stiffness (NL-PS) for S2-glass/HDPE composite laminates (Erkendirci & (Gama) Haque 2012)

Yahaya et al. also used quasi-static penetration tests in order to investigate the penetration energies and resistances of kenaf-aramid fibre hybrid composites in different stacking sequences (Yahaya et al. 2014). They achieved higher penetration resistance forces and total absorbed energy values by combination of kenaf and aramid layers, however the specific energy absorption (per areal density) of hybrid configurations was negatively affected.

Erkendirci investigated the energy absorption behaviour of Carbon fibre/HDPE resin (high density polyethylene) laminates for two different thicknesses (Erkendirci 2016). The author observed that thinner laminates dissipated more energy compared to the thicker ones, because of the large effective displacement for complete penetration.

Sutherland and Guedes Soares carried out quasi-static testing in order to compare the failure modes and energy absorption behaviour of glass fibre composite laminates with the drop-weight impact tests (Sutherland & Guedes Soares 2012). They achieved good agreement in terms of delamination onset in both test cases. However, the fibre failure happened earlier in quasi-static tests than it did in the dynamic tests which can be explained by the higher strain rate effects of glass fibre reinforced plastics (GFRP). Overall, they concluded that quasi-static test method is a useful and cost effective tool to predict lower energy impact events for marine industry applications.

Liang et al. performed quasi-static punch shear testing on satin weave carbon/epoxy laminates in order to provide a better understanding of the damaging events via using visual techniques such as X-ray computed tomography (X-CT) scanning and optical microscopy (Liang et al. 2015). They also produced numerical models via ABAQUS software to support the damage visualisation because of the lack of damage identification of X-CT scanning. Many different failure modes were captured by the optical microscopy such as inter-laminar crack, intra-laminar crack, fibre breakage, and fibre-matrix de-bonding for different displacement points. The failure mode sequence in the perforation process of the plates was observed as; matrix cracks (reason: high transverse stress), intra and inter laminar cracks (reason: crack propagation), delamination (reason: inter-laminar cracks), fibre-matrix de-bonding (reason: loss of support) and finally shear plug. The numerical model underestimated the load-displacement curve, reasoning the parameter that controls the stiffness degradation. The comparison of the X-CT scanning and the numerical model showed that the numerical model provided more detail on specific type of failure, while X-CT showed a combination of damage types.

Bulut and co-workers conducted quasi-static punch shear loading in order to investigate the hybridization effects (Figure 45) resulted in by combining different layers of woven Kevlar, S-glass, and carbon fibres (Bulut et al. 2016). Authors used double as well as triple combination of fibres and obtained energy absorption and penetration resistance forces of each material type to conclude whether the hybridization effect was positive or negative. Combination of carbon-Kevlar-carbon fibre layers resulted in best performance, while carbon-glass-carbon fibre layers sample had the lowest performance (Figure 46). It was also observed that the variation caused by the stacking sequence effects were greater in double fibre configurations than triple fibre configurations, and it was attributed to the presence of third fibre balancing the others.

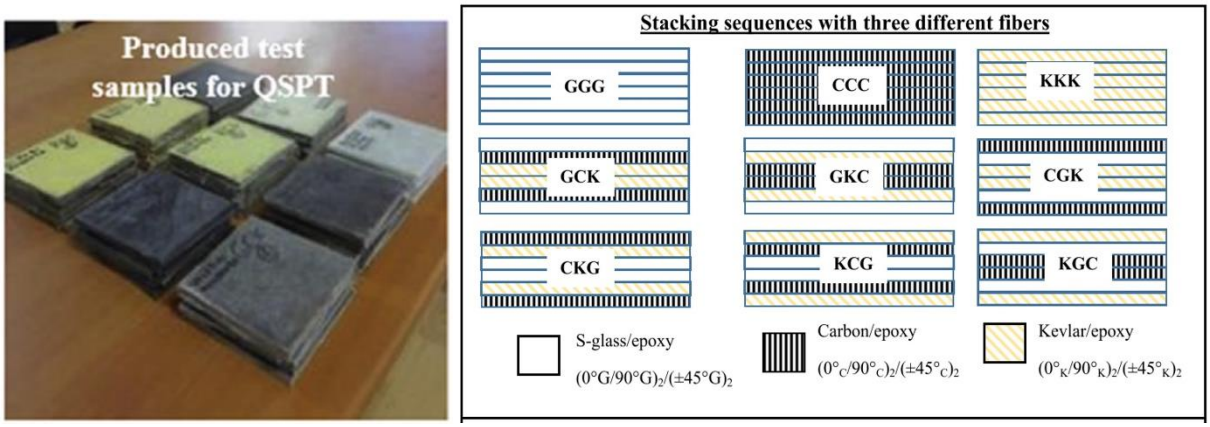

Figure 45 Hybrid laminates manufactured from woven Kevlar, S-glass, and carbon fibres (Bulut et al. 2016)

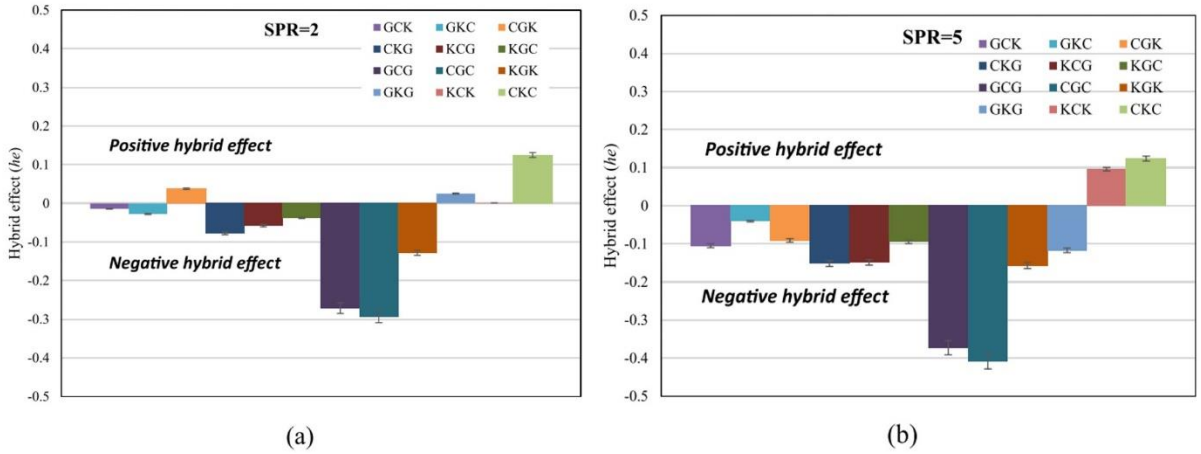

Figure 46 Hybridization effect in tested laminates (Bulut et al. 2016)

Manzella and co-workers studied the effect of specimen thickness and punch dimension on the confined transverse compression behaviour of S2 glass fibre/SC15 epoxy composite laminates (Manzella et al. 2011). They investigated a ratio range for (D_p/ H_c):0.48-5.00 (punch diameter (D_p) to specimen thickness (H_c)) by testing 29 different combinations. It was reported from the test results that fracture angle and applied stress at failure are the invariants for all of the considered cases. Upon observing contradictive finite element results, the authors compared 6 failure criteria namely; maximum stress, Tsai-Wu, Tsai-Hill, hydrostatic crush, deviatoric stress, and finally Mohr-Coulomb criterion, to reveal the internal stress distribution during loading. Among these criteria, Mohr-Coulomb criterion provided the most accurate description for compression-shear interaction.

2.4.2 Findings

Clearly, the available research in this field is not limited. However, what has been reported highlights the important aspects, the current understanding, and the state-of-the-art research of impact on laminated composites that is relevant to the current research. Examples of such aspects were presented with a wide range of parameters including: fibre type and architecture, laminate thickness, effect of fracture mechanics and toughness, fibre-matrix interface, inter-laminar properties, failure modes, damage propagation, strain rate effects, boundary conditions, projectile mass and properties, impact velocities, analytical and numerical modelling, and failure inspection.

One of the most common finding was the effect of laminate thickness. It was apparent that the thicker the laminate, the better the performance against impact loading in terms of the amount of absorbed energy and the penetration resistance force. Therefore, thickness of the laminates should be maximised to resist higher loads and absorb more energy. The effect of thickness, however, influences the failure mode responsible for the loss of load bearing capability. In general, the dominant mode of failure (as well as for the energy absorption behaviour) appears as the tensile failure in fibre direction for thin specimens, whereas dominant out-of-plane (OOP) shear and delamination failure distinguishes the thicker laminate targets.

It was seen that the reinforcement type has significant effect on the impact performance of laminates. Both CFRPs and GFRPs are adequate against impact loading. Depending on the fibre and matrix combination it is possible to tailor the damage containment and residual properties. It was reported by many that FRPs with higher strain/strain energy to failure should be preferred in order to have a better impact resistance performance, which explains why glass fibres can be preferred over CFRPs. In terms of fibre architecture and laminate configuration, purely unidirectional reinforced laminates are inferior compared to the multiaxial or fabric reinforcements, and should be avoided against impact loading. Woven fabric laminates create adequate structural properties against impact loading compared to multi-axial and unidirectional counterparts. It was reported that, a 90° change between neighbouring layers causes mismatch in bending stiffness, leading to an increased interface failure. Therefore, in case of the use of multi-axial reinforcements, the lay-up orientation of multilayers should be made in a gradual fashion instead of a dramatic fashion. Although this is not the case for woven fabrics since the warp and weft fibres interlace each other.

The fibre-matrix interface and interlaminar interface allow a compromise between failure containment and penetration resistance, considering the needs of the application. If no-penetration is desired and residual properties are not important, then the interphase region should be weaker to encourage failure through gross splitting and delamination. If damage containment is required, then the interphase should be strong so that the matrix cracks and delamination can be arrested.

It was observed from the review of previous QSPT practices that the fixtures and test setups didn't have a common particular specification, some researchers used the same configuration but not the others. This shows that the technique is not standardised. Nonetheless, it was evident that the method provides valuable information on the penetration behaviour of composite targets. Strong correlation was observed by many in terms of failure modes and sequence between QSPT and high-velocity impact. It was demonstrated by some that it was possible to predict a structures' energy absorption capability by QSPT without performing dynamic testing. Therefore, all of the studies reviewed here supports the hypothesis that a simpler and cost effective prediction method would be greatly beneficial.

Significant progress has been made in numerical modelling of composite targets against impact loading. FRPs are especially notorious for the challenge and complexity in their numerical material modelling. However, with the rigorous efforts of many researchers, this challenge has mostly been overcome to date. Various proposed material models have shown the very accurate results obtained with respect to experiments in terms of ballistic performance, failure modelling, and damage progression both for fibre and matrix based micromechanics.

2.5 Literature review: Impact loading response of sandwich composites

Mines et al. conducted static and low-velocity perforation experiments with sandwich panels for offshore applications (Mines et al. 1998). Two different sandwich configurations were tested: glass fibre/vinyl ester resin skins combined with Coremat core, and glass fibre/epoxy resin skins combined with honeycomb core. The panel dimensions were 500 mm wide, 10 mm thick for Coremat core, 13 and 26 mm for honeycomb core. Figure 47 illustrates that in static penetration experiments the failure sequence differs with respect to core material. In Coremat sandwich panel lower skin failure preceded the top skin failure, while it was the reverse in honeycomb core sandwich panels – which was explained by the influence of the core density. The authors presented simple perforation equations to investigate the influence of material type and structural behaviour. It was found that sandwich panels can absorb more energy with

respect to increasing impact energy. The work also provided recommendations on how to increase the energy absorption performances of such structures by, for example, skin material should be strong in tension and bending whereas the core material should be able to exhibit a progressive crushing behaviour.

Reid and Wen studied the penetration and perforation of foam core sandwich composite materials and made a comparison between ballistic impact tests and quasi-static penetration (Figure 48) (Reid, Wen, et al. 2000). They developed an analytical model which incorporates the high velocity impact intrinsic event of composites. This event namely wave-dominated perforation was researched by using flat, hemispherical and conical nosed projectiles. They observed in quasi-static testing that energy absorbed up to failure of bottom skin and peak load was highly influenced by the thickness of skins, and the core material was responsible for the failure behaviour.

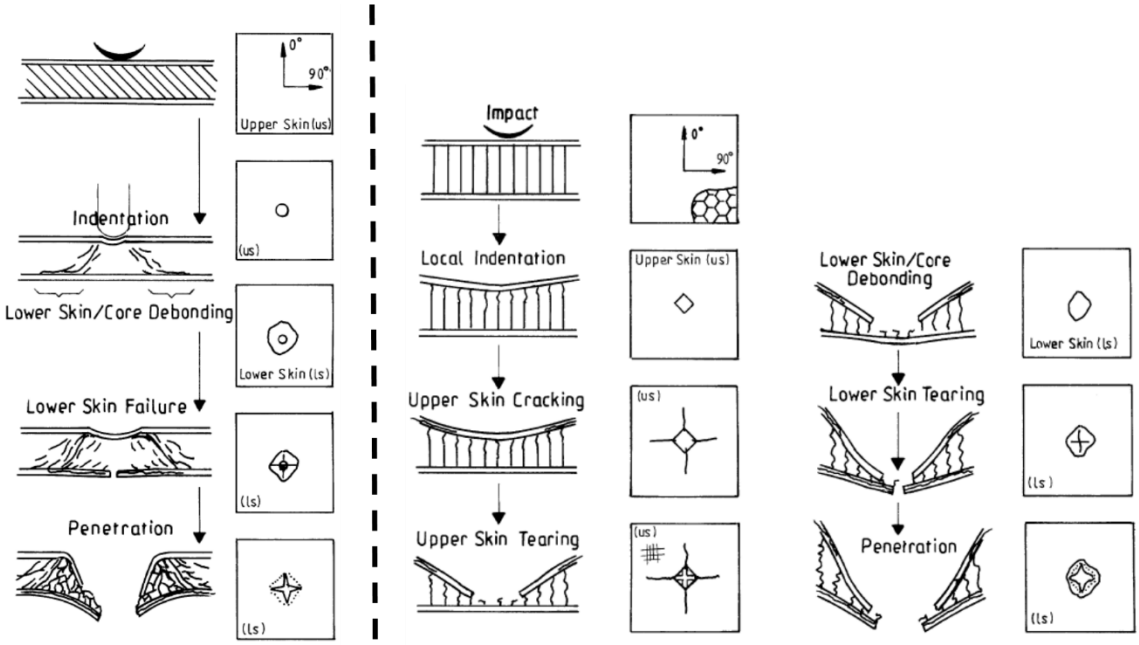

Figure 47 Failure modes and sequences differ with respect to core material in static penetration (Mines et al. 1998)

For ballistic test analysis they concluded that ballistic limit increases with increased laminate thickness while the effect of core was insignificant. For wave-dominated perforation, theoretical model was in good agreement with both the experimental data and with previous data from other researchers such as (Guoqi et al. 1992; Mines et al. 1999).

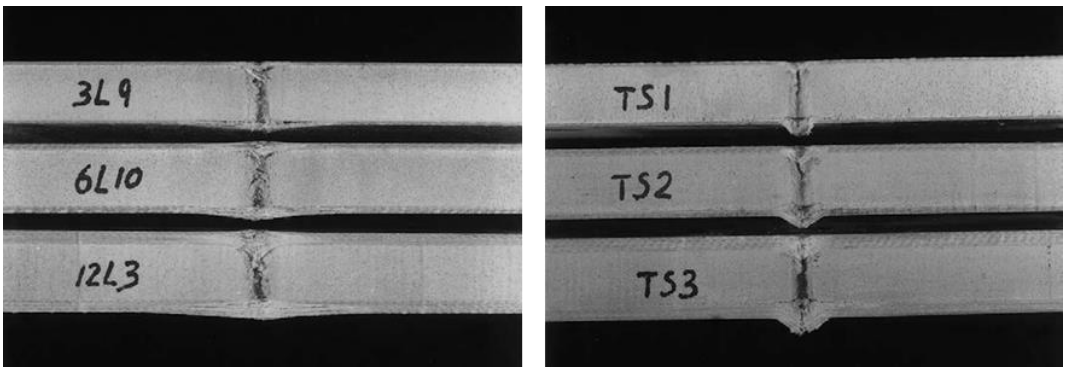

Figure 48 Section of damage extend of sandwich samples deformed by hemispherical ended projectile: (left) ballistic loading, (right) quasi-static loading (Reid, Wen, et al. 2000)

Hoo Fatt and Sirivolu approached high velocity impact behaviour of sandwich panels with an analytical model that doesn't take into account delamination and de-bonding .They considered simply the change in load resistance (Hoo Fatt & Sirivolu 2010). The authors divided the high velocity impact into two phases, i.e. phase 1-through thickness wave propagation, and Phase 2-local core crushing and back facesheet deformation; each subdivided in itself and representing the damage sequence. They compared the analytical model with FE simulation of impacted composite plate in terms of transient deflection, and also with the results from a previous research in terms of projectile residual velocity (Figure 49).

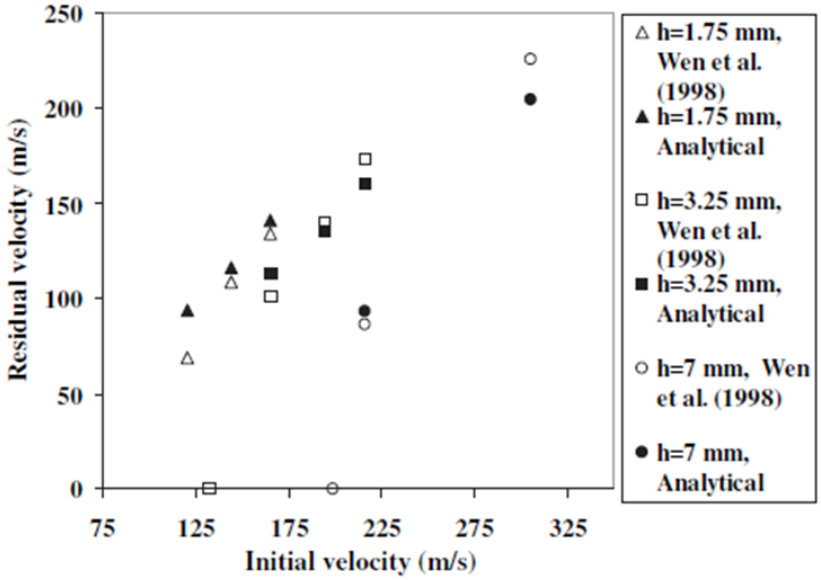

Figure 49 Comparison of analytical model and experimental tests for residual velocities of the projectiles (Hoo Fatt & Sirivolu 2010)

In conclusion, they reported that the generated model agreed well with finite element analysis up to core densification stage, and stated that the disagreement arose because of the FE

formulation provided by the core material model, and they added that further improvements can be made with much better mesh refinements although it requires excessive amounts of computation.

In another analytical study of high velocity impact behaviour of composite sandwich structures impacted by cylindrical projectile, Feli and Namdari Pour investigated the aluminium honeycomb core sandwich panels (Feli & Namdari Pour 2012). They considered the complete penetration event in three phases, which were the skin penetration, core perforation and back face penetration. After generating the analytical model, they compared their results with the available experimental and numerical data in the literature. Even though their model considered fewer number failure criteria compared to others, they achieved good agreement with both experimental and FEA data in terms of predicted residual velocities. However, the projectile geometries were different between the compared studies, and the mode of deformations were different up to ballistic levels. Above this level, both projectiles affected similarly. In addition, effects of skin materials, front/back facesheets, and aluminium honeycomb core were investigated and it has been found out that the main energy absorption was provided by the facesheets.

Aktay and co-workers validated their numerical models with high-velocity impact tests on sandwich panels made of aramid honeycomb and polyetherimide foam core combined with carbon fibre facesheets (Aktay et al. 2005). The impact tests were performed by using concrete projectile to represent runway debris impact against aircrafts. 60 m/s impact velocity resulted in partial penetration of the sandwich panels, i.e. the top skin was fully penetrated and the projectile was caught by the core material. Orthotropic elasticity model was implemented to simulate the unidirectional carbon fibre response, while crushable foam and non-linear bi-phase solid material model was used for foam and honeycomb core, respectively. It was concluded that current model was able to predict the impact response, and reasonable correlation was obtained in terms of penetration resistance, energy dissipation, and damage development. However, it was stated that further refinement of the model as well as different modelling approaches were required to get more accurate representation of impact events.

Buitrago et al. investigated the high velocity impact behaviour of carbon-epoxy/honeycomb sandwich composite with experiments and FE simulations using ABAQUS (Brenda L. Buitrago et al. 2010). The authors carried out experimental tests on 25 samples by using a gas gun in a velocity range of 92 m/s to 548 m/s. Comparing the numerical model with the experiments in terms of ballistic limit, residual velocity and contact time, they obtained %2 difference for

ballistic limit comparison, and reported very good agreement for contact time and residual velocity. They also stated the dominant energy absorbing damage mechanisms as fibre breakage in face skins and plastic deformation in honeycomb core.

Ballistic performance of E-glass/polyester skin and PVC foam core sandwich composites was numerically investigated by Ivanez and co-workers (Ivañez et al. 2011). Simulations were carried out in 400-800 m/s velocity range. Validating their numerical model with the experimental results generated by Buitrago et al. (B. L. Buitrago et al. 2010), the authors analysed the contribution of the core material by simulating the ballistic impacts with the spaced laminates (no foam core in between facesheets). The results showed that the absence of foam core resulted in slight decrease (4.2%) of the ballistic limit, but significant change (36%) of the residual velocities of the projectile. It was found that at higher impact velocities, the contribution of foam core to the energy absorption was negligible. In addition, the presence of the foam core reduced the damage area of top skins, and increased the damage area of the bottom skin. The authors contributed this difference to the evolution of the projectile velocity, while Buitrago et al. suggested that the stress wave propagation difference between foam and air can influence the damage.

Balsa core with carbon fibre reinforced facesheets was investigated in ballistic experiments by Jover (Jover et al. 2014). In contrast to most of other research on sandwich structures loaded by high velocity projectile, the authors carried out multiple steel spherical ball firings on each plate, 19 in total, and supported the visual inspection of damage extend with non-destructive testing (NDT) such as tap testing (Figure 50 left). One of the benefits of this NDT method reported by the authors was that overlapping damage areas could be identified. After performing the tests, it was observed that subsequent impacts didn’t make the first damage propagate further, and the structure maintained its integrity in every impact point. Damaged areas reported to increase with the increasing absorbed energy, as expected. The samples that were impacted three times has shown larger damage compared to the previous impacts. In conclusion, the relevant samples were found to be safe to use in a protective environment. The tap testing method has been found as a useful tool for damage assessment, however it required highly skilled operator and was prone to human error.

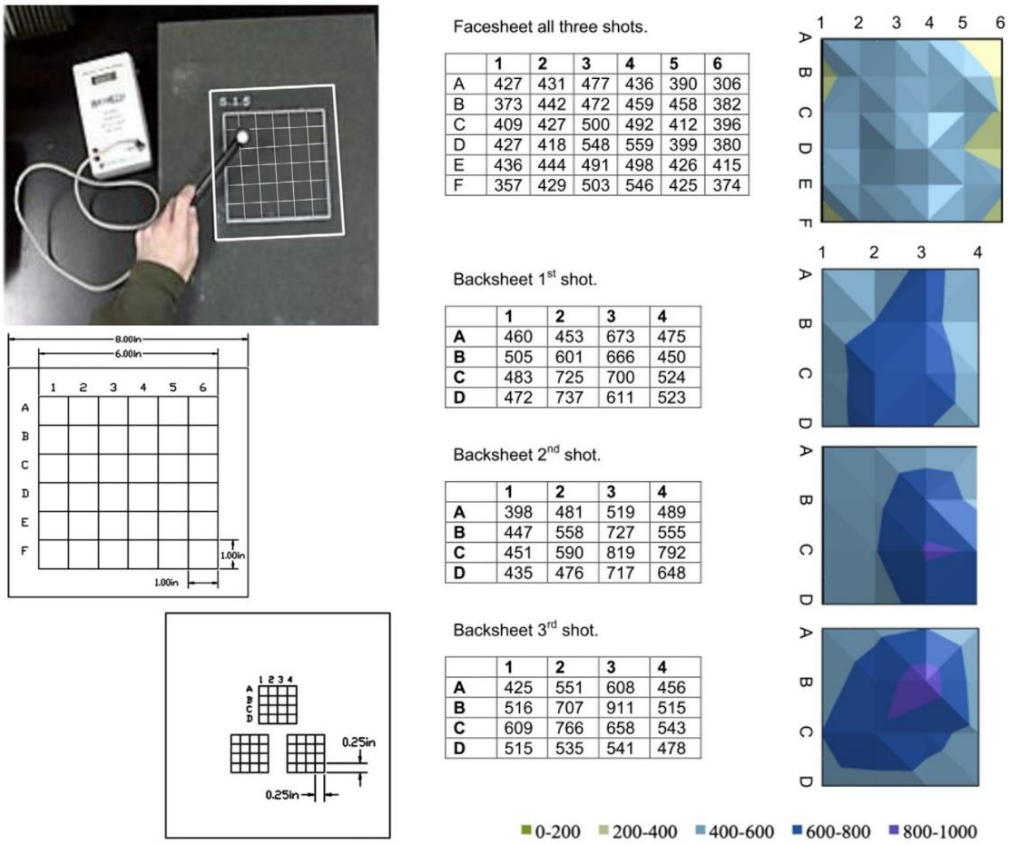

	1	2	3	4	5	6
A	427	431	477	436	390	306
B	373	442	472	459	458	382
C	409	427	500	492	412	396
D	427	418	548	559	399	380
E	436	444	491	498	426	415
F	357	429	503	546	425	374

	1	2	3	4
A	460	453	673	475
B	505	601	666	450
C	483	725	700	524
D	472	737	611	523

	1	2	3	4
A	398	481	519	489
B	447	558	727	555
C	451	590	819	792
D	435	476	717	648

	1	2	3	4
A	425	551	608	456
B	516	707	911	515
C	609	766	658	543
D	515	535	541	478

Figure 50 Tap testing (NDT): device and grid used (left) and obtained imaging results from impacted sandwich structures (right) (Jover et al. 2014)

Hassan and Cantwell investigated the relationship between perforation resistance and the Mode II work of fracture for nine different foam materials (Hassan & Cantwell 2012). To identify the failure modes in the impact event, the authors carried out compression and shear tests to characterize the foam materials with varying density and material. They stated that the work of shear dominant mode of fracture (Mode II) was greater compared to Mode I fracture in perforation and energy absorption of sandwich panels. With a testing programme that considers different boundary conditions, they built up a connection between overall absorbed energy to fail the sandwich structure completely and the work of Mode II fracture (Figure 51), which can be used as a simple benchmarking of the penetration behaviour of foam cored sandwich structures.

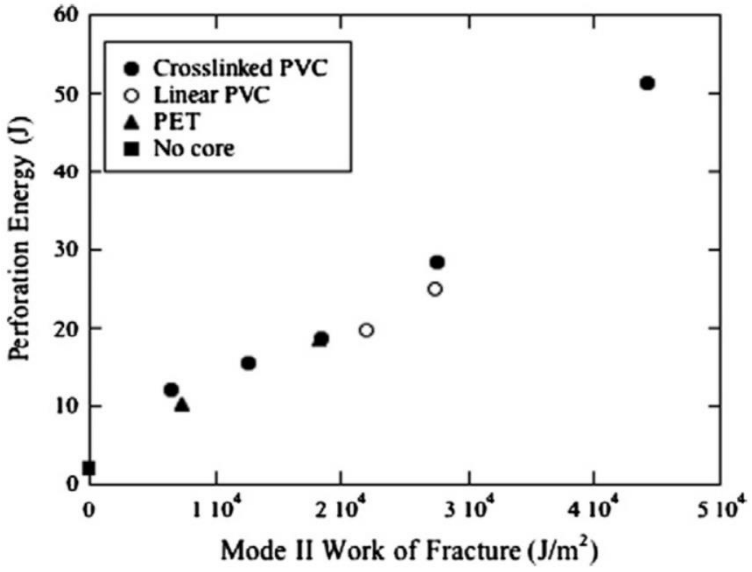

Figure 51 Relationship between Mode-II work of fracture and energy absorption by the sandwich showing performance increases with increasing foam density (Hassan & Cantwell 2012)

Six different foam densities (37 to 240 kg/m^3) in glass fibre sandwich composites were investigated under high-velocity impact conditions by Nasirzadeh and Sabet (Nasirzadeh & Sabet 2014). Experiments were carried out with a 10.7g hemispherical ended projectile in velocity range of 100-150m/s. In contradiction to the findings of (Hassan & Cantwell 2012), their ballistic tests results showed that 49 kg/m^3 foam core outperformed the others in terms of ballistic limit velocity and energy absorption. The reason for this was attributed to the yawing of the projectile in 49 kg/m^3 foam core, resulting in the projectile impacting the reverse face with its side rather than its tip, which in turn leading to an extended area of damage at the reverse side of the sandwich (Figure 52). Absence of yawing in higher density cores were also attributed to the foam morphology, of which the Scanning Electron Microscopy (SEM) analysis showed that foam morphology, i.e. cell wall thickness and strut, plays a vital role in energy absorption. Although this connection seems possible, no information was given about the number of repetition for each test configuration. Therefore, more tests could reveal if that was the case. In addition, it was reported that as the density increases, the foam becomes more brittle and exhibited total foam collapse, leading to lower energy absorption.

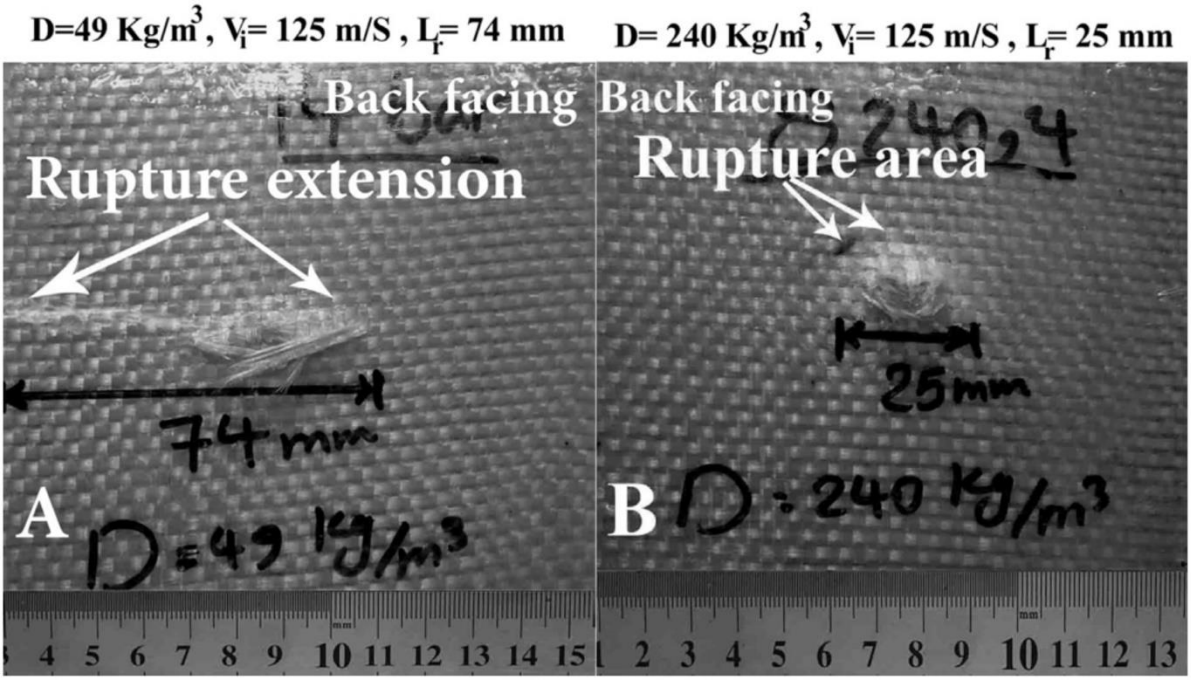

Figure 52 Extended damage at the reverse side of the sandwich caused by the yawing of the projectile (A), normal impact to the reverse side (B) (Nasirzadeh & Sabet 2014)

Rizov and co-workers studied numerical modelling of foam core indentation (Rizov et al. 2005). Rohacell WF51 PMI (polymethacrylimide) foam core combined with glass fibre laminates was tested with spherical indentation setup. To mimic the plastic deformation behaviour of the foam at the indentation point, they used crushable foam material model to match the experimental data and achieved good correlation in terms of load-unload and load-damage zone relationship.

Gama and Garbys investigated the ballistic penetration performance of glass fibre/honeycomb core sandwich structures (Gama & Gabrys 2007). Using previously validated finite element model, the effect of boundary conditions and energy absorption properties were presented, and it was concluded that ballistic limit velocity of the sandwich panels increases as the constraining boundary increases. It has also been found out that the addition of honeycomb core in between the laminated skins increases the penetration resistance of thick laminates by changing the energy absorption failure modes.

Flores-Johnson and Li experimentally investigated the indentation behaviour of carbon fibre facesheet polymer foam sandwich materials with various indenter nose shapes (Flores-Johnson & Li 2011). Sandwich materials were manufactured by combining woven fabric carbon fibre face sheets and PMI (polymethacrylimide) foam cores with different densities. The nose shapes

considered in their study were conical, truncated (2 type), flat, and hemispherical (3 type). The flat indenter resulted in highest penetration resistance as opposed to the authors' previous research (Flores-Johnson & Li 2010) in which the lowest indentation resistance into foams was achieved by the flat indenter. Quasi-static perforation tests were carried out with two different boundary conditions; namely solid support and framed support (constraining the two edges of the panels). The authors identified varying failure mechanisms (Figure 53) during loading of the sandwiches. The effect of support conditions revealed that bending response achieved by framed support decreases the indentation resistance. Therefore, it was concluded that sandwich panels may be more fragile if they are not properly constrained in service. It was observed that energy absorption doesn't have a linear increase or decrease with respect to the density, it was rather a wave-like characteristic in the considered density range (Figure 54). In addition, the higher the density, the stiffer the panels, therefore the damaged area decreases with respect to density increase.

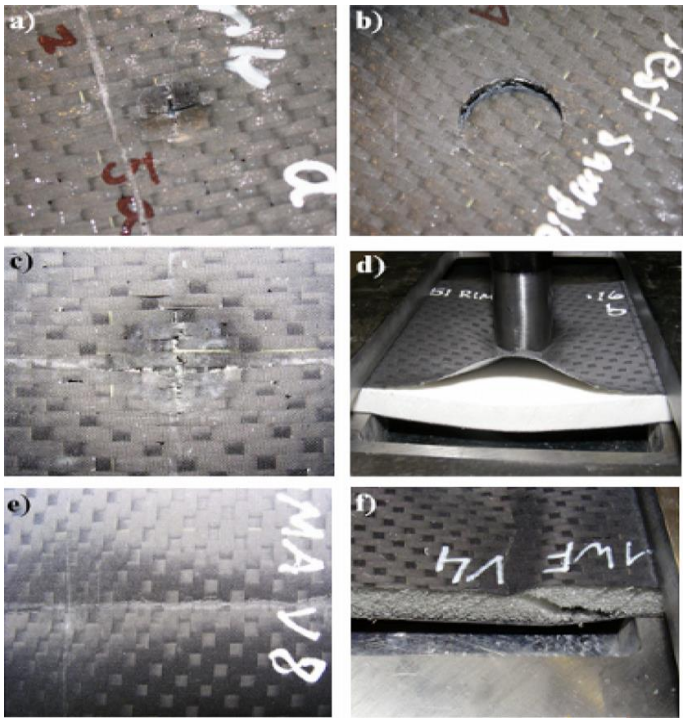

Figure 53 Failure modes observed during indentation: failure of face: (a) cruciform shape; (b) shear plugging; (c) cruciform shape with fracture of fibres; (d) skin/core de-bonding, (e) fracture of the face, (f) core shear (Flores-Johnson & Li 2011)

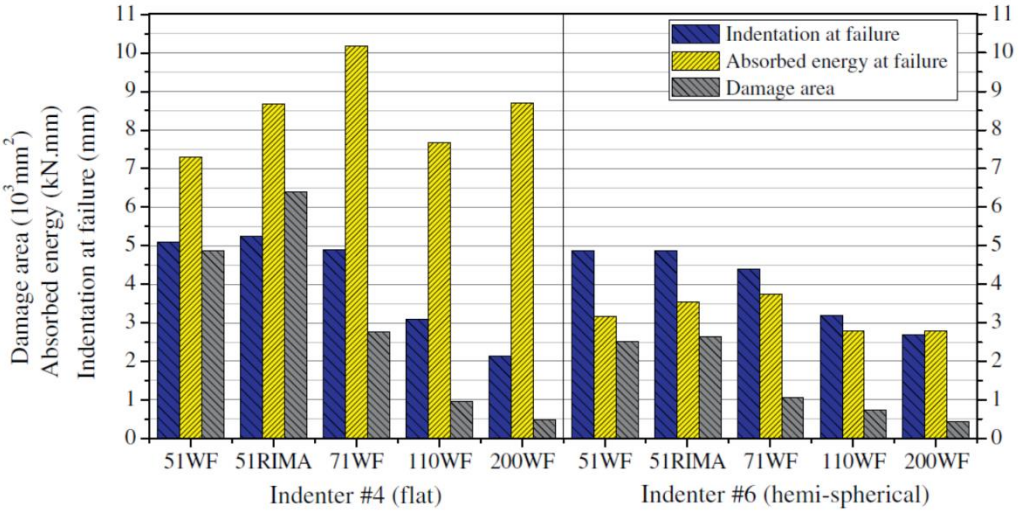

Figure 54 Effect of density on energy absorption, damaged area, and indentation at failure (Flores-Johnson & Li 2011)

In this study, the effect of strain rate was considered for the composite laminates but not for the foam core. The main reason for ignoring this effect for the foam core was the previous research which showed that a mild effect was observed in most cases unless the strain rate exceeds 100 s^{-1}. Strain rate effect on mechanical properties becomes more significant for high density foams, while the changes were negligible for low to mid densities. In addition, the resistance of foam cores to the penetration of the sandwich plates were insignificant as previous studies shown.

Effect of strain rate and temperature on the compression behaviour of polymethacrylimide (PMI) foam was studied by Arezoo et al. (Arezoo et al. 2013). Four relative densities (ratio of measured density to parent polymer density (1416 kg/m^3 for this specific PMI)) were considered of which the compression tests were carried out in 10^{-3} – 5000 s^{-1} strain rate range and 203-473 K temperature range. Among four densities, three of them showed mild response to increasing strain rate (Figure 55) while the effect was more distinct for the highest density foam (D). It was reported that progressive embrittlement was the cause for the enhanced collapse properties. Mild strain effect on the compressive properties of the foam cores were almost negligible (+ 0.1-0.5 MPa levels). On the other hand, foams were found more sensitive to temperature change where the behaviour tend to change from rubbery type to elastic-brittle with respect to decreasing temperature.

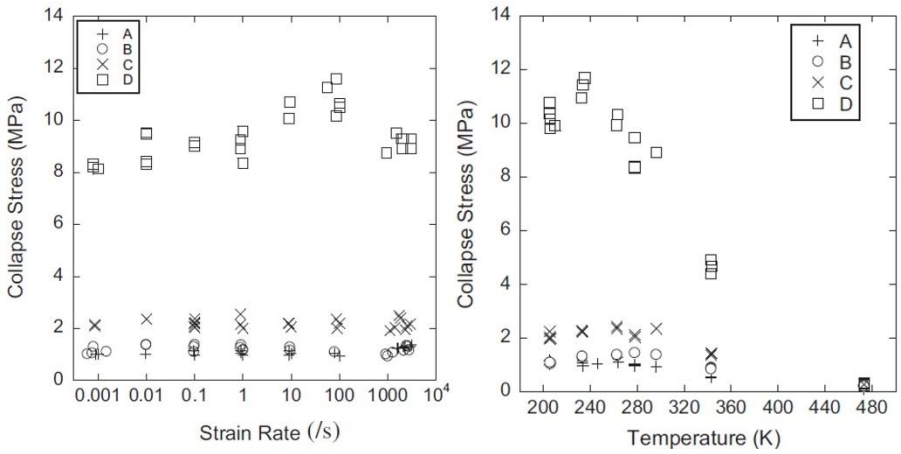

Figure 55 Effect of strain rate (left) and temperature (right) on compressive behaviour of foam (Arezoo et al. 2013)

2.5.1 Findings

The literature review has shown that impact response of sandwich composites has been increasingly studied in the past years. The majority of the research has been focusing on low-velocity impact behaviour, while the high velocity impact behaviour found lesser attention. Regarding the sandwich composite response under high velocity impact loading, following conclusions can be drawn:

- Given the same loading conditions, failure modes and sequences can be different from one sandwich configuration to another.
- The thickness of the facesheets greatly influences the performance of a sandwich composite against impact loading. However, the effect of thickness of the core material to the ballistic limit of the structure is negligible.
- There is no clear linear trend in energy absorption for varying densities of a given foam core material. The performance of the core material is influenced by the morphology of the foam cells and struts.
- Progressive crush behaviour of the core material is an important parameter for maximising the energy absorption under impact loading.
- Crushable foam material model was used by many and was found as a suitable material model for foam core simulation, even though some limitations exist from one model to another such as physical representation of the damage.

- A common finding from the literature review suggests that facesheet laminate properties and thickness should be maximised for a superior impact loading resistance and energy absorption.

2.6 Conclusions

Chapter 2 reported the examples of main load bearing composite material applications in railway vehicles together with the current state-of-the-art research on impact behaviour of composites. Regarding these applications, the timing of the past research (in the last 10 to 15 years) suggests that the interest in this field is relatively recent and the amount of available research was limited. Furthermore, the railway specific requirements of impact loading were missing. However, it has been seen that the interest in composites in railways is growing rapidly. Considering no standards have been established yet in the railway industry for composites, clearly there is a need for more research in many relevant areas. It is believe that the outcome of this thesis would benefit the assessment procedures required for the object impact resistance of composite rail carbodies which will be explained in Chapter 3.

Lightweight FRPs and sandwich composites are known to be susceptible to impact loading which can compromise the structural integrity. The literature review has shown extensive amount of research in this field which covers a very diverse range of parameters and material configurations. Collectively, these studies highlight the effectiveness of these structures despite their sensitive nature. Even though the subject was deeply and well understood, the evidence presented in this chapter suggests that every application case should be investigated individually, because of the fact that the response of the composites against impact loading is a combination of material and projectile parameters.

The important theme emerged from the reviewed studies is the use of quasi-static punch testing (QSPT) procedures as a prediction method. Many researchers proved the benefit of their own static methods to investigate the impact resistance, energy absorption, and damage propagation. However, it is important to note that these QSPT methods did not follow a standardised procedure, which does not allow an effective comparison between studies. This method has the potential to be a worthy and practical approach as long as it is verified through observation and analytical/numerical modelling.

Chapter 3. Impact risks to the rail vehicle carbodies

This chapter identifies the main types of object impact against rail vehicles during their service life. The various existing railway standards are introduced and their relevance to the present study is discussed.

3.1 Analysis of relevant railway vehicle standards and requirements

In terms of vehicle categories identified by EN12663, the focus of this thesis will be on coaches (P1) and fixed units (P2) that are operated on intercity mainline and high-speed lines (Figure 56).

Figure 56 A Siemens EMU (electric multiple unit) fixed unit (P2) with coaches (P1)

In the vicinity of a mainline rail track there are different types of objects with varying mass and material, as well as different types of threats (Figure 57). For example, in "Rail High Speed Network Security Handbook", a published report by UIC, stone throwing is identified as an act of vandalism against railway system and it is a rail safety threat (UIC 2016). This threat obviously influenced some of the requirements written into rail vehicle standards (Ingleton 2005), as can be seen in Table 2, which shows the various standards in Europe and UK for different cases of object impact requirements.

In addition, based on the information obtained from REFRESCO deliverable WP7 - D7.2 below (REFRESCO WP7-D7.2 2016), it is safe to say that it is challenging to cover all the possible object strike scenarios:

- *"It exists many various national standards which regulate different aspects of damage scenarios; it is to recommend a harmonisation of these.*
- *The damages that occur are very different, the classification of the severity and frequency is very difficult.*
- *It would be good if a database of damages exists in order to have the capability of evaluation through statistical analyses. For future use, it is recommended to develop such a database."*

Given the variety of striking objects, the consequences will vary accordingly. Therefore, a parameter (or parameters) has to be identified which classifies different impact cases. This will answer one of the research questions that was proposed in Section 1.2. Notice that some of the standards in Table 2 are requirements for windscreens or body side windows. The reason to include those in the table is the fact that the complete carbody shells can be built using composite materials. In this case, the impact requirements for windscreens or body side windows apply for the composite shell structures as well.

Figure 57 Different object strikes to carbodies: Bird strike on HSTs (top), stone throwing against mainline train (bottom)

Clearly, in addition to the vehicle body shell, other adjacent parts such as underframe structure and the running gear (bogie) are affected from object strikes as well. These vehicle parts can also be manufactured fully/partially from composite materials to decrease the weight of the whole vehicle and these were demonstrated by many in the literature. However, the main concern of this study involves with the passenger and driver safety. Therefore, vehicle parts surrounding the people inside were considered only.

Although European standard EN12663 describes the expected structural performance from a railway vehicle carbody in service, there is insufficient information provided in this standard regarding flying object strike against rail carbodies. Therefore, other available standards in the same area were provided in the following sections. In Great Britain, Railway Group Standard GM/RT2100 (Section 3.3.3) describes missile protection requirements as:

a) *Forward facing surfaces of vehicles occupied by people shall have an equivalent impact resistance to that required for the vehicle cab windscreens.*

b) *Roofs over areas which are freely accessible to passengers, personnel or train crew during normal service shall withstand, without penetration, the impact of a 100 kg concrete cube with an edge length of 0.36 m dropped from a height of 3.0 m above the roof. The cube shall be dropped so that a flat surface hits the roof* (GM/RT2100 – Issue 5, (RSSB 2012)).

Standard	***Definition***	***Impactor mass***	***Impactor velocity***	***Specifications***
GM/RT2100	Missile protection	1000 g	V_{max} + 160 km/h	94 mm diameter Hemispherical tip
GM/RT2100	Roof structure resistance	100 kg	Equivalent of 3m drop height	Cubic concrete with 0.36m edge length
GM/RT2100	Body side window impact (laminated)	250 g	100 km/h	Solid steel ball
GM/RT2100	Body side window impact (toughened)	250 g	50 km/h	Solid steel ball
GM/RT2100	Body side window impact - containment	5000 g	34 km/h	Solid steel ball
EN 15152	Gravelling impact	20 g	V_{max} + 20 km/h	Conical tip with 90° cone angle
NF-F07-101	Ballast impact	60 g	$V_{Imp} < 1.1\ V_T$	Conical tip with 105° cone angle

NF-F15-818	Windscreen requirement	4000 g	V_{max} + 160 km/h	120 mm diameter Cylindro-pyramidal projectile
UIC	Windscreen requirement	1000 g	V_{max} + 160 km/h	94 mm diameter Hemispherical tip

V_{max}: Maximum vehicle operating speed, V_T: train speed, V_{Imp}: impact speed

Table 2 Different railway standards for object strike against rolling stock

Requirement a) leads to the EN15152 standard which has two different impact requirement: gravelling impact (small object), and impact from a large projectile (missile protection, as specified in Table 2). Within the scope of this thesis gravelling impact resistance will be analysed with respect to proposed method, since missile protection and requirement b) is not suitable for the testing equipment and can cause the structure to exhibit global response rather than local.

GM/RT2100 also defines the requirements for bodyside windows for two different types of windows. From Table 2, impact for laminated window will be analysed in this thesis because the impact velocity is higher compared to the toughened version, thus there is no necessity for the slower impact. Containment requirement is out of scope since it is a low-velocity impact case and it requires a sequence of loadings in addition to the one described in Table 2.

French standard NF-F07-101 is a specifically defined standard for ballast strike resistance and classifies the impact into 11 categories (K1 to K11) depending on the energy levels. Another French standard NF-F15-818 describes the protection requirements of frontal windscreens of conventional trains and HSTs, and was designed considering the stone drops from bridges. NF-F07-101 ballast strike standard will be analysed in this thesis. NF-F15-818 windscreen standard will not be considered because its specifications are similar to missile protection.

In his doctoral thesis on the design of a composite cab for structural applications, Ingleton highlighted the importance of object strikes and stated (Ingleton 2005):

"*Impact resistance is an important aspect of the cab design as this provides protection to the driver from projectile such as track ballast 'whipped up' by the slip steam of passing trains and more seriously stones and bricks deliberately thrown at trains by vandals."*

The author reported previously conducted tests for missile protection requirement from various national rail vehicle/operators (Table 3). Very few of these examples provide a detailed outcome of the tests. The reported failure modes were localised facesheet damage or partial

penetration. But in all cases the composite configurations were found to have sufficient resistance. In addition, the author reported that around 87% of the damaging missile strikes against windscreens and drivers in UK during the years 1996/97 are based on vandalism acts of humans, and this type of attack has increased in later years (Ingleton 2005).

Rolling stock	Structural part	Material Configuration	Impactor mass	Impact velocity	Reference
Locomotive 2000 for Swiss Federal Railways	Front cab	E-glass fibre/polyester resin skins bonded to PVC core. Additional GFRP laminate in the middle of the core	1 kg	280 km/h (77 m/s)	(Cortesi et al. 1991)
C20 Stockholm metro car	Front facing surface	Knitted multiaxial glass fibre/polyester resin laminates combined with balsa wood core	1 kg	130 km/h (36 m/s)	(Werne 1997)
Intercity 125 HST	Front cab	GFRP/polyurethane foam core sandwich panels. The laminate facesheets were manufactured from unidirectional fibre layers oriented in [0°/90°] angles and supported by chopped strand mat (CSM) layers.	0.9 kg	400 km/h (111 m/s)	(Morton-Jones & Ellis 1986)
ETR 460 HST for Italian Railways	Front cab	Foam core sandwich structure	n/a	n/a	(Sistema Compositi 2016)
Gardermoen HST Airport Shuttle	Front cab	Stitched glass fibre fabric/phenolic resin laminates and polyetherimide (PEI) foam core	0.9 kg	400 km/h (111 m/s)	(Brevik 1997)
Italian Locomotive E464	Front facing surface	Sandwich composite - no other details available	1 kg	360 km/h (100 m/s)	(Marchetti et al. 1999)

Table 3 Previous applications of missile protection requirement for composite structures (Ingleton 2005)

3.2 Flying ballast phenomenon

The desire and ambition to become a more effective transportation mode and compete with other transportation modes naturally forces the industry to find solutions to improve the performance of the mode. One of these improvements is to decrease the travelling times which can be attainable by increasing the operation speed of the vehicles. As a result of this ambition the railway industry witnessed the introduction and development of high-speed rail (HSR) lines in the past decades. Although this evolution provided great improvements to the system, it involuntarily brought its own drawbacks. One of these drawbacks is called 'flying ballast phenomenon', which occurs due to the displacement of ballast particles on the track by various forces. As a consequence, airborne ballast particles can contact and damage rolling stock and infrastructure during service. Throughout the thesis, the term "flying ballast strike" is more appropriate instead of the "flying ballast phenomenon". The rationale is that the research presented here is addressing merely one of its consequences, rather than the phenomenon itself, which covers various conditions leading to the displacement of particles in time and space.

The literature review on this subject revealed that the majority of the previous research has been dealing with the causes of the displacement of the particles (ballast flight): 'under which circumstances are the particles displaced?', 'which mechanisms are relevant?', 'what are the risk factors?', 'what are the critical parameters and their values?', 'how can it be mitigated?' However, the question 'what is the aftermath?' still remains substantially unanswered as the literary review holds scarce amount of research (Sakly et al. 2016; Onder et al. 2016). The following section will detail only the relevant studies with this thesis (particle velocity, mass, shape), although the author is aware of the context of the rest of the research which can be generally classified as:

- Train aerodynamics (Ido et al. 2008; Quinn & Hayward 2008)
- Track response (Saat et al. 2015; Jing et al. 2012)
- Ground effects (Saat et al. 2015)
- Atmospheric conditions (Saat et al. 2015)
- Field tests (Quinn et al. 2010; Lazaro et al. 2011)
- Risk analysis studies (Saussine et al. 2011; Bedini-Jacobini et al. 2013)

In an earlier research Luo and co-workers reported that ballast particles can be accelerated to 10 m/s^2 under train velocities of 270 km/h and above (Figure 58) (Luo et al. 1996). This means

that ballast particles can overcome gravity with the minimal force inputs from other sources such as vibration.

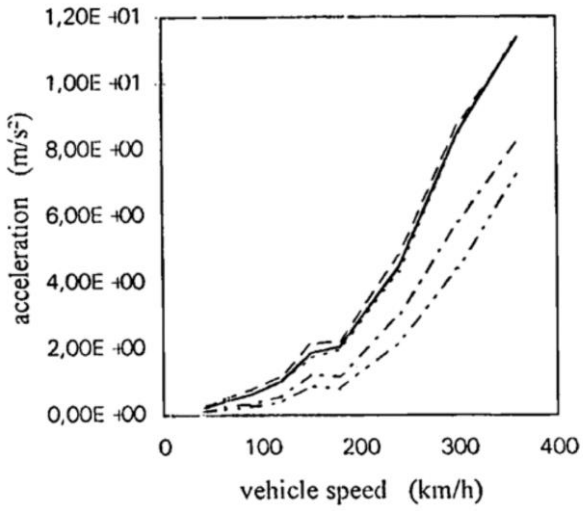

Figure 58 Train speed vs acceleration levels graph, showing ballast particles can overcome gravity above 270 km/h (Luo et al. 1996)

In HSR lines the passage of trains can generate enough air force to move the ballast particles. Kwon and Park investigated this air force in a wind tunnel experiment, i.e. the cross wind velocity levels at which different shaped and sized ballast particles move or are totally blown out (Kwon & Park 2006). Ballast particles obtained from Seoul-Busan high-speed line were classified as flat, hemi-spherical, and spherical shape, with their mass up to 200 g (Figure 59). It can be seen from the figure that irrespective of their shape, most of the particles starts to move at around 20 m/s wind velocity and it is defined as critical velocity. The lighter spherical ballast has lower blown out velocity which can be explained with the lower resistance to rolling while lighter flat and hemi-spherical particles have more resistance to air flow and rolling on track surface. Supporting Kwon and Park's work, it was also reported in (Saat et al. 2015) that ballast flight may occur at lower train speed levels in tunnels. Stating a likely threshold value of 260 km/h for a ballast flight outside of tunnels, the study reported evidence of significant damage to the sign posts from object strike, in a tunnel where the velocity limits were around 140 km/h. This implies that two train passing in a tunnel may damage each other more easily via ballast projection.

Jing and co-workers carried out wind tunnel tests and computational fluid dynamics (CFD) analysis to study the airflow effects on ballast particles with different shape and mass (Jing et al. 2014). Supporting the findings of (Kwon & Park 2006), the authors reported that 25m/s

wind velocity is the critical value for most of the ballast particles (Figure 60), which can be generated by an HST. It was observed that particle mass has more influence over critical wind velocity than particle contact area with the ground.

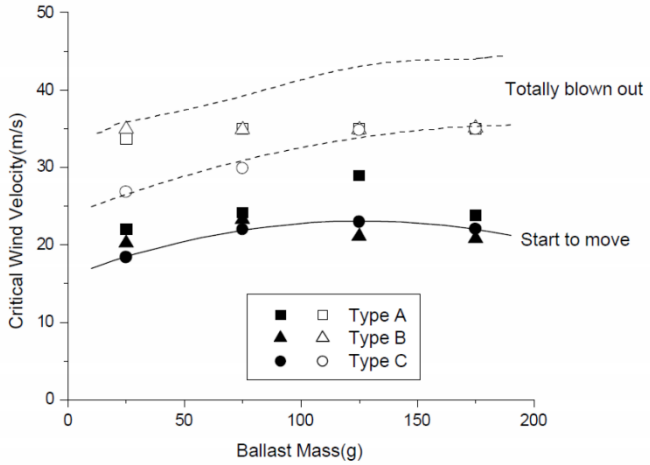

Figure 59 Critical wind velocity levels at which the ballast particles move. Type A: flat shape, Type B: hemi-spherical shape, Type C: spherical shape (Kwon & Park 2006)

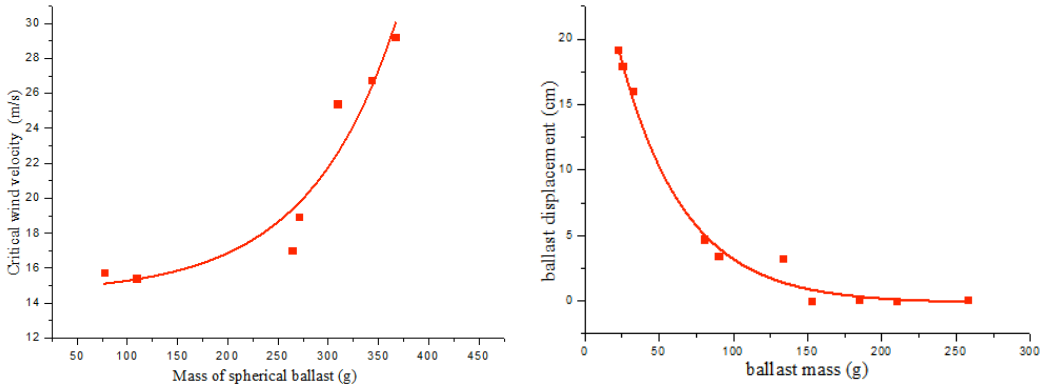

Figure 60 Critical wind velocity and particle displacement with respect to ballast mass (Jing et al. 2014)

It was reported by Italian authorities in (Saat et al. 2015) that during the certification of the HSR line between Rome and Naples, a ballast strike was observed at 270 km/h operating speed, striking the middle carbodies in train set and resulting in visible damage (Figure 61). This type of damage, from composite materials perspective, may require inspection for the integrity of the structure because delamination failure mode generally precedes other failure/damage modes such as indentation or scratches (shear) (Figure 61). It was also reported that ballast particles were found embedded inside the cone of the front cab. This indicates that the front end can also be considered as one of the susceptible areas of the rail vehicle for flying ballast strikes.

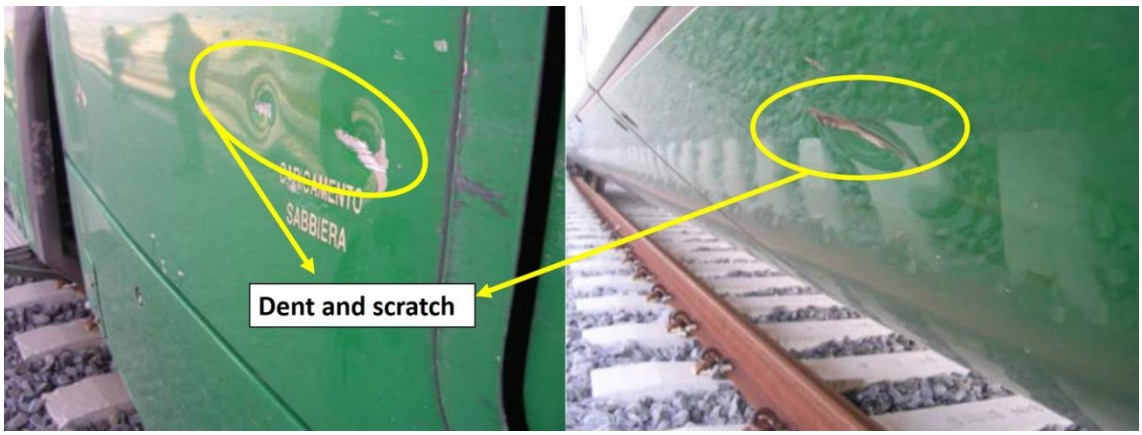

Figure 61 Dents and scratches after ballast strike on carbody ((Agretti 2012) in (Saat et al. 2015))

In their very recent study, Sakly et al. investigated composite sandwich structures for railway applications under low-velocity impact (Sakly et al. 2016). The authors introduced a specialised test bench and carried out low-velocity impact tests according to the French railway standard NF-F07-101, which describes how to simulate a ballast impact against foam-based components. Two different sandwich configuration were investigated for their damage resistance: PES foam with glass/epoxy skins, and PET foam with glass/acrylic skins. Oblique and temperature dependant impact tests were carried out as well. Results showed that successive (four) impacts increased the indentation depth up to 3mm. While matrix cracks and delamination were found to be main failure modes, fibre rupture was also observed after sectioning the sandwich composites. Expectedly, cooling the materials (-25°C) before the impact caused degradation in mechanical response, making it more rigid, and introducing shear failure to the core material. Although the authors supported the foam cavitation phenomenon with numerical study, it could have been improved if they have introduced a failure criterion to the GFRP skins in the model since the skin failure was present in experiments.

A preliminary study of the proposed simplified assessment method for impact performance prediction of composites was presented by the author and co-workers (Onder et al. 2016). E-glass/polyester laminates were subjected to quasi-static punch shear test (QSPT) and the similarities of the failure progression between static tests and ballistic impact of composite laminates were presented. The developed numerical model underestimated the penetration resistance of the laminates with a 22.2% difference in the force at failure (Figure 62 top). The reason for this higher underestimation was the capability of the material model, which is generally used for relatively brittle composites. On the other hand, the model provided accurate

prediction of failure modes between static and dynamic impact cases (Figure 62 bottom). It was concluded that further refinement of the numerical model was required (which is an aim of this thesis) and the alternative approach was found to have high potential as a simpler and cost effective prediction method.

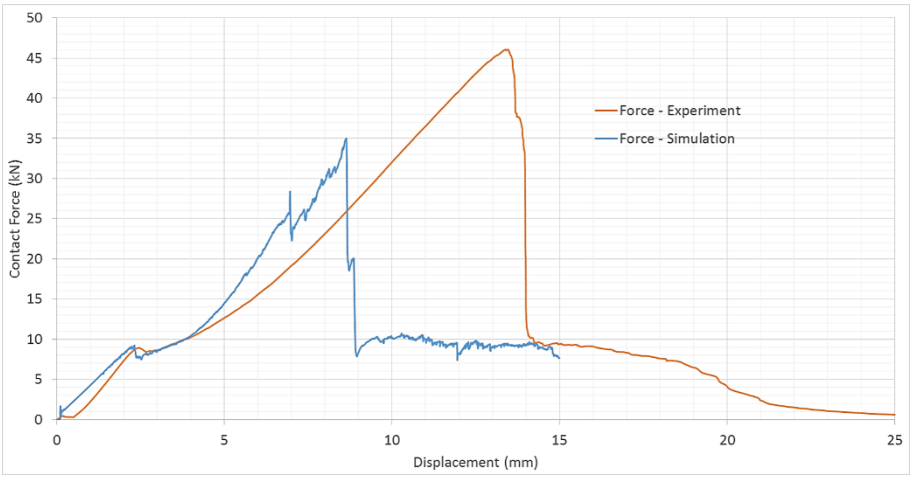

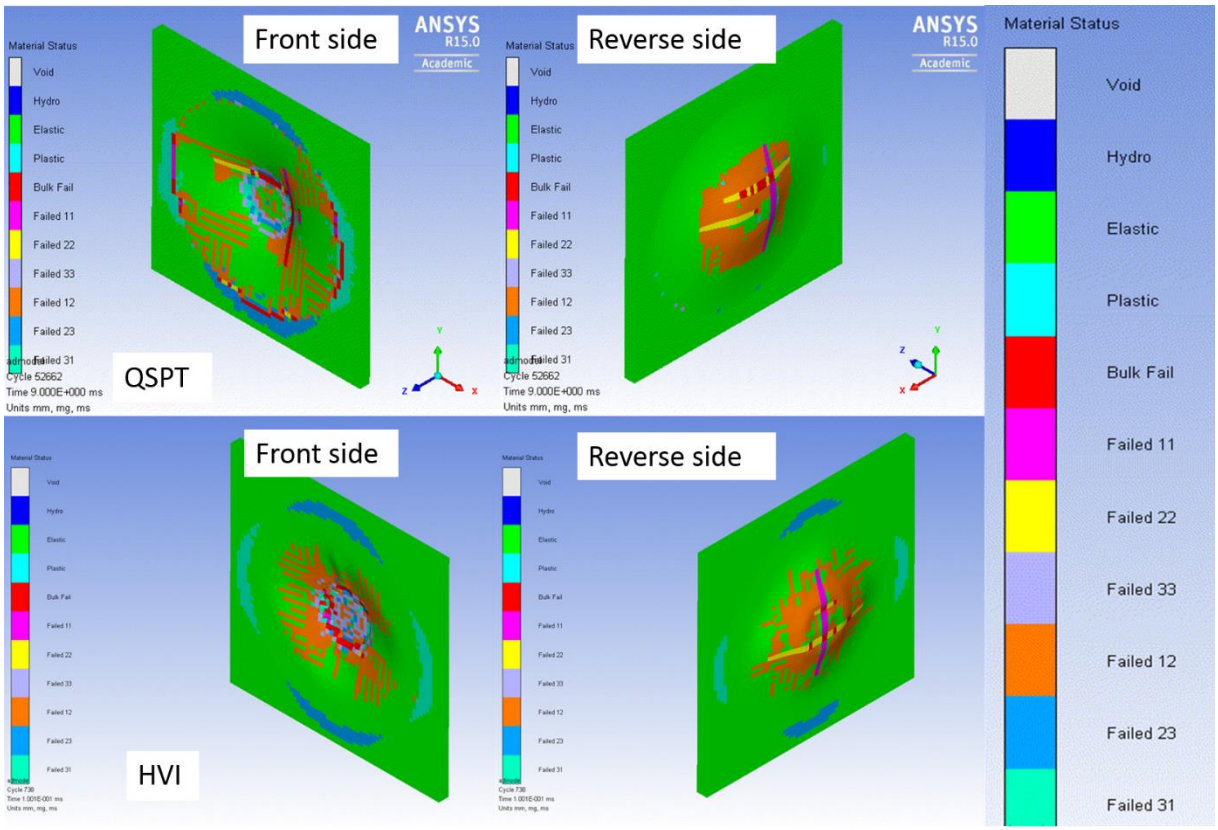

Figure 62 Numerical model prediction of penetration resistance of GFRP laminates (top) showing the variation. (Bottom) Front and reverse side figures of the laminates under QSPT and high-velocity impact (HVI) showing the failure modes were similar (Onder et al. 2016)

3.3 Conclusion

It is clear from the information presented in this chapter that during their service life, object strikes against rail vehicle carbodies (especially against HSTs) are highly likely. It is not possible to predict the type of impact precisely, given the variety of conditions. However, it can be anticipated that smaller object strikes such as gravelling or ballast are more likely compared to other more severe cases, considering the nature and conditions of the service. Various standards were provided and it was seen that most of them have no direct or little relationship with the others. Therefore, generating a method that can unify and harmonise case specific requirements would be beneficial, for example in terms of testing and materials cost. In conclusion, this chapter emphasized the need for such a method.

Chapter 4. Development of the impact response prediction method

After clarifying the gap in the field and the need for a different assessment approach in the previous chapter, this chapter presents the basis of the prediction method with the reasons behind it, and describes the resources used, how it was carried out, and what the important points were.

4.1 Proposed methodology and hypothesis

Previous research (Potti & Sun 1996; Gama & Gillespie 2008) has shown that laminated composites tested using the quasi-static punch test (QSPT) exhibit similar failure modes and damage progressions to high-velocity impact (HVI) events. If sufficient information could be identified regarding the mechanisms involved and their effects, and if logical connections could be made between two cases, then it means that creating an alternative low speed method would be viable for the rail industry not only in terms of cost and time saving, but also for a preliminary prediction. Therefore, the thesis hypothesis is:

"The combination of quasi-static punch testing and finite element (FE) modelling can provide a reasonable degree of confidence for the prediction of dynamic impact response of composite materials, and therefore can be competitive to costly ballistic experiments (Figure 63)."

In essence, the assessment method can answer these two main questions;

- Does the structure have enough resistance against complete penetration?
- If the structure has enough resistance against complete penetration, what could be the extent of damage in the aftermath of an impact scenario?

The answer to the first penetration question could be predicted roughly by means of analytical models and other approaches available in the literature. However, the answer to the second resistance question could be complex. Although relevant safety codes define this as an absolute requirement – in this case the penetration of a foreign object into the occupied parts of the vehicle is not allowed – in some cases, the aftermath of a non-penetrating impact event requires further examination for repairs or even replacements. Therefore, to cope with the level of complexity, any information (or data) from various aspects of the phenomenon proves useful in the analysis process which can be achieved via numerical means such as commercial

software. Acquiring the history log of the event from various aspects not only enhances the understanding, but helps designers on decision making as well.

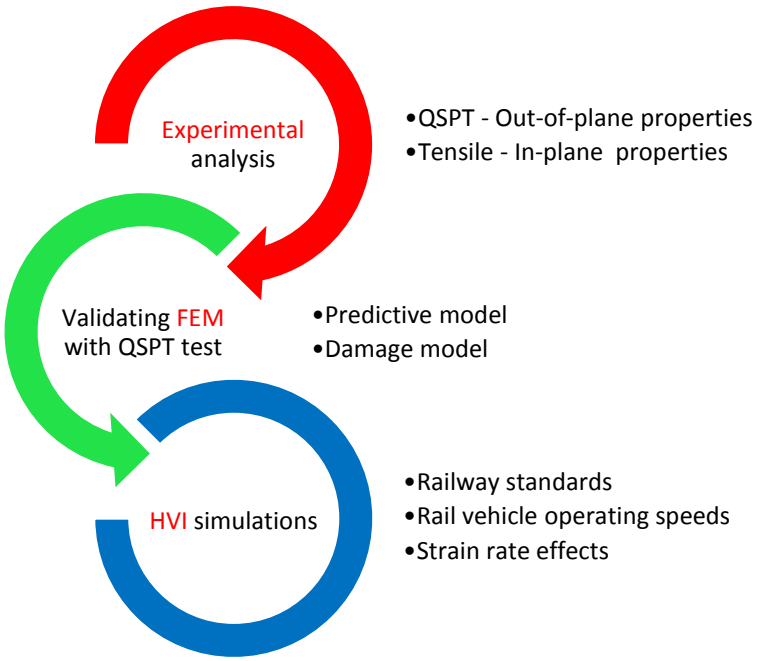

Figure 63 General schema of the proposed methodology

Figure 64 shows the application of numerical means in the aviation industry (top) currently and in a foreseeable time period, and the strategy for the rail industry (bottom). It depicts that the trend in experimental investigation will be superseded by simulations, reducing the vast number of test specimens, hence resulting in cost savings. This is also the case for the railway industry since a similar building block approach is applicable in design.

"The aftermath" of a non-penetrating impact may raise question to the reader about the residual strength of the structure. Composite materials are susceptible to impact type loading which results in delamination failure. It is a critical mode of failure especially under compression loading in the fibre (or in-plane) direction. The residual strength is particularly important in the aviation and aerospace industries for composite structure design, and for this reason standardized test methods called compression after impact (CAI) tests were developed. However, the CAI concept is not as crucial for rail vehicles as it is for aviation/aerospace vehicles since the service can be terminated in case of an emergency – or the vehicle can be taken to immediate repair before the catastrophic failure happens. Therefore, residual strength is not included in the scope of this thesis, but it would be worthwhile to conduct linking research in the future.

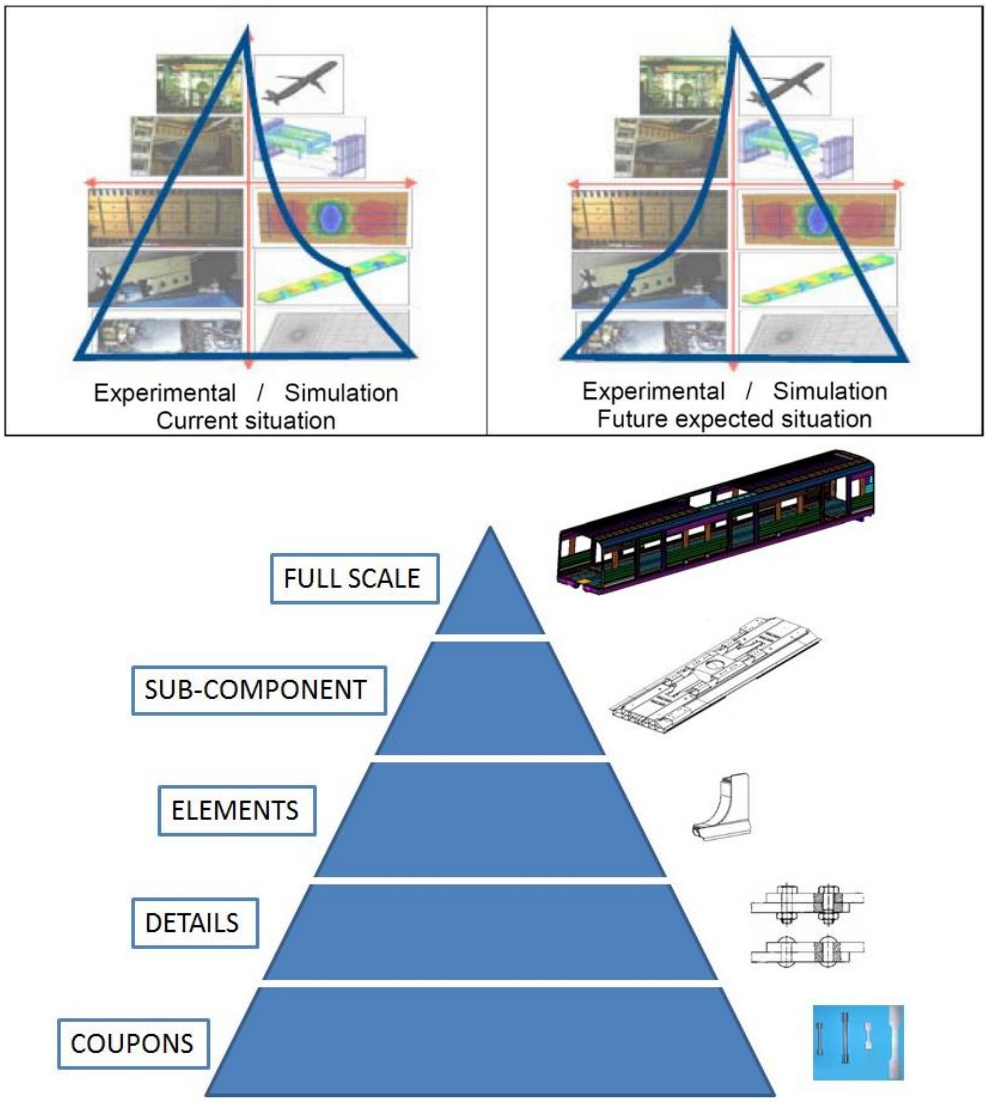

Figure 64 Current and future balance between experimentation and simulation (top), building bock strategy in railway industry vehicle design (bottom) (REFRESCO WP7-D7.3 2016)

4.2 Materials and samples

4.2.1 Laminate configuration

As this thesis addresses railway specific impact risk, the choice of materials should reflect the realistic applications accordingly. Carbon, glass, and aramid fibre reinforcements are widely used in structural applications. Among these, glass fibres are not only cost effective, but they also have a better impact response and damage tolerance (Reid, Zhou, et al. 2000). FRPs paved the way for light-weighting in other sectors such as aviation with the extensive use of carbon fibre. Unfortunately, strength and stiffness properties aside, carbon fibre is still one of the most expensive reinforcement. Therefore, it was ignored in this study.

Aramid fibres are mainly used in defence industry for ballistic protection of personnel. They have good impact resistance, but are also more expensive. In addition, larger scale structural applications of aramid fibres are not advantageous over glass or carbon fibres. Therefore, aramid fibres were not considered.

Reinforcing materials other than glass, carbon, and aramid fibres such as novel natural and recyclable fibres were not considered because of the limited and invalidated knowledge on their current capabilities, manufacturing process, and long-term life cycle characteristics.

For these primary reasons experimental studies were carried out with E-glass fibre/polyester resin composite laminates. The type of polyester resin used in this study was DRT P4 TV-129 pre-accelerated unsaturated polyester with no additives. This thermoset resin is the most widely used resin type in many industries, is easy to use in low batch manufacturing as it requires low pressure for moulding, and is perfectly suitable for hand lay-up method. GFRP plates were manufactured by the hand lay-up technique using 800 g/m^2 plain woven rowing glass fabric and polyester resin matrix. Since in plain weaving architecture the fibres stretch in and interlace perpendicular to each other, each ply was laid in the same orientation which resulted 0° being the *x (longitudinal or 1)* direction and 90° being the *y (transverse or 2)* direction, respectively. This orientation is conventional in terms of obtaining quasi-isotropic in-plane properties and is a common configuration. Material characterisation tests were carried out in accordance with ISO standards and the results are presented in Section 5.1 in detail. In addition, the fibre volume fraction (v_f) of the laminates was calculated as 55-60% through mass fraction method (also known as burn-out method). The dimensions of each plate were 200x200 mm^2 with 6 mm thickness (Figure 65 left).

4.2.2 Sandwich configuration

Based on the information given in Section 2.2.1, sandwich composite of foam core combined with E-glass fibre/epoxy facesheets was preferred in this research (Figure 65 right). AIREX® T90.100 closed cell PET (polyethylenterephtalate) foam was used in this research which was obtained from Trident Foams Ltd. UK. AIREX® T90 is a closed-cell, thermoplastic and recyclable, structural PET rigid foam with excellent fire, smoke, and toxicity (FST) properties. It is suitable for lamination with all types of resins and processes; it is easy to thermoform and process mechanically. It also offers great chemical resistance, is resistant against ultra-violet (UV) rays, and does not absorb water. Curing and post curing at increased temperatures is unproblematic as it is very heat-resistant and does not post expand or outgas. This foam core

has high level mechanical and fatigue properties as well as excellent fire, smoke and toxicity properties, thus completely suitable for railway applications. Material characterisation tests were carried out with 100x100x50 mm foam blocks, 50 mm being the thickness. However, for validation of case studies, a thickness value was chosen for the sake of having an optimised light-weight structure. In order to decide on a suitable core thickness, specific energy absorption, i.e. energy absorption performance per mass (J/kg) – analysis was performed via QSPT simulations for four thicknesses (20, 30, 40, 50 mm – the results were presented in Chapter 5 – Section 5.3.1). Foam core was bonded to 2 mm thick E-glass fibre/epoxy facesheets and these facesheets were also characterised separately for their tensile and shear properties. ILSS properties were taken from the resin manufacturer data sheet. The E-glass fibre used was 300 g/m^2 plain weave fabric, and the epoxy resin used in these facesheets were RS-L135 epoxy resin. This low viscosity laminating system has been designed for the manufacture of glass, carbon and aramid fibre composite components requiring high static and fatigue strength properties. The resins and hardeners contain neither solvent nor fillers, making the RS-L135 epoxy laminating system particularly suitable for marine applications and the manufacture of wind energy turbine blades (PRF Composite Materials 2013). The RS-L135 epoxy resin system exhibits good mechanical properties after curing at room temperature. If high temperature strength is not required, finished products made with the selection of hardeners up to RS-H136 may be used without further heat treatment. Post curing (heat treatment) will further enhance the mechanical properties and will also increase the heat resistance (PRF Composite Materials 2013). The fibre volume fraction (v_f) of the sandwich laminates was calculated as 57.40 %.

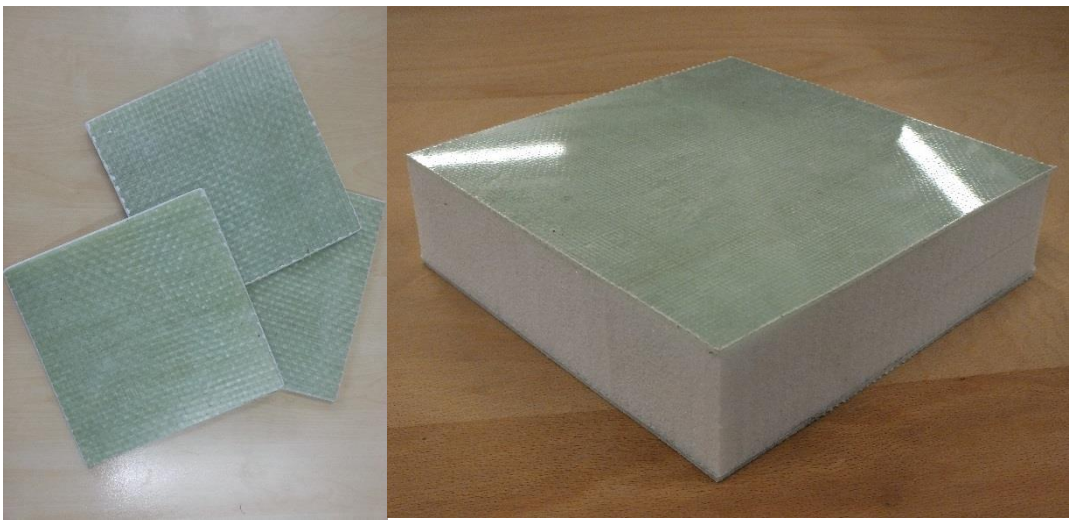

Figure 65 Glass fibre/polyester laminates (left) and foam core - Glass fibre/epoxy facesheet sandwich composite (right) used in this study.

4.3 Quasi-static punch tests (QSPT)

Before describing the main testing method used in this thesis, other methods used by researchers to assess impact response of composites were investigated.

The techniques to measure impact related parameters for metals have also been implemented on composites in the past. These include basic testing methods such as Charpy and Izod tests (Figure 66 a), drop-weight impact (Figure 66 c), and more advanced techniques like Hopkinson bar test, and gas gun impact (Figure 66 b), which can achieve higher strain rate loading. Since the way composites dissipate impact energy is different than the way metals do, Charpy and Izod test results tend to be influenced predominantly by the geometry of the specimens, hence providing inappropriate data for realistic scale applications (Cantwell & Morton 1991). Nevertheless, these methods can be used for the sake of ranking different materials.

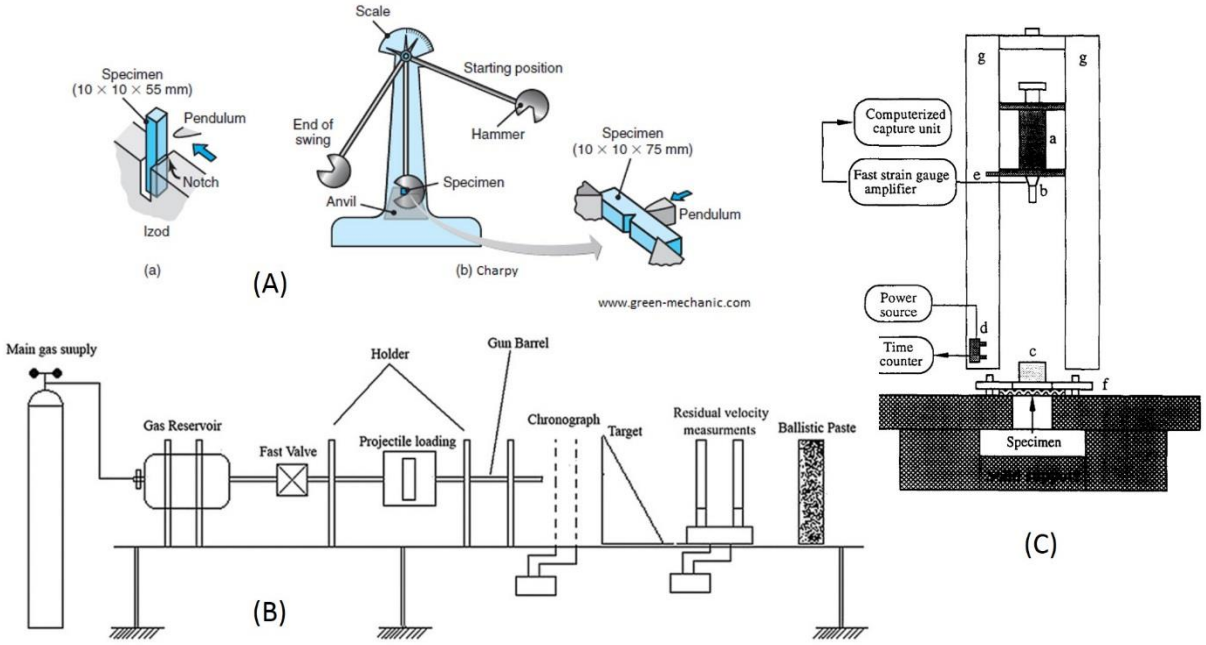

Figure 66 Various impact testing rigs: (A) charpy and izod (Green Mechanic 2017), (B) gas-gun (Sabet et al. 2011), (C) drop-weight impact test rig (Zhou & Davies 1994)

Drop-weight (drop-tower) testing is most commonly used for low-velocity impact response of composites. An instrumented head with adjustable mass and drop height impacts the specimen after a free fall, perpendicular to in-plane direction (Figure 66 c). The impact head generally has a force sensor which enables the generation of force-time history, but a displacement sensor could be used as well to determine energy absorption by the specimen. Incident energy (or incident kinetic energy) can easily be calculated through equations of motion. With this test

method, reasonable degree of strain rate effects can be achievable in addition to a wider range of specimen geometry.

More advanced impact testing methods such as ballistic/gas gun (Figure 66 b) or Hopkinson pressure bar can reach to thousands of hertz strain rate loading which can produce crucial information in designing high performance composites for many industrial applications. However, these high energy/velocity involving experimental testing methods require specific and expensive testing equipment such as sensors for determining the impact velocity, high-speed cameras to capture visual information, fast data acquisition systems, and even specialised personnel in some cases. Therefore, generally it is not readily available and is challenging to access to these facilities.

In addition to these more classical methods, there has been a growing trend towards using quasi-static test methods for impact damage investigation. When compared to the others, many advantageous aspects standout such as the requirement of simple equipment, it being easier to perform, and especially the good level of repeatability.

One of the issues about impact strength/resistance of both sandwich and laminated materials is that there is no existing common standard, and one has to select from many different methods, some of which are standardised but others are not. Hildebrand compared three test methods which determine the impact strength and the failure modes of FRP sandwich structures (Hildebrand 1996). Various sandwich structures composed by glass fibre skins (both fabric mat and chopped strand mat) and polymer foam core material (polystyrene, polyurethane and PVC) were subjected to indentation in the through-thickness direction in accordance with ISO 6603, Pyramid method (developed by VTT Technical Research Centre of Finland), and slow impact (developed by KTH Royal Institute of Technology in Stockholm) test methods. All three methods are the same in principal, with variations in boundary conditions and impactor shape/size. The author concluded that the pyramid method appears to be more practical since it could capture a multitude of different failure modes. One inconsistency of this study is that the rate of loading was much higher (forty times) in both the ISO 6603 and pyramid methods compared to the slow impact method, Hence, practicality aside, the failure loads are also important along with the failure modes, which in this case were influenced by higher rate loading.

In this thesis, an experimental test - namely quasi-static punch test (QSPT/QSP test) - was performed with a custom-made steel fixture. First practices of this type of test dates back to the

mid-90's (Zhou & Davies 1994; Potti & Sun 1996; Potti & Sun 1997). Researchers have made use of this particular method (with variations in testing setup) for different industrial areas such as protection/armour ballistics (Nguyen et al. 2016), aerospace (Clegg et al. 2006; Riedel et al. 2006; Wicklein et al. 2008) and in the marine/offshore industry (Sutherland & Guedes Soares 2012; Gibson 2003). No research references have been found incorporating the use of this experimental analysis for the railway industry. It can be argued that the essence of this test method is analysing the protection performance of the material in question. Being a part of the main structural construction of a front cab/end for example, composites are not specifically designed as armour type structures in rail vehicles. For this reason, an assessment has to be carried out in order to reveal the compliance with the relevant existing/future standards.

Being easily applicable and fully controllable, QSPT provided more detail about the failure and damage mechanisms and their sequences in penetration of the samples. In particular, the slow and controllable nature of this method ensures excellent repeatability which is a concern in composite testing. For every fixture-punch setup, the samples were loaded stepwise (predefined displacements) to reveal the failure sequence. The number of steps were decided according to the change in the load behaviour of a fully penetrated sample. Relevant steps and corresponding punch crosshead displacements are given in Table 4.

In this research, quasi-static punch tests were performed using a custom-made steel fixture and two different punch tips, i.e. circular flat (CF) and hemispherical (H). The rationale behind the preference of these particular nose shapes is based on the recent work of Jordan and Naito who carried out extensive ballistic limit identification tests to investigate the effect of eight impactor nose shapes (Figure 67 top) on three different thicknesses of glass fibre reinforced laminates (Jordan & Naito 2014). The authors analysed the displacement profiles of each projectile in a full penetration case, and also identified the dominant failure modes. Ballistic limit comparisons were made between their study and two analytical prediction models (Wen 2000; Jeng et al. 1994). The comparison revealed that Jeng's model gave inconsistent results at certain impact cases although the error levels were less than 20%, while Wen's model required the refinement of empirical parameter (β) for each different nose shapes. Nevertheless, these refined parameters resulted in accurate predictions. Results of ballistic tests revealed that hemispherical and chisel nose shapes were the most efficient penetrators, while Right Circular Cylinder (RCC), cube, and parallelepiped nose shapes were the least efficient (Figure 67 bottom). It was concluded that energy absorption and ballistic limit of composite laminates predominantly

depend on the impactor shape. Based on this finding, circular flat and hemispherical ended impactors were selected in order to cover a good range of penetration efficiency.

	Step 1 (mm)	Step2 (mm)	Step 3 (mm)	Step 4 (mm)	Step 5 (mm)
SPR1.2 – CF	1.5	3	4	4.25	9
SPR1.2 – H	1.5	4	6	6.9	9
SPR4.1 – CF	3	8	13	25	-
SPR4.1 - H	3	8	12	25	-

Table 4 Number of steps and corresponding crosshead displacement for QSPT setups (CF: circular flat punch head, H: hemispherical punch head)

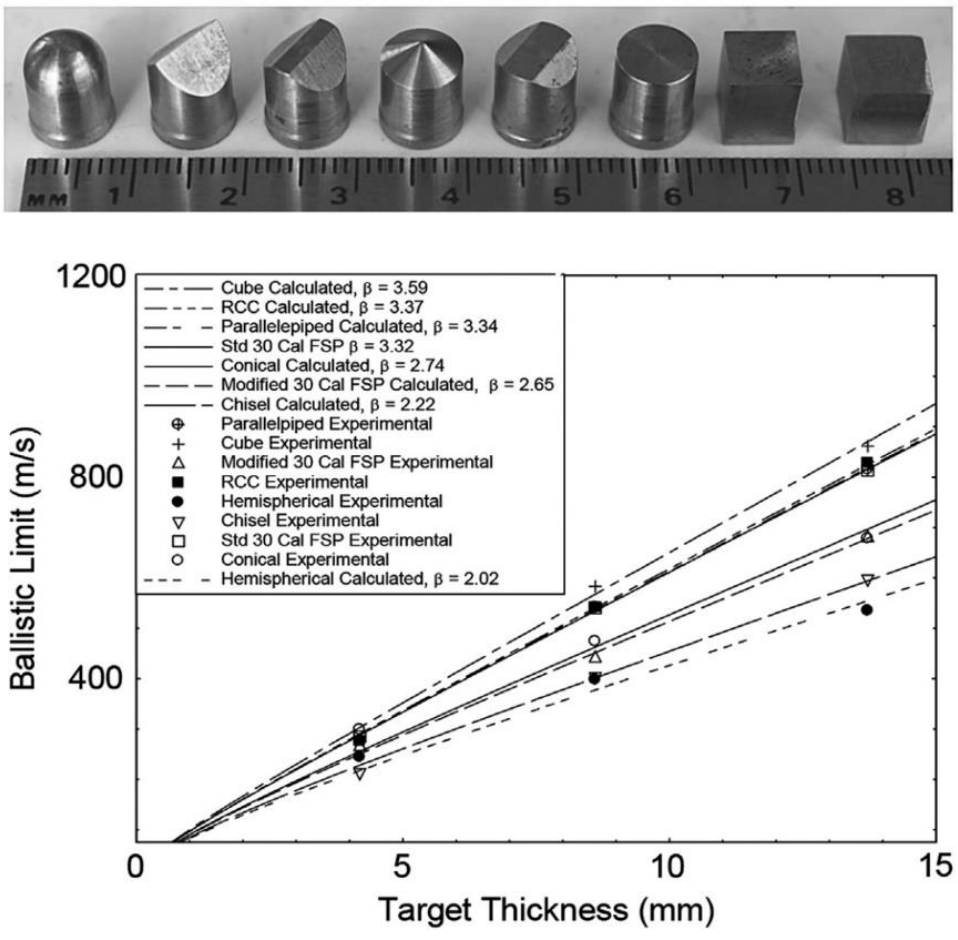

Figure 67 Various projectile nose shapes (top), ballistic limit tests and predictions by the modified analytical models (bottom) (Jordan & Naito 2014)

The QSPTs were carried out by using a Shimadzu universal tensile test rig of 100 kN capacity, TRAPEZIUM software which processes the data obtained from the sensors embedded in the crosshead of the test rig, and a custom-made fixture made of steel to hold the samples. The custom-made fixture has a central circular ring (span) which enables the penetration of the samples. Geometrical and dimensional details of the fixture can be seen in Figure 68. The rig was used in compression loading, by attaching a long steel punch to the moving head, and applying compression force normal to the samples held by the custom-made fixture which was mounted on the base plate of the rig. The punch heads used have the same diameter (25.4 mm) which results in span-to-punch diameter ratio (SPR) of SPR 4.1. All tests were carried out with a constant crosshead displacement control of 2 mm/min. The sensors in the test rig crosshead enable to obtain the applied force and displacement levels of the punch head. These two are the main experiment parameters, which were processed through TRAPEZIUM software to generate force-displacement (F-d) graphs and energy absorption values (the area under the F-d graph).

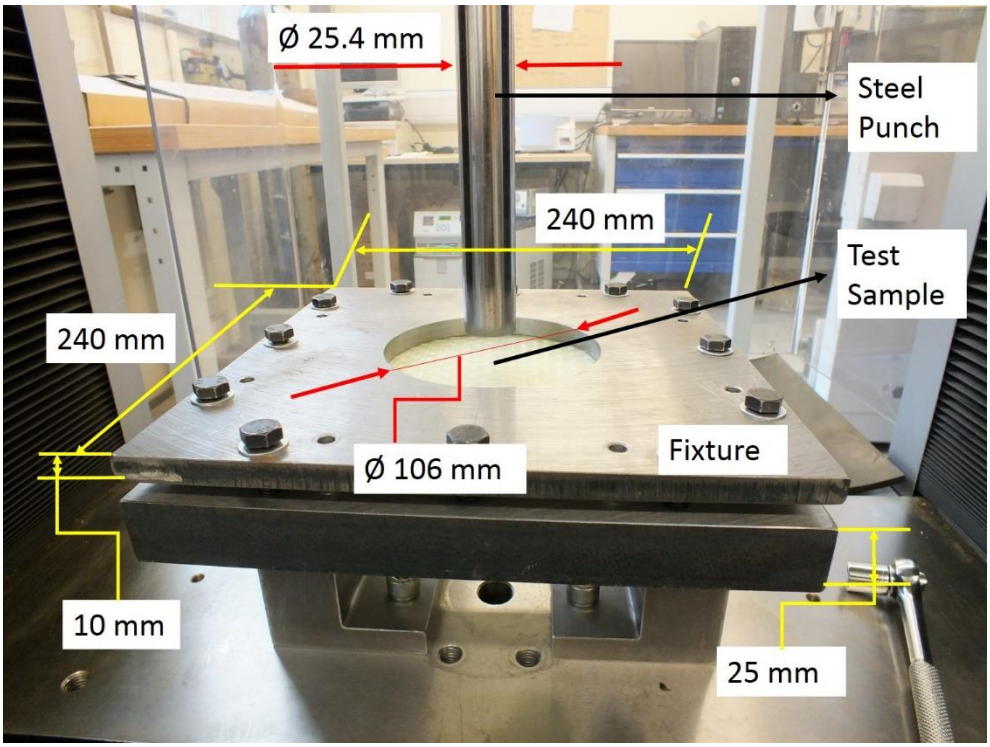

Figure 68 Quasi-static punch test setup showing the dimensions of the custom made fixture

The reason to choose SPR 4.1 is, based on the information stated by Gama and Gillespie that the possible transition from shear dominated deformation to bending dominated deformation starts at SPR>4 (Gama & Gillespie 2008). Other numerous researchers also used varying SPR values, however, no information regarding such transition value could be found. An additional fixture of a smaller diameter (31 mm – resulting in SPR1.2) was used to measure the out-of-

plane shear strength of the laminates (Section 5.1.3) in a similar manner as it was used by Clegg and co-workers (Clegg et al. 2006).

4.3.1 Numerical modelling approach

As the proposed methodology requires extensive use of FE modelling, it is important to detail the numerical modelling process with all the details corresponding to material behaviour, loading type, and the variables of results. It is obvious that numerical modelling methods vary depending on the system being questioned in addition to the needs and expectations of the user. Therefore, the detailed information provided here reflects only the techniques and modelling that is relevant to the specific application, viz. impact loading of composite materials.

First of all, the overall approach throughout this thesis on numerical modelling was introduced in two parts; firstly, the model validation based on quasi-static experimentation (Section 5.3.1), and secondly the application of the same model to HVI case simulations (Chapter 6). Before presenting the risk scenarios however, the credibility of HVI simulations will be discussed. Even though the material model and solution process stays the same, the inertial effects caused by the highly dynamic nature of the impact influences the material properties of the GFRP target, i.e. strain rate effects.

Slight differences were present in the models for each different scenario. For example, in order to keep a good mesh aspect ratio for the model, the number of elements vary depending on the type of the impactor. Nevertheless, the general principals remained the same. The next subsections will provide details and a description about the numerical modelling.

4.3.2 Time integration: Explicit over implicit

Widely used commercial stress-strain analysis software are basically built on two time integration schemes: implicit and explicit. In simple terms they describe how the position-force-acceleration relationship of masses are solved with respect to time. Both integrations have advantages and disadvantages over the other, however, when highly dynamic or nonlinear behaviour is of concern, explicit time integration is the superior and the next sections will explain why. In general, explicit solvers were designed to overcome the difficulties arising from:

- Nonlinear material response,
- Complex contact between bodies,

- Large deformations and strains,
- Stress/Shock wave propagations,
- Penetration/perforation of bodies,
- Complex material failure and damage.

An impact loading scenario may exhibit one, many, or all of these complex mechanisms. Furthermore, explicit time integration is highly suitable for rapid occurrence of events which happens in milliseconds or even at a microsecond level. Table 5 and Table 6 gives a brief comparison between two time integration methods and the general material response with respect to varying loading conditions, respectively.

Solver type	***Impact velocity (m/s)***	***Strain rate (1/s)***	***Effect***
Implicit		$< 10^{-5}$	Static / Creep
	< 50	$10^{-5} – 10^{-1}$	Elastic
	50 – 1000	$10^{-1} – 101$	Elastic-Plastic (material strength significant)
	1000 – 3000	105 – 106	Primarily Plastic (pressure equals or exceeds material strength)
	3000 – 12000	106 – 108	Hydrodynamic (pressure many times material strength)
Explicit	> 12000	> 108	Vaporization of colliding solids

Table 5 Implicit analysis vs explicit analysis (reproduced from (Jaiswal 2011))

Velocity	***Low***	***High***
Deformation	Global	Local
Response time	ms - s	ms - µs
Strain	< 10%	> %50
Strain rate	$< 10^{-1}$	$> 10000\ s^{-1}$
Pressure	< Yield stress	10 – 100 times yield stress

Table 6 General material response to varying impact velocities (reproduced from (Jaiswal 2011))

Implicit time integration solvers are suitable for linear problems. A linear structural response means the structural stiffness remains constant and the internal load of the structure is

proportional to the displacement. These conditions, together with the required parameters for specific integration schemes (e.g. Newmark method or Hilber-Hughes-Taylor method (HHT-α)) allows the governing equations to become unconditionally stable, which means time step can be defined without the stability concern of the solution.

In a nonlinear response however the structural stiffness is not always constant, so the solution requires the inversion of dynamic equivalent stiffness matrix which is time consuming. In implicit time integration, nonlinearity results in usage of small iterative time steps to achieve convergence which is not always guaranteed. In addition, the solution is obtained through linear approximation methods. At this point the explicit time integration becomes advantageous for nonlinear problems since the integration method allows the equations to become uncoupled, and therefore can be solved directly (explicitly) for each element. Because the equations are uncoupled, there is no need for small iterative time steps and convergence checks which makes the simulation time efficient and more accurate. Although explicit time integration is superior to its counterpart in data processing and solution, one important detail to mention is that the method used in explicit dynamics does not allow to choose a time step (time spent per cycle) manually, unlike that of implicit integration in which the user can define the time step, therefore influencing the accuracy, stability, and efficiency of the problem. Therefore, a criterion is used to automatically specify the time step, i.e. CFL (Courant-Friedrichs-Levy) condition (Eqn. 1).

$$\Delta t \leq f * \left[\frac{h}{c}\right]_{min} \qquad \text{Eqn. 1}$$

Where Δt is time increment, f is the stability time factor (0.9 is default), h is characteristic cell dimension of an element which is calculated differently for various element types (hexahedral, tetrahedral, beam, etc.), and c is the local material sound speed in an element in m/s. CFL criteria implies that the time step must be limited so that a stress wave cannot travel further than the smallest characteristic element dimension in the mesh (ANSYS Help Viewer 2013). This condition, in turn, makes the analysis mesh size dependant. Therefore, model mesh should be optimized to provide sufficient accuracy while avoiding unnecessary long run time at the same time.

4.3.3 Explicit dynamics governing equations

The equations that define a system in explicit dynamics are the conservation equations of mass, energy and momentum. Lagrange formulation are supported in AUTODYN explicit solver, in which the mesh moves and deforms together with the geometry and material it models, unlike

it is in Euler formulations in which the mesh is stationary and the geometries move in the predefined area (Figure 69). Therefore, the conservation of mass is satisfied automatically in Lagrange type formulations. Based on mass conservation, the density is determined by the current volume by the following equation (Eqn. 2);

$$\frac{\rho_0 V_0}{V} = \frac{m}{V} \qquad \text{Eqn. 2}$$

Where m is the mass, V is the current volume, V_0 is the initial volume, and ρ_0 is the current density of the element. The conservation of momentum depends on the acceleration - stress tensor relationship by the partial differential equations below (Eqn. 3);

$$\rho\ddot{x} = b_x + \frac{\partial\sigma_{xx}}{\partial x} + \frac{\partial\sigma_{xy}}{\partial y} + \frac{\partial\sigma_{xz}}{\partial z}$$

$$\rho\ddot{y} = b_y + \frac{\partial\sigma_{yx}}{\partial x} + \frac{\partial\sigma_{yy}}{\partial y} + \frac{\partial\sigma_{yz}}{\partial z} \qquad \text{Eqn. 3}$$

$$\rho\ddot{z} = b_z + \frac{\partial\sigma_{zx}}{\partial x} + \frac{\partial\sigma_{zy}}{\partial y} + \frac{\partial\sigma_{zz}}{\partial z}$$

Where $\ddot{x}, \ddot{y}$, and $\ddot{z}$ are nodal acceleration in each material direction, ρ is the density, σ_{ij} is the stress tensor, and $b_{x,y,z}$ are the body acceleration components. And finally, the conservation of energy is expressed with Eqn. 4 below:

$$\dot{e} = \frac{1}{\rho}\left(\sigma_{xx}\dot{\varepsilon}_{xx} + \sigma_{yy}\dot{\varepsilon}_{yy} + \sigma_{zz}\dot{\varepsilon}_{zz} + 2\sigma_{xy}\dot{\varepsilon}_{xy} + 2\sigma_{yz}\dot{\varepsilon}_{yz} + 2\sigma_{zx}\dot{\varepsilon}_{zx}\right) \qquad \text{Eqn. 4}$$

Where σ_{ij} and $\dot{\varepsilon}_{ij}$ are stress and strain tensors, respectively.

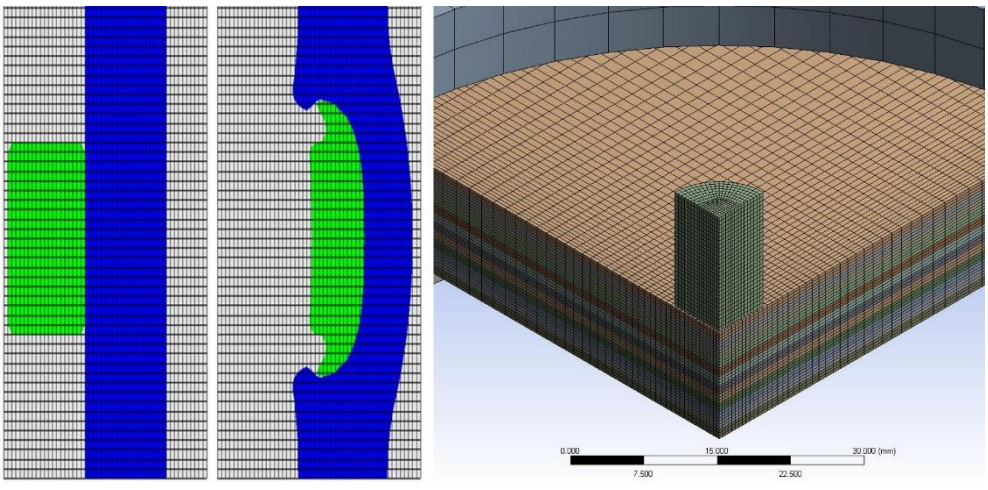

a b

Figure 69 Mesh functioning in Euler (a) and Lagrange (b) solvers

Basic formulations performed in explicit time integration are briefly described next. These formulations are solved in nodal scale, then for every mesh element in the model which is formed by a number of nodes, the conservation equations mentioned previously are solved individually. In order to establish a complete model to run in explicit analysis, at least one quantity (such as force or motion) should be defined in the system. Starting from this point and taking into account the contact and boundary conditions, the nodal accelerations (Eqn. 5) are derived from the nodal forces divided by mass:

$$\ddot{x}_i = \frac{F_i}{m} + b_i \qquad \text{Eqn. 5}$$

Where:

$\ddot{x}_i$: are the nodal acceleration components (i=1, 2, 3)

F_i: are forces at nodes

b_i: are the components of body acceleration

m: is the mass assigned to a node.

After the accelerations are obtained at time n, they are used to obtain velocities ($\dot{x}_i$) at time $n + 1/2$ with the Eqn. 6 below:

$$\dot{x}_i^{n+1/2} = \dot{x}_i^{n-1/2} + \ddot{x}_i^n \Delta t^{n+1/2} \qquad \text{Eqn. 6}$$

And lastly the position of nodes (x_i) (Eqn. 7) at time $n + 1$ are derived from velocity equations:

$$x_i^{n+1} = x_i^n + \dot{x}_i^{n+1/2} \Delta t^{n+1/2} \qquad \text{Eqn. 7}$$

4.3.4 Modelling the material behaviour

Modelling of GFRP laminates

Numerical modelling of composite materials such as laminates first of all requires the capability to model anisotropy, in other words the direction dependant behaviour. That being said, material models such as isotropic elasticity are not sufficient enough to capture elasticity behaviour and composite intrinsic mechanisms accurately. For this reason, orthotropic material models have been developed in the past years to represent the direction dependant behaviour arising from the characteristics and the distribution of the constituents, i.e. fibre and matrix phase.

In this thesis, ANSYS AUTODYN explicit solver was used to model quasi-static punch and impact behaviour of E-glass/polyester laminates and sandwich materials. AUTODYN has

extensive material modelling capabilities and techniques for composite modelling, covering a range from simple structural applications to highly non-linear behaviour such as shock effects induced by high/hyper velocity impact loading (Clegg et al. 2006; Riedel et al. 2006; Lassig et al. 2015). AUTODYN uses the Orthotropic Constitutive Model, which can be built by using the combination of Orthotropic Elastic Models, Strength and Hardening Models, and Failure models. Figure 70 shows the available material models. It is important to note that not all the sub-models are compulsory. For example, Equation of State (EOS) models are used if the type of loading result in shock effects such as hypervelocity impact (1000m/s and above impact speed). Moreover, if the material has a brittle characteristic, or does not show significant non-linear behaviour/plasticity, then brittle material models can be used. Previously, the author used the brittle material model as well to simulate quasi-static punch behaviour of GFRP laminates (Onder et al. 2016). However, it was found that accuracy of this model was not sufficient. Therefore, in this thesis, the orthotropic elastic model was used in combination with orthotropic yield (strength) and orthotropic softening (failure) material models to simulate the quasi-static and dynamic behaviour of GFRPs.

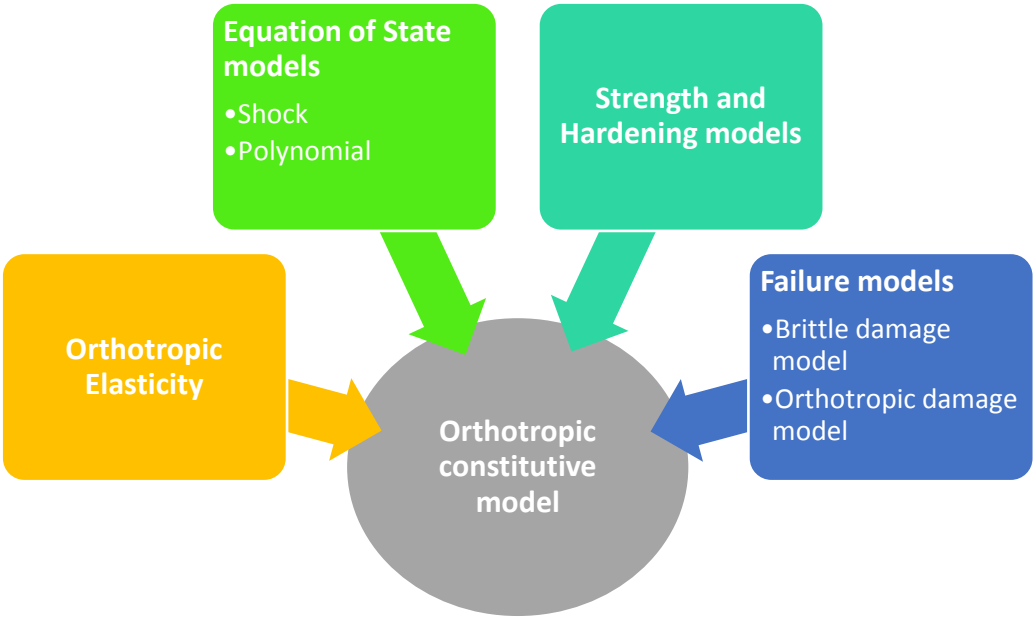

Figure 70 Available material model combinations in AUTODYN for composite modelling.

Orthotropic elastic model: This material model is used to provide basic direction dependant properties of the composite material in question: Young's moduli (E), shear moduli (G), and Poisson's ratios (ν) in each direction.

***Strength and hardening model – Orthotropic yield*:** Most of the fibre and matrix combinations are known to exhibit brittle behaviour. This statement is relatively true when they are compared with metallic materials, however it is not entirely true when the focus is only on polymer matrix composites. While high-performance carbon fibre reinforced composites fail by an immediate break/rupture (Lassig et al. 2015), other composites such as glass fibre or aramid composites, can exhibit significant non-linear behaviour both before and after the catastrophic failure of the material (Clegg et al. 2006). This relatively ductile behaviour that arises from micro-cracking, plasticity of polymer matrix, or re-orientation of fibres, is referred to as hardening in AUTODYN. A yield function (Eqn. 8) based on nine parameters (Chen et al. 1997) is implemented in this material model and it requires plasticity parameters, and also the effective stress-strain values in combination as inputs (ANSYS Inc. 2013). a_{ij}'s are called plasticity parameters, and parameter k varies with the effective inelastic strain in the material and can be used to represent hardening behaviour. Plasticity parameters would ideally be calibrated from the experimental stress-strain data obtained from three simple uniaxial tension tests and three pure shear tests. The six parameters associated with the normal stresses are then determined from the definition of a master effective stress-effective plastic strain relationship.

$$f(\sigma_{ij}) = a_{11}\sigma_{11}^2 + a_{22}\sigma_{22}^2 + a_{33}\sigma_{33}^2 + 2a_{12}\sigma_{11}\sigma_{22} + 2a_{23}\sigma_{22}\sigma_{33} + 2a_{13}\sigma_{11}\sigma_{33} + 2a_{44}\sigma_{23}^2 + 2a_{55}\sigma_{31}^2 + 2a_{66}\sigma_{12}^2 = k \quad \text{Eqn. 8}$$

***Material Failure Model – Orthotropic damage model*:** Orthotropic damage model is used in order to discriminate the failure modes during the loading of the samples. This material model characterises the limit response of the material in a two phase approach: failure initiation and damage. The criteria (Eqn. 9) used in failure initiation of this AUTODYN model is a modified version of the Hashin criterion, which has been widely used for composite modelling. However, Hashin criteria takes into account the in-plane stresses for the failure of fibre and matrix. As an addition to the original Hashin criteria, Hou et al. presented the failure criteria (Hou et al. 2000) by taking into account the delamination criterion and out-of-plane shear stresses for fibre and matrix cracking, which then was implemented in AUTODYN.

In 11 direction: $$e_{11f}^2 = \left(\frac{\sigma_{11}}{\sigma_{11fail}}\right)^2 + \left(\frac{\sigma_{12}}{\sigma_{12fail}}\right)^2 + \left(\frac{\sigma_{31}}{\sigma_{31fail}}\right)^2 \geq 1$$

In 22 direction: $$e_{22f}^2 = \left(\frac{\sigma_{22}}{\sigma_{22fail}}\right)^2 + \left(\frac{\sigma_{12}}{\sigma_{12fail}}\right)^2 + \left(\frac{\sigma_{23}}{\sigma_{23fail}}\right)^2 \geq 1 \quad \text{Eqn. 9}$$

In 33 direction: $$e_{33f}^2 = \left(\frac{\sigma_{33}}{\sigma_{33fail}}\right)^2 + \left(\frac{\sigma_{23}}{\sigma_{23fail}}\right)^2 + \left(\frac{\sigma_{31}}{\sigma_{31fail}}\right)^2 \geq 1$$

Failure is initiated when the stress reaches the value required for failure σ_{fail}. After the initiation of failure which indicates that a stress state that is outside of the allowable region is found, a backward-Euler algorithm is used to return the stress to the failure surface region. The resulting inelastic increment in strain is then accumulated as crack strain ε^{cr}. The maximum stress that can be sustained in an element is then reduced as a function of crack strain.

$$G_f = \int_{\varepsilon^{cr}=0}^{\varepsilon^{cr}=\varepsilon^u} \sigma L d\varepsilon^{cr};\ \varepsilon^u = \frac{2G_f}{\sigma_{fail}L};$$

$$h = \frac{L\sigma_{fail}^2}{2G_f};\ Dam = \frac{h\varepsilon^{cr}}{\sigma_{fail}};\ \sigma_{max} = \sigma_{fail}(1 - Dam) \qquad \text{Eqn. 10}$$

In Eqn. 10, L is the characteristic cell dimension in the direction of failure, h is the gradient of the linear softening slope, $G_f$is the fracture energy, and Dam stands for damage which at initiation ε^{cr}=0, therefore Dam=0. When the cell has no strength Dam=1. At any point between these times the maximum tensile material stress that can be supported in the cell is calculated as $\sigma_{max} = \sigma_{fail}(1 - Dam)$. After the initiation of failure, the damage parameter influences the failure criteria mentioned above as Eqn. 11 shows:

$$e_{11f}^2 = \left(\frac{\sigma_{11}}{\sigma_{11fail}(1-D_{11})}\right)^2 + \left(\frac{\sigma_{12}}{\sigma_{12fail}(1-D_{12})}\right)^2 + \left(\frac{\sigma_{31}}{\sigma_{31fail}(1-D_{31})}\right)^2 \geq 1$$

$$e_{22f}^2 = \left(\frac{\sigma_{22}}{\sigma_{22fail}(1-D_{22})}\right)^2 + \left(\frac{\sigma_{12}}{\sigma_{12fail}(1-D_{12})}\right)^2 + \left(\frac{\sigma_{23}}{\sigma_{23fail}(1-D_{23})}\right)^2 \geq 1 \qquad \text{Eqn. 11}$$

$$e_{33f}^2 = \left(\frac{\sigma_{33}}{\sigma_{33fail}(1-D_{33})}\right)^2 + \left(\frac{\sigma_{23}}{\sigma_{23fail}(1-D_{23})}\right)^2 + \left(\frac{\sigma_{31}}{\sigma_{31fail}(1-D_{31})}\right)^2 \geq 1$$

Modelling of foam core of sandwich materials

Sandwich materials were modelled in the same way as the laminated composites except the different material model assignment to foam core while keeping the same modelling for face layers. Therefore, only the core modelling is provided in this section.

In AUTODYN, the material models suitable for foam characteristics are classified as porosity models; Porosity-Crushable foam, Compaction EOS Linear, Compaction EOS Nonlinear, and P-alpha EOS. These models basically depend on the volume, density and pressure relationship. Among these, P-alpha EOS is the most comprehensive model. However, the required input is

somewhat unconventional, viz. Porosity (α) – Pressure (*P*) curve, and also the Porous sound speed data. Compaction EOS models require Pressure (*P*) – Density (ρ) loading or unloading curve which is not practical as well. On the contrary, Porosity-Crushable foam material model requires shear and tensile strength along with the compression stress-strain curve to define the foam characteristic which is easily obtainable with ISO-844 standard. Although it is a rather simple model compared to others, this material model is used by many researchers (Rizov et al. 2005; Flores-Johnson et al. 2008; Wang et al. 2013), and it provides reliable results especially in impact loading conditions where cyclic behaviour is unimportant. Therefore, crushable foam material model was preferred in this thesis to simulate foam core behaviour of the sandwich composite. The required parameters were obtained through material characterisation tests described in Section 5.1.4.

4.3.5 Element formulation and meshing

Different approaches could be followed to model a composite laminate such as micro-scale, meso-scale, and macro-scale modelling. In micro and meso scale modelling, the individual or bundle of constituents (fibre and matrix) can be modelled and analysed to study how they influence or interact with each other. Predictably, this is not a realistic approach if we think about actual engineering structures since the computational effort would be tremendous. Macro-scaling approach on the other hand considers the constituents as a whole, with different properties in predefined directions, which is more adequate for current study as well as for larger full/sub structure modelling. Macro-scale models can be created either as a continuum volume or as a sub-laminate volume. Continuum volume approach requires crack propagation information to represent delamination and matrix cracks and for this reason this approach was not favoured in this thesis. For every numerical model carried out in this work, a sub-laminate model approach was preferred as it will be described in detail in Section 4.3.7. In AUTODYN each layer of the laminate is not explicitly modelled, rather continuum elements representing equivalent homogeneous anisotropic solids are used to represent laminates consisting of a number of repeating lamina (ANSYS Help Viewer 2013). It was shown by Nguyen et al. in a recent paper (Nguyen et al. 2016) that target numerical model discretized into sub-laminate enables the decoupling of out-of-plane tensile and shear failure modes, and provides a more accurate prediction of ballistic response of laminated composites.

The element types (or formulations) used to describe the materials can be done in a couple of different ways while using shell and/or solid elements. Solid elements generally give more

accurate results compared to shell elements but they require more computational effort in return. Moreover, the complexity of the model increases as the element formulation changes from shell to solid. The important point is to decide on the level of complexity required to solve the problem in the most efficient and accurate way. Software enables the identification of geometric models in 2D or 3D. When 2D (plane) geometry is used, all of the laminate properties can be identified as a stacked ply which includes the information for all layer materials, layer thickness, orientation, and stacking sequence. Shell elements are used in such cases, and even though it is computationally effective, the drawbacks are the lack of through-thickness delamination representation, the insufficient through-thickness stress propagation, and the inaccurate representation of 3D wave propagation caused by highly dynamic impact. Therefore, shell elements were ignored and solid element formulations were used in all of the models considered in this thesis based on the fact that through-thickness behaviour is important and the geometric scale of the model is not excessive.

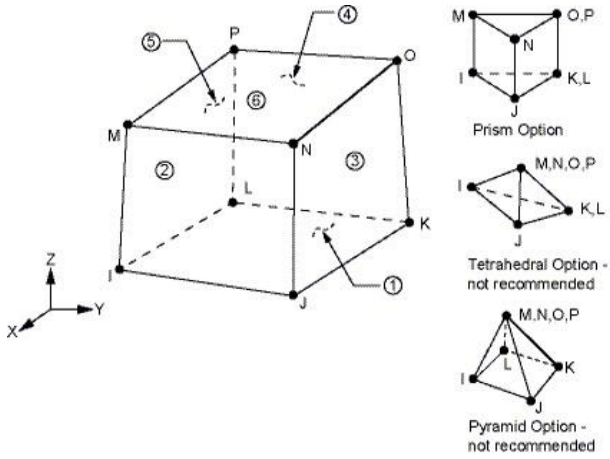

Figure 71 SOLID185 element: coordinate system, nodes, and geometrical variations (ANSYS Help Viewer 2013)

The element type used in the numerical modelling was three dimensional SOLID185 (Figure 71). This element is used to model solid structures and is defined by 8 nodes. The element has three degrees of freedom at each node allowing translation in x (*longitudinal or 1*), y (*transverse or 2),* and z (*through-thickness or 3*) directions. Different geometrical types such as prism or pyramid (Figure 71) are allowed as well even though some of these are not recommended because of the accuracy and stability concerns. Hexahedral type elements were used in this thesis for maximum accuracy. The element is also capable of capturing plasticity, stress stiffening, large deflections and large strains throughout the simulation.

It is well known that the outcome of the numerical methods depends on the quality and metrics of the mesh unless a parameter or algorithm exists to remove this dependency. It was reported in the literature for dynamic impact of similar studies to the current study that 1mm element mesh size at the impact location provides sufficient accuracy (Xin & Wen 2015). Element mesh size smaller than 1 mm was found to increase computation effort unnecessarily (Roth & Oudry 2009).

In the current study, meshing of the laminate/sandwich was done by dividing the edges into desired number of parts which resulted in rectangular mesh elements. Mesh size of 0.5 - 1 mm was achieved at the impact location in order to obtain sufficient results reported in Section 5.3. This mesh size provided an element aspect ratio between 1 - 1.1 at the impact point which is very desirable. At the far field geometry coarser mesh was used to save computation time.

4.3.6 Interface and contact modelling

The complete physical model of the system being questioned was achieved by creating thin solid bodies which represent each individual ply, then joining these plies together by a surface-to-surface contact definition to form the laminate/sandwich. The aim of using contact definition is to define the matrix layer in between plies and mimic the delamination behaviour arising from the matrix crack and failure between laminae. In ANSYS platform, there are two main methods to model the flow of the cracks and de-bonding mechanisms, namely VCCT-based (Virtual Crack Closure Technique) crack growth simulation, and Cohesive Zone modelling. Former of these techniques is based on the critical energy release rates in different types of separation: Mode-I, Mode-II, and Mode-III type delamination (Figure 72). The latter technique on the other hand, simulates the de-bonding according to the definition of the surface between joining bodies, via either interface elements or contact elements.

VCCT-based crack growth technique requires crack energy release rates in multiple directions and modes, hence it results in more experimental testing. In addition, this model needs a predefined crack path which is not conventional for the current work.

In Cohesive Zone (or elements) technique, existing contact pairs can be assigned a normal and shear stress criterion to simulate delamination response, and all modes of delamination (Figure 72) are allowed as well. Therefore, because of the practicality, simplicity and the fewer input parameters required this contact modelling was preferred in this thesis. This approach also helps avoid unnecessary computational effort and testing (critical crack energy release rate) in order

to characterise the structure for simulation purposes, hence saving effort, time and cost. It will be discussed in Section 5.3.1 whether this model is capable of providing a good validation with respect to experiments.

The elements used in contact surfaces are CONTA173 and TARGE170 (Figure 73). CONTA173 is a 4-node surface-to-surface contact element which can be used to represent contact, sliding, and the separation of bonded contact pairs to simulate delamination failure. TARGE170 is the associated surface target element for CONTA173, hence these two elements form a contact pair. The criteria used in these contact pair for de-bonding (or delamination) is the normal and shear stresses acting on the contact surface which can be obtainable by interlaminar shear strength (ILSS) tests (Section 5.1.2).

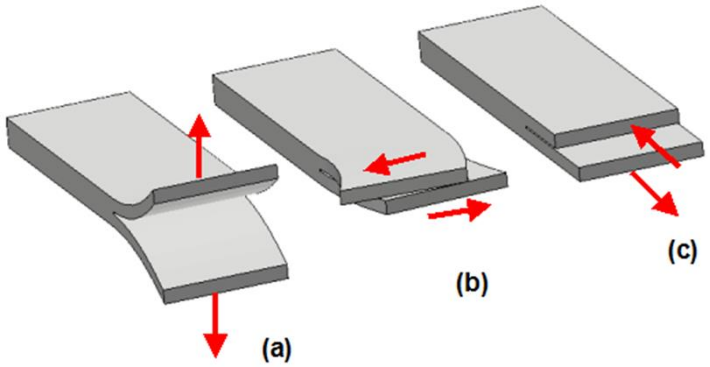

Figure 72 Delamination modes in a laminate; a) Mode-I (normal separation), b) Mode-II (shear separation), c) Mode-III (shear or mixed separation) (ANSYS Help Viewer 2013)

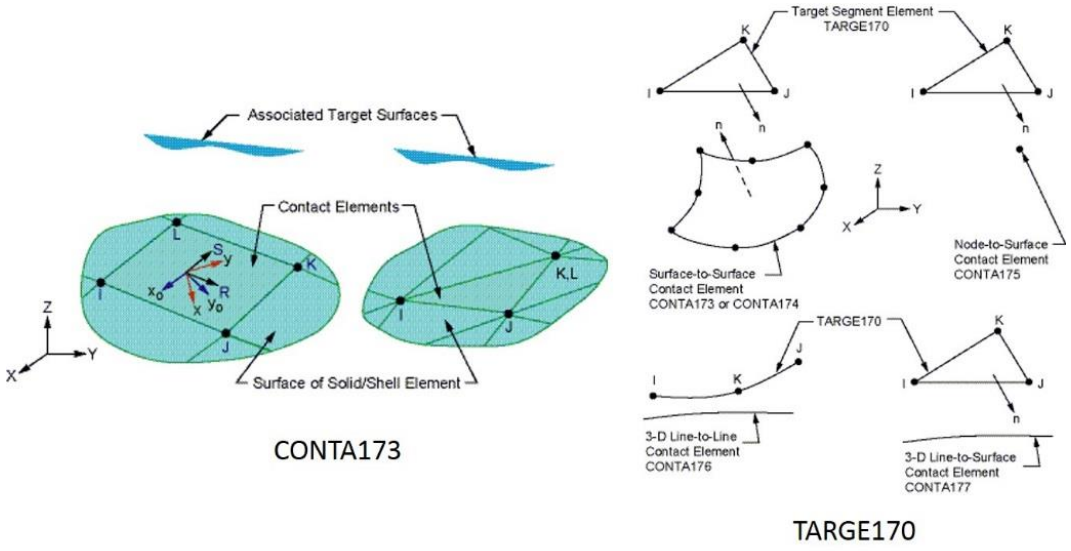

Figure 73 Contact elements; CONTA173 and TARGE170 (ANSYS Help Viewer 2013)

The interaction between bodies such as the punch and the laminate was defined as frictional contact with a friction coefficient of 0.25. AUTODYN recommended contact algorithm trajectory contact detection and penalty formulation were used between bodies. This contact definition is time efficient because it does not constrain the time step. In simple terms, the trajectories of faces of bodies are tracked and if an intersection occur between these faces or nodes then the contact is detected. Penalty formulation, supporting the trajectory contact, calculates a penalty force to push a penetrating node back to its place in order to help conserving linear and angular momentum. The numerical values of these contact parameters and formulations were selected in line with the recommendations of the software, and default values were used. These default values work for most of the systems and they are determined by performing many number of parametric simulations.

An important parameter for the contact of penetrating bodies in impact modelling is called erosion. An eroding contact enables the bodies to penetrate into each other while deleting excessively distorted elements and nodes from the bodies in order to provide a stable time step to the simulation. Erosion parameter was included to ensure a stable simulation time via the removal of excessively distorted elements and the effect of this parameter will be discussed in Section 5.3.1.

4.3.7 Definition of the numerical model

During the numerical model creation, efforts made to mimic the physical experimental setup as much as possible, however, restrictions were taken into account for the sake of time and computational efficiency. Such an example is the quarter modelling approach. If two perpendicular plane of symmetry of solid bodies exist as well as it does for the direction of loading, then it is possible to run the solution over a quarter model. The geometric model shown in Figure 74 is used with minor differences in most of the validation and analysis scenarios, unless otherwise specified.

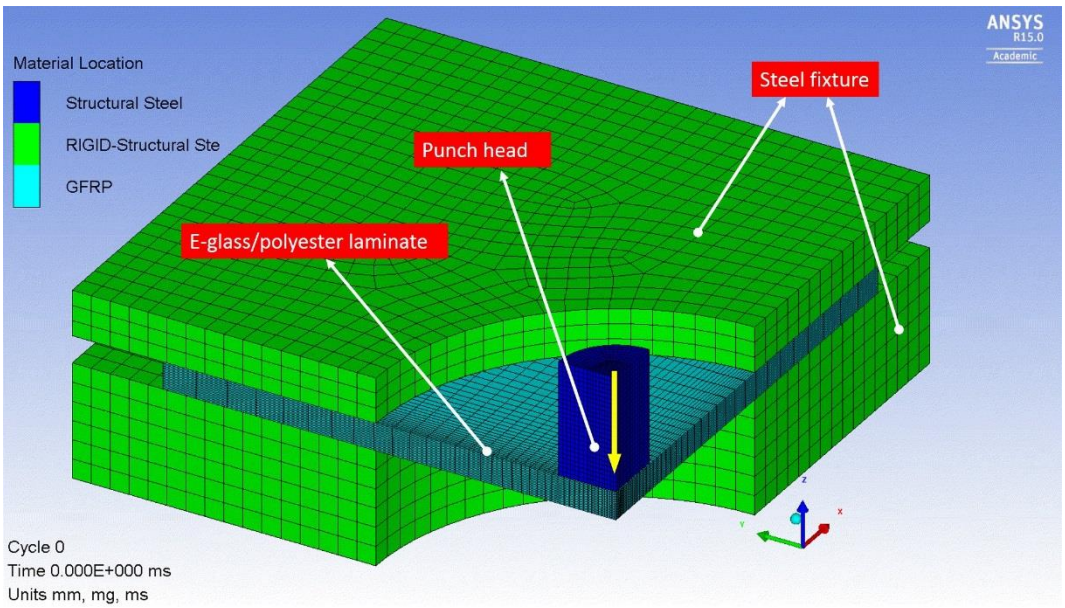

Figure 74 Numerical model used for QSPT and high velocity impact simulations. Quarter model is created in order to decrease computation time.

As mentioned in Section 4.3.5, the sub-laminate approach was proposed which consists of the stack of real-life representative fibre reinforcement layers. 6 mm thick GFRP laminate was created by bonding 10 plies of solid bodies (each 0.6 mm) with an interface between every ply using contact elements, defined by normal and shear stress failure criteria to simulate delamination. The same approach was applied to the sandwich plate numerical model as well. The contact between the fixture and the sample was modelled as a surface-to-surface bonded contact to represent no-slippage. The punch head and fixture were both modelled with steel material predefined in the software, and the fixture was modelled as rigid solid, while the punch was modelled as elastic solid.

Fixed support was applied to the fixtures, while a velocity value was assigned for the punch tip in the thickness direction. Every component was meshed with solid (brick) elements. Fine mesh was used around the punch tip while coarser mesh was used for the rest of the plate, and every ply was meshed with 2 elements in thickness direction, i.e. 20 elements in total through thickness. On average, the quarter model consists of 73635 elements in total, 32000 elements for composite laminate, 28800 contact elements, and 6850 elements for punch tip, respectively.

4.3.8 Notes on quasi-static simulations

It is desirable to simulate an event within its real natural occurrence time. However, it is impractical to do this in QSPT simulation cases without the necessary modifications in

modelling, because the time increments in an explicit dynamics analysis is at $1x10^{-10}$ s levels, which leads to millions of simulation cycles for a real-time-equivalent analysis. One of the ways to obtain logical results in a reasonable time period is to load the material with a maximum crosshead speed which doesn't exceed 1% of the wave (sound) speed of the material. With this method, inertial forces remain insignificant and do not affect results significantly and the first deformation mode of the structure in the QSPT case doesn't change. The typical wave speed of GFRP material is around 3 km/s, and 1% of this value is equal to 30 m/s. The quasi-static simulations presented in this thesis were carried out with 1m/s crosshead speed in order to obtain a good signal with low oscillation or noise.

Another technique to perform in a quasi-static simulation is called mass scaling. Section 4.3.2 explained the limit condition of the time step (CFL condition – Eqn. 1) in explicit analyses and showed that it is inversely proportional to the sound speed of the material, viz. inversely proportional to the stiffness-density ratio of the material (Eqn. 12). Therefore, introducing additional mass to the system enables to increase the time step of the solution. So basically, artificially increasing the density of the material will result in shorter simulation times.

$$\Delta t \propto \frac{1}{c} = \frac{1}{\sqrt{\frac{C_{ij}}{\rho}}} = \sqrt{\frac{m}{VC_{ij}}} \qquad \text{Eqn. 12}$$

In Eqn. 12, c is the sound speed of the material, C_{ij} is the material stiffness, ρ is material density, m is mass and V is the volume. Although this is a useful technique especially when dealing with larger scale models, it was not used in this thesis since the author is not experienced enough with this technique to obtain desired results. It should be noted that artificially introducing mass to the system could result in a change in inertial properties, leading to unrealistic or physically irrational results.

4.3.9 Notes on high velocity impact simulations

Determination of the impact velocity range relevant to this research has been made according to two factors. The first consideration is based on the UIC and GM/RT2100 standards (Table 2). These codes specify the testing velocity of the projectile as maximum operating vehicle speed plus 160km/h (44m/s). Considering the HST velocity in UK – 125mph (200km/h=55m/s), HST velocity in Europe – 300-360km/h (83-100m/s), and finally taking into account the possible advances in HST velocity in future up to 400km/h (111m/s) operating velocities, the corresponding velocity range could be limited in between 40-160m/s.

Another consideration is based on the flying ballast phenomenon, in which Jing et al. (Jing et al. 2014) reported that:

"*HSR operators worldwide suggest that ballast flight have appeared to occur at speeds above 260 km/h, which the wind speed is usually between 20- 30 m/s.*"

The authors concluded in the same study that most of the ballast particles – independent of size and shape- starts to move at wind velocities of 15-20m/s levels. A European HST travelling at max speed of 360 km/h (100m/s) can generate wind speeds of 20-30m/s, so it is possible that it can induce a ballast flight. The airborne ballast might strike to a passing train travelling in opposite direction, resulting in a collision velocity of 120-130m/s levels. Such a scenario can be seen in Figure 75 where French TGV trains were struck by ice fall. Even though it is not a ballast particle in this example, it proves that two passing trains could suffer from bilaterally induced objects.

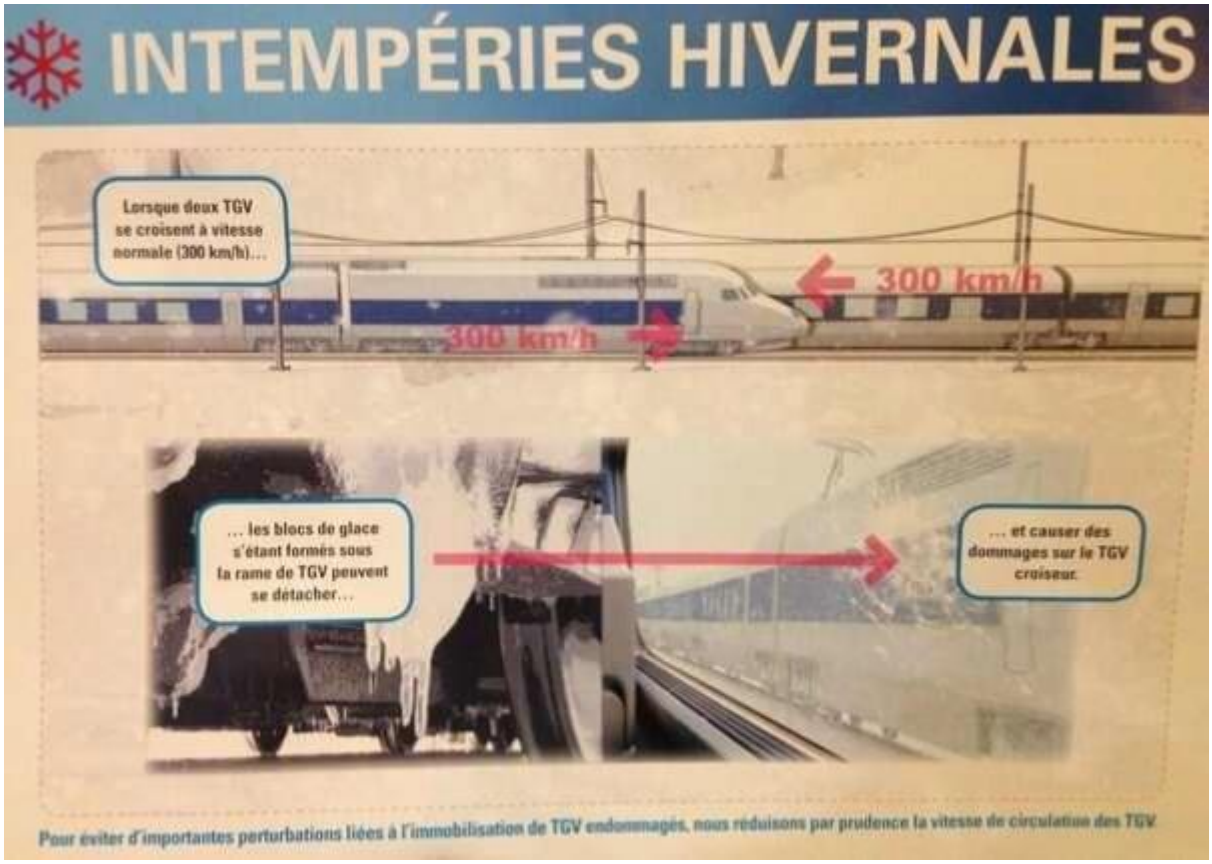

Figure 75 French TGV train subjected to hard ice strike from another passing train (REFRESCO WP7-D7.2 2014)

The literature review has shown that although projectile strike against both laminated and sandwich composites has been studied by many, it has been seen that the impactors with

particular size and mass in this PhD research was not common. The majority of the previous research on QSPT in literature studied the 12.7 mm punch which is too small for a ballast particle, therefore not very realistic. The reason behind the particular selection of projectile mass and dimensions is the consideration arising from the size of a ballast particle.

This rather greater size results in greater kinetic energy levels for the impactor, meaning that this energy level can easily be compared to high-velocity impact scenario, with higher strain rate loading effects. The size of the punch used in this thesis is within the range of minimum size of a ballast particle in various European countries.

It is practically irrational to make a clear decision for an impactor mass due to the probability and the randomness of impact. Indeed the track ballast has standardized specifications. However, the mass of a ballast has been reported as 60gr in some references and 200gr in other references (REFRESCO WP7-D7.2 2014; REFRESCO WP7-D7.3 2016). As the concept of this research is just the beginning, it is fair to consider a reasonable mass for the time being and a more extensive study could be carried out in the future. Therefore, the weight of the CF and H projectiles was decided as 100 g, based on the specifications of the impactors in the three considered standards; GM/RT2100 (250 g) > QSPT (100 g) > (NF-F07-101) 60 g > (EN15152) 20 g.

4.3.10 Result variables

The analysis of numerical model results was carried out with various contour plots exists in AUTODYN (Table 7). Particular attention was paid to the damage contours to check whether the failure sequence matches with experiments. In addition, the stress values were plotted to identify and validate the responsible failure modes. As for the delamination failure, BOND STATU variable was plotted and compared with experiments.

Variable name	*Contour plot*	*Value*
Stress/Strain	STRESS(*ij*) – STRAIN(*ij*)	Variable
Damage/failure	DAMAGE (*ij*)	0 (intact) – 1 (fully damaged)
Delamination	BOND STATU	0 (bonded) – (-1) (fully separated)

Table 7 Results variables in AUTODYN (ANSYS Inc. 2013)

4.4 Determining the strain rate dependency

When an FRP material is subjected to loadings in a very short amount of time, they exhibit large amounts of strain depending on the magnitude of loading. This rapid loading affects the material properties negatively or positively. Although not every structural composite is sensitive to different rate of loadings, glass fibre composites are well known as strain rate sensitive materials. Thus, it is important to take into account the strain rate effects for intended applications. A literature review on strain rate dependency of composites revealed that many different test rigs (drop weight, hydraulic/pneumatic, explosive/expanding, pressure bar, flyer plate) and loading conditions (tensile, compression, shear, and interlaminar properties) were studied by researchers. Table 8 summarises the notable findings from the literature review with respect to varying strain rate testing conditions (all of the findings are with respect to increasing strain rate). The evidence presented in the table suggests, although a general trend exists that higher strain rate loading results in an increase in mechanical properties, it is not practical to identify a common or clear enhancement level (*ENL*) – given the wide range of material configurations and testing methods. In addition to the studies shown in Table 8, various other authors reported a general increase in material properties with respect to increasing strain rate (Newill & Vinson 1993; Pintado et al. 1993; Harding 1993; Jenq & Sheu 1993; Powers et al. 1995; Saka & Harding 1990).

However, the degree of enhancement – so to say – is more obvious for glass FRPs compared to carbon/graphite counterparts. Powers and co-workers (Powers et al. 1995) reported their findings from compressive pressure bar tests on graphite/epoxy composites where the ultimate strength, elasticity modulus, and strain energy density to failure in all three principal directions showed rate insensitive behaviour. This behaviour was attributed to the brittle nature of the graphite. On the other hand, (Wang 1995) observed that E-glass fibre bundles are rate sensitive so that higher loading rates indicated a transition from brittle to ductile behaviour.

Specimen	***Test method & Conditions***	***Findings***	***Reference***
E-glass/epoxy - UD & CP S-glass/epoxy - UD	Drop weight - up to 6.8m/s impact velocity	Energy absorption is rate dependant, up to 40% increase in failure strength	(Broutman & Rotem 1975)
E-glass/epoxy - UD & 7 different angle ply	Drop weight - up to 4.2m/s impact velocity	25% Failure strength increase	(Lifshitz 1976)

Glass fibre/polyester, Glass/fibre epoxy	Dynamic 3-pt bending - up to 80/sec loading rate	Increased flexural and shear strength, greater rate effects for polyester compared to epoxy	(Boukhili et al. 1991)
Glass/Epoxy - woven and UD	Tensile test - High strain rate loading up to 160 Hz	Up to 50% increase in tensile strength, however no significant change in Tensile modulus, 400% increase in toughness	(Ou & Zhu 2015)
Glass/phenolic - UD, Satin weave, multiaxial Glass/polyester - Mat, rowing, continuous	Tensile test - Strain rate loading up to 6 Hz	Increase in tensile modulus, tensile and shear strength properties	(Barré et al. 1996)
S-glass/epoxy	Tensile test - Strain rate loading up to 500/sec	Up to 50% increase in tensile strength, decrease in average failure strain	(Armenakas et al. 1973)
Carbon/epoxy angle ply, Carbon/glass/epoxy angle ply	Expanding ring tensile test up to 300/sec strain rate loading	Significant increase in transverse modulus (300%) and strength (200%), while very little increase in longitudinal modulus (30%) and strength (negligible)	(Daniel et al. 1995)
Carbon/epoxy	Explosive compression test	Similar response in longitudinal direction compared to static loading, 50% increase in transverse strength	(Daniel & LaBedz 1983)
Graphite/epoxy	Various high strain rate testing - up to 150/sec	Significant increase in transverse modulus and tensile strength, moderate increase in transverse compressive strength, small effect on interlaminar properties.	(Daniel et al. 1980; Daniel et al. 1982; Daniel & LaBedz 1983)
Glass - aramid - carbon fibre reinforced angle ply tubes	Explosive tensile test - strain rate up to 150/sec	Negligible effect in strain rates below 20/sec, strength increase in strain rates 100/sec and above	(AI-Salehi et al. 1989)
E-glass/epoxy - UD, quasi-isotropic Graphite/epoxy - UD, quasi-isotropic	SHPB Compression test - strain rate up to 400/sec	Increase in ultimate strength, decrease in time-to-fracture	(Choe et al. 1988)
Graphite/epoxy, Carbon/glass CMC - UD, CSM	SHPB Compressive test - strain rate up to 2000/sec	Decrease in ultimate stress for graphite/epoxy, increase in ultimate stress for CMC composites	(Frey, Vinson & Prewo 1991)
Glass/polyester	Pressure bar test - strain rate up to 2000/sec	Yield and ultimate stress levels observed together at strain rates less than 754/sec	(Frey, Vinson & Hall 1991)

Graphite/PEEK - X ply	Drop tower - strain rate of 8/sec	42% increase in strength, 25% increase in failure strain	(Montiel & Williams 1992)

Table 8 Strain rate effects on various laminated composite configurations

In general, the available literature highlights the importance of the strain rate dependant nature of the FRP materials. Therefore, strain rate effects should be considered for the intended application. In the absence of available experimental testing, for the present study, modification of the material properties for high-strain loading was made in the light of all the previous research in the literature, and in particular (Armenakas et al. 1973; Zhou & Davies 1994; Gama & Gillespie 2011).

Armenakas and Sciammarella investigated the strain rate dependency of S-glass fibre/epoxy resin laminated specimens subjected to tensile loading along fibre direction up to 30.000 in/in/min rate of strain (Armenakas et al. 1973).

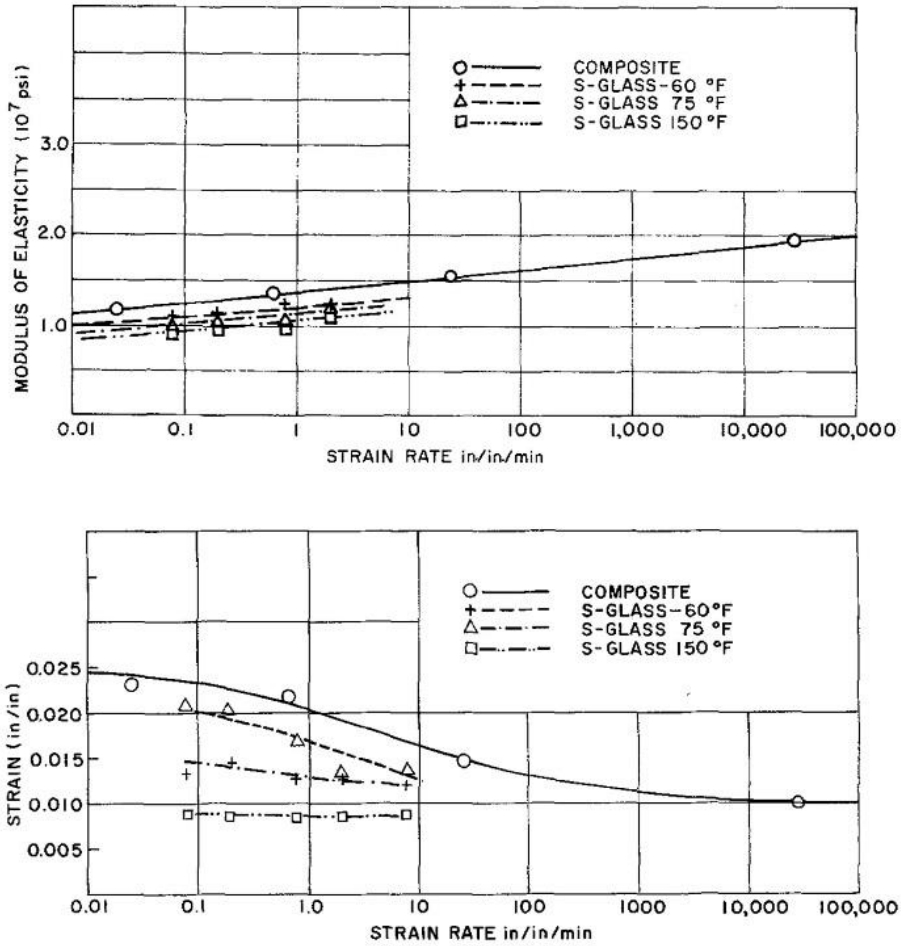

Figure 76 Effect of strain rate on individual fibres and composite laminate: (left) elasticity modulus, (right) average strain (Armenakas et al. 1973)

High strain tensile tests were carried out by a specially built rig and mechanical properties were compared with quasi-static tensile loading results in terms of failure mode, ultimate load, and corresponding strain levels. The authors observed considerable increase in the number of broken fibres which occurred below ultimate failure load and in random areas of the specimens in higher strain rate loadings. Accordingly, the results have shown linear stiffness behaviour up to ultimate failure, and an increase in modulus while decrease in average strain over the testing range (Figure 76).

On the other hand, Gama and Gillespie obtained good ballistic performance prediction by enhancing the material properties (via numerical parameter) such as all material strength levels, shear moduli and through-thickness elasticity modulus, and as well as the transverse modulus of the laminates. One common thing in (Gama & Gillespie 2011) and (Zhou & Davies 1994) is that the impact energy ranges for the dynamic impact cases are 17J-4500J and up to 1500J, respectively. This information which was also backed by numerical means suggests that it is rational to apply 30-50% increase to the static material properties in order to obtain more realistic prediction on dynamic loading response.

In addition to the major material properties, interface strength values were increased as well. Naik and co-workers carried out shear tests with Torsional Split Hopkinson Bar (TSHB) at high strain rates (up to 1000 /s) on plain weave carbon/epoxy and E-glass/epoxy thin walled specimens (Naik et al. 2007). Their findings suggest that interlaminar shear strength is enhanced under higher strain loadings compared to quasi-static testing (Figure 77). Evidently the enhancement was similar for both carbon and E-glass fibre composites. This is probably the case caused by the use of epoxy matrix in both specimens, and usually matrix cracking strength is responsible for the interlaminar shear. Similar behaviour was reported by Lataillade and co-workers as well (Lataillade et al. 1996).

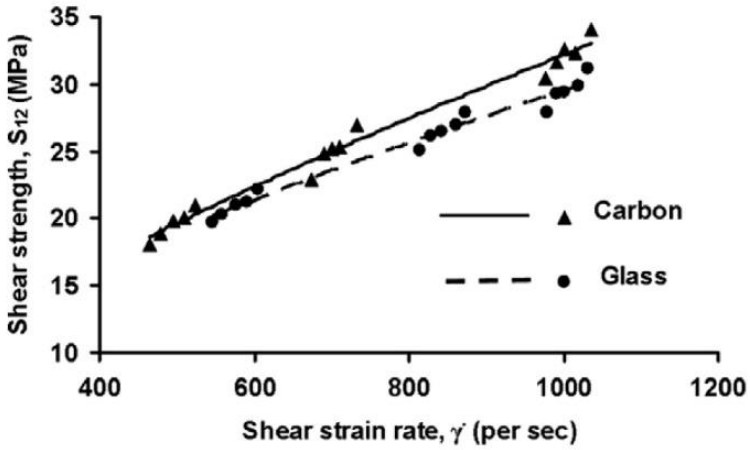

Figure 77 Enhancement of interlaminar shear stress under high strain rate loading (Naik et al. 2007).

In AUTODYN, the influence of strain rate effects can be included by modifying the plasticity parameters a_{ij}. Figure 78 shows how the slope of the stress-strain relationship (elasticity modulus) is affected with respect to various a_{11} values. Therefore, a_{ij} will be addressed as strain rate modifier in this thesis. Two level of enhancements was considered for this study: 30% and 50% increase in material properties. a_{11}=0.7 value represents the static material property, while a_{11}=1.2 value results in 30% increase in static properties (Gama & Gillespie 2011; Zhou & Davies 1994), and a_{11}=1.55 represents the 50% increased material properties (Ghalami-Choobar & Sadighi 2014; Hoo Fatt et al. 2003; Armenakas et al. 1973).

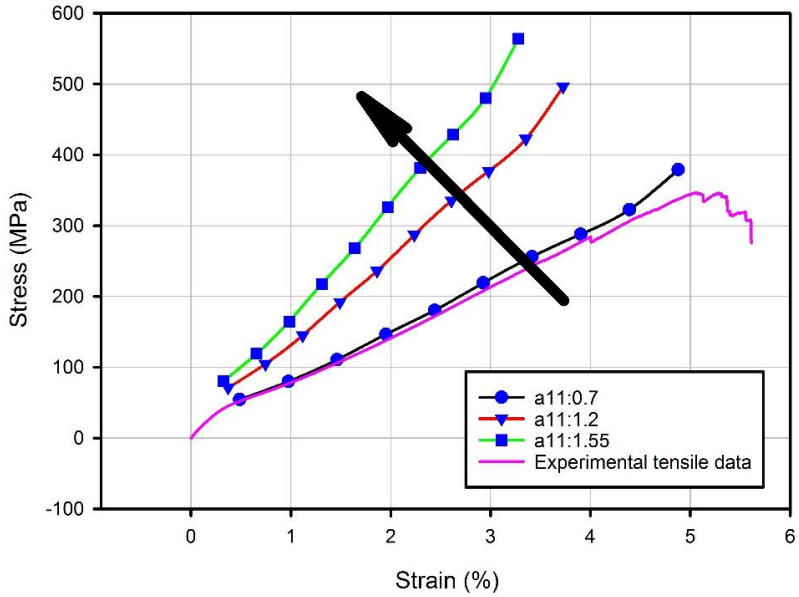

Figure 78 Strain rate effect: a11 is the plasticity parameter in fibre (1) direction. Increasing values of a11 results in enhancement in fibre direction elasticity modulus and tensile strength.

It is definitely more appropriate and rational to consider the strain rate effects in numerical models, however, it is not sufficient and realistic to carry out such an approach without a control mechanism. In the end, the question arises: how to decide if the enhancement level (*ENL*) is accurate? For this reason, in order to provide a control mechanism and to evaluate the accuracy of the strain rate enhancement level, analytical models from the literature relevant with impact on composites were used. Three analytical models: one ballistic limit (V_{BL}) prediction and two penetration models (impact velocity (V_I) vs residual velocity (V_R)) will be described in the next section.

4.4.1 Wen's ballistic limit velocity prediction model

Wen generated simple perforation equations for FRP composite laminates and foam core sandwich composites under different impact velocity range and impactor nose shapes (ogival, conical, flat, and hemispherical) (Wen 2000; Wen 2001). The author stated that the resistance of the material can be divided into two parts, which are quasi-static resistive pressure and dynamic resistive pressure. These equations are functions of penetration depth and based on wave-propagation after impact which shows that the damage is localised. The results obtained by the proposed equations (Eqn. 13) were reported to be in good agreement with experimental tests. This approach was also verified with finite element analysis in a further publication by Wen and co-authors (He et al. 2008).

The equation to predict ballistic limit velocity is:

$$V_{BL} = \frac{\pi\beta\sqrt{\rho_t\sigma_e}D^2T}{4G}\left[1+\sqrt{1+\frac{8G}{\pi\beta^2\rho_tD^2T}}\right] \qquad \text{Eqn. 13}$$

Where;

V_{BL} : Ballistic limit velocity,

β : Parameter for projectile profile, default: 2 for flat ended, 1.5 for hemispherical ended.

ρ_t : Density of the target material,

σ_e : Elastic limit stress of target material in through-thickness direction,

D : Projectile diameter,

T : Target thickness

G : Projectile mass.

Wen introduced the compression elastic limit (σ_e) in thickness direction to the analytical model as an input, considering that in the early phase of an impact event high inertia forces result in hydrostatic compression forces. Although this rationale is correct, it is not entirely accurate. When we look at the flat ended projectile punch test, it was observed that the area contact was lost during the loading, instead the load was applied through the circumference of the punch, hence line contact (Figure 79). This finding is consistent with what was reported by Choi and Chang (Choi & Chang 1991). So the effect at the contact area is shearing rather than pure compression. According to this observation, the maximum shear force obtained from SPR1.2 test was used to calculate ballistic limit velocity.

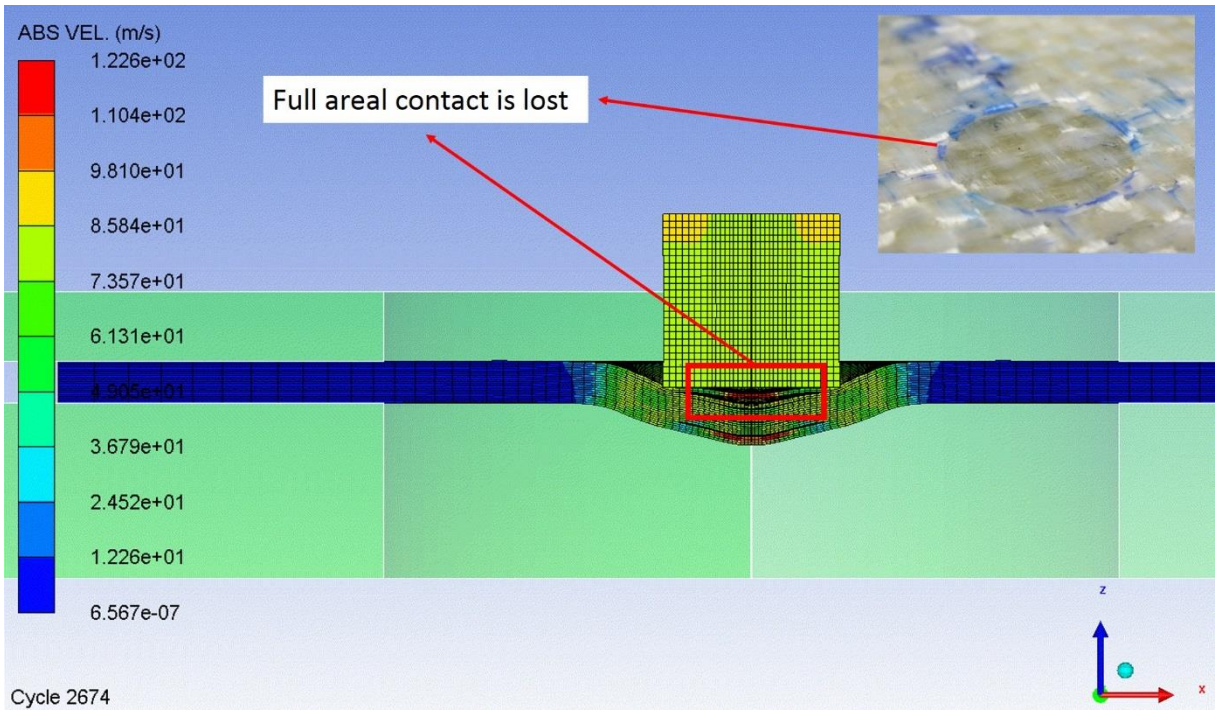

Figure 79 Loss of area contact during static experiment and HVI simulation

It is not uncommon to use modified model specific parameters according to the needs of individual studies. Such an example was presented in the work of Jordan and Naito as they obtained more accurate results while using different β values (Jordan & Naito 2014). However, the authors failed to include the correct elastic limit property in their work. Their calculation takes into account the in-plane compression elastic limit of laminate which should have been out-of-plane elastic limit. Though it is possible that they might have used the in-plane property in the absence of particular adequate property. Nevertheless, their detailed study proves that penetration model parameters should be adapted accordingly for independent studies. In this study, the selection of empirical parameters for Wen's model was done by following the

guidelines of the author, together with the information from similar studies available in the literature.

Wen proposed the β parameter for conical nosed projectiles as well, however impact of conical nosed projectile was not performed in the scope of this thesis. The reason is, gravelling and ballast impact requirements incorporates the use of conical projectiles which has relevant cone angles (θ) of 90° and 105°, respectively. The parameter β for conical tip was defined as 2Sin($\theta/2$) in (Wen 2000), resulting in 1.41 and 1.5 respectively, which is almost the same as original β parameter for hemispherical nose shape. In addition, as Wen stated in the same study that "*To a first approximation, the formula obtained for hemispherical-tipped indenters is applicable to conical-nosed punches.*" Supporting this, Mines et al. reported that conical and hemispherical indenters give similar penetration characteristics for GFRP laminates (Mines et al. 1999). Therefore, this case will be discussed in Chapter 6 if this assumption is sufficient or not.

4.4.2 Ballistic penetration models

Two analytical models from the literature were used to evaluate the residual velocities of the projectile in complete penetration cases. The first model considered was Lambert & Jonas model (Eqn. 14) which is sufficiently simple and was also considered by any in the field (Lambert & Jonas 1976). Stating a more flexible model was needed, the authors improved the simple ballistics model by introducing the parameter p, of which the value close to two was found satisfactory.

Lambert-Jonas (L&J) penetration model is described as:

$$V_R = \left(\beta\left(V_I^p - V_{BL}^p\right)\right)^{1/p} \qquad \text{Eqn. 14}$$

Where

V_R : Residual velocity,

β : Curve fitting parameter: slope of the function, $0 < \beta \leq 1$

V_I : Impact velocity,

V_{BL} : Ballistic limit velocity,

p : Curve fitting parameter: shape factor controlling the slope of function.

The second model considered in this thesis was presented by Haque and Gillespie. The authors reviewed the previous classic ballistic limit analysis models including (Ipson & Recht 1963; Ipson & Recht 1975; Giere 1964; Lambert & Jonas 1976) and reported that although these models were and still are quite successful, they fail to include conservation of momentum and energy at the same time (Haque & Gillespie 2015). Therefore, they presented a new penetration equation model (Eqn. 15) that satisfied the previous weaknesses.

$$V_R = ((V_T^{max})^2 + \beta^*[\xi V_I^2 - V_{BL}^2])^2 \qquad \text{Eqn. 15}$$

Where

V_R : Residual velocity,

V_T^{max} : Jump velocity at ballistic limit, default can be assumed $V_T^{max} = 0.10\ V_{BL}$

β^* : Model parameter,

ξ : Model parameter, can be assumed as 1

V_I : Impact velocity,

V_{BL} : Ballistic limit velocity.

Different than the others, the authors considered the velocity of the projectile as a sum of target velocity in contact with the projectile, and relative velocity of the projectile with respect to the target in contact. Previous ballistic data was fitted to the new equation to determine the model parameters. As a result, the new model was found satisfactory to predict ballistic impact behaviour both in penetrating and non-penetrating scenarios. The jump velocity (V_T^{max}) encountered in experiments (Figure 80) was successfully predicted as well, which represents any anomaly in the target or small differential kinetic energy that causes a jump in the residual velocity at and around ballistic limit which is a common phenomenon in the literature. This model, along with L&J model, was used in this thesis to investigate residual velocity curve obtained from the simulations to determine whether the results are acceptable. The model parameters were decided following the guidelines of both studies (Table 9): V_T^{max} is the jump velocity at ballistic limit, a default value can be taken as V_T^{max}= 0.10V_{BL}, β^* and ξ are the model parameters - for all practical purposes $\xi \leq 1$ can be assumed.

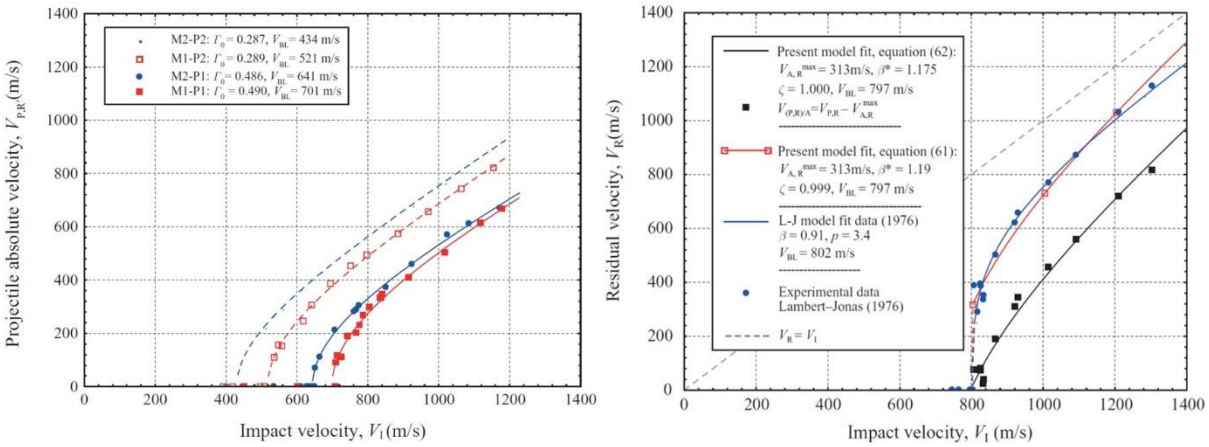

Figure 80 Predictions by the Haque & Gillespie model (M1-2: materials, P1-2: projectiles). Right figure shows the successful prediction of jump velocity.

	Lambert-Jonas model		***Haque-Gillespie model***		
Projectile	β	p	V_T^{max}	β	ξ
Circular flat	0.999	2.25	9.4	0.999	1
Hemispherical	0.998	2.08	8.4	0.98	1

Table 9 Penetration model parameters used in this study

Chapter 5. Experimental and numerical investigation of the impact response prediction method

Following the hypothesis of this research and the explanation of the proposed methodology, this chapter presents the experiment results of and the finite element analysis before validating the methodology in relation to the railway related impact risks.

5.1 Materials characterisation

This section describes the methods used to characterize the materials in this research in accordance with relevant standards, and presents the results of those experiments. Table 1 in Section 2.1 summarized the test methods for polymer matrix laminated composites with ASTM and ISO/EN standards. It can be seen from the table that many different tests must be performed to fully characterize a specific material system. However, it is more practical to identify the needs of the intended application then decide which properties are crucial and which properties are not necessary. For example, the in-plane compression and through-thickness tensile properties are rarely significant in most impact applications, therefore they can be neglected. For the present study, in-plane tensile and through-thickness shear resistance are of major importance and therefore the materials were characterized in this respect. Results of these tests were compiled and reported at the end of Section 5.1.3 for the sake of collectiveness.

5.1.1 In-plane tensile properties

Tensile tests were carried out in accordance with the ISO 527-1 and 4 standards in order to measure the elasticity modulus, tensile strength, and tensile failure strain properties in fibre direction.

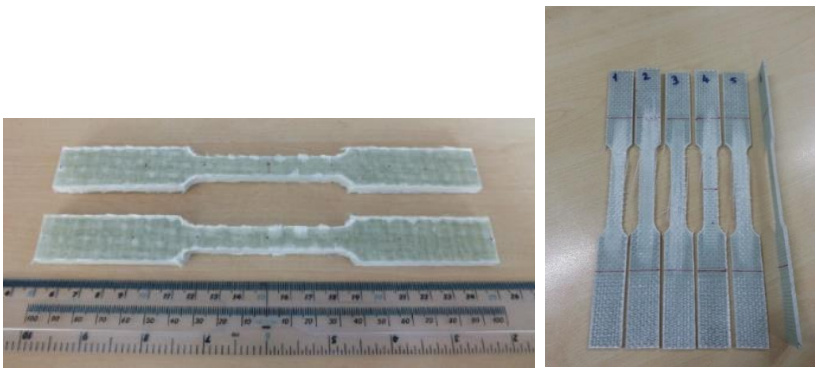

Figure 81 Dog-bone tensile test specimens for characterisation of: intact E-glass/polyester laminated plate (left) and tested E-glass/epoxy sandwich facesheet (right)

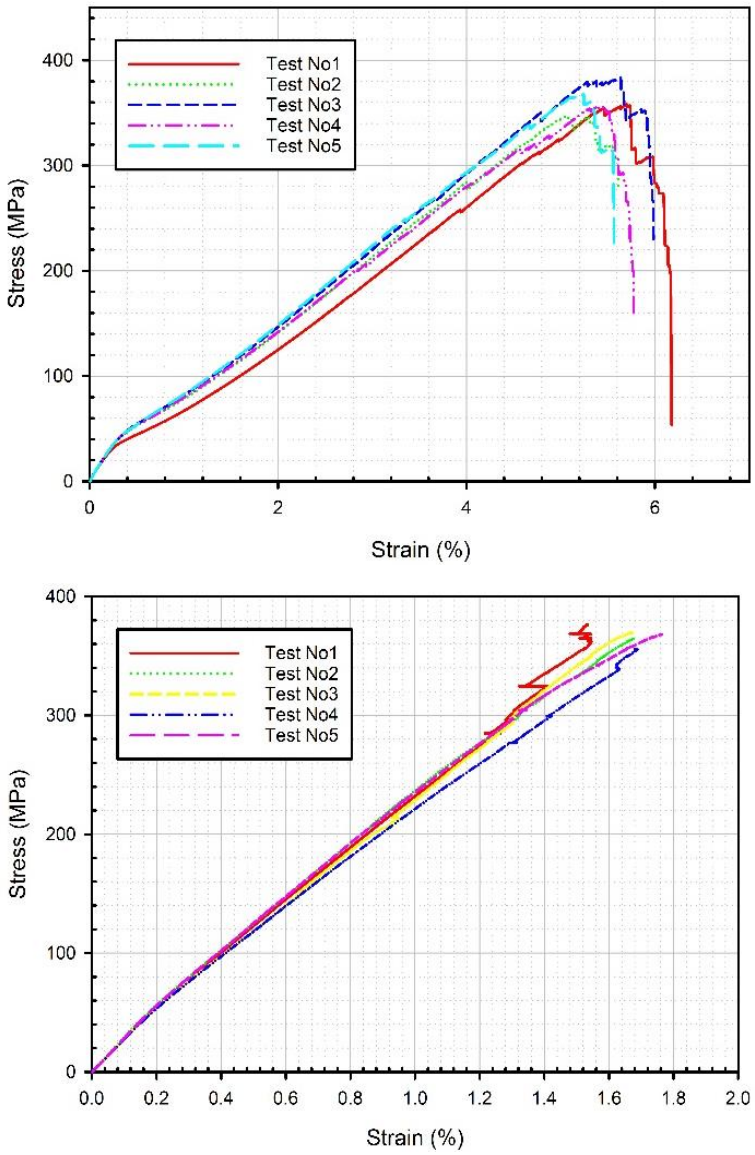

Figure 82 Tensile test results for E-glass/polyester laminates (top), and E-glass/epoxy sandwich facesheet samples (bottom)

The plain weave structure of the glass fabric (0° and 90° orientation in the same layer) supports the assumption that the laminates have quasi-isotropic in-plane properties, i.e. same properties in fibre (1) and transverse (2) direction. Therefore, tensile properties were analysed as "in-plane", rather than separate longitudinal or transverse properties. This is a common practice while carrying out numerical model analysis. Dog-bone shaped specimens were used in the tests for both laminated and sandwich facesheet samples (Figure 81) to initiate the failure in initial gauge area. An extensiometer was used to measure the strain levels during tensile tests. Sample dimensions were 200x20x6 mm for both E-glass/polyester and E-glass/epoxy laminates, and each fabric ply laid in the same orientation which resulted 0° being the *x (longitudinal)* direction and 90° being the *y (transverse)* direction, respectively. It can be seen

from the (Figure 82) that all the tests were consistent with each other and no abnormal case was observed. Towards the end of the test, the deviation increases as a results of the relative random deformation such as matrix cracking and delamination. Since the laminates were manufactured by hand lay-up method, this level of deviation was acceptable and similar results were reported in the literature as well. In all five tests, the samples exhibited predominant delamination before the major load carrying capability loss, and subsequently fibre rupture at major failure and during softening (Figure 83). As usual, the elasticity moduli of the samples were obtained from the slope of the early part of the graph – between 0.0005 and 0.0025 strain, and the tensile strength was calculated as average value of all individual tests.

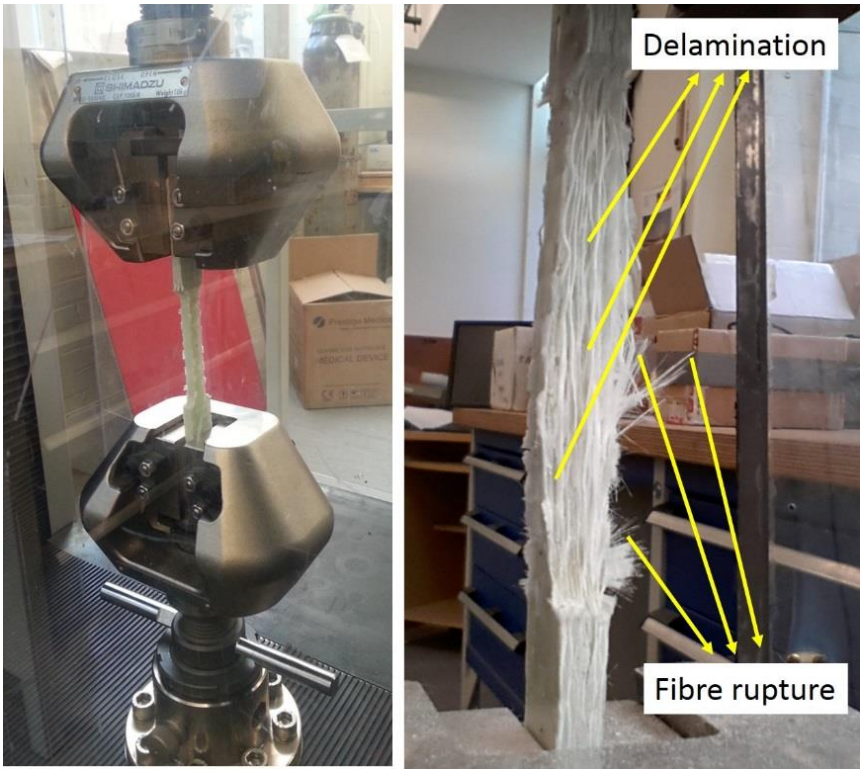

Figure 83 Tensile test setup (left) and failure modes of GFRP at the end of the test (right)

5.1.2 Inter-laminar shear strength (ILSS)

To determine the interface strength between plies of the laminate, inter-laminar shear strength test method was carried out in accordance with ISO 14130 standard. This characterisation method is basically a 3-point bending test but rather than using a conventional long beam specimen, a short-beam sample (Figure 84) is used. The short-beam sample is loaded vertically from the middle while the back face is supported by cylindrical elements as seen in Figure 84. Throughout the test the load-displacement relationship is tracked and the maximum load value before the first clear non-linearity is recorded to calculate the inter-laminar shear strength. This

test was needed in order to provide the ILSS as an input to the numerical model when the contact elements are used to model delamination behaviour.

ISO-14130 standard describes how to calculate the interface strength with the equation below (Eqn. 16);

$$\tau = \frac{3}{4}\frac{F}{bh} \qquad \text{Eqn. 16}$$

Where F is the failure load in (N), b is the width, and h is the thickness of the samples in (mm). Sample dimensions were identified based on 6 mm thickness which complies with the standard, resulting 30 mm width and 60 mm length for each sample. Since samples was cut from laminated plates, they had the same configuration as the laminates in terms of fibre and resin material and configuration.

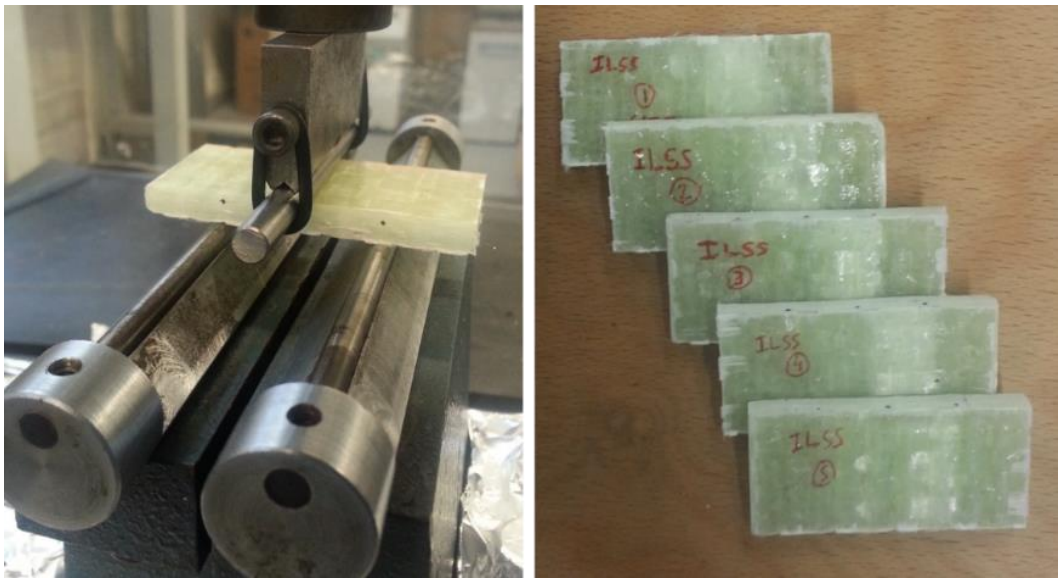

Figure 84 Inter-laminar shear strength (ILSS) test setup and tested samples showing the similar stress concentrations (whitened areas) at around loading point.

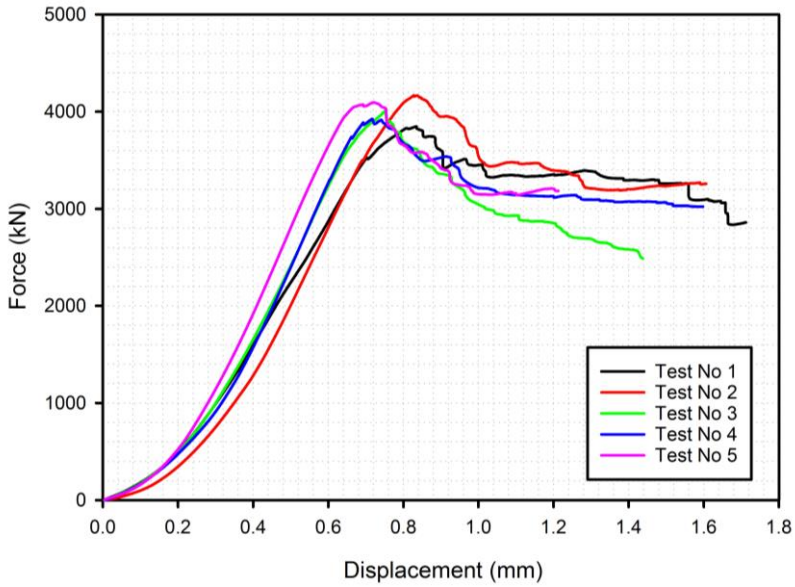

Figure 85 Results of ILSS tests of laminated GFRP plate samples

Figure 85 shows the results of repeated tests with this method which were consistent. Based on the average failure load values, 17 MPa was calculated as ILSS by using the (Eqn. 16). It should be noted that during the tests delamination should be the first failure mode, indicating the first load drop. This means compression failure at the loading or support members, or tensile failure at free reverse surface are not acceptable. This condition was ensured for all the tests samples in current study.

5.1.3 Through-thickness shear properties

It has been mentioned that this research evolved around the through-thickness performance of the composite materials. Therefore, to determine the out-of-plane (OOP) properties, a test setup was used in a way to initiate pure shear failure at the loading point following the assumption that the failure would be localised around the projectile in high velocity impact.

This approach reveals the resistance and strength of the material against this specific loading condition. A similar application was considered by Clegg and co-workers for material characterisation (Clegg et al. 2006), and it was demonstrated by Gama as well (Gama & Gillespie 2008) that pure shear strength of the fibre reinforced laminates could be obtained via SPR values between 0-2. The setup used in this test was a smaller version of the QSPT setup (Figure 68) which has a circular opening of 31.6 mm and uses a circular flat punch head with 25.4 mm diameter, resulting in span-to-punch ratio of 1.2 (SPR1.2). Since OOP flexibility/bending of the laminates were restricted a great deal, the delamination progression

was fairly confined. Therefore, 100x100 mm samples were found sufficient for this test. Figure 86 shows a sample tested with this setup and then sectioned in half to prove that the failure was shear predominant.

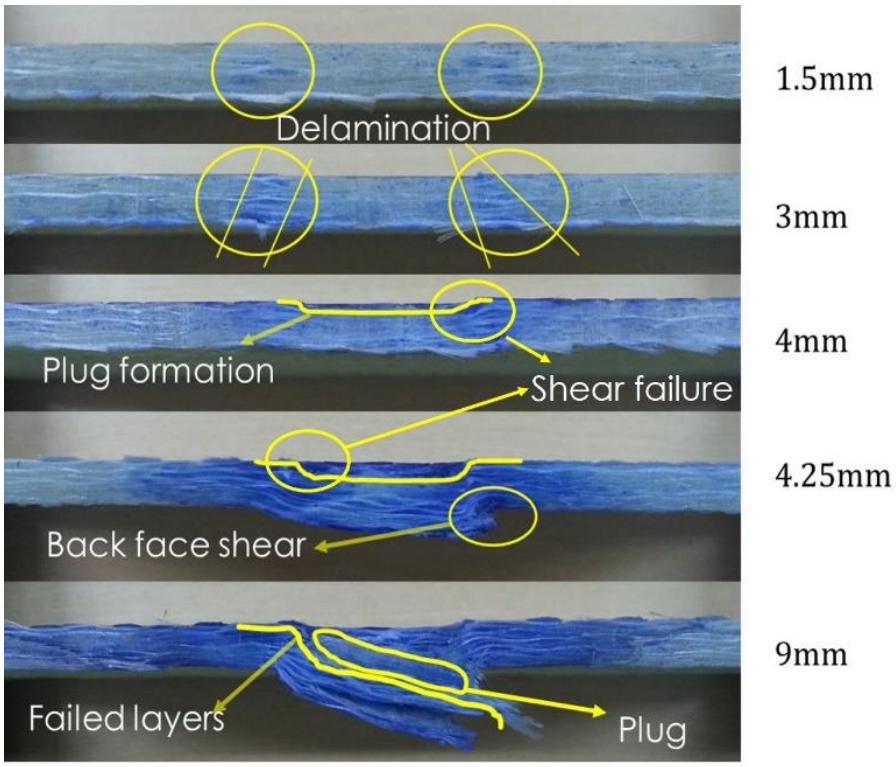

Figure 86 Quasi-static punch test to determine through-thickness properties of the laminates showing the shear predominant failure modes observed after each crosshead displacement value of 1.5 mm to 9 mm

Figure 87 was taken from the tests with a flat and a hemispherical ended punch and depicts the stepwise testing (Section 4.3) in order to capture the failure sequence. Based on the load change of a fully pierced sample, a new sample was loaded and taken out after each load change. Afterwards, the sample was sectioned in half and dipped in blue dye to ease the visual inspection. Tests showed that the failure shape at the reverse face appeared as a circle rather than a cross (which a tensile failure would display). A hemispherical ended punch was also considered to investigate whether the failure mode was specific to the flat punch. Figure 88 depicts the impact and reverse face failures of loaded laminates. The reverse face shear failure (Figure 88 left)) was observed independent of punch profile, while in hemispherical loading (Figure 88 right) a compressive type crush failure caused by point contact was observed. However, it was observed from the tests that the crush failure occurred almost at the same time as the reverse face shear failure occurred.

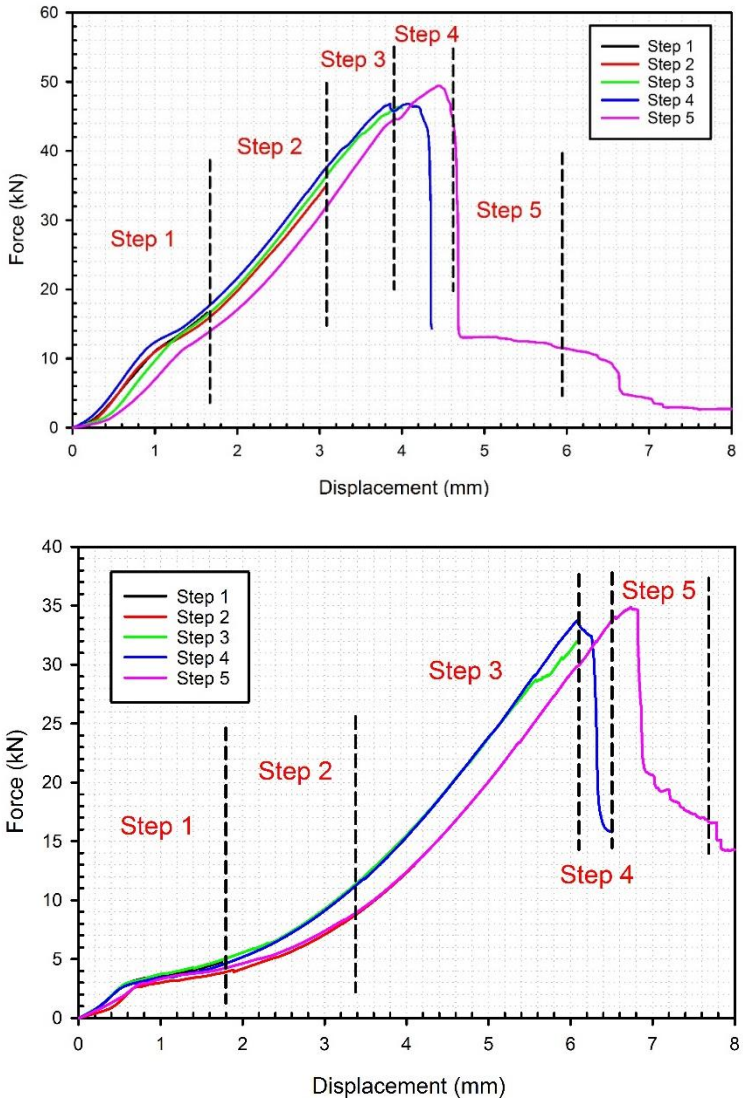

Figure 87 Stepwise testing in SPR1.2 - CF setup (top) and SPR1.2 - H setup (bottom). The end of each line indicates a separate test

Based on the SPR1.2 test program, the out-of-plane (OOP) shear strength of the laminates (S_{13}=S_{23}) were calculated by using Eqn. 17 below:

$$S_{23} = S_{13} = \frac{F_{max}}{2\pi rt} \qquad \text{Eqn. 17}$$

Where S_{13} and S_{23} are the through-thickness shear strength in 13 and 23 planes, F_{max} is the maximum failure force obtained from the experiments, r is the radius of the flat ended punch, and t is the thickness of the laminate. This calculation is based on the fact that the load is applied through the circumference of the punch (Section 4.4.1). The Eqn. 17 yielded 97 MPa shear strength for E-glass/polyester laminates, and 95 MPa for E-glass/epoxy sandwich laminates.

Thus, these observations show that the punch profile does not influence the responsible failure mechanisms. The failure sequence during this test is in the next section and Table 10 summarises the findings. Similar failure sequence was observed with hemispherical punch loading except the crush type failure at the impact side. For this reason, Table 11 was given to describe the failure sequence of hemispherical punch loading for brevity. In addition, delamination response in these setups were also analysed in Section 5.2.3.

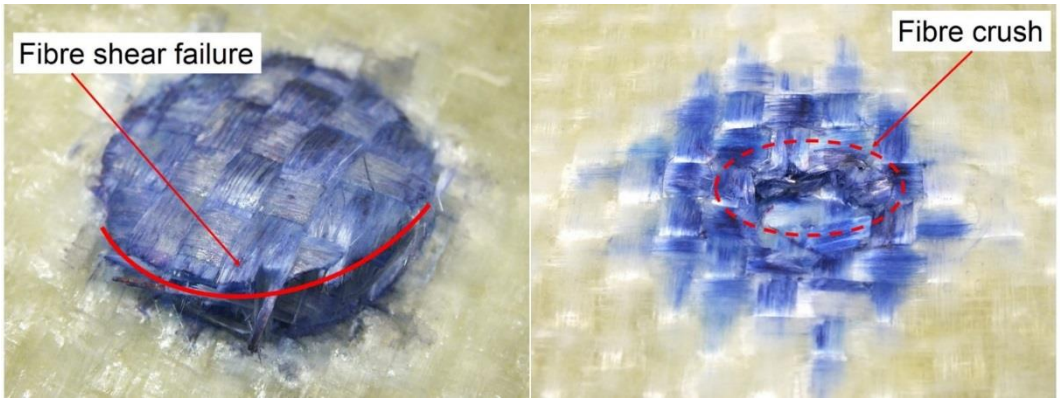

Figure 88 Shear failure at the reverse face (left) and fibre crush at the impact face (right) after SPR1.2 tests

1.5mm displacement: No fibre or matrix failure occurred at the contact and reverse side. Due to the shape of the punch (CF) and fixture ring, a circle shape was visible on both sides as stress-whitened areas (Figure 89). This indicates that the load was applied through the circumference of the punch, rather than the whole area because the portion beneath the punch tip undergoes bending and thus the surface-to-surface contact was lost.

3mm displacement: No major fibre and matrix damage was observed on either side, but the shape of the punch became more visible on the contact side.

4mm displacement: Fibre shear failure started at the contact side and formation of shear plug under the punch began at this step (Figure 89). On the reverse side, a slight bulge was present due to the plug formation, indicating the change in the force value in the force-displacement graph (Figure 87 top).

4.25mm displacement: The displacement of the plug inside the laminate was observed clearly from the contact side, showing multiple layers had suffered from shear fibre failure (Figure 89). On the reverse face, more than one ply de-bonded from the laminate under the punch, indicating the biggest load drop in the force-displacement graph (Figure 87 top). From observation of the

reverse face, it can be seen that the fibres in the inner plies also suffered from shear damage and were broken, forming a clear circular shape plug just like the contact side fibres did.

9mm displacement: The plug was fully detached from the laminate due to the extensive fibre shear failure and pushed out from the reverse face (Figure 89), indicating the decreasing force levels after the maximum load on the force-displacement graph (Figure 87 top). It can be seen from close up observation that the inner plies were mostly de-bonded (which occurred in step 4) from each other in addition to the fibre failure.

	Failure Mode				
	Front face		**Back face**		**Delamination**
Displacement	***Fibre failure***	***Matrix failure***	***Fibre failure***	***Matrix failure***	
1.5 mm	no	no	no	no	34 mm
3 mm	no	no	no	no	43 mm
4 mm	OOP shear	yes	no	no	52 mm
4.25 mm	OOP shear	yes	OOP Shear	yes	53 mm
9 mm	OOP shear	yes	OOP shear	yes	54 mm

* no: no damage, yes: damage was present, (OOP Shear): out-of-plane shear

Table 10 Failure sequence of E-glass/polyester laminates in SPR1.2 - CF setup with respect to increasing displacement of the crosshead

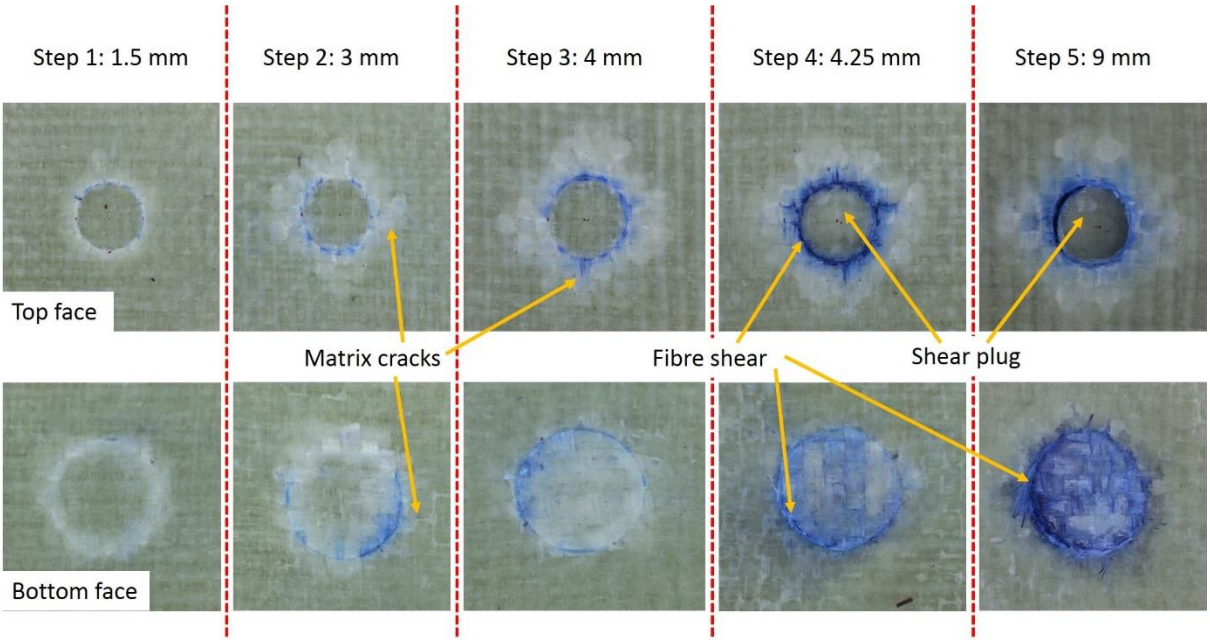

Figure 89 SPR1.2 setup with CF punch showing the damage progression at each step denoted above and the failure modes intrinsic to impact loading

	Failure Mode				
	Front face		Back face		Delamination
Displacement	***Fibre failure***	***Matrix failure***	***Fibre failure***	***Matrix failure***	
1.5 mm	no	Minor crack	no	no	15 mm
4 mm	no	yes	no	no	45 mm
6 mm	no	yes	no	no	55 mm
6.9 mm	OOP crush	yes	OOP shear	yes	62 mm
9 mm	OOP crush	yes	OOP shear	yes	62 mm

* no: no damage, yes: damage is present, (OOP): out-of-plane

Table 11 Failure sequence of E-glass/polyester laminates in SPR1.2 - H setup with respect to increasing displacement of the crosshead

Collectively, the previous two sections have described the in-plane tensile and out-of-plane shear response of the laminates which are the major responsible parameters to control the failure of the laminates. Table 12 and Table 13 below gather the data obtained by these tests together with the complementary properties for E-glass/polyester laminates and E-glass/epoxy sandwich facesheets, respectively.

E_x *(GPa)*	12.895	G_{xy} *(GPa)*	-	S_{xC} *(MPa)*	122
E_y *(GPa)*	12.895	G_{xz} *(GPa)*	1.5	S_{yC} *(MPa)*	122
E_z *(GPa)*	-	G_{yz} *(GPa)*	1.5	S_{zC} *(MPa)*	-
υ_{xy}	0.15	S_{xT} *(MPa)*	373	ε_{max} *(%)*	5.54
υ_{yz}	0.3	S_{yT} *(MPa)*	373	S_{xy} *(MPa)*	-
υ_{xz}	0.3	S_{zT}*(MPa)*	-	S_{xz} *(MPa)*	97
ρ *(kg/m3)*	1850	*ILSS (MPa)*	17	S_{yz} *(MPa)*	97

Table 12 Material properties of E-glass/polyester laminates obtained by the testing program described in the previous sections. E: elasticity moduli, G: Shear Moduli, ρ: density, S: relevant strength values, ILSS: interlaminar shear strength, ε_{max} :failure strain, υ**:** Poisson's ratio, subscripts x, y, z material coordinates, T for tensile and C for compression.

E_x (GPa)	26.3	G_{xy} (GPa)	-	S_{xC} (MPa)	-
E_y (GPa)	26.3	G_{xz} (GPa)	2.1	S_{yC} (MPa)	-
E_z (GPa)	-	G_{yz} (GPa)	2.1	S_{zC} (MPa)	-
υ_{xy}	0.1	S_{xT} (MPa)	366	ε_{max} (%)	1.60
υ_{yz}	0.3	S_{yT} (MPa)	366	S_{xy} (MPa)	-
υ_{xz}	0.3	S_{zT}(MPa)	-	S_{xz} (MPa)	95
ρ (kg/m3)	1960	ILSS (MPa)	42	S_{yz} (MPa)	95

Table 13 Material properties of E-glass/epoxy laminates of sandwich composite obtained by the testing program described in the previous sections. E: elasticity modulus, G: Shear Modulus, $\boldsymbol{\rho}$: density, S: relevant strength values, ILSS: interlaminar shear strength, $\boldsymbol{\varepsilon_{max}}$:failure strain, υ**:** Poisson's ratio, subscripts x, y, z material coordinates, T for tensile and C for compression.

5.1.4 Characterisation of foam core

Characterisation of the foam core was carried out via a unidirectional compression test (as described in Section 2.2.1), density measurement in accordance with ISO-845 standard, and the information obtained from the manufacturer data sheet (3A Composites 2016). 50 mm thick square blocks of 100x100 mm foam samples were used for both density measurements and compression tests (Figure 90) and the results can be seen in Table 14. For ILSS properties of the interface between foam core and GFRP laminates, resin manufacturer data was used (PRF Composite Materials 2013).

Density (kg/m³)	110	**Shear Strength (MPa)**	8
Tensile strength (MPa)	2.2	**Shear Modulus (MPa)**	20
Tensile Modulus (MPa)	120	**Compression Strength (MPa)**	1.34
Shear Elongation at break (%)	10	**Compression Modulus (MPa)**	45.75

Table 14 Mechanical properties of AIREX T90.100 foam

Figure 90 shows the result of compression tests of the foam material. Three typical regions can be observed as: stress increase up to yield point, constant stress plateau indicating continuous plastic deformation of foam cells, and finally compaction region resulting in density increase. Stress-strain data in Figure 90 of these tests were provided as inputs to the crushable foam material model as well as the inputs from Table 14.

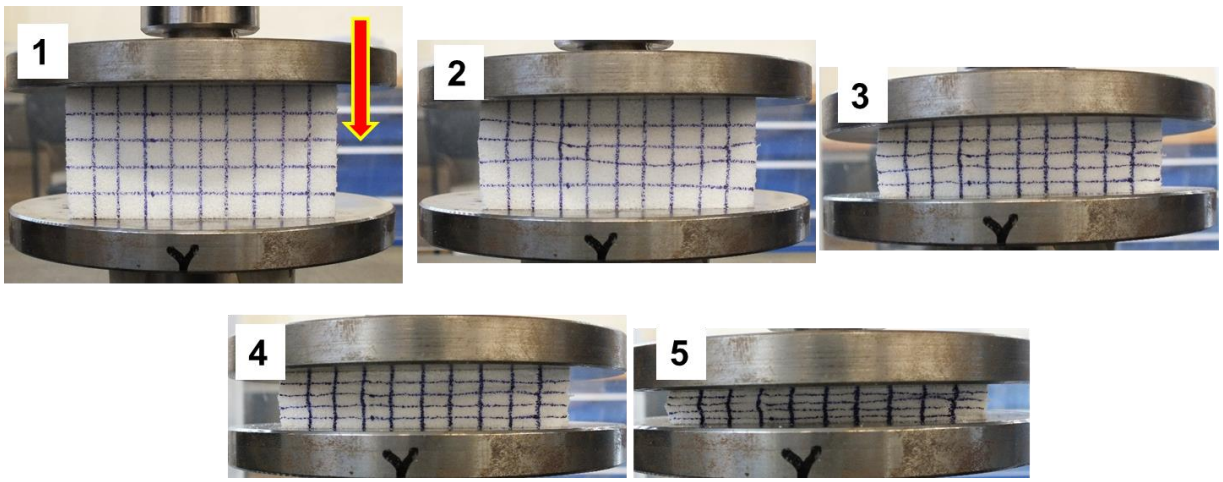

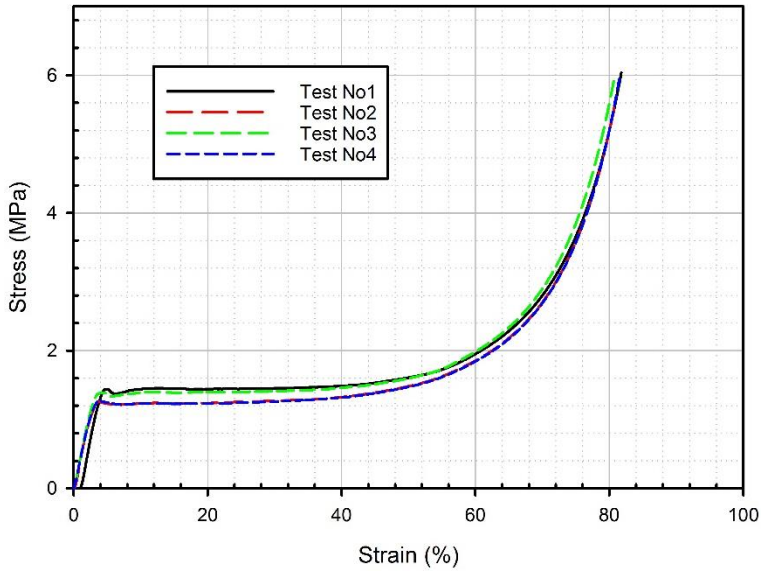

	Comp Strain (%)	Comp Stress (MPa)
1	0.02	0.91
2	0.04	1.38
3	0.1	1.38
4	0.2	1.39
5	0.3	1.41
6	0.4	1.46
7	0.5	1.6
8	0.6	2.2
9	0.75	3.85
10	0.8	5.58

Figure 90 Foam material characterisation: uniaxial compression experiment showing the progressive collapse of the foam (top 1 to 5), the result of the experiments (bottom left), and stress-strain inputs for crushable foam material model (bottom right) obtained by these tests

5.2 Quasi-static punch tests results

This section reports the results and observations from QSPT tests which was used primarily for the proposed assessment method. Detailed analyses were given for each test setup to explain the failure mechanisms and sequence of damage modes. Visual inspection of delamination is presented in Section 5.2.3.

5.2.1 Damage progression: SPR 4.1 with CF ended punch

3mm displacement: Minor matrix cracks due to OOP compression in a circular shape was present on the contact side (Figure 91). No fibre and matrix damage was observed on the reverse side. A delamination diameter of 63 mm was measured under bright light.

8mm displacement: The beginning of a plug formation under the punch can be observed at the contact face, accompanied by matrix cracks in line with the fibre orientations (Figure 91). This step can be considered as the onset of irreversible damage. No major fibre damage was present at the reverse face, but minor matrix cracks due to contact pressure at the fixture ring periphery was observed. Delamination was observed to reach to the fixture ring periphery (106 mm diameter) and also included the area under punch.

13mm displacement: As the punch tip continues to move, a clean circular cut started to form due to fibre shear failure, and shortly after shear plug completion, fibre tensile failure occurred on the reverse face (Figure 91). This indicates the major load drop on the force-displacement graph. Matrix cracks increased simultaneously to the fibre damage on the contact and reverse side. Delamination damage appeared to be progressing slightly towards the boundary of the laminate.

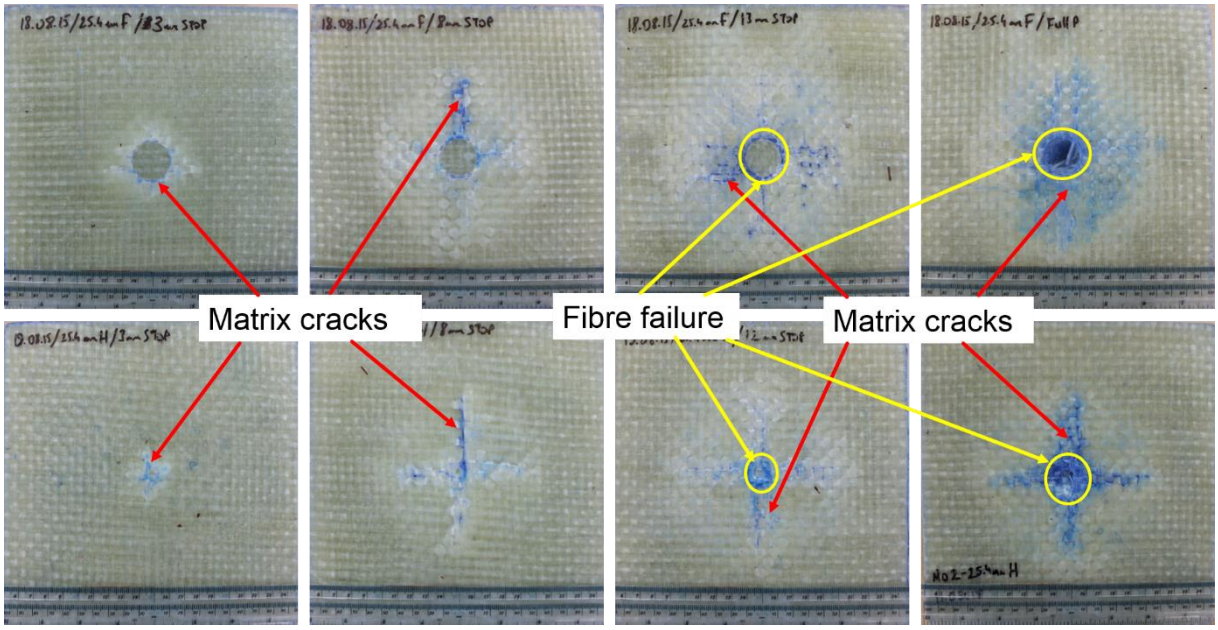

Figure 91 Damage progression in SPR4.1 setups. Top row shows the experiments with CF punch at 3-8-13-25 mm displacements, and bottom row shows the experiments with H punch at 3-8-12-25 mm displacements.

25mm displacement: Further fibre breakage was observed on the reverse face as the plug was pushed away from the laminate and created a brush-like shape (Figure 92). A clean circle shape cut can be seen from the contact face through the whole thickness of the laminate. The area of delamination didn't change compared to the previous step.

5.2.2 Damage progression: SPR 4.1 with H ended punch

3mm displacement: No major fibre damage on either side, but minor matrix cracks were present on the contact side. In addition, delamination area around 30 mm diameter was measured under bright light.

8mm displacement: Minor fibre damage was observed on the contact side, no more than half bundle of fibres. The matrix cracking extended in both in-plane fibre directions on the contact side, but no matrix damage was observed on the reverse face (Figure 91). The area of delamination progressed through the boundaries of the fixture ring (106 mm diameter).

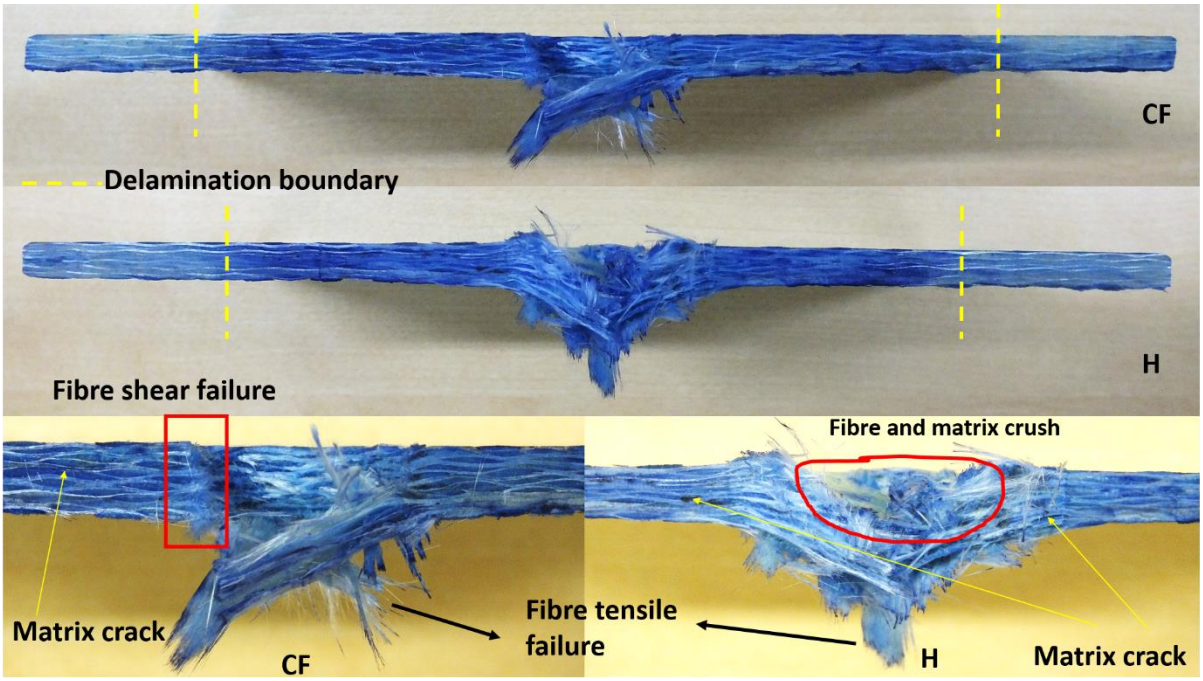

Figure 92 QSPT experiments after full penetration (25mm) showing differences in CF and H ended punches in SPR4.1 setup

12mm displacement: Fibre breakage/crush (Figure 92) due to OOP compression and shear was observed on the contact face (Figure 91) and fibre damage due to excessive tensile stress was observed on the reverse face, which in this step indicates the load drop in the force-displacement

graph. Matrix damage increased on both sides, concentrated at the broken fibre areas. Slight increase in delamination area was observed towards outside of the ring periphery.

25mm displacement: Increase in the fibre breakage was observed on both sides as the penetrating tip progresses further. Matrix damage also increased in parallel with the fibre damage (Figure 91). The area of delamination didn't show an increase compared to the previous two steps.

5.2.3 Delamination failure

Figure 93 shows the progression of delamination observed by illuminating the laminates from the reverse side (thanks to the opacity of GFRPs), and the delamination progression in each loading step for SPR1.2 is shown. While the overall response was similar in both cases, delamination along fibre orientations (like a cross shape) was clearer for the H punch tip, however, for CF tip it starts as a circular shape and transforms into a diamond shape later.

Figure 94 illustrates the delamination progression for SPR4.1 setup with CF (left) and H (right) punch tips. It can be seen for both cases that the delaminated area extended to the span periphery at the end of 2nd step. Weak-shaped discontinuities at the 3rd and 4th steps were due to the clamping bolts. For CF tip, the length of delamination at the end of 1st step was measured as 60 mm in diameter, while for H tip it was 30 mm diameter.

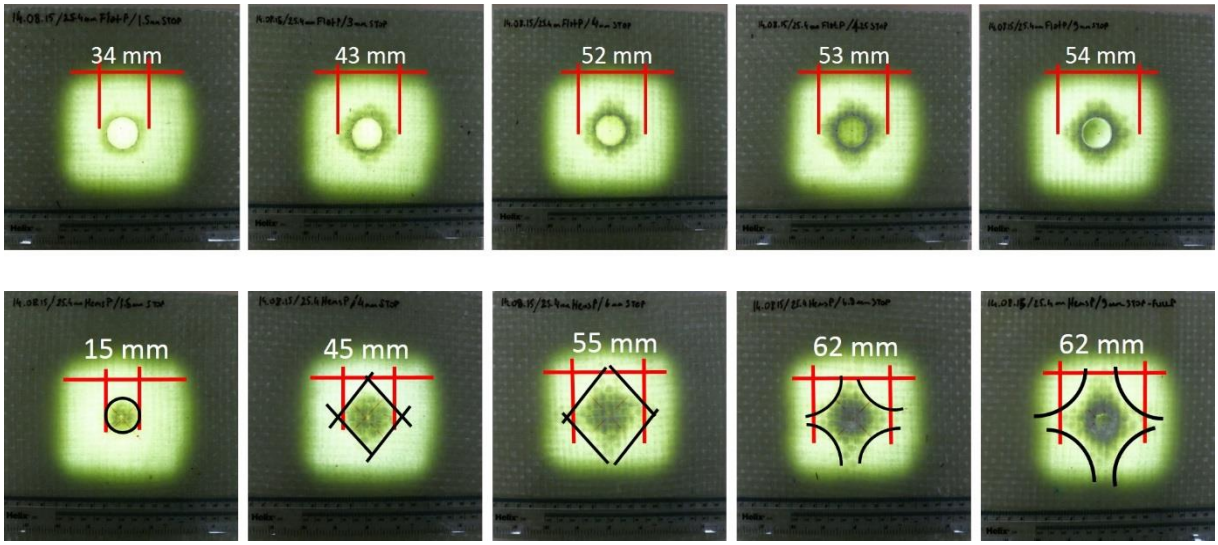

Figure 93 Delamination progress in SPR1.2 setups: CF punch (top row) at 1.5, 3, 4, 4.25 and 9 mm displacements, H punch (bottom row) at 1.5, 4, 6, 6.9, and 9 mm displacements

However, as it can be seen from (Figure 94), the area under the CF punch was not delaminated. Therefore, the fact that delamination was the only damage mode in both cases at the end of 1st

step, the energy absorbed by the samples were quite close to each other (as will be discussed in the following section). At the end of the 2nd step the delaminated region is darker for CF tip compared to H tip, indicating that absorbed energy is greater. The contribution of delamination to the absorbed energies is hard to decipher after the 2nd step since in both cases the complete span is delaminated. These images are not able to provide information on the through-thickness delamination progress. Sectioning can resolve this issue and determine the contribution to energy absorption. This will be determined using numerical models.

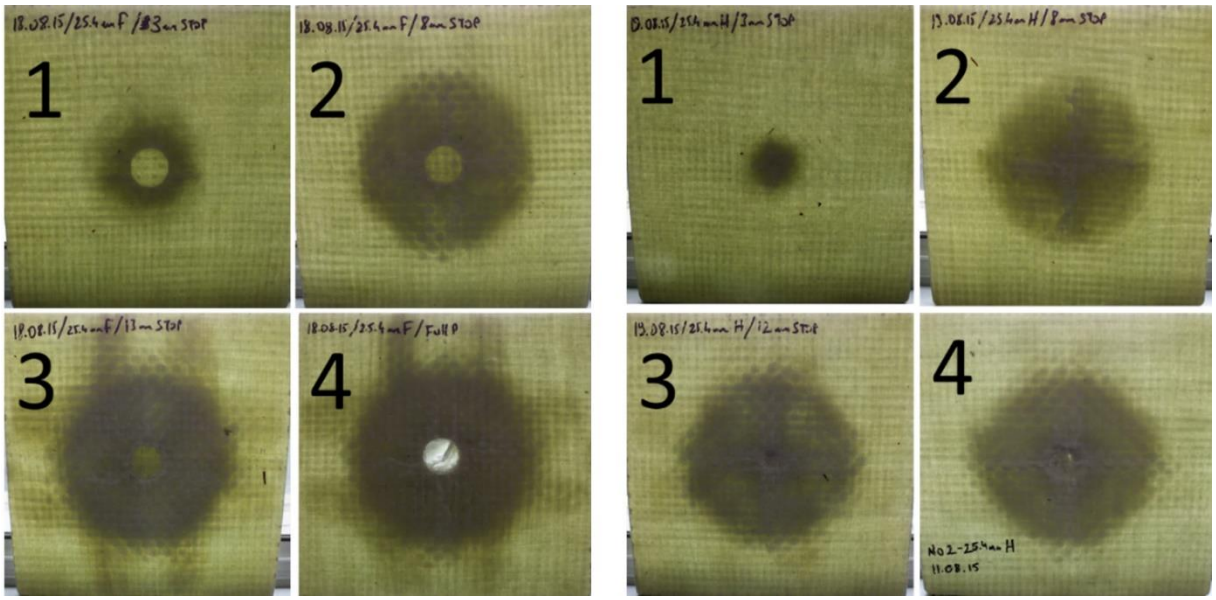

Figure 94 Delamination progress at each loading step (from 1 to 4) in SPR4.1 setups: CF punch (left) at 3, 8, 13, 25 mm displacements, H punch (right) at 3, 8, 12, 25 mm displacements.

5.2.4 Energy absorption behaviour

The energy values shown in Figure 95 to Figure 98 were obtained by using test bench software TRAPEZIUM, from the area under the force-displacement graphs which is the indication of the energy spent to damage/penetrate samples, that is (Eqn. 18):

$$E = \int_0^x F(x)dx \qquad \text{Eqn. 18}$$

Where E is the energy spent to damage the material and x is the final displacement of the punch head. The noticeable detail is that the energy absorption graph shows a higher energy absorption rate for SPR4.1 between the 2nd and 3rd steps for CF profile (Figure 95 and Figure 98). For SPR4.1 setup, at the end of 2nd step the extent of delamination was observed at the span periphery. During the 3rd step, there was an increased amount of fibre damage since more plies

were subjected to shear failure. In addition, at the end of the 3rd step, the fibre tensile failure occurred at the reverse face which indicates the biggest load drop in the force-displacement graph. This observation suggests that, in SPR4.1 setup, fibre shear damage was the dominating failure mechanism for energy absorption. However, for SPR1.2-CF setup, the rate of energy absorption was similar for every transition (Figure 97), which exhibited fibre shear damage, matrix damage and delamination. It is not entirely clear which failure mode is the dominant one in SPR1.2-CF setup. However, considering that the delamination spreading was small, then it is possible to say that fibre shear damage could be the dominant energy absorber for SPR1.2 as well.

For H profile, the energy absorption behaviour was similar to CF punch for the SPR1.2 setup, with minor differences (Figure 97). In SPR4.1-H setup (Figure 96), at the end of 2nd step, the delamination progress appeared to reach the fixture ring, just like in CF case. No fibre shear damage was observed, but there was some out-of-plane compression damage in a small concentrated area under the tip. The energy rate change slightly increases after 2nd step as well, even if not as drastic as the CF tip. This difference can be explained by the amount of fibres subjected to failure since the fibre breakage was in a more concentrated area in H punch case. Therefore, it is not as obvious as it is in CF punch case, to decide whether the fibre breakage or any other failure mechanism is the dominant energy absorber.

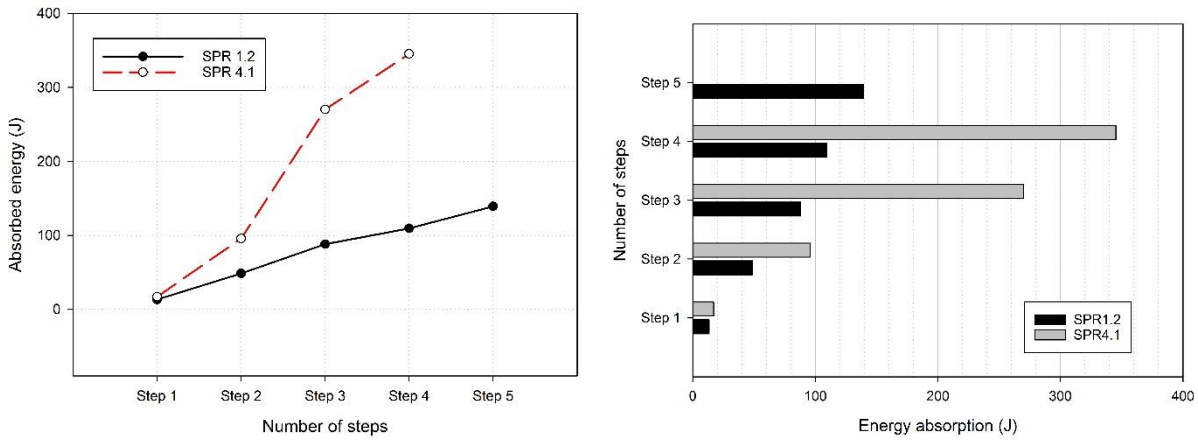

Figure 95 Energy absorption in SPR1.2 and SPR4.1 setups with circular flat ended punch showing more energy was spent in SPR4.1 because of the bending of the samples

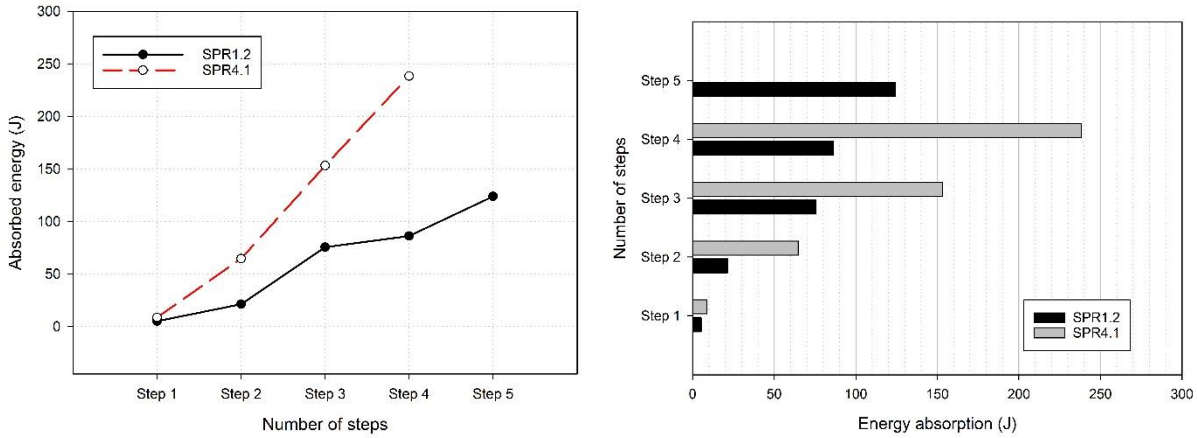

Figure 96 Energy absorption in SPR1.2 and SPR4.1 setups with hemispherical ended punch

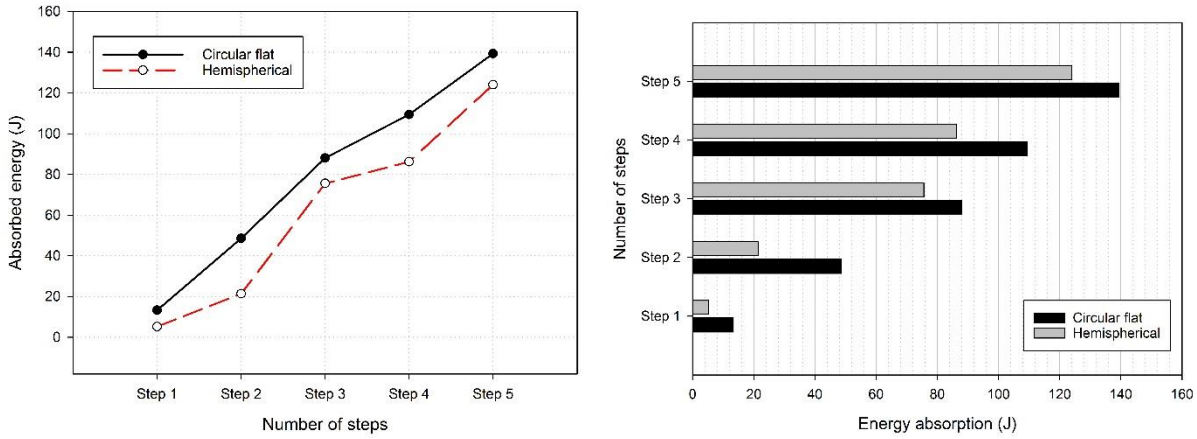

Figure 97 Energy absorption in SPR1.2 setup: comparison of impactors showing minor differences between circular flat and hemispherical ended punches

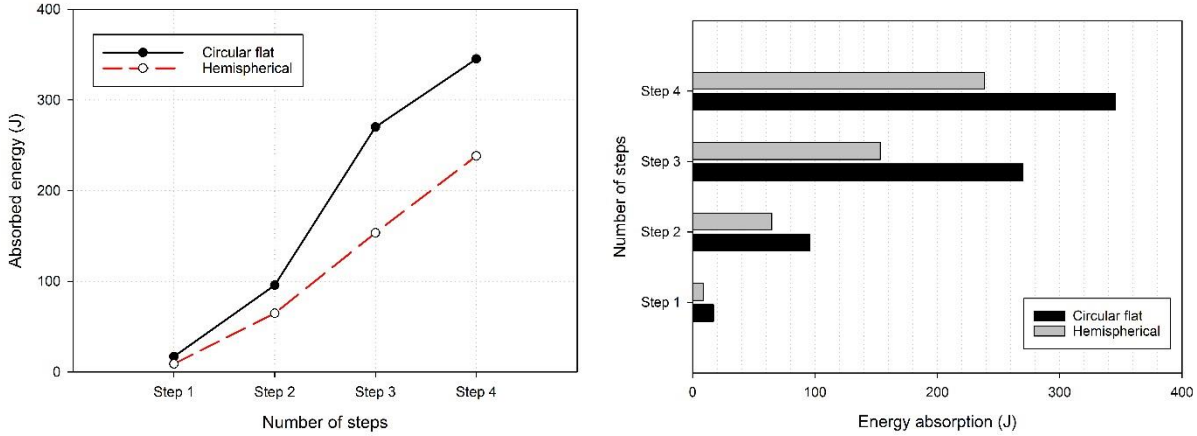

Figure 98 Energy absorption in SPR4.1 setup: comparison of impactors showing circular flat punch requires more energy to damage a specimen

5.2.5 Quasi-static punch test of sandwich composite

Punch tests of foam core sandwich plates were performed by following the same procedure as the glass fibre laminate testing (Section 4.3). Tests were carried out with circular flat ended punch at 2 mm/min crosshead displacement rate.

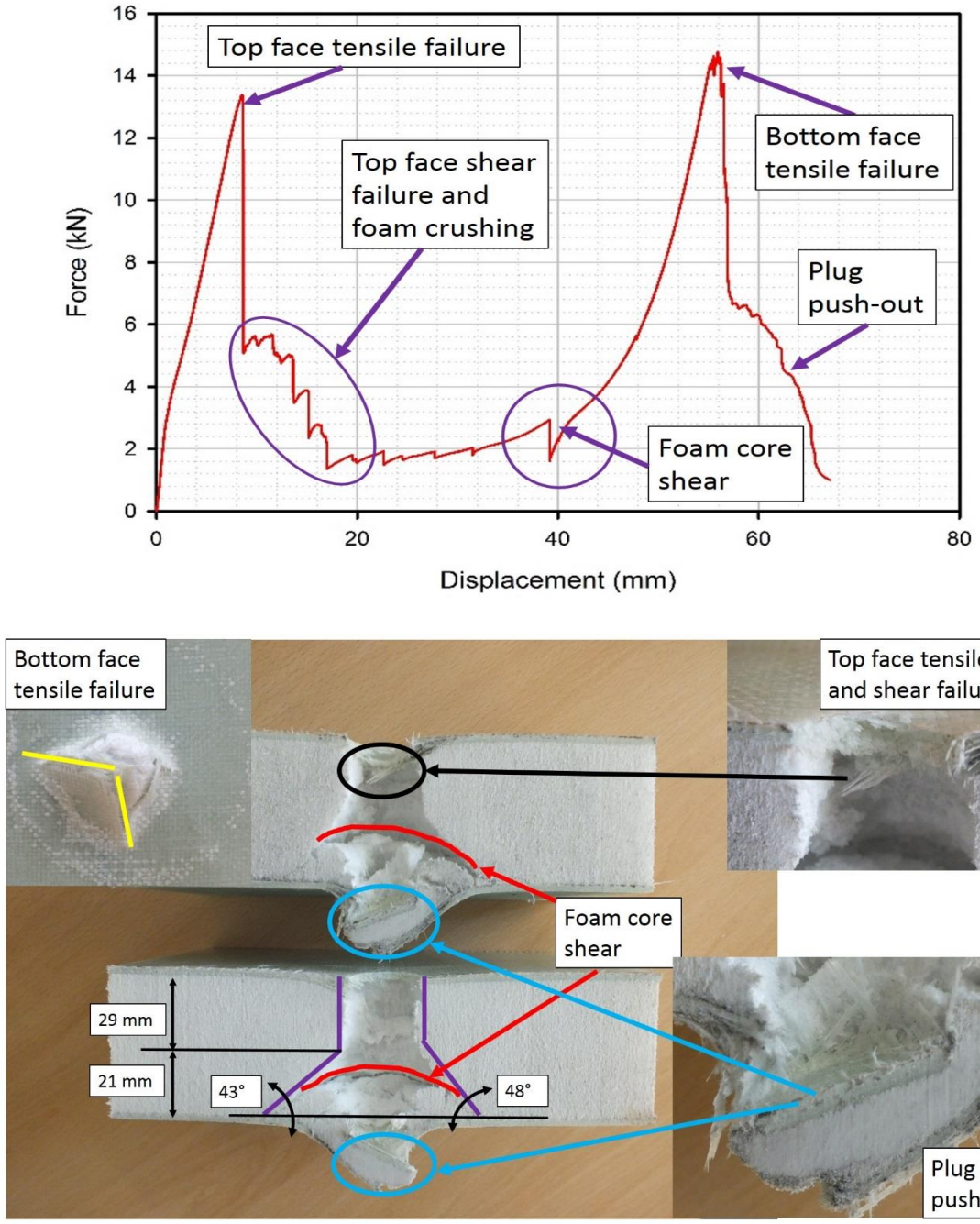

Figure 99 QSPT response of sandwich plate. Force-displacement output (top) describing the failure modes associated with each load change. Sectioned images of the sandwich (bottom) indicating the failure modes and details observed

Figure 99 (top) shows the force-displacement graph obtained from the test and illustrates the failure modes associated with each load change. The overall response of the sandwich was roughly similar to what has been observed for the monolithic laminates.

The slope of the load exhibited a slight change between 1-2 mm displacements which is believed to be delamination in the top facesheet layers although overall delamination levels were observed to be negligible. Following, the load continues to increase without any apparent fibre or matrix failure, and displays the first major load drop as a tensile failure of the top face. It is worth clarifying that at this point the failure was also accompanied by the shear of the top face and the crushing of the foam core as well. This mode of failure was reported in the literature (Flores-Johnson & Li 2011) and addressed as shear plugging. It is true that a shear failure caused by the shape of the circular flat indenter was obvious for the present case as well. However, judging from the pulled out fibre bundle (Figure 99 bottom) and the absence of a clear indentation into the glass fibre layer during the major load drop, it can be concluded that the preceding failure mode was tensile which was rapidly followed by the shear plugging. The plateau section between the 20-40 mm displacement levels indicates the continuous foam crushing followed by foam shear. Through the end of this section, at 39 mm, the continuous collapse of the polymeric foam cells and the densification result in a through-thickness tensile stress accumulation inside the foam core. This accumulation causes the foam to exhibit a conoid shaped shear failure (Figure 99 bottom). The angle of the conoid was measured as 43° and 48° which also agrees with the typical shear failure of foam core which is around 45°. Conoid foam shear was observed by others as well (Flores-Johnson & Li 2010; Rajaneesh et al. 2014b). The penetration process was finalised as the bottom face layer exhibited tensile failure in parallel with fibre directions (0° and 90°), and the GFRP skin/foam shear plug was pushed-out from the plate. Reverse face tensile failure was shown in (Figure 99 bottom) with yellow lines indicating the separated layer.

5.3 Numerical model validations

5.3.1 Model validation: Quasi-static punch tests

The numerical model described in Section 4.3.1 was compared with the QSPT experiments for validation. The material response in fibre direction (*1*) and (*2*) were found similar as expected given the fact that the laminates have quasi-isotropic properties in in-plane (*1-2 plane*). For this reason, the failure contour in *1* direction (DAMAGE 11) will be shown only for brevity. Data

sets of material property and numerical parameters are given in Table 15 for E-glass/polyester laminates and in Table 16 for E-glass/epoxy facesheets of sandwich plate.

Equation of State: Orthotropic	**Value**	**Strength Model: Orthotropic yield** [b]	**Value**	**Plasticity Parameters**	**Value: Static/ 30% /50%** [c]
Young's Modulus - E_x (GPa)	12.895	Eff Stress 1 (kPa)	5.30E+04	a11	1 / 1.2 / 1.55
Young's Modulus - E_y (GPa)	12.895	Eff Stress 2 (kPa)	7.80E+04	a22	1 / 1.2 / 1.55
Young's Modulus - E_z (GPa)	8[a]	Eff Stress 3 (kPa)	1.08E+05	a33	1 / 1.2 / 1.55
Poisson's ratio - ν_{xy}	0.15	Eff Stress 4 (kPa)	1.43E+05	a12	-0.25 / -0.3 / -0.38
Poisson's ratio - ν_{yz}	0.3	Eff Stress 5 (kPa)	1.76E+05	a23	-0.45 / -0.54 / -0.69
Poisson's ratio - ν_{xz}	0.3	Eff Stress 6 (kPa)	2.14E+05	a13	-0.45 / -0.54 / -0.69
Shear Modulus - G_{xy} (GPa)	1.79[a]	Eff Stress 7 (kPa)	2.50E+05	a44	1.5 / 1.8 / 2.32
Shear Modulus - G_{yz} (GPa)	1.5	Eff Stress 8 (kPa)	2.81E+05	a55	1.5 / 1.8 / 2.32
Shear Modulus - G_{xz} (GPa)	1.5	Eff Stress 9 (kPa)	3.15E+05	a66	1.5 / 1.8 / 2.32
		Eff Stress 10 (kPa)	3.70E+05		
Failure Model: Orthotropic Softening	**Value**			**Erosion strain**	0.5
Tensile Strength - S_x (MPa)	373	Eff Strain 1	5.00E-03		
Tensile Strength - S_y (MPa)	373	Eff Strain 2	1.00E-02		
Tensile Strength - S_z (MPa)	1E+20	Eff Strain 3	1.50E-02	**ILSS –** Normal stress (MPa)	
Shear Strength - S_{12} (MPa)	1E+20	Eff Strain 4	2.00E-02		15
Shear Strength - S_{23} (MPa)	97	Eff Strain 5	2.50E-02		
Shear Strength - S_{13} (MPa)	97	Eff Strain 6	3.00E-02	**ILSS –** Shear stress (MPa)	
Fracture energy - G_{f1} (J/m^2)	-	Eff Strain 7	3.50E-02		17
Fracture energy - G_{f2} (J/m^2)	-	Eff Strain 8	4.00E-02		
Fracture energy - G_{f3} (J/m^2)	-	Eff Strain 9	4.50E-02	**Damage coupling coefficient (*C*)**	
Fracture energy - G_{f12} (J/m^2)	-	Eff Strain 10	5.00E-02		0
Fracture energy - G_{f23} (J/m^2)	-				
Fracture energy - G_{f13} (J/m^2)	-				

[a] These parameters were given an estimated value for the sake of providing material property to the FE model. They do not have any influence on the results.
[b] Effective stress and strain values were determined from experimental tensile stress-strain data and piecewise master curve was generated by these points.
[c] 30% and 50% values of Plasticity parameters amplify the Effective stress-strain data accordingly to represent higher strain rate loading response of the material. Higher strain rate plasticity parameters were determined in parallel with material strength under higher strain loading.

Table 15 Numerical model data set for E-glass/polyester laminate

Equation of State: Orthotropic	**Value**	**Strength Model: Orthotropic yield** [b]	**Value**	**Plasticity Parameters**	**Value: Static/ 50%** [c]
Young's Modulus - E_x (GPa)	26.3	Eff Stress 1 (kPa)	5.14E+04	a11	1 / 1.65
Young's Modulus - E_y (GPa)	26.3	Eff Stress 2 (kPa)	9.68E+04	a22	1 / 1.65
Young's Modulus - E_z (GPa)	8[a]	Eff Stress 3 (kPa)	1.37E+05	a33	1 / 1.65
Poisson's ratio - v_{xy}	0.1	Eff Stress 4 (kPa)	1.78E+05	a12	-0.1 / -0.165
Poisson's ratio - v_{yz}	0.3	Eff Stress 5 (kPa)	2.18E+05	a23	-0.3 / -0. 495
Poisson's ratio - v_{xz}	0.3	Eff Stress 6 (kPa)	2.60E+05	a13	-0.3 / -0. 495
Shear Modulus - G_{xy} (GPa)	2.5[a]	Eff Stress 7 (kPa)	2.96E+05	a44	1.5 / 2.475
Shear Modulus - G_{yz} (GPa)	2.1	Eff Stress 8 (kPa)	3.39E+05	a55	1.5 / 2.475
Shear Modulus - G_{xz} (GPa)	2.1	Eff Stress 9 (kPa)	3.82E+05	a66	1.5 / 2.475
		Eff Stress 10 (kPa)	4.31E+05		
Failure Model: Orthotropic Softening	**Value**			**Erosion strain**	0.5
Tensile Strength - S_x (MPa)	366	Eff Strain 1	1.2E-03		
Tensile Strength - S_y (MPa)	366	Eff Strain 2	2.4E-03		
Tensile Strength - S_z (MPa)	1E+20	Eff Strain 3	3.7E-03	**ILSS –** Normal stress (MPa)	
Shear Strength - S_{12} (MPa)	1E+20	Eff Strain 4	4.9E-03		42
Shear Strength - S_{23} (MPa)	95	Eff Strain 5	6.1E-03		
Shear Strength - S_{13} (MPa)	95	Eff Strain 6	7.3E-03	**ILSS –** Shear stress (MPa)	
Fracture energy - G_{f1} (J/m^2)	-	Eff Strain 7	8.6E-03		45
Fracture energy - G_{f2} (J/m^2)	-	Eff Strain 8	9.8E-03		
Fracture energy - G_{f3} (J/m^2)	-	Eff Strain 9	1.1E-02	**Damage coupling coefficient (*C*)**	
Fracture energy - G_{f12} (J/m^2)	-	Eff Strain 10	1.22E-02		0
Fracture energy - G_{f23} (J/m^2)	-				
Fracture energy - G_{f13} (J/m^2)	-				

[a] These parameters were given an estimated value for the sake of providing material property to the FE model. They do not have any influence on the results.
[b] Effective stress and strain values were determined from experimental tensile stress-strain data and piecewise master curve was generated by these points.
[c] 30% and 50% values of Plasticity parameters amplify the Effective stress-strain data accordingly to represent higher strain rate loading response of the material. Higher strain rate plasticity parameters were determined in parallel with material strength under higher strain loading.

Table 16 Numerical model data set for E-glass/epoxy sandwich facesheets

SPR4.1 – Circular flat punch

A summary of failure analysis for this experiment setup is shown in Table 17. It can be seen in the contact force-displacement graph (Figure 100) that the numerical model predicted the overall non-linear behaviour of GFRP laminates with reasonable accuracy. For the 0-2mm displacement, there is a change in the loading rate which was observed as delamination onset, followed by a uniform section of increasing load (hardening), and the major load drop (catastrophic failure and softening) indicated out-of-plane (OOP) shear and fibre tensile failure. The same major damage mechanisms are reported in (Sutherland & Guedes Soares 2012), and similar behaviour was reported in (Gama & Gillespie 2008) and (Xiao et al. 2007). Although the model underestimated the force values at delamination onset and at maximum (major) failure, it captured the corresponding displacement levels well. The variation issues for the delamination force values were reported previously and the reason was indicated as the initial contact instability (Gama et al. 2004). The variation between experiments and numerical model for maximum failure load is calculated as 11%, and 45.05% for the delamination onset. In terms of corresponding displacements, 7.6% and 8.29% error was calculated for major failure displacement and delamination onset, respectively.

	Failure Mode				
	Front face		**Back face**		**Delamination**
Displacement	***Fibre failure***	***Matrix failure***	***Fibre failure***	***Matrix failure***	
3 mm	no	Minor crack	no	no	63 mm
8 mm	Minor	yes	no	Minor	106 mm
13 mm	OOP shear	yes	Tensile	yes	107 mm
25 mm	OOP shear	yes	Tensile	yes	107 mm

* no: no damage, yes: damage is present, (OOP Shear): out-of-plane shear

Table 17 Failure sequence of E-glass/polyester laminates in SPR4.1 - CF setup

Figure 101 visually compares the FE model and the repeated QSPT experiments with flat punch in terms of failure behaviour. Figure 101 (c) indicates that the fibres began to be fully damaged at 12.4mm crosshead displacement. In Figure 101 (d) the first ply of the laminate exhibited shear failure after 13mm displacement and later the damage extended to the back face at 15mm (Figure 101 e). This outcome matches the experiments quite well (Figure 101 a, b). In support, Figure 101 (f, g) shows the stress distribution during the loading, which also supports evidence that the reverse face failure occurred due to the fibre tensile stress exceeding a strength value of 373MPa.

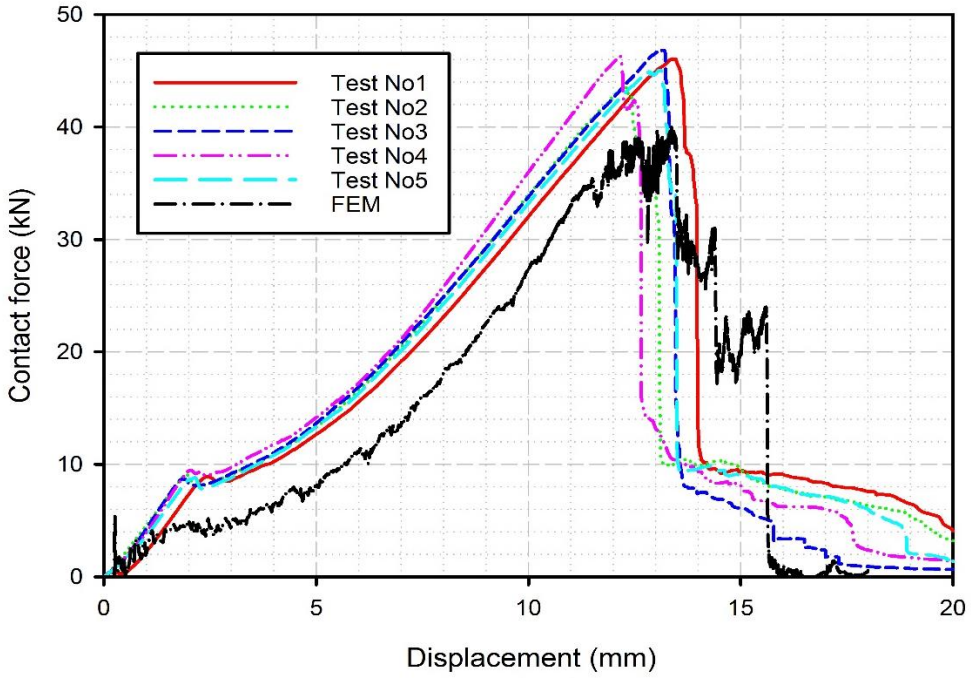

Figure 100 Contact force-displacement graph showing the agreement between FE model and the experiments (dotted lines) for CF ended punch

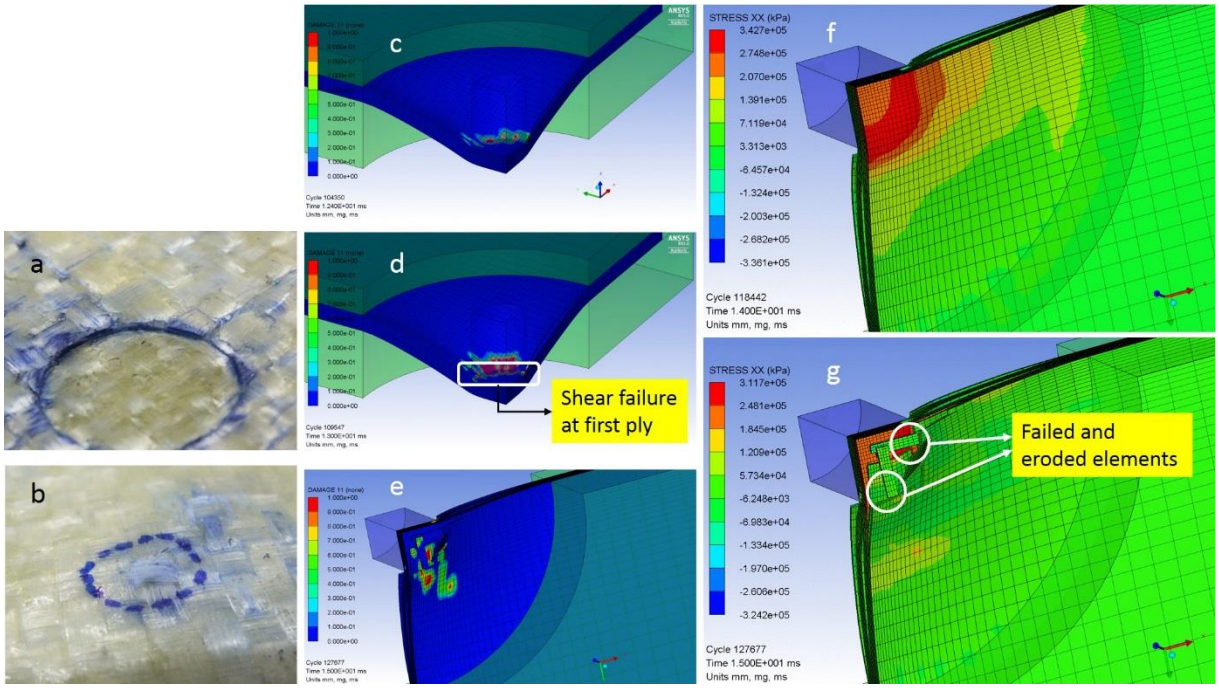

Figure 101 Numerical model prediction at major failure; a) experiment: shear failure at impact side, b) experiment: tensile failure at reverse side, c) to e) FE model is showing shear failure followed by tensile failure, f) to g) tensile failure at reverse face

SPR4.1 – Hemispherical punch

Summary of the failure sequence analysis for this experiment setup is shown in Table 18 and Figure 102 shows the experiment-FEM comparison of contact force-displacement levels. As it was in the CF ended punch case, the prediction agreed to a reasonable degree with the experiments, showing an underestimation at delamination onset. However, this time the variation levels were found to be lower: 2.4% (26.864kN vs 26.2kN) for the failure force, and 8.9% (11.75mm vs 12.8mm) for failure displacement. The major failure of the laminates was observed due to the tensile failure at the reverse face at crosshead displacement around 12 mm. It is apparent from the Figure 102 that the load drop after maximum load was considerably different. There is a sharp load drop after a short section of softening. A possible explanation for this might be the effect of softening parameters (Xiao et al. 2007). This should be investigated in more detail in the future and the author believes that it is likely to solve the issue with additional testing methods. Figure 103 shows the back face stress distribution of the laminate in fibre (1) direction. In parallel with the experiments, the tensile stress reaches to its predefined value (373 MPa) after 12 mm and fails before 13 mm displacement, causing a stress release underneath the punch.

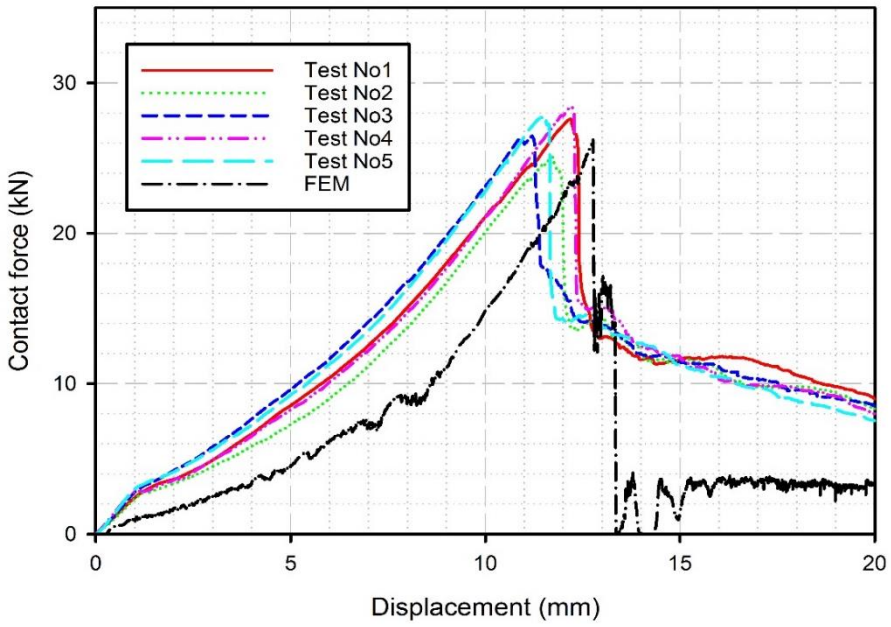

Figure 102 Contact force-displacement graph showing the validation of FE model with the QSPT experiments for H ended punch

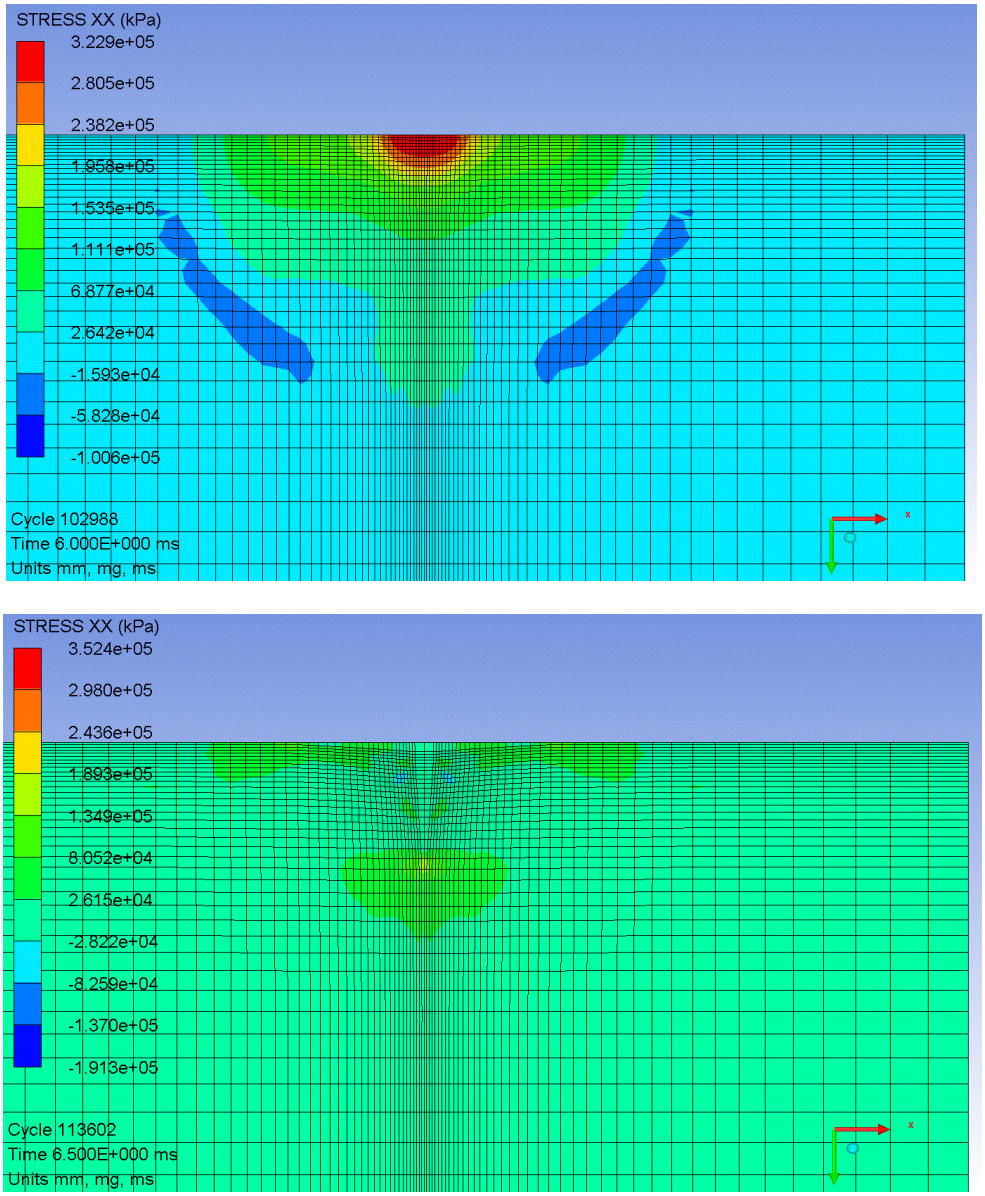

Figure 103 Back face stress levels (STRESS XX) in fibre (1) direction at 12 mm (top) and 13 mm (bottom) crosshead displacement.

	Failure Mode				
	Front face		**Back face**		**Delamination**
Displacement	***Fibre failure***	***Matrix failure***	***Fibre failure***	***Matrix failure***	
3 mm	no	Minor crack	no	no	30 mm
8 mm	Minor	Extended cracks	no	no	106 mm
12 mm	OOP shear	yes	Tensile	yes	107 mm
25 mm	OOP shear	yes	Tensile	yes	107 mm

* no: no damage, yes: damage is present, (OOP Shear): out-of-plane shear

Table 18 Failure sequence of E-glass/polyester laminates in SPR4.1 - H setup

Delamination response

Delamination is a crucial failure mode of laminated composites and it is important to capture this mode accurately as stated by many (de Moura & Marques 2002). Delamination failure of GFRP plates under quasi-static punch loading was captured via BOND STATU result variable (ANSYS Help Viewer 2013). Failure occurs when the contour level is between 0 and -1. Figure 104 and Figure 105 compares the experimental observation and the prediction of FE model for CF and H ended punches, respectively. Excellent correlation was achieved - 6.6% error for 3mm displacement and 1.88% error for 8mm displacement for CF punch, while for H punch 3mm correlation was predicted exactly and 7.54% difference calculated for 8mm displacement. Section 5.2.3 stated that the contribution of delamination to the energy absorption behaviour after 2nd loading step in SPR4.1 setup was not clear, and a sectioning study could reveal this issue. At this point, we can use the advantage of a finely correlated simulation, not only to analyse the delamination advance but also to validate the use of light source to detect delamination.

(Figure 106) demonstrates the delamination progression in 3D contour (as a half symmetry model) between 8-18mm crosshead displacements. The advance of the delamination and increased intensity can be clearly seen from the figures; after the middle interface layer delamination extending to the span periphery (8mm), the intensity increases at the outer areas during 9mm and 10mm. Later, this intensity trend switches back to the punch periphery (11mm) and the interfaces which were already de-bonded continues to advance away from the impact point (12 to 18mm). It is worth mentioning that these results match with those presented in (Figure 94) (the slight change in contrast), supporting the obvious advantage of software modelling, which provides more insight without the need of extra imaging techniques. These figures prove that using contact elements with interlaminar shear strength criterion to mimic delamination behaviour of GFRP laminates is a practical, sufficient, and accurate approach.

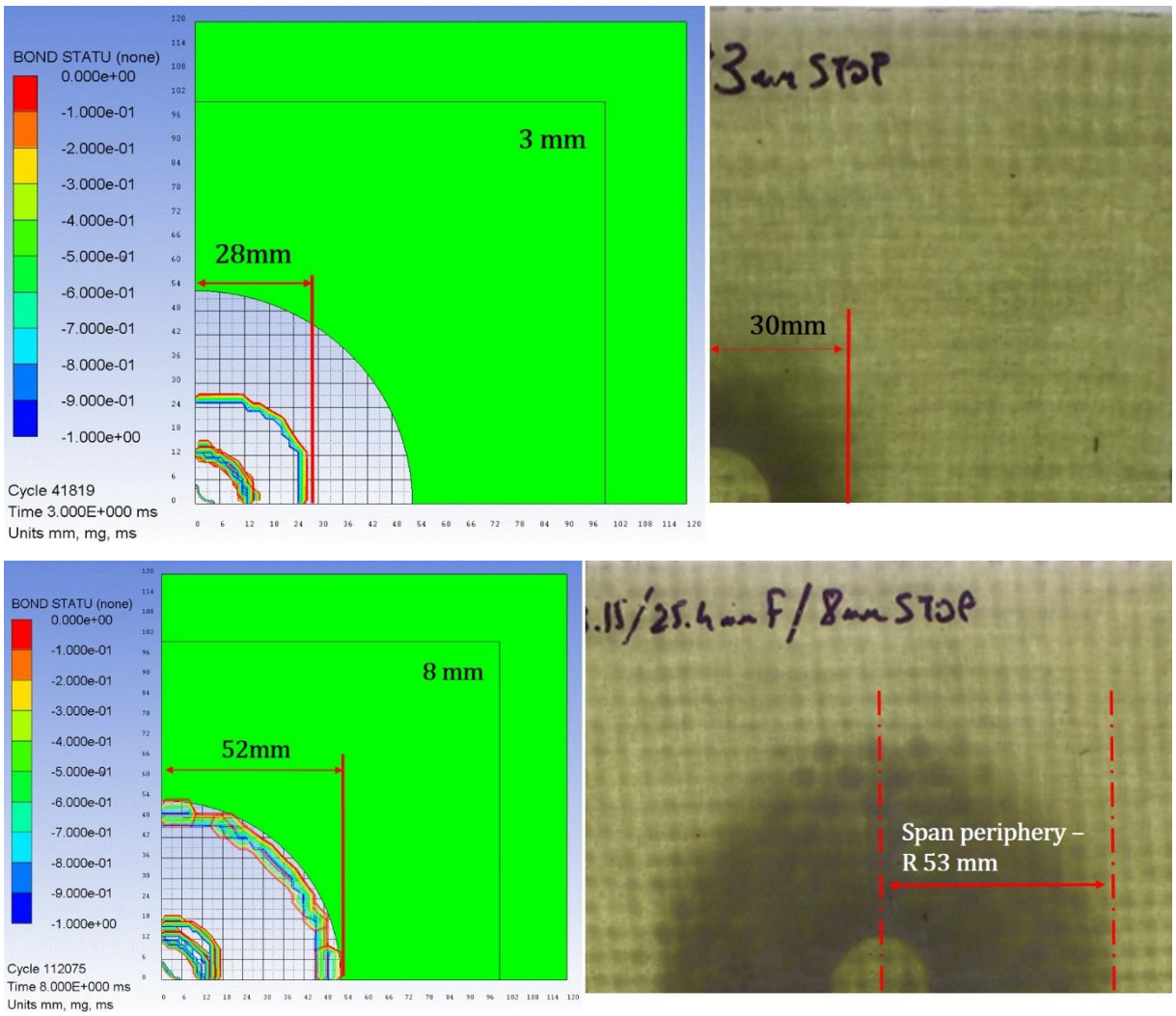

Figure 104 Validation of delamination at 3mm (top row) and 8mm (bottom row) crosshead displacement (CF ended punch)

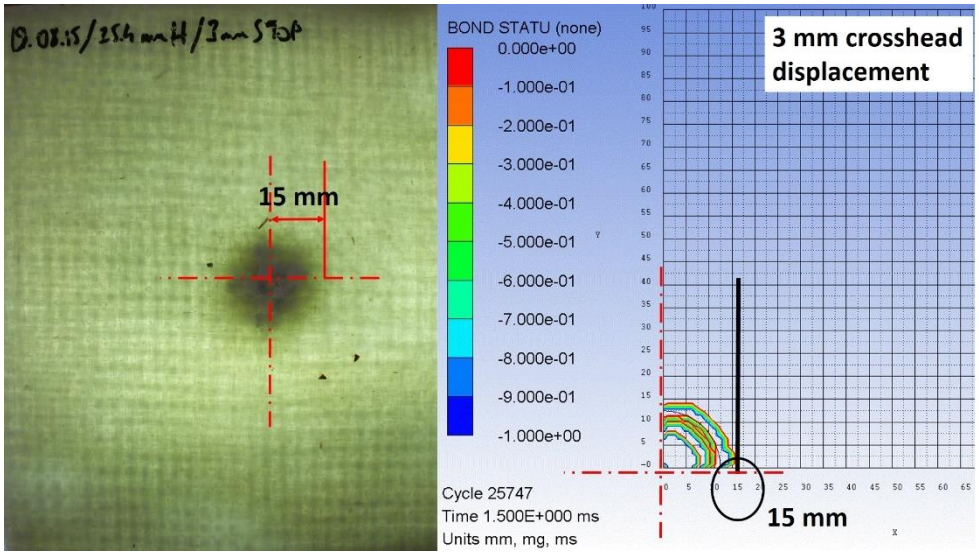

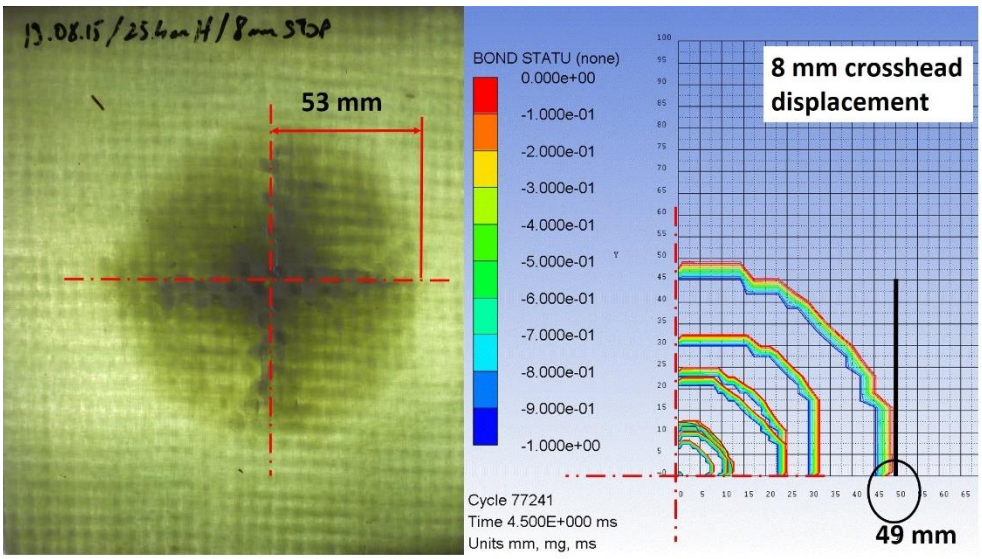

Figure 105 Validation of delamination of laminates in SPR4.1 setup with hemispherical punch: 3mm crosshead displacement (top), 8 mm crosshead displacement (bottom)

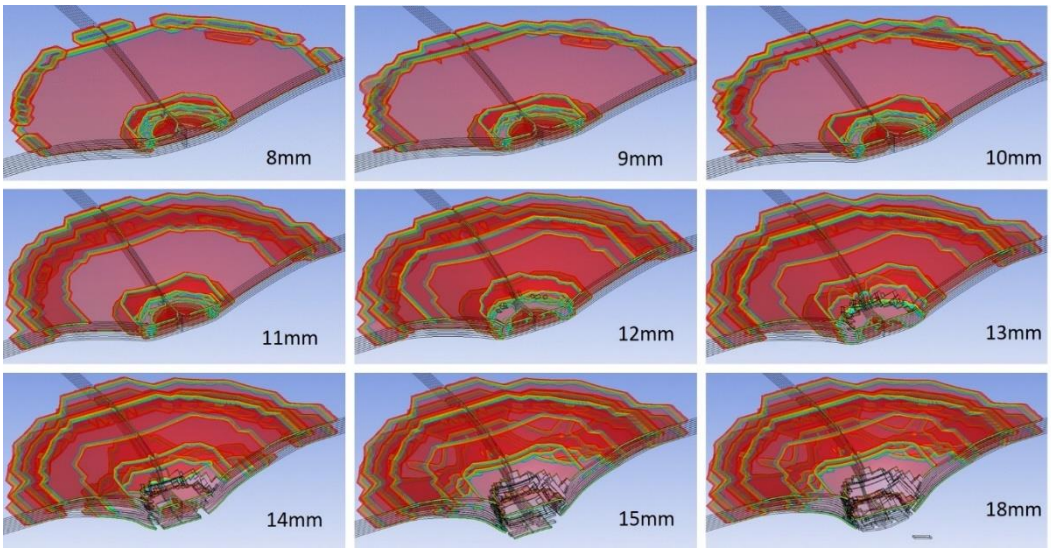

Figure 106 Progression of delamination in 3D (half symmetry) between 8-18mm crosshead displacements

Energy absorption

Internal energy (IE) change of the GFRP laminates over displacement was observed during the simulations. In Figure 107, the IE of the laminate increased to 323 J at the end of 18 mm crosshead displacement.

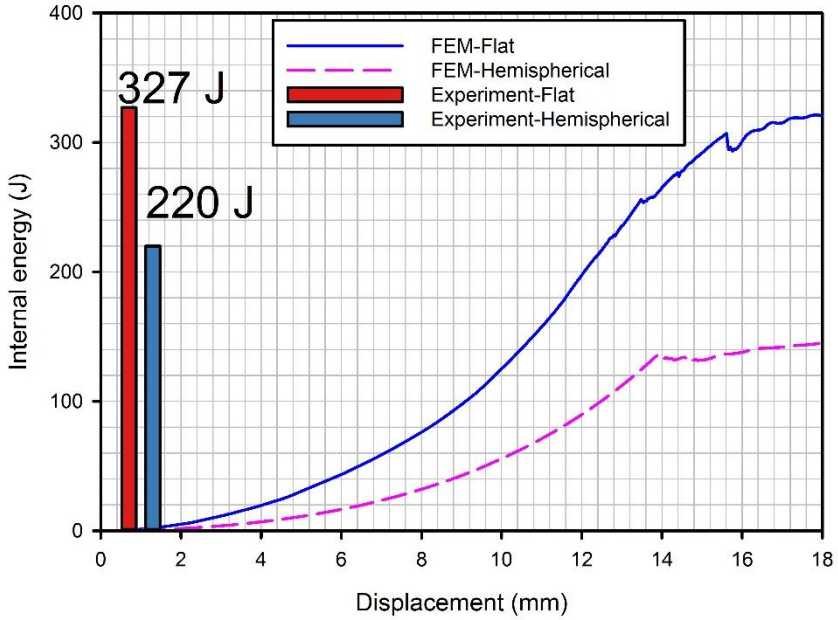

Figure 107 Energy absorption in experiments (bars) and FE model (lines)

When compared with the experimental average value of 327.82 J, 1.47% variation was calculated for energy absorption for SPR4.1-CF setup. However, the variation was much higher - 28% - for H punch setup when compared with the experimental average value of 220 J. This can be explained by the variation of the contact force which was influenced by the likely effect of erosion parameters. In general, the rate of energy increase starts to change at the beginning of major failure. Figure 107 supports the evidence of fibre failure dominated energy absorption for CF impactor as 77J absorbed up to 8mm, and 246J absorbed in the rest of the perforation which mostly consists of fibre damage accompanied by additional delamination.

QSPT of sandwich composite

Figure 108 shows the correlation between the experimental QSPT and the numerical model of the sandwich plate. Three numerical model predictions can be seen, each representing the effect of erosion strain parameter assigned to the foam material model: 0.8, 1.2, and 1.5. Overall, the numerical model provided excellent correlation except the final failure load of the bottom facesheet failure. The stiffness prediction of the sandwich at early stages and at the first major load drop was consistent with the experiments. The failure load of the top facesheet was predicted with a 7.57% difference, and the displacement at failure was predicted with 7.2% variation. The shear failure of the top facesheet accompanied by the foam crush (the jagged section after first load drop) was simulated accurately as well. The consistency continues until the middle of the second load increase, which is the hardening behaviour of sandwich caused

by the densification of the crushed foam and the bending of the bottom facesheet. After this point, the numerical model underestimated the final failure load of the bottom facesheet with a 28.57% difference. However, the displacement at failure was predicted accurately, with a 1.52% variation. The reason of the inconsistency is believed to be the shortcoming of the penetration modelling, which arises from the interaction between the foam core and the bottom laminate. In reality, crushed and densified foam was attached to the laminate during the facesheet failure (Figure 99). However, in FE model, extremely distorted elements should be removed from the model in order to facilitate the penetration phenomenon. This possibly causes a mismatch between experimental and numerical failure load levels. Therefore, this should be investigated in a future work. Nonetheless, reasonable and sufficient prediction was achieved overall.

Among three numerical models in Figure 108, FEM-2 (erosion strain: 1.2) provided more accurate foam response compared to the others. The foam crush plateau between 20-40 mm and the foam conoid shear failure just before 40 mm crosshead displacement was captured accurately whereas other models failed to display a clear indication of this failure mode. Therefore, 1.2 value was used for foam erosion in all the sandwich impact simulations.

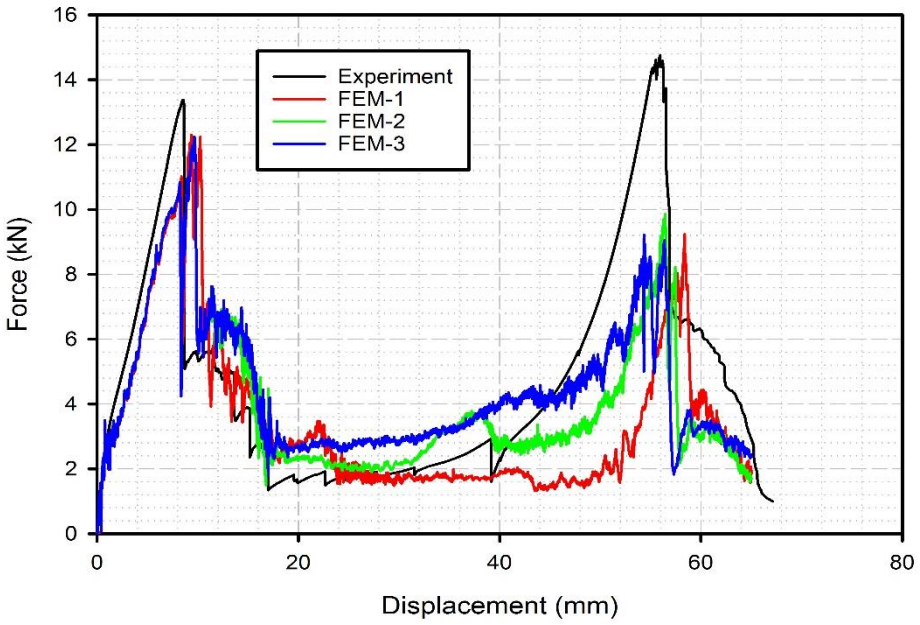

Figure 108 Comparison of force-displacement levels of the experiment and numerical model for sandwich composite. FEM 1, 2, and 3 indicates the model with different element erosion parameters assigned to the foam core (0.8, 1.2, and 1.5, respectively) for a more accurate material response

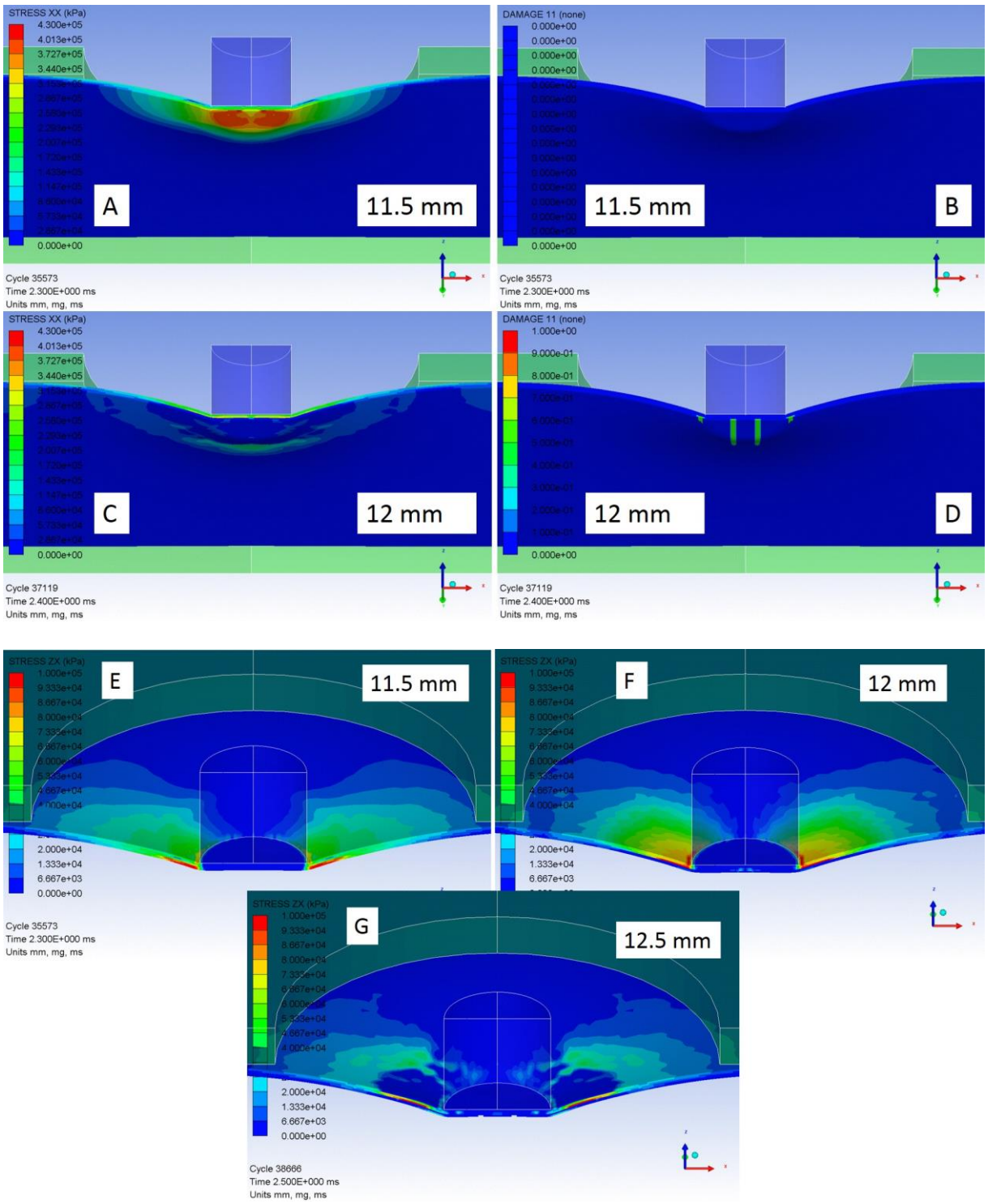

Figure 109 STRESS XX (A and C) and DAMAGE 11 (B and D) contour plots showing the tensile stress distribution and associated fibre tensile failure of the sandwich top facesheet at indicated crosshead displacements. STRESS ZX contour plot (E to G) shows the through-thickness stress distribution at indicated crosshead displacements. Tensile failure precedes the shear failure by 0.5 mm crosshead displacement

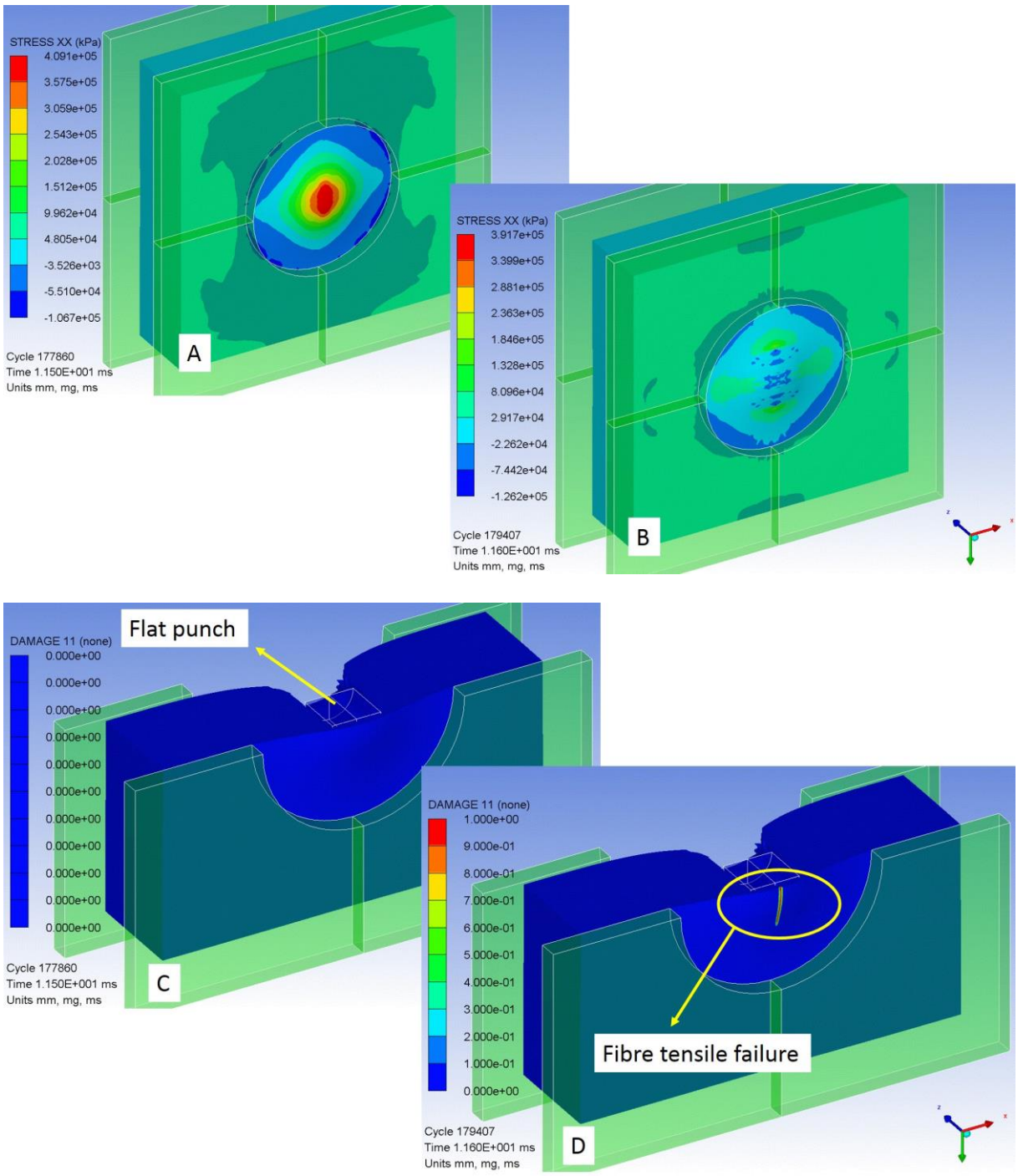

Figure 110 STRESS XX contour plot (top) showing the sandwich reverse face stress distribution in fibre direction before (A) and after (B) the laminate failure. The stress levels decrease after the back face tensile stress reaches to maximum strength level (431 MPa). DAMAGE 11 contour plot (bottom) shows the fibre failure before (C) and after (D) the reverse face failure for the corresponding STRESS XX levels

Figure 109 illustrates the mechanism responsible for the sandwich top laminate failure. Top face tensile failure occurred at 12 mm crosshead displacement (A to D), and rapidly followed by top face through-thickness shear failure (E to G) at 12.5 mm crosshead displacement. This finding clarifies and supports the evidence in Section 5.2.5 that experimental fibre tensile failure preceded the fibre shear failure. Figure 110 depicts the failure mode responsible for the sandwich bottom laminate failure which was observed as fibre tensile failure. As the STRESS XX contours show that the stress levels increases up to the maximum allowable levels just before the failure (Figure 110 A), and a stress release (decrease) was observed after the failure (Figure 110 B). Correspondingly, the DAMAGE 11 contour plot indicates the tensile failure at the bottom laminate (Figure 110 D).

The energy absorption of the sandwich plate was observed as well during the simulation of QSPT, and the internal energy (IE) change was illustrated in Figure 111. It is clear that the foam core contributed a great amount to the energy absorption, only to be outperformed by the GFRP laminate at the latest stages of the penetration. The energy absorption rate of GFRP decreases after top face failure (after 10 mm displacement) and the slightly ascending plateau indicates the contribution from bending resistance of the bottom facesheet. On the other hand, the foam core continues to absorb more energy by foam crushing, until conoid foam shear occurs at 40 mm displacement, after which the energy absorption starts to decrease. Lastly, the energy was absorbed mainly by the resistance of the bottom GFRP facesheet.

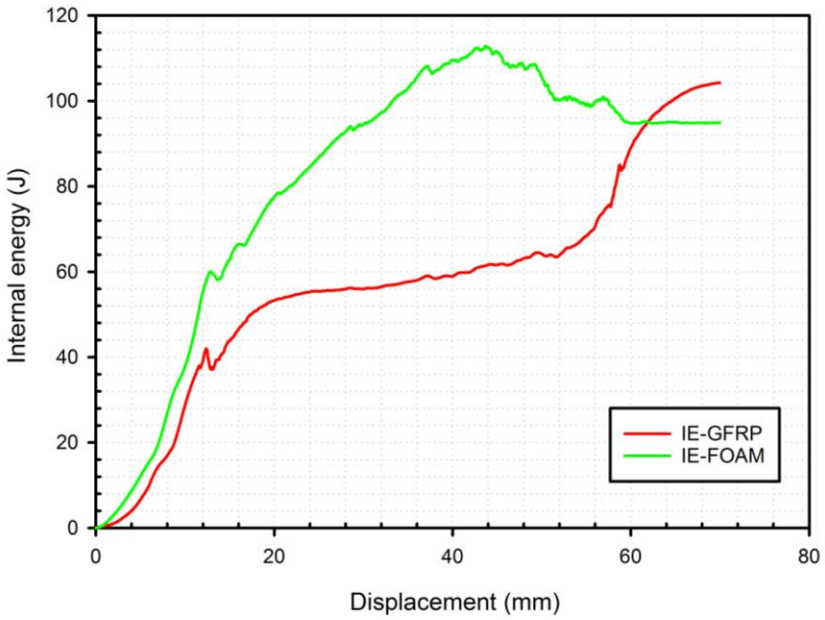

Figure 111 Internal energy change of the GFRP facesheets and foam core during the QSPT simulation

Taken together, the sandwich plate absorbed 220 J of energy by fibre tensile, fibre shear, foam core crushing, and foam core shear failure mechanisms. When compared with the energy required to penetrate the samples in QSPT experiment: 315 J, 30.15% difference was calculated. This inconsistency was due to the variation in the bottom face failure load prediction described earlier in this section. Therefore, this subject needs further investigation together with the late-phase penetration modelling and the effect of foam-bottom facesheet interaction.

Determination of the foam core thickness

As mentioned previously, the characterisation of the GFRP/foam sandwich plate was performed with 50 mm thick core. However, before carrying out simulations to investigate the railway impact standards, an appropriate thickness value has to be selected. The criteria for this preference was the essential reason to use composites in railway vehicles which is light-weighting purposes. Therefore, static penetration simulations were carried out considering different thickness foam cores in order to the find the optimized energy absorption behaviour. The results of energy absorption per weight – specific energy absorption (SEA) – for sandwich plates with 20, 30, 40, and 50 mm thick foam core is illustrated in Figure 112 and reported in Table 19. Based on these results, the sandwich plates with 30 mm foam core was selected to investigate the railway standards.

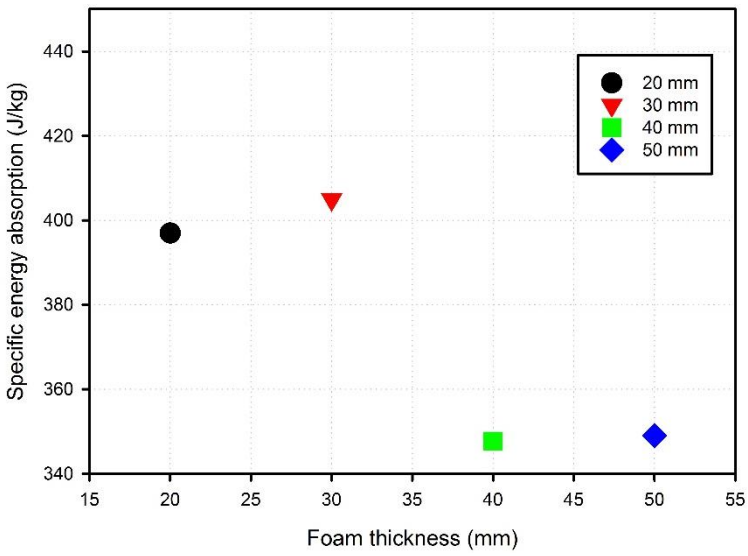

Figure 112 Specific energy absorption (SEA) with respect to foam thickness for Airex T90.100 foam core sandwich plates

Sandwich core thickness (mm)	Total weight (kg) (GFRP+Foam)	Total energy absorption (J)	Specific Energy Absorption (J/kg)
20	(0.31+0.088)	158	396.98
30	(0.31+0.132)	179	404.97
40	(0.31+0.176)	169	347.73
50	(0.31+0.220)	185	349.05

Table 19 Specific energy absorption (SEA) with respect to varying foam core thicknesses of sandwich composite

5.3.2 Model validation: High velocity impact

It has been shown in the previous section that the quasi-static FE model was validated with the experiments. However, due to the absence of ballistic testing facilities and due to budget limitations to have the materials tested elsewhere, the high velocity impact experiments could not be performed. Since same FE models will be used in HVI simulations, it has to be shown that the considered FE approach has been fully understood, and the model works for dynamic loadings as well in order to be credible. This challenge has been overcome in two stages, i.e. first remaking a published study from the literature, in this case the work of Gama & Gillespie (Gama & Gillespie 2011), and secondly investigating the strain rate effects (Section 5.3.3) in dynamic loading by correlating the HVI simulations with analytical ballistic penetration models. This section deals with the former.

Comparison with published study: There were two main reasons for selecting the work of Gama & Gillespie (Gama & Gillespie 2011) to support the assumption that an accurate prediction could be obtained in the absence of physical ballistic testing. Firstly, the availability of the material inputs, and secondly but more importantly is that the published work was carried out with LS-DYNA software, whereas in this thesis it was ANSYS AUTODYN. Both of these software are explicit solvers, however there are differences in modelling and certain parameters. Thus, this section shows that despite the differences, the developed numerical model was capable of providing accurate predictions and the consideration of strain rate effects were validated.

It was detailed in the literature review section that S-2 glass/SC-15 epoxy laminates were investigated under ballistic loading both experimentally and numerically (Gama & Gillespie 2011). Validation was obtained by comparing various impact parameters such as contact force,

ballistic limit velocity, energy balance, and overall material failure. Figure 113 shows the energy balance comparison for this published work and the AUTODYN results. The results obtained from AUTODYN shows a decrease in total energy. The reason for this decrease is believed to be the lack of consideration of friction energy between impactor and target material. So it doesn't necessarily mean there is a loss in the total energy of the system. This is why the top right graph was also shown in Figure 113 indicated the error levels of the simulation. In AUTODYN, if the error level is within 10% of the total energy, then it is considered as a reliable simulation. It shows that the error level remained almost unchanged. Other indicators such as kinetic energy and internal energy change of the projectile/target are also consistent with the original results. Minor differences in the graphs are present due to the differences in hardware and simulation setup such as mesh density and computing performance. Nevertheless, it is concluded that the numerical model was able to capture the energy balance for the system.

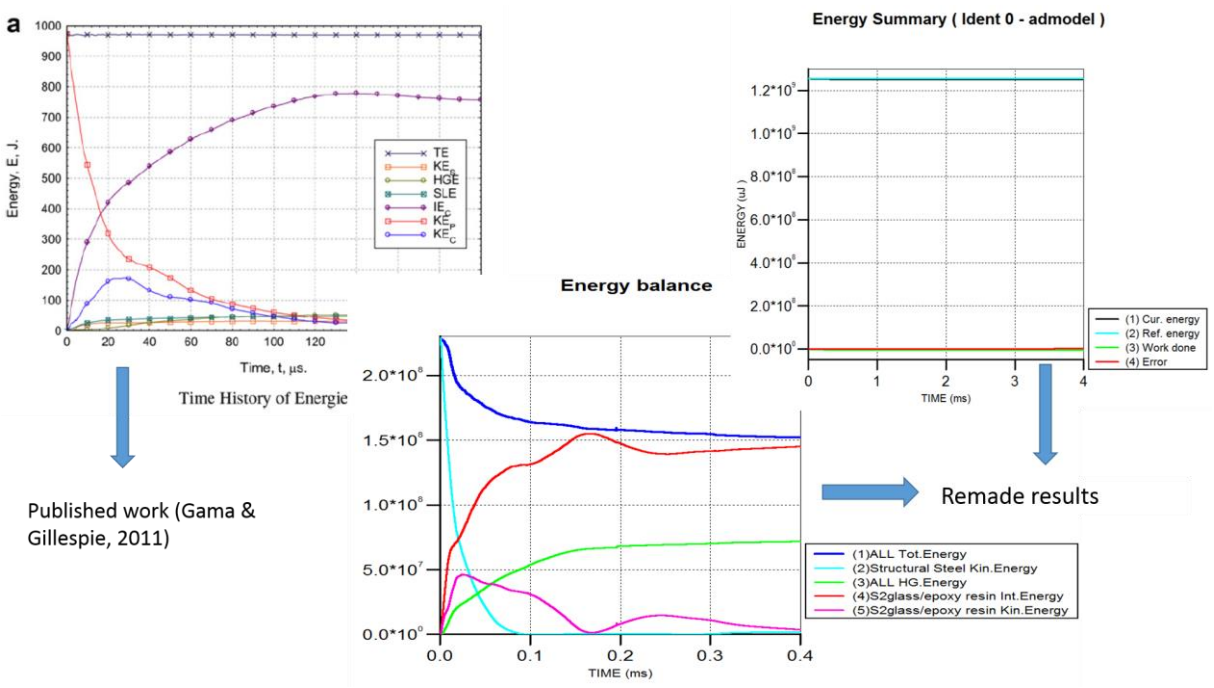

Figure 113 Comparison of energy dissipation and balance

Remade results are the results obtained from AUTODYN simulations. The error level in energy summary is not changing and remains below allowable limit (10%). In energy summary graph (top right), Current Energy overlaps with Reference Energy, and Work done overlaps with Error line.

Another parameter to compare was the contact force between projectile and target, i.e. penetration resistance of the target material. Figure 114 shows the contact force levels with

respect to projectile displacement in the reference work, whereas AUTODYN model shows the contact force vs time graph. Overall the resistance force values match well between the two cases (150kN level).

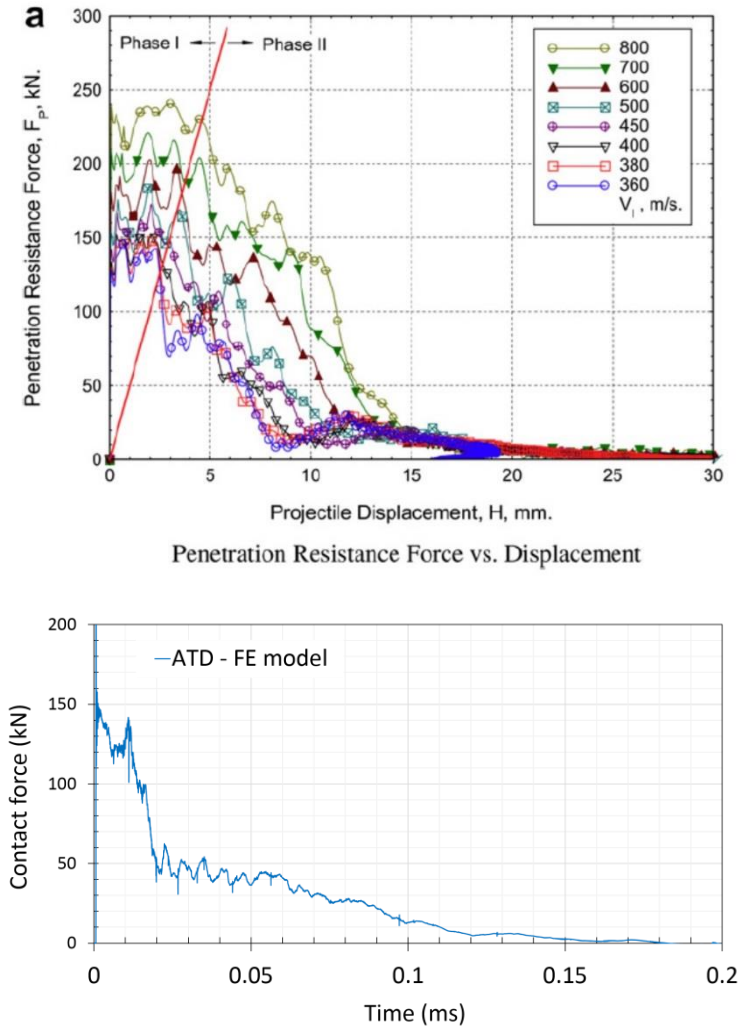

Figure 114 Comparison of contact force during 360m/s velocity impact showing the AUTODYN model captured the initial penetration resistance of the laminate accurately with respect to published results

In Figure 115 velocity history results from the simulations was presented by the authors at above ballistic limit velocity. Based on their report of experimental velocity levels - V_{BL}: 367m/s and V_R: 38.3m/s – AUTODYN simulation was carried out for 367m/s impact velocity and 34m/s residual velocity was obtained, resulting in 11.22% variation between two models.

Last but not least, the overall failure of the target material at the end of the impact was compared for both the numerical and experimental reported results. The extent of delamination at 360m/s impact which is nearly at the ballistic limit is shown in Figure 116 along with the AUTODYN

model result. AUTODYN model slightly overestimated the propagation despite the fact that the delamination modelling method was different between the two studies.

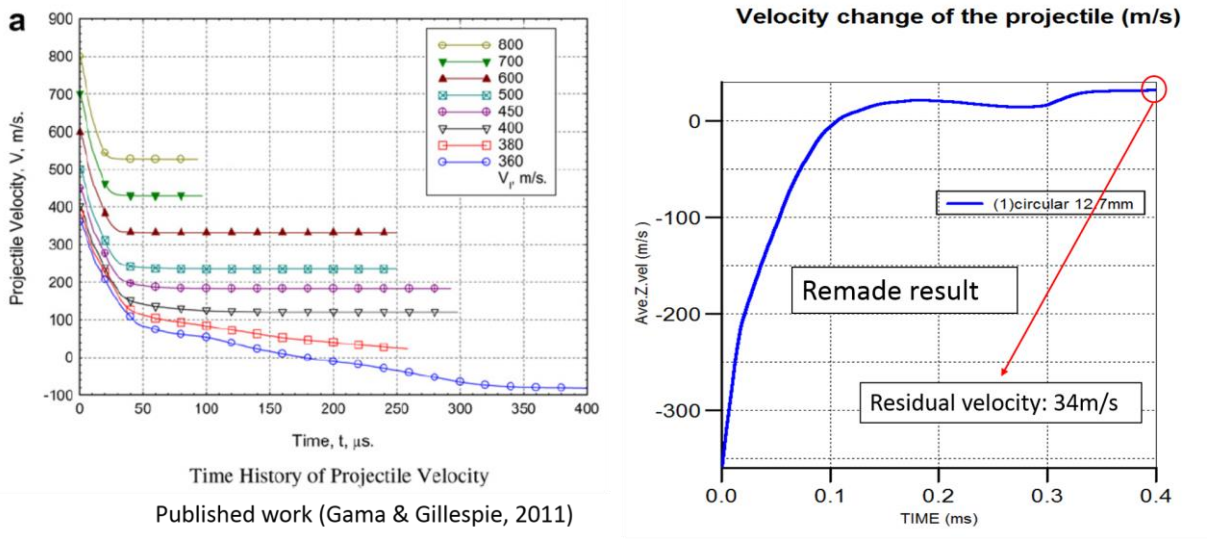

Figure 115 Comparison of residual velocity for 360m/s velocity impact showing 34 m/s residual velocity was predicted by AUTODYN with an 11.22% variation in comparison to published work

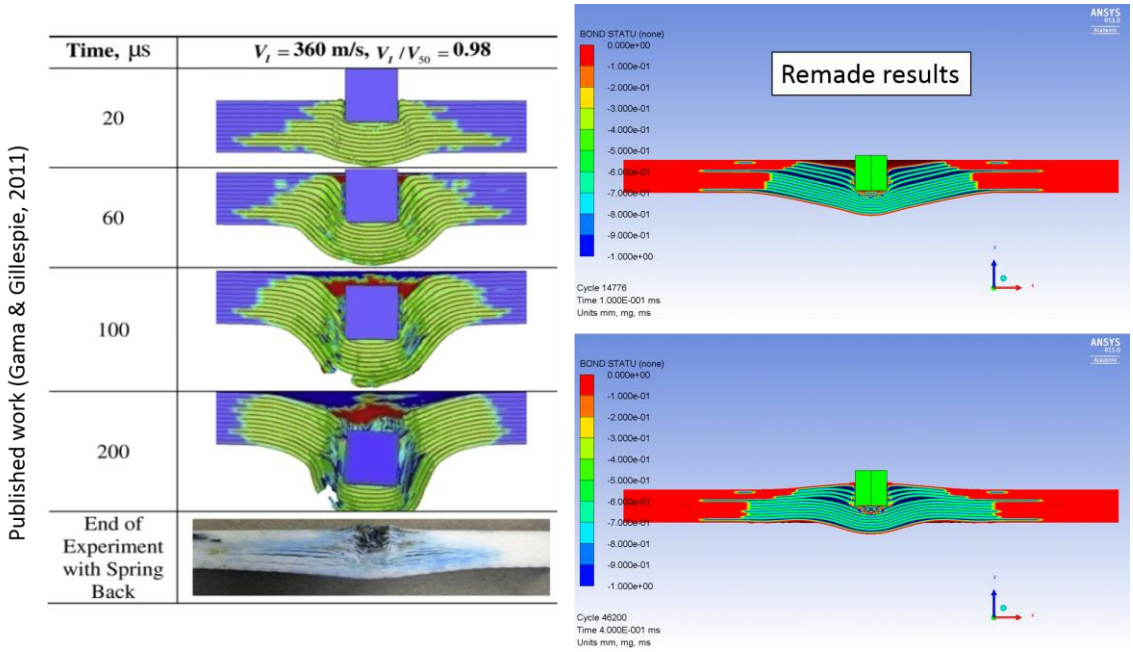

Figure 116 Delamination and depth of penetration comparison showing AUTODYN results (right) are very accurate in comparison to the ballistic experimental result (bottom left)

LS-DYNA Model 162 has the capability to predefine delamination without the need of additional contact or cohesive elements. However, definition of delamination in AUTODYN

model has been done through contact elements with a stress criteria assigned to them. On the other hand, the prediction for the depth of penetration (almost half of the laminate thickness) was in good correlation with the experimental result although it was predicted more excessively by the authors' numerical model. These comparisons prove that the numerical model can be used with confidence for dynamic impact analysis.

5.3.3 Strain rate effect analysis

Section 4.4 highlighted the effects of higher strain rate loading on glass fibre reinforced composites as an increase in material strengths and elasticity moduli in general. However, a certain level of enhancement does not exist. Therefore, in this study, two dynamic material sets were considered to represent the effect of strain rate, i.e. 30% and 50% increase in material properties. Impact simulations were carried out with CF and H ended projectiles in 40-160 m/s velocity range (section 4.3.9) with three sets of material properties (static, 30%, and 50% increase). The results of these simulations were compared with the analytical ballistic and penetration models provided in Section 4.4. The purpose of this section therefore is to investigate the credibility of the material response in dynamic loadings, by analysing a velocity range that covers no-penetration, ballistic limit (partial penetration), and full-penetration cases.

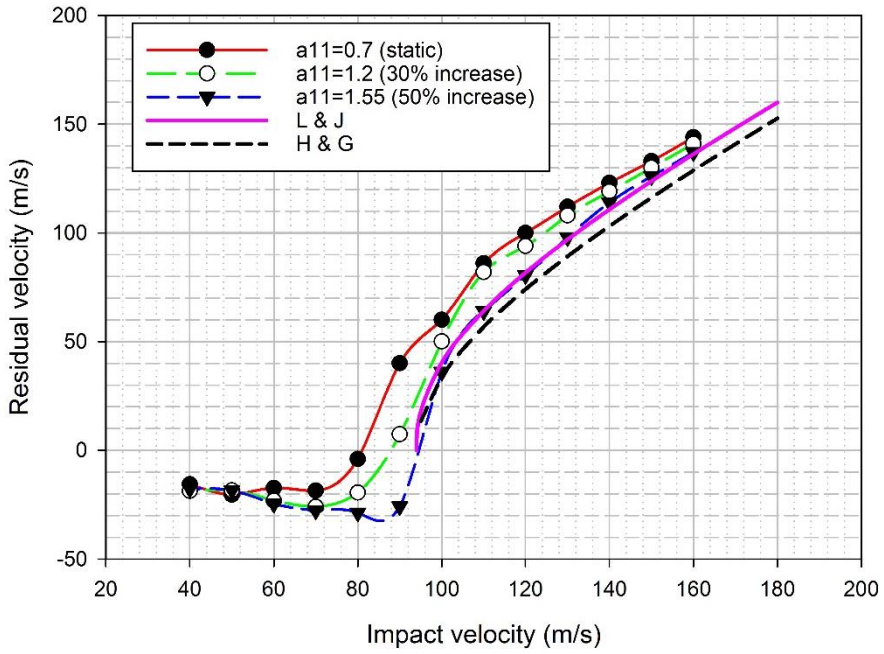

Figure 117 Residual velocity vs impact velocity graph of CF ended projectile with three material property sets showing the penetration model fits to the numerical data. L&J: Lambert-Jonas model, H&G: Haque-Gillespie model.

Figure 117 and Figure 118 present the numerical predictions along with the Lambert-Jonas and Haque-Gillespie penetration models fit to these data. The ballistic limit for each projectile was calculated using Wen's model and this data was later fed in to the penetration models to generate curve fittings. The following parameters were used to calculate ballistic limit velocity of laminates; projectile profile parameter β=1.25 for CF and β=0.6 for H projectile, projectile mass G=100g, target thickness T=6mm, projectile diameter D=25.4mm, target density ρ_t=0.00185gr/mm^3, and target through-thickness elastic limit σ_e=97MPa.

Ballistic limit velocity was calculated as 94.53 m/s for CF ended impactor, while for H ended impactor it was 84.89 m/s. It can be seen from Figure 117 and Figure 118 that the 30% increase in material property resulted in little improvement over static material property simulations for both projectiles. The influence of the enhancement seems more defined around the ballistic limit velocity, while for impact resulted in complete penetration, the effect diminishes gradually, making the residual velocities similar. On the other hand, ballistic limit velocities obtained using Wen's model coincides well with the 50% increase curve predicted by the simulations. To be more precise, additional impact simulations were carried out to obtain near zero residual velocity for both projectiles to find the error between analytical prediction and the numerical model.

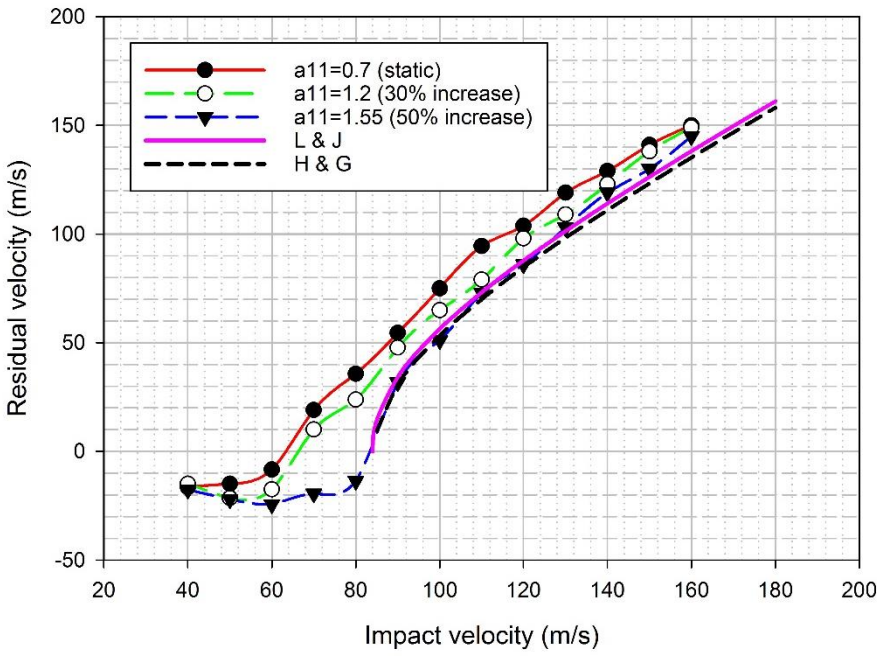

Figure 118 Impact velocity vs residual velocity graph of H ended projectile with three material property sets showing the penetration model fits to the numerical data. L&J: Lambert and Jonas model, H&G: Haque and Gillespie model.

The lowest full penetration for CF projectile was predicted at 97m/s (V_R=12m/s) and highest partial penetration was predicted at 95m/s (rebound velocity V_R=20m/s). Considering 96m/s is the predicted limit velocity, 1.55% variation is calculated between Wen's model prediction and the numerical model. For H ended projectile lowest full penetration was predicted at 81m/s (V_R=1.4m/s), and highest partial penetration was predicted as 80m/s (rebound velocity V_R=13.6m/s), consequently resulting 5.17% variation between Wen's model and numerical prediction if we take ballistic limit velocity as 80.5m/s. These results prove that it is rational to carry out impact simulations with a 50% increase in material properties. It is also in parallel with the findings of (Zhou & Davies 1994) that the strain rate enhancement is higher for thin laminates compared to thick ones, noting that laminates in question can be classified as thin taking into account the impactor diameter (*h/D*=6/25.4=0.236).

Supporting the findings above, it has been found that both penetration models gave excellent fit to the residual velocity data obtained from the simulations that incorporates the 50% increased material properties due to the strain rate effects. The reason for the variation between the two analytical models is believed to be the insufficient experimental data provided in the H-G model since it is influenced by the jump velocity (V_T^{max}) which represents any anomaly in the target or small differential kinetic energy that causes a jump in the residual velocity at and around ballistic limit.

Based on the reliability of the results of laminated plates, the same principals were applied to GFRP facesheet/foam core sandwich plates as well. However, only the ballistic limit velocity range was considered this time rather than the full velocity range (40-160 m/s). Figure 119 presents the results of two ballistic impacts on sandwich plate, 76 m/s and 85 m/s, which resulted in partial penetration and complete penetration, respectively. The projectile rebounded from the sandwich plate with a V_R= -10 m/s residual (rebound) velocity after 76 m/s impact, while after 85 m/s impact, it penetrated the sandwich fully and exited with a residual velocity of V_R= 8 m/s. Based on this data, the average ballistic limit velocity V_{BL} was calculated as 80.5 m/s. The analytical prediction of V_{BL} using Wen's model was calculated as V_{BL}= 75.7 m/s. These results show that only a 6% variation exists between the numerical model and the analytical prediction. Therefore, it proves that the adoption of strain rate effects is viable for sandwich plate as well even though the materials used were slightly different (epoxy resin instead of polyester resin).

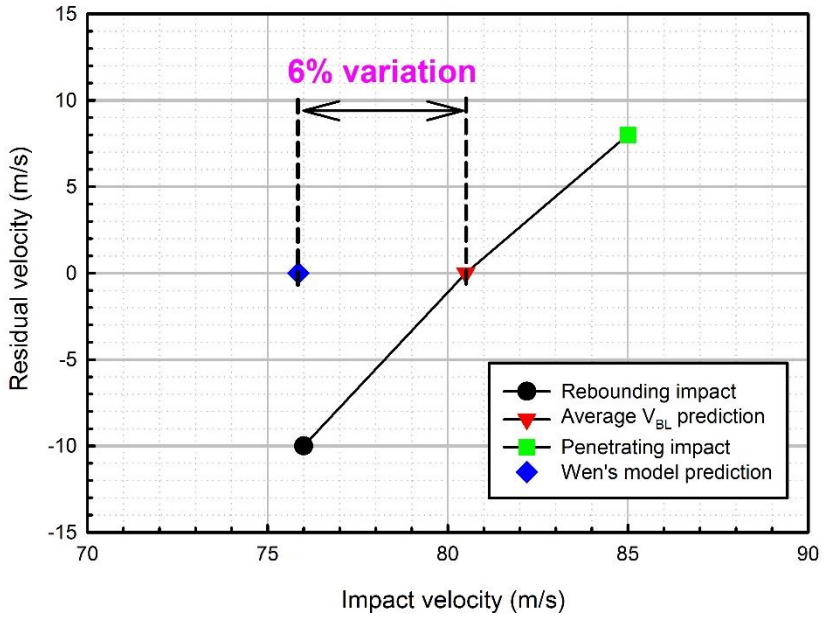

Figure 119 Ballistic velocity prediction of numerical model compared to Wen's model prediction. Numerical model achieved good prediction, with a 6% variation compared to analytical model

5.3.4 Extent of delamination in dynamic loading

Composite laminates subjected to high velocity impacts exhibit two consequences. If the impact results in full penetration, the damage will be localized around the area of impact. In a non-penetration or partial penetration case, the damage will most likely be spread inside the material (along with possible fibre damage at the impacted face) because the impact energy is dissipated by matrix failure mechanisms such as matrix cracking and delamination. Therefore, it is important to determine the extent of internal damage in case of a non-penetrating impact. Figure 120 shows the radius of delamination at the end of each impact simulation (based on 50% enhanced material properties), which increases up to limit velocity levels for both projectiles and after that decreases as a result of full penetration and localized material response, in parallel with what was previously reported (Potti & Sun 1997). The highest measured radius was 55 mm which occurred in 100 m/s impact and this value is slightly larger than the fixture ring (106 mm diameter). This result indicates that within the considered velocity range the delamination damage did not reach to the edge of laminates, therefore the size of laminates was sufficient and the boundary conditions did not affect the outcome of simulations results.

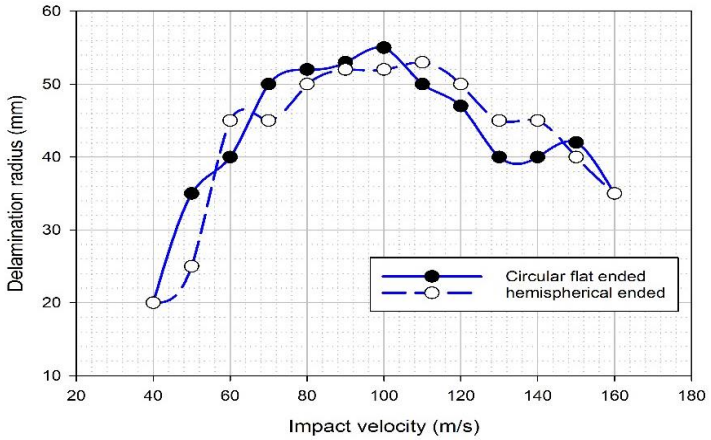

Figure 120 Delamination length with respect to impact velocity showing maximum measured length is within the boundaries of the samples. This means the sample dimensions are sufficient

5.4 Energy absorption behaviour under dynamic loading

Internal energy change (i.e. energy absorption) of the glass fibre laminates were presented in Figure 121 and Figure 122 with respect to impact velocity. The trend in energy absorption increases gradually with respect to impact velocity until the ballistic limit velocity, then after this point it decreases and stabilises with respect to increasing impact velocity, indicating that the damage was getting more and more localised. This result agrees with what has been reported in (Hosur et al. 2004). For the CF ended projectile, with every set of material property, i.e. static properties, 30% and 50% increased material properties, the energy absorption is almost equal in the 40-80m/s range which is expected since all the projectile's energy was consumed before the projectile stopped. At 90m/s impact velocity the energy absorption difference between static and dynamic material properties is clear, indicating that limit velocity value starts to change at this point because the higher strain rate loadings result in increased material property and a better structural performance. This can be seen better in 0-400J and 0-300J energy range in Figure 123 and Figure 124, respectively, which shows the energy profile of impacted laminates by CF and H projectiles, i.e. absorbed energy (E_a) with respect to impact energy (E_i). An impact resulting in complete penetration can be understood when the slope of the curve started to deviate from unity.

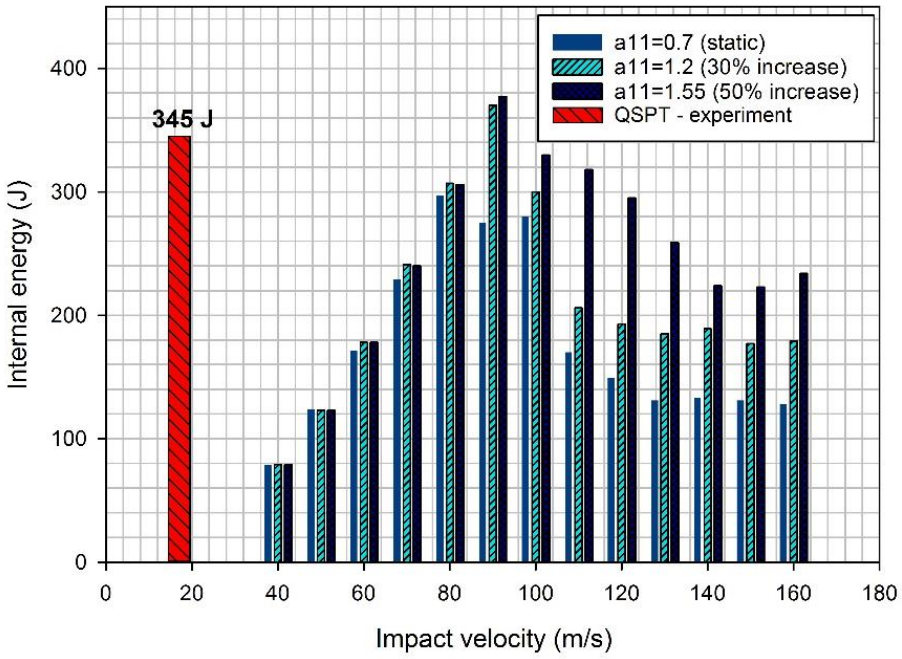

Figure 121 Internal energy change of laminates under impact loading and QSPT experiment for CF ended projectile showing how the different material sets affect the energy absorption before and after ballistic limit velocity (94.53 m/s). a11 being the material property modifier in AUTODYN, a11:0.7 represents static material property set, while a11:1.2 and a11:1.5 represent 30% and 50% increased (dynamic) material property sets, respectively

The energy required to fully penetrate glass fibre laminates in QSPT was also included in Figure 121 and Figure 122. Compared with the absorbed energy at near ballistic limit velocity, the energy required in static perforation resulted in 8.48% and 15% differences for CF ended and H ended projectiles, respectively. This result is in parallel with what was reported previously by many that energy consumed by specimens in dynamic penetration was higher than in static penetration. The higher variation of energy levels for H ended projectile is believed to be the erosion parameter in numerical model. The energies of excessively distorted and deleted elements are stored in the total energy count, and since point contact results in concentrated deformation the number of distorted elements were less. These findings suggest that performing QSPT test with the setup described in this study can give reasonable prediction on the energy absorption capability of the structure in intermediate to high velocity impact events.

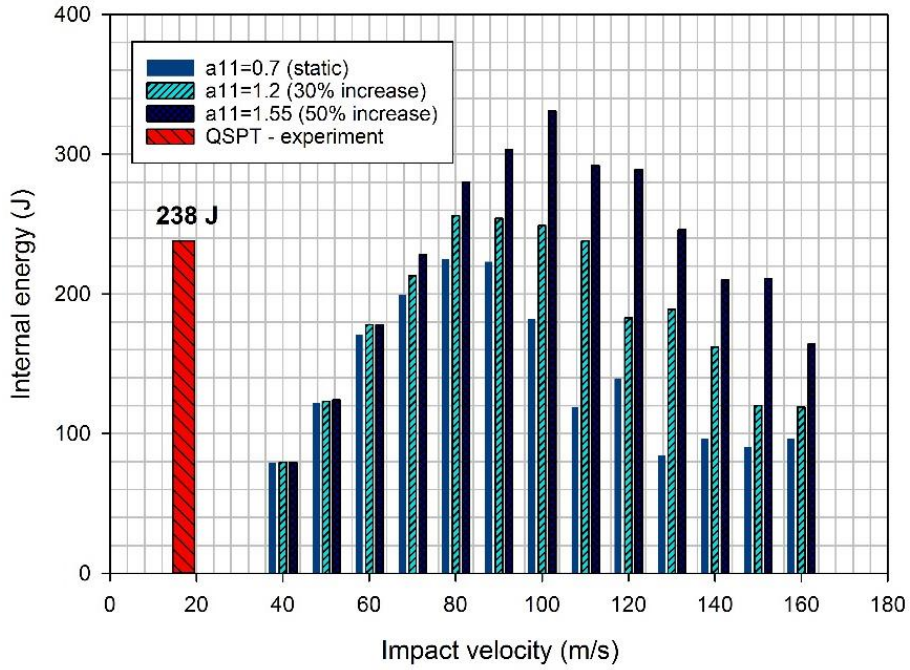

Figure 122 Internal energy change of laminates under impact loading and QSPT experiment for H ended projectile showing how the different material sets affect the energy absorption before and after ballistic limit velocity (80.5 m/s). a11 being the material property modifier in AUTODYN, a11:0.7 represents static material property set, while a11:1.2 and a11:1.5 represent 30% and 50% increased (dynamic) material property sets, respectively

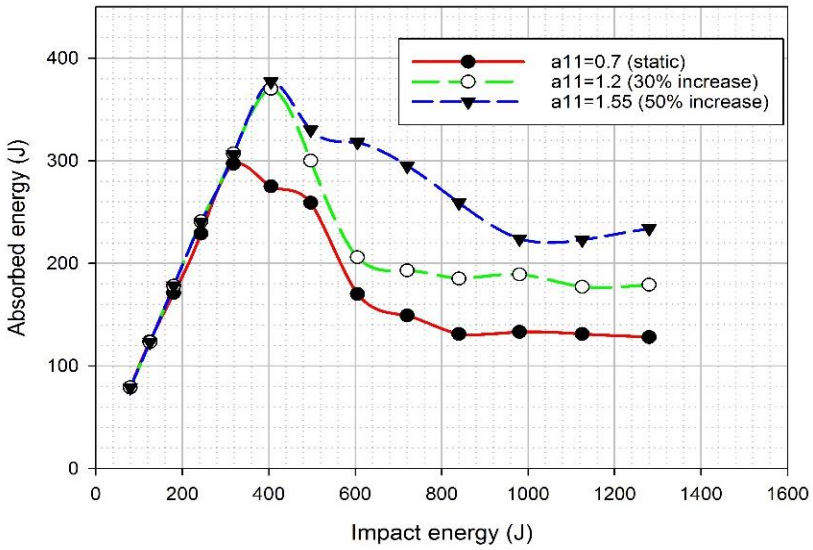

Figure 123 Energy absorption profile of materials with static and dynamic material property sets for CF ended projectile impact, indicating the peak of each slope defines the limit of the structure's energy absorption capability

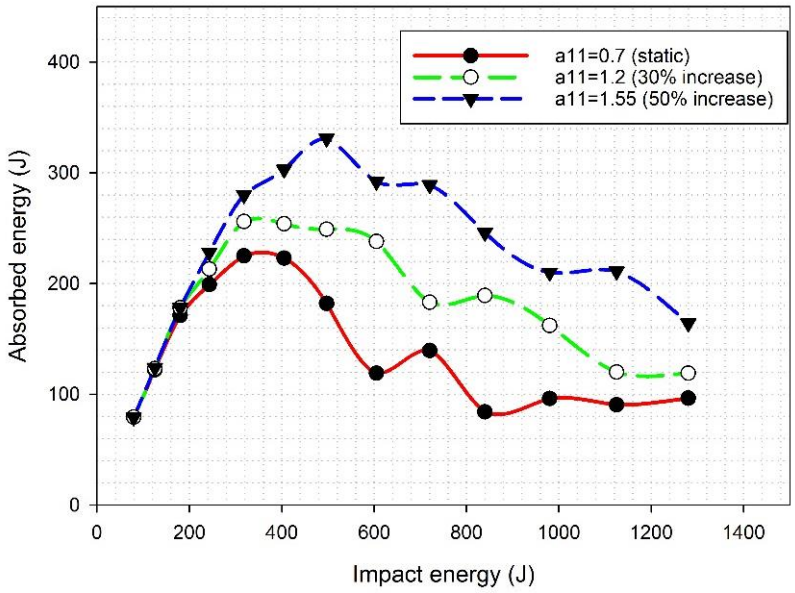

Figure 124 Energy absorption profile of materials with static and dynamic material property sets for H ended projectile impact, indicating the peak of each slope defines the limit of the structure's energy absorption capability

5.5 Discussion and conclusion

This chapter presented the findings from the experimental program, and then validated the numerical models with experiments and analytical models available in the literature. The primary material properties were identified as the tensile strength in fibre direction, the OOP shear strength, and the interlaminar shear strength. Next these properties were investigated in detail. Performing QSPT with SPR1.2 setup enabled to obtain the resistance of the structure against shear forces arisen by the impactor contact. Since both the impact and reverse face failure was due to the shear failure (rather than tensile failure in reverse face), the outcome of this setup could be useful even though a different material is used, given the fact that, e.g., relatively brittle carbon FRP laminates tend to show more distinct shear plugging when subjected to ballistic impacts.

The focus was given to the QSP tests with SPR4.1 setup which is the essence of the proposed method. These experiments confirmed that the failure mechanisms were indeed quite similar to an actual ballistic impact case, which later allowed the use of numerical models in dynamic impact simulations based on the static models. The use of shear strength obtained from SPR1.2 tests as a material property in simulations was found satisfactory in controlling the load bearing loss along with tensile strength. Excellent correlation has been achieved for circular flat

impactor case, however, even though it was sufficient at the time, further numerical and experimental investigation could improve the correlations for hemispherical case.

In general, based on what has been reported, it is fair to say that the correlation level between the prediction models and the physical tests were very satisfactory. This is indeed the case especially for the dynamic impact loading and the material behaviour since that particular analysis itself was a prediction, hindered by the limitations in ballistic testing. However, the prediction methodology depends on valid and a rational foundation which was supported by the available literary information. Obviously, discrepancies will exist if it were possible to obtain physical ballistic results. However, it is strongly believed that this limitation has been overcome with confidence.

High velocity impact analysis showed that the effect of strain rate on the material properties have significant influence over ballistic performance of the composite materials. It was therefore concluded that the 'enhancement level' caused by higher strain rate loading is the most important impact parameter in this research, and this parameter denoted as '*ENL*' for future reference.

The current method uses the SPR4.1 custom-made testing setup, and the energy absorption values were found quite close to each other in static and dynamic impact cases. This has not been seen in the previous research for this particular case. Therefore it would be interesting to conduct further research with various materials and various thicknesses to see whether this is a case-specific finding. In connection with this finding, it will be discussed further (after the analysis of case studies in Chapter 6) that whether the energy absorption is a better parameter on the assessment of structures.

Chapter 6. Validation of the prediction method using flying object risk scenarios

Previous chapter explained the technical aspects and details of impact risks against carbodies. This chapter investigates whether it is viable to promote the proposed method by comparing it with the relevant standards (Table 2 (page 72) from three points of view:

[1]. ***Simulating the standard***: Firstly, impact scenarios were simulated as they appeared in each standard, including all necessary specifications such as sample dimensions and characteristic impact parameters.

[2]. ***Effect of sample size and boundary conditions***: Secondly, each scenario was simulated with the QSPT fixture while maintaining the *impactor geometry and velocity as they are described in the standards*. These results will reveal the possibility to alter the sample size and boundary conditions.

[3]. ***Effect of projectile geometry***: Lastly, impact simulations of *flat and hemispherical ended projectiles with the same incident energy* were presented, together with the previous two cases for comparison. These comparisons will reveal whether the use of a case specific projectile is strictly needed.

Each scenario was analysed in terms of energy transfer from the projectile to the sample, projectile velocity change, and the penetration resistance characteristics together with the visible and invisible damage of the structure. The results of monolithic laminates were presented first and the results of sandwich composite were presented afterwards. A general discussion on findings and the applicability of the results are presented at the end of this chapter along with a conclusion.

6.1 EN 15152 – Gravelling impact risk

European standard for the windscreen requirements describes the gravelling impact as repeated impact from small objects and states:

"The risk of this type of damage will vary according to train speed, the aerodynamic conditions on the exterior of the driving cab and the construction of the infrastructure on which the train will operate. It is therefore the choice of the customer whether to demand that resistance to gravelling is demonstrated. If a resistance to gravelling is required, then the test requirements shall be as defined in 6.2.9. (EN 15152)."

According to this requirement, test pieces with nominal dimensions of 500x500 mm (±2.5 mm) are held by a rigid steel mounting with a central cut-out size of 460x460 mm, and were impacted by a conical aluminium projectile (grade 2017A) (Figure 125) travelling in normal direction to the surface with an impact speed of $v_{imp} = (v_{max} + 20) km/h$. Here v_{max} is the maximum operating speed of the rail vehicle. Simulation setups for both cases are shown in (Figure 126).

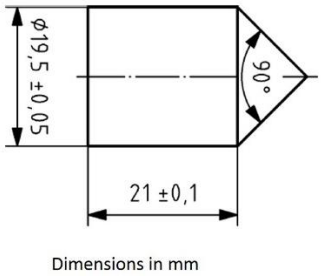

Figure 125 Specifications of gravelling impact projectile made of aluminium (EN15152)

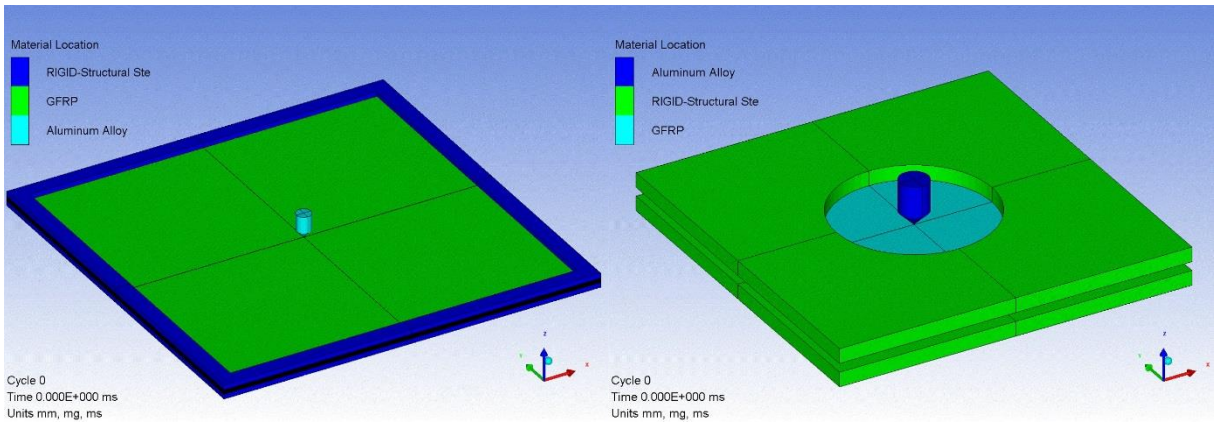

Figure 126 FE models of: EN 15152 setup (left), QSPT setup (right)

6.1.1 Results & discussion – monolithic laminate

Since this standard is required for high-speed train (HST) windscreens, the impact velocity for this scenario was determined as follows:

$$v_{imp} = (400 + 20) = 420\ km/h = 116\ m/s$$

Even though 400 km/h is not a frequently achievable operating speed in Europe, this preference was made while considering future improvements and applications in HST service. For a 20 g aluminium projectile, 116 m/s impact velocity results in 135 J of impact kinetic energy. Figure 127 shows that the energy transfer from the projectile to the laminate has similar characteristic in all cases, i.e. EN15152 standard setup (denoted as STND), QSPT setup with conical, flat and hemispherical impactor. At around 0.3 and 0.35 ms, kinetic energies reached to zero level,

indicating that the projectiles were caught by the laminate. In terms of energy transfer from the projectile to the laminate, a difference can be seen between incident kinetic energy (KE) (135 J) and maximum internal energy (IE) levels of the laminate in standard (STND) and QSPT setup with conical projectile. After reaching the maximum IE, the energy levels stays nearly the same until the end of impact because all of the projectile's KE was dissipated by the structure by then and the projectile was stuck in laminate. These indicate that the laminates in STND and QSPT-conical setup were capable of absorbing 110 J and 105 J of energy by elastic deformation, respectively. The rest of the impact energy (25 J and 30 J) was dissipated through plastic deformation (damage) and negligible forms of energy such as friction, heat, and sound. The damage appeared as fibre failure at laminate-projectile contact area (Figure 128), and delamination predominantly in two interfaces with radii of 25, 31, and 50 mm (Figure 129).

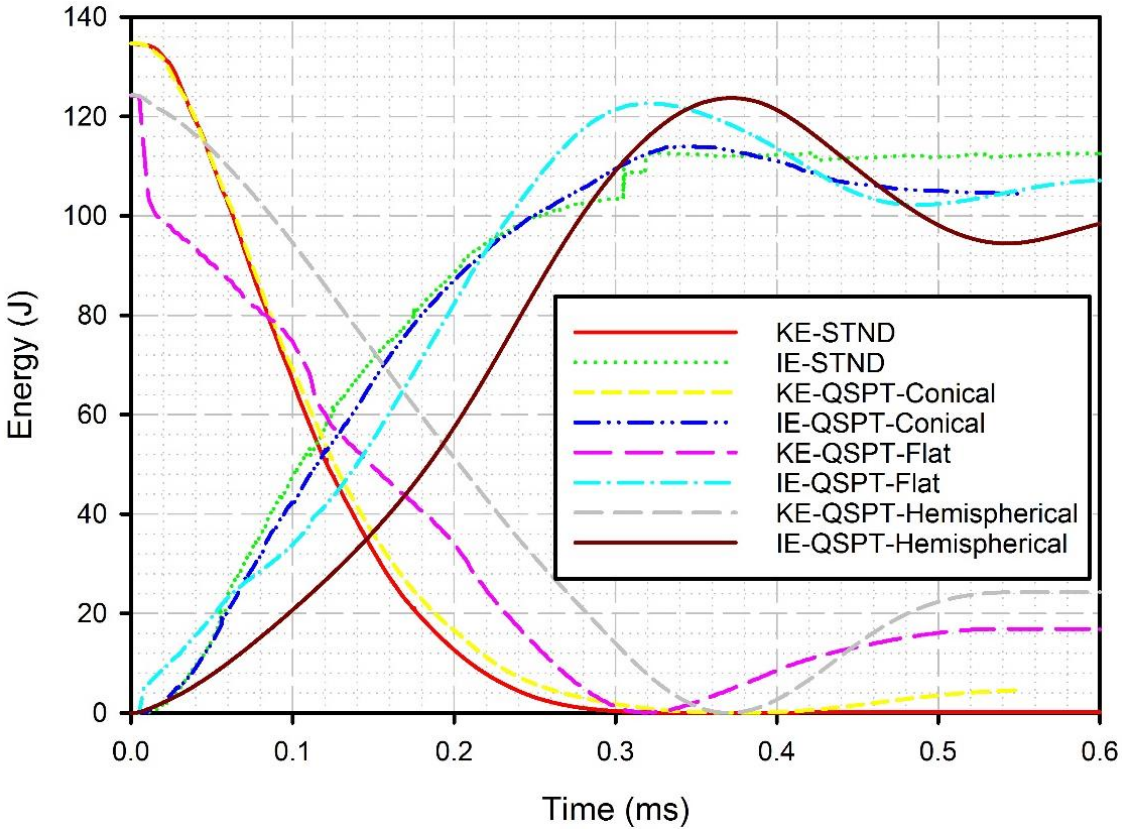

Figure 127 Kinetic energy (KE) change of the projectile and internal energy (IE) change of the GFRP laminates for EN15152 (STND) and QSPT setup with conical, flat, and hemispherical projectiles showing similar responses were obtained for each impact

The response of the laminates against flat and hemispherical ended projectiles in Figure 127 indicates that the energy transfer characteristics match well with both standard and QSPT-conical setups. For flat and hemispherical ended projectile impact, IEs increases up to incident

KE which indicates the impact caused no material failure except delamination. The decrease in the IEs after the maximum point indicates that the elastic energy stored in the laminate is then transferred back to projectile due to the flexibility of the laminate, which causes a spring-back and an increase in projectile KE.

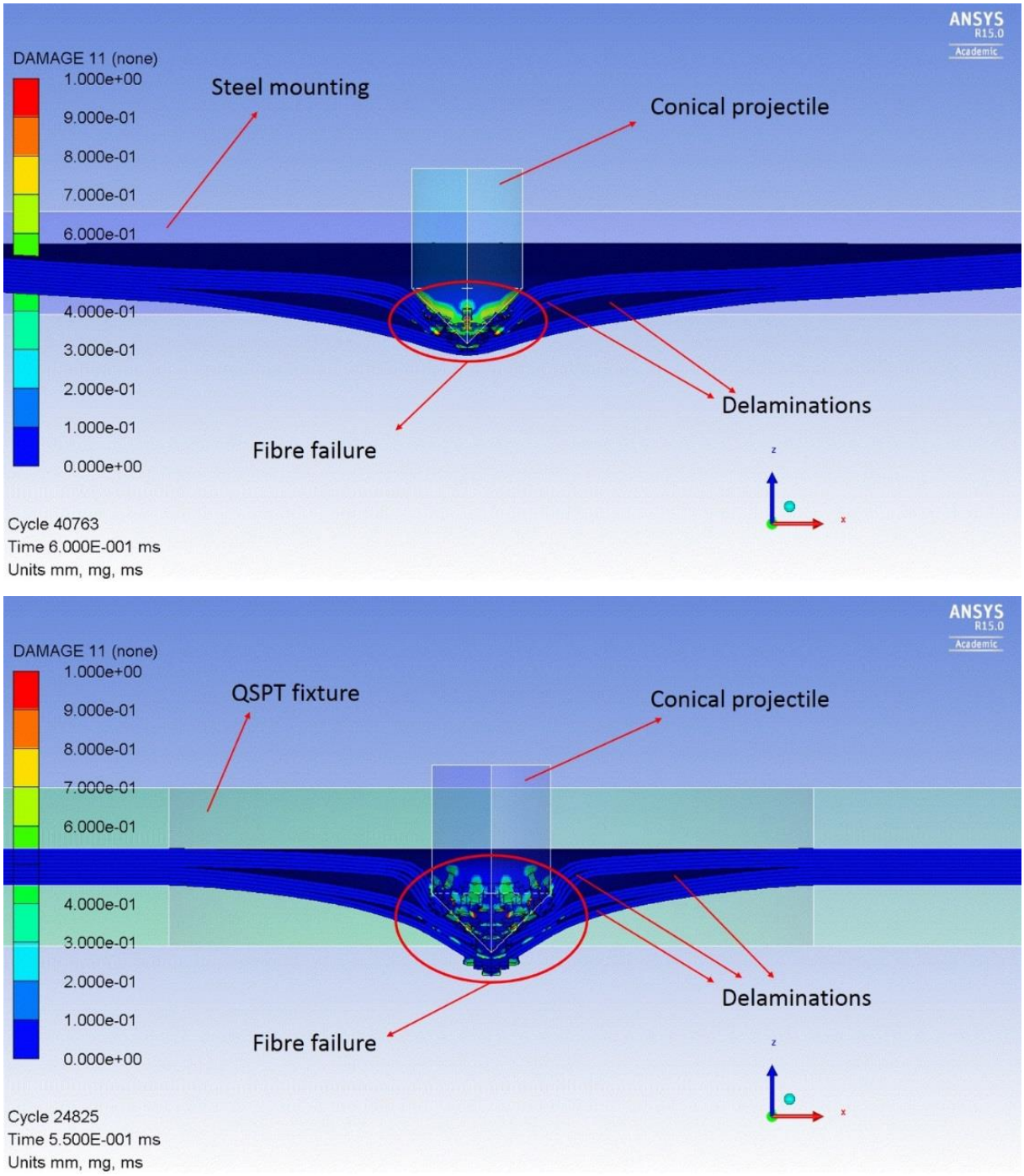

Figure 128 Failure in GFRP laminates after 116m/s impact: EN15152 setup (top), QSPT setup (bottom) showing the extent of fibre damage via contour plot (DAMAGE 11), and the delamination between layers

Failure analysis of the simulation results in Figure 128 reveals that visible failure occurs in a concentrated area beneath the impactor. The penetration level of the projectile was slightly greater in QSPT setup compared to STND setup. In the case of invisible failure – delamination – quite similar response was predicted with little variation (Figure 129) and the extent of delamination was captured as 50-51mm.

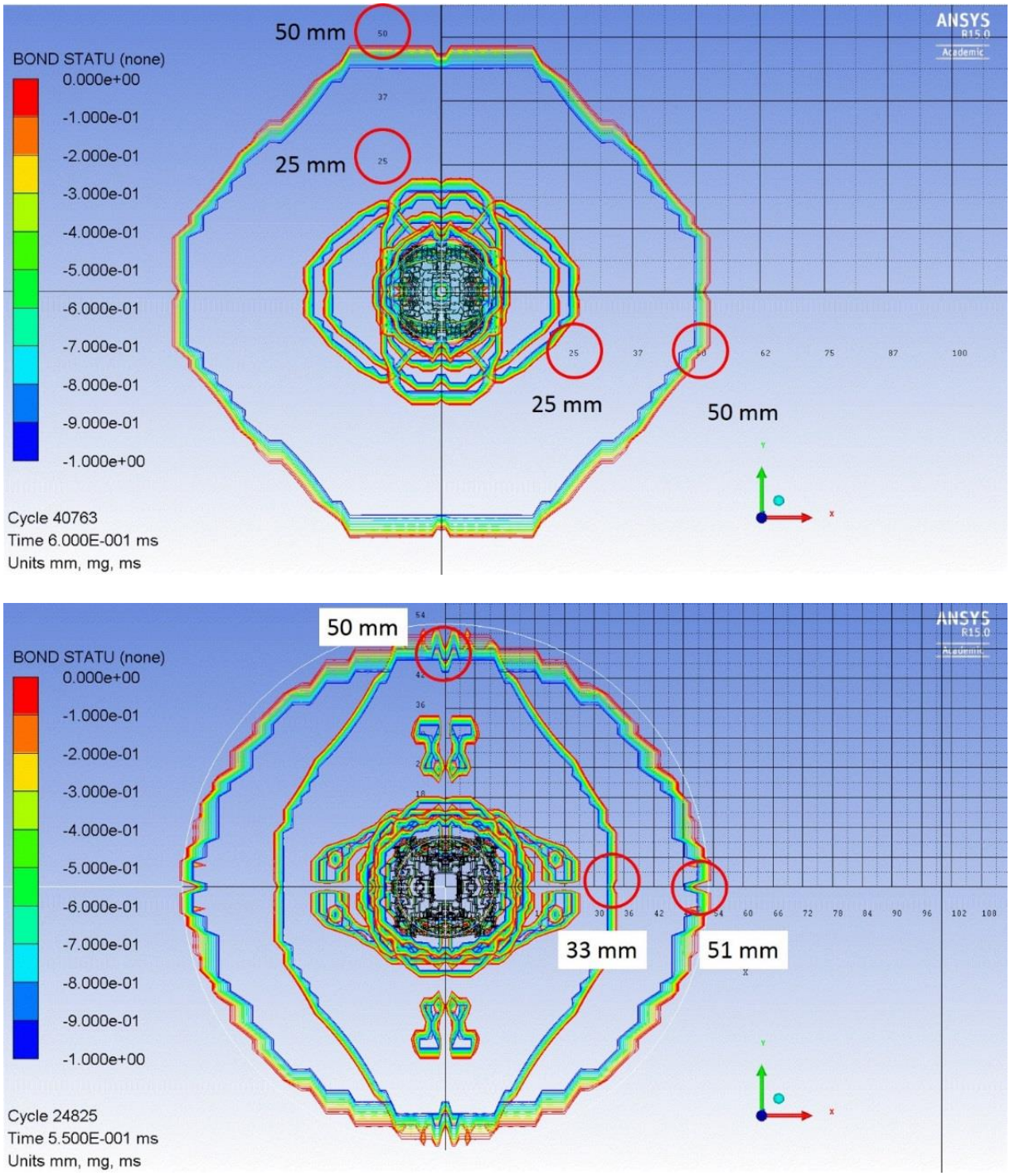

Figure 129 Simulation results showing the delamination extent via BOND STATU contour plot after 116m/s impact in: EN15152 setup (top), and QSPT setup with conical projectile

(bottom). The custom-made QSPT fixture (hence boundary conditions) has negligible influence on the invisible failure

Penetration resistance of the laminates can be seen in Figure 130. The noise (or oscillation) in time history signals was due to the contact instabilities, in other words, they are not an indication of material failure. The maximum contact force was calculated in the order of 10 kN for the STND and QSPT setup with conical projectile. For flat and hemispherical projectiles, the contact force was calculated as much higher (25 kN), even though their velocities were lower. This greater value is the result of greater projectile size (19.5 mm vs 25.4 mm), and also the shape of the flat ended projectile which causes a line contact. Hemispherical and conical projectiles cause point contacts. However, the conical projectile mass was lower (20 g vs 100 g) and therefore had a lower contact force value.

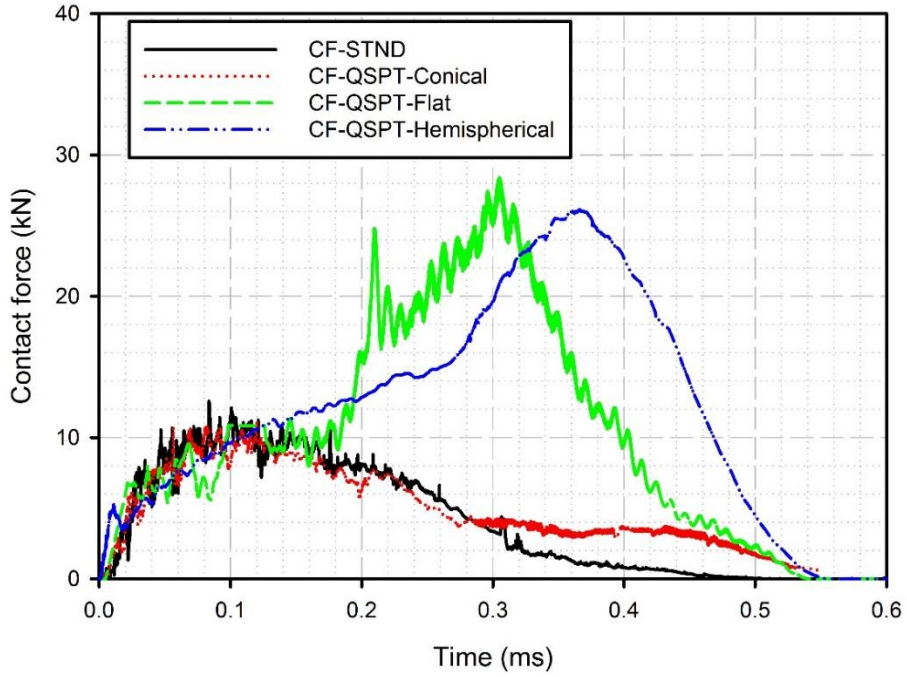

Figure 130 Contact force (CF) obtained from the projectile in: original EN15152 setup (denoted as STND) and in QSPT setup

The impact velocity (v_{imp}) change of the projectiles with respect to time is shown in Figure 131. In all cases the projectile was caught by the laminate between 0.3-0.4 ms ($v_{imp} = 0$) at the end of a gradual velocity decrease. Later, the sign of the velocity changes from negative to positive, indicating the rebounding of the projectile from the laminate. Again, as a result of boundary conditions, the spring back velocity was found higher for the QSPT setup ($v_R = 20\ m/s$) compared to the standard setup ($v_R = \sim 5\ m/s$), while in both cases the velocity

profile is very similar. The residual velocity of both the flat and the hemispherical ended projectiles were similar to the conical counterpart. These results indicates that it is possible to reduce the sample size and hence the boundary conditions.

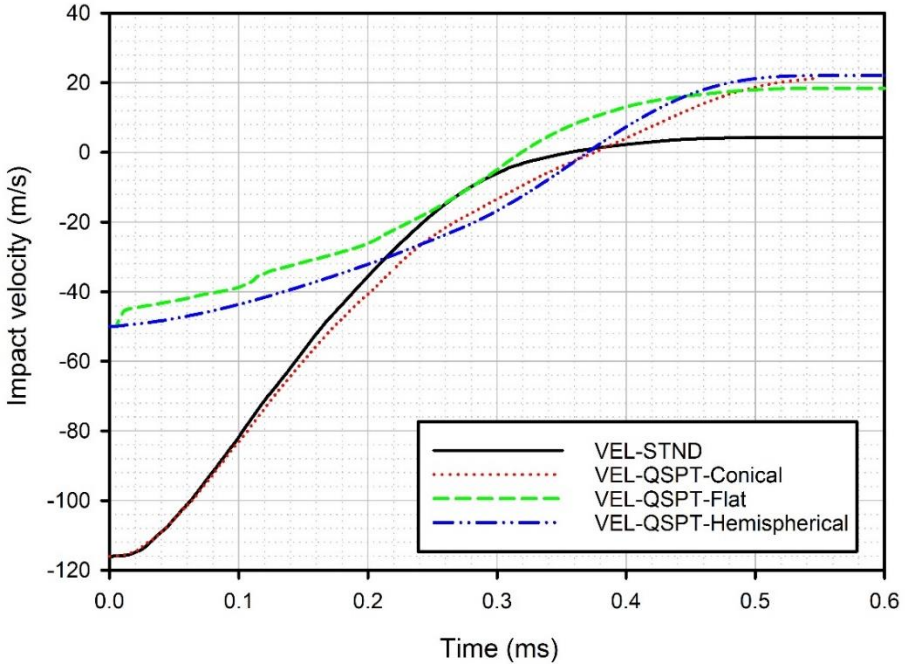

Figure 131 Impact velocity (VEL) of the projectile with respect to time in: original EN15152 setup (denoted as STND) and in QSPT setups showing the residual velocities were similar

6.1.2 Results & discussion – sandwich composite

Figure 132 depicts the energy absorption results of sandwich plates obtained from the numerical models of EN15152 standard (STND) and QSPT setup with conical, flat, and hemispherical projectiles. In comparison to the monolithic laminate, the response of sandwich plates was slightly different. A possible explanation to this variation might be the local stiffness difference between the monolithic and sandwich material at the impact point. Even though the sandwich plate has much greater thickness compared to the monolithic laminate (34 mm vs 6 mm), the foam core insert makes the sandwich less stiff in through-thickness direction. This local stiffness difference can be realised easier if Figure 133 and Figure 130 are compared. Average contact force obtained from the impactors were much higher (2 to 5 times) for monolithic plates.

It is apparent from the Figure 132 that the impact of hemispherical projectile occurred over a longer time scale. This is mainly due to the partial penetration of the sandwich plate. The hemispherical projectile was caught at the bottom facesheet even though the bottom facesheet also failed (Figure 134). Coincidentally, the impact was at near ballistic limit. This outcome

was different than the others; the conical projectile impact exhibited full penetration, while flat ended projectile impact concluded with a complete rebound from the plate, causing only delamination failure at the impact point.

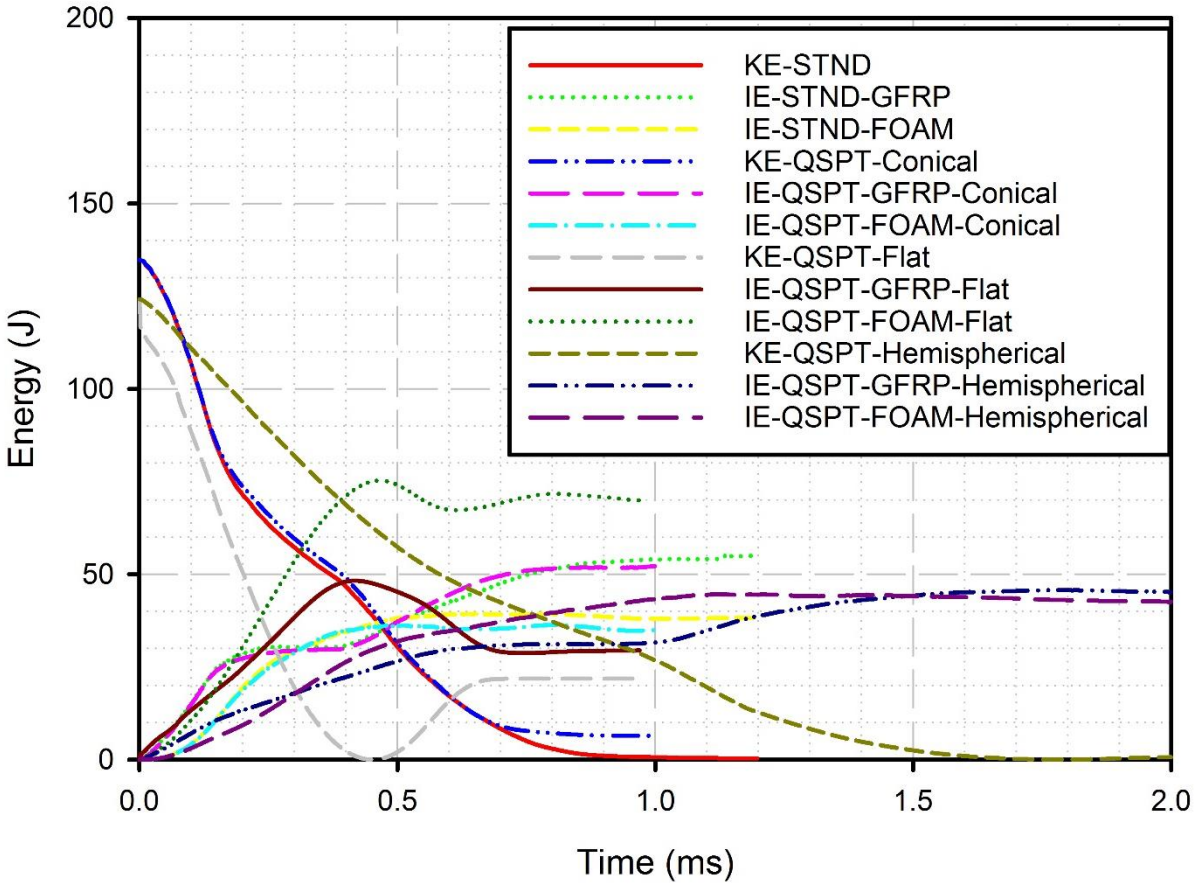

Figure 132 Energy transfer characteristics in EN15152 (STND) and QSPT simulations for GFRP/foam core sandwich plate with three different projectiles. Internal energy (IE) of the sandwich was divided into GFRP facesheets and foam core

In Figure 132, the KE of the conical projectiles in EN15152 (STND) and QSPT setup display a steeper two-step decrease between 0-0.5 ms which indicates the top and bottom facesheet penetration, respectively. On the other hand, the KE of the hemispherical projectile decreases relatively more stably, also influenced by the shape and the relatively greater size of the projectile compared to the conical counterpart. In relation to the KE change, the IE of the glass fibre facesheets (GFRP) and the foam core values are closer to each other in hemispherical projectile impact. In conical projectile impact the difference was greater, which is the result of the complete penetration, as both facesheets contributed to the energy absorption. Overall, both conical impact cases resulted in very similar material behaviour in terms of energy dissipation

(Figure 132) and penetration resistance (Figure 133), and showed minor difference between the residual velocities (Figure 135).

The surprising result from this scenario was the flat ended projectile impact. With a thinner facesheet, a partial penetration was expected at least. However, the impact caused only delamination failure in the top facesheet (Figure 136), with a diameter equal to the projectile diameter. This is most likely due to the bending resistance performance provided by the sandwich structure. The circular flat projectile creates a circular line contact with the GFRP, and since the flat projectile failed to penetrate the GFRP facesheet, the continuous movement of the projectile causes a "larger" effective foam surface area to react to the impact. The sandwich is supported by the custom-made fixture and the centre of the sandwich is allowed to move. Thus, the projectile pushes the sandwich into the span ring (Figure 136), causing a local out-of-plane bending. The highest penetration resistance to the flat ended projectile in Figure 133 resulted in highest energy absorption by the foam core among all the cases in Figure 132. This finding is in consistent with what has been reported by Aktay et al. (Aktay et al. 2005).

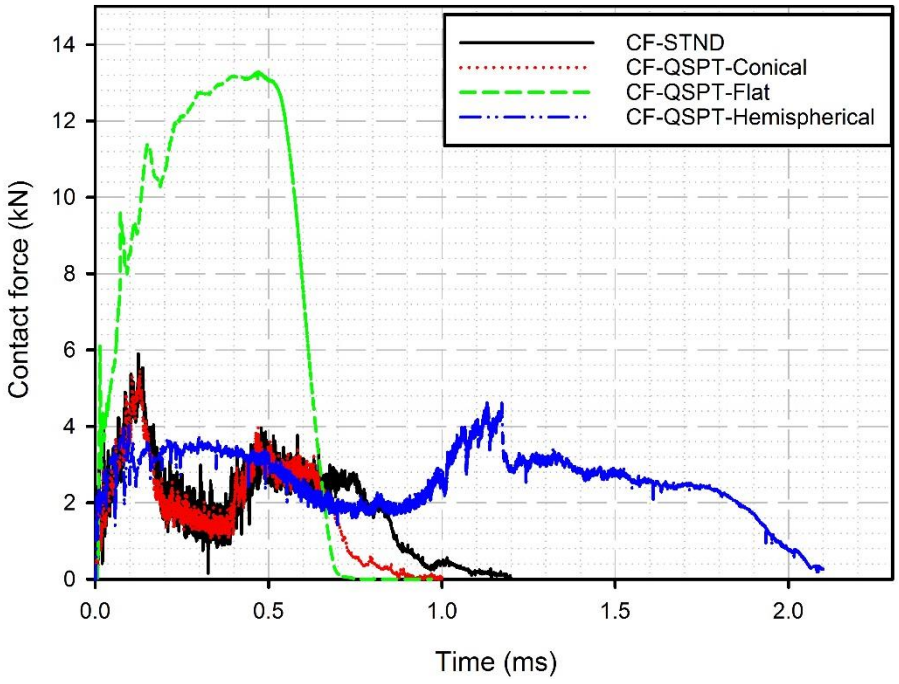

Figure 133 Penetration resistance of sandwich plates against impact of conical, flat, and hemispherical projectiles in gravelling impact scenario. Shape effect of circular flat projectile (line contact) is distinctive while point contact from conical and hemispherical projectiles exhibited similar behaviour

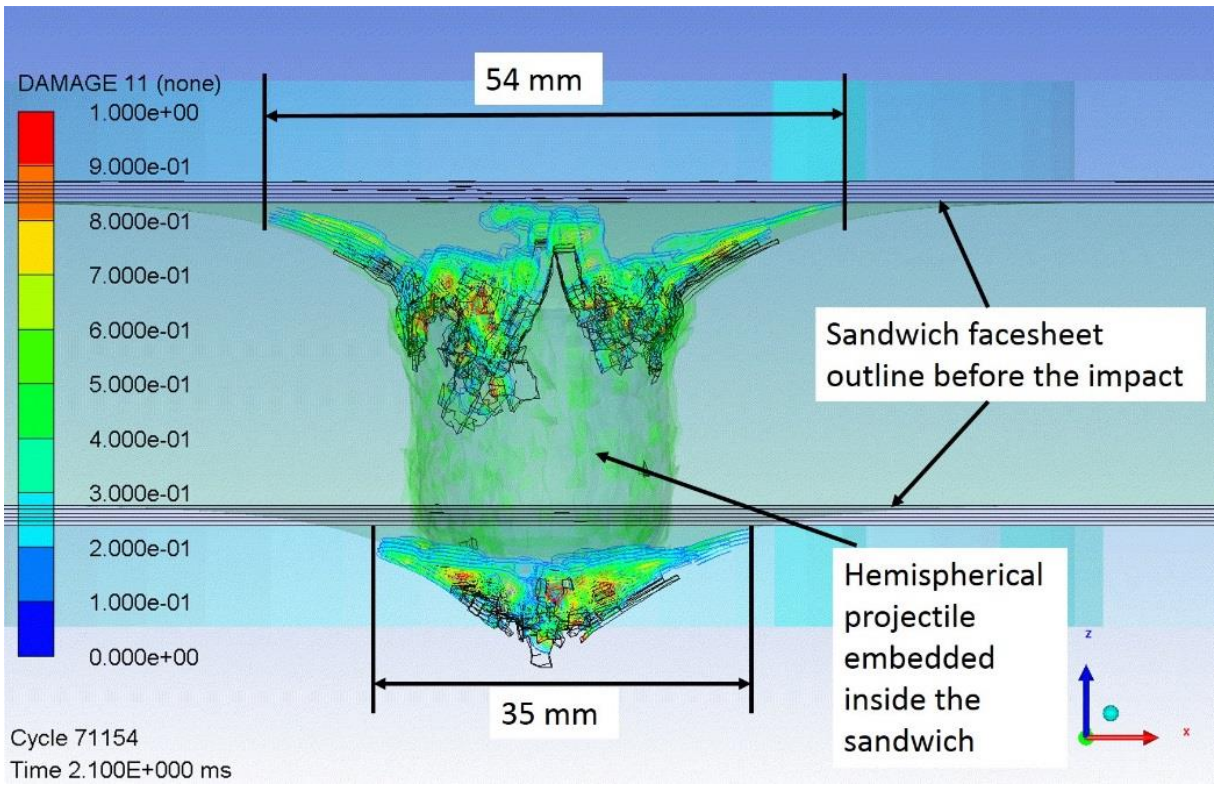

Figure 134 DAMAGE 11 contour plot showing the extent of fibre failure at upper and lower facesheets at the end of the hemispherical impact. The projectile was embedded inside the material

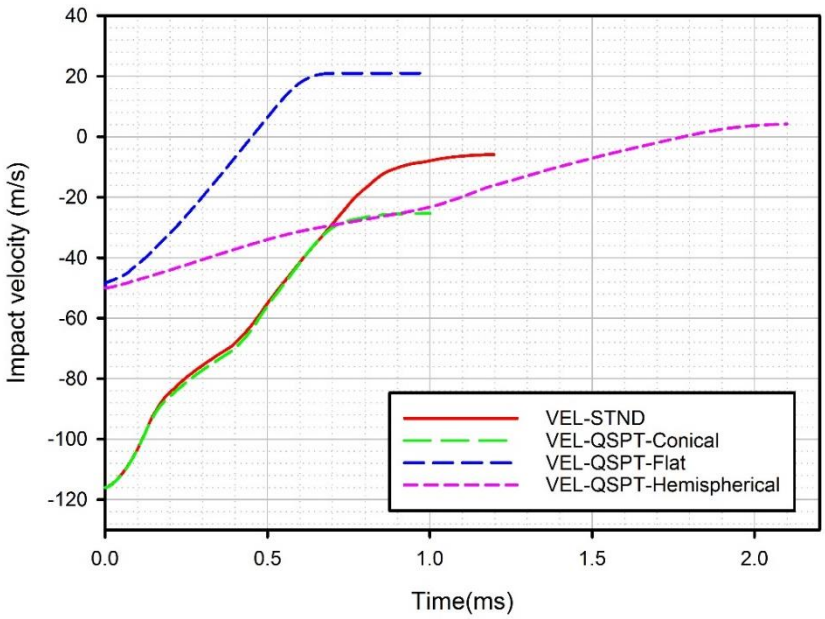

Figure 135 Velocity profiles of the projectiles in EN15152 (STND) and QSPT simulations. Conical projectiles in STND and QSPT resulted in complete penetration, while flat and hemispherical projectiles were caught by the sandwich

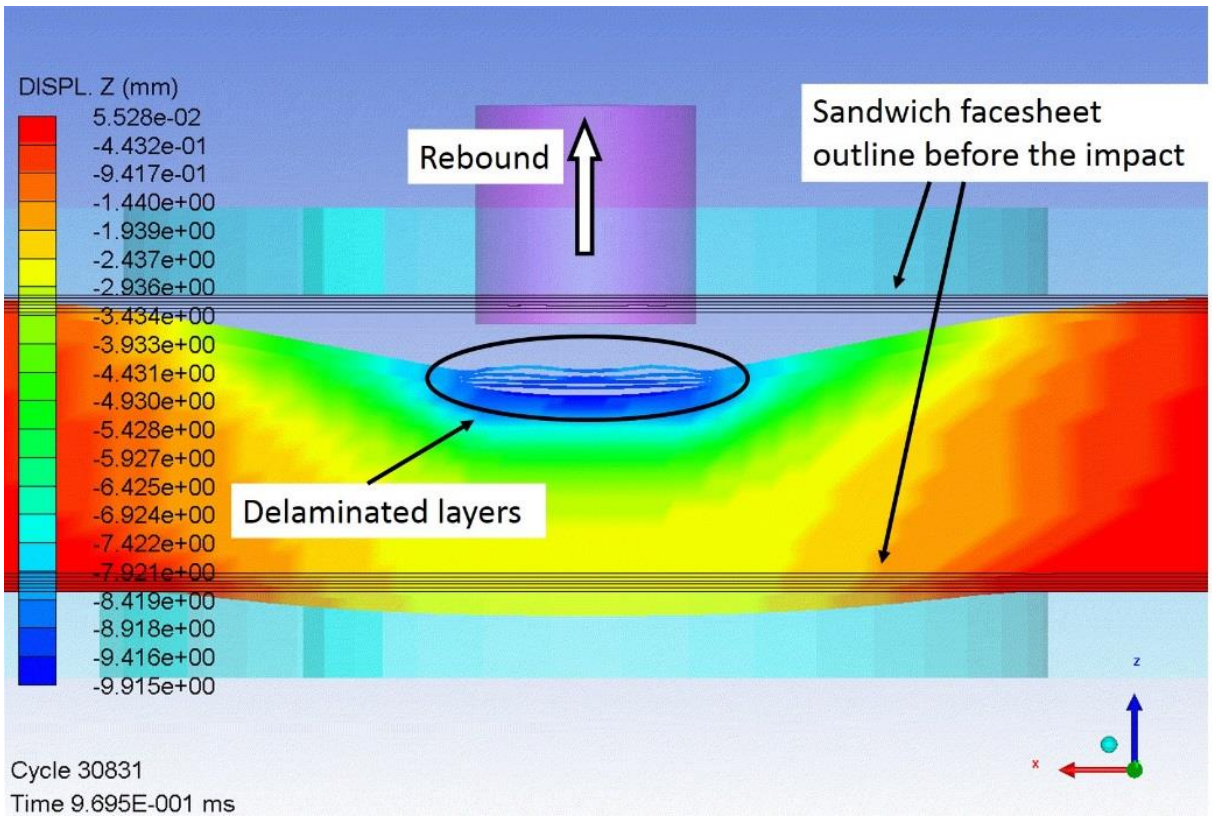

Figure 136 Flat projectile impact showing the delamination failure at the end of the simulation in which a larger volume of the foam core was subjected to bending

6.2 GM/RT2100 – Bodyside window impact resistance

Originally, two different test conditions exist in the standard for this requirement as it is quoted below (GM/RT2100 – Page 47):

- *"For testing laminated safety glass or laminated double glazed window units the steel ball shall be travelling at a speed of 100 km/h, ± 3 km/h, at the point of impact."*
- *"For testing toughened safety glass window units the steel ball shall be travelling at a speed of 50 km/h, ± 3 km/h, at the point of impact."*

In both conditions, the impactor is a solid steel ball of a mass of 0.25 kg. In the present work, since the rail vehicle carbody shell is of concern rather than the window structure, it is rational and sufficient to analyse only the first testing condition. The specimen for this requirement is a rectangular plate with minimum dimensions of 1100x900 mm which is subjected to testing as they are in installed condition, hence clamped in all edges, while the solid steel ball impacts the centre of the specimen. FE models for the simulation of this scenario can be seen in Figure 137.

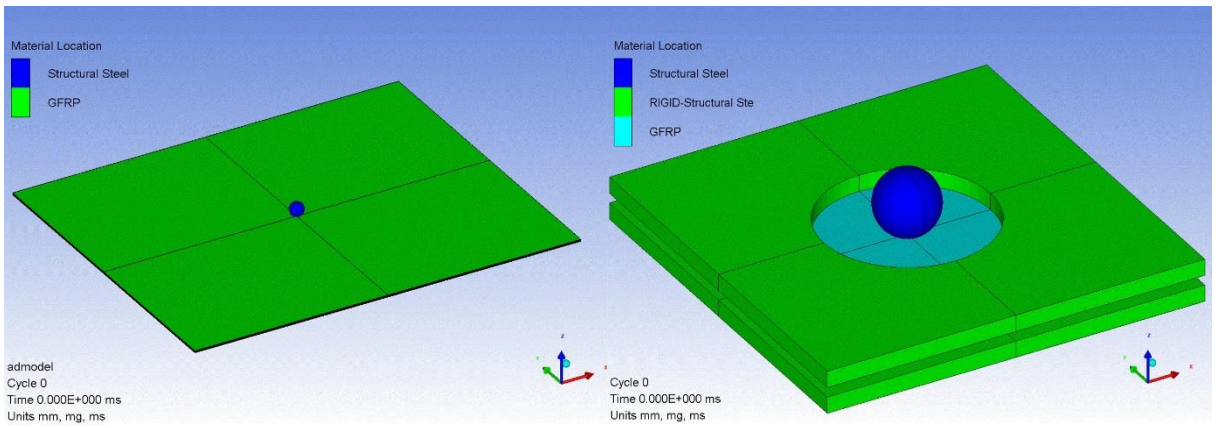

Figure 137 FE model of: GM/RT2100 setup (left), and QSPT setup (right)

6.2.1 Results & discussion – monolithic laminate

Impact simulations were carried out with 28 m/s (100 km/h) impact velocity which resulted in 98.8 J impact kinetic energy. Figure 138 shows the kinetic energy (KE) and internal energy (IE) history during the impact scenarios. In all cases, the kinetic energies have become zero which indicates that the projectile failed to pierce the target.

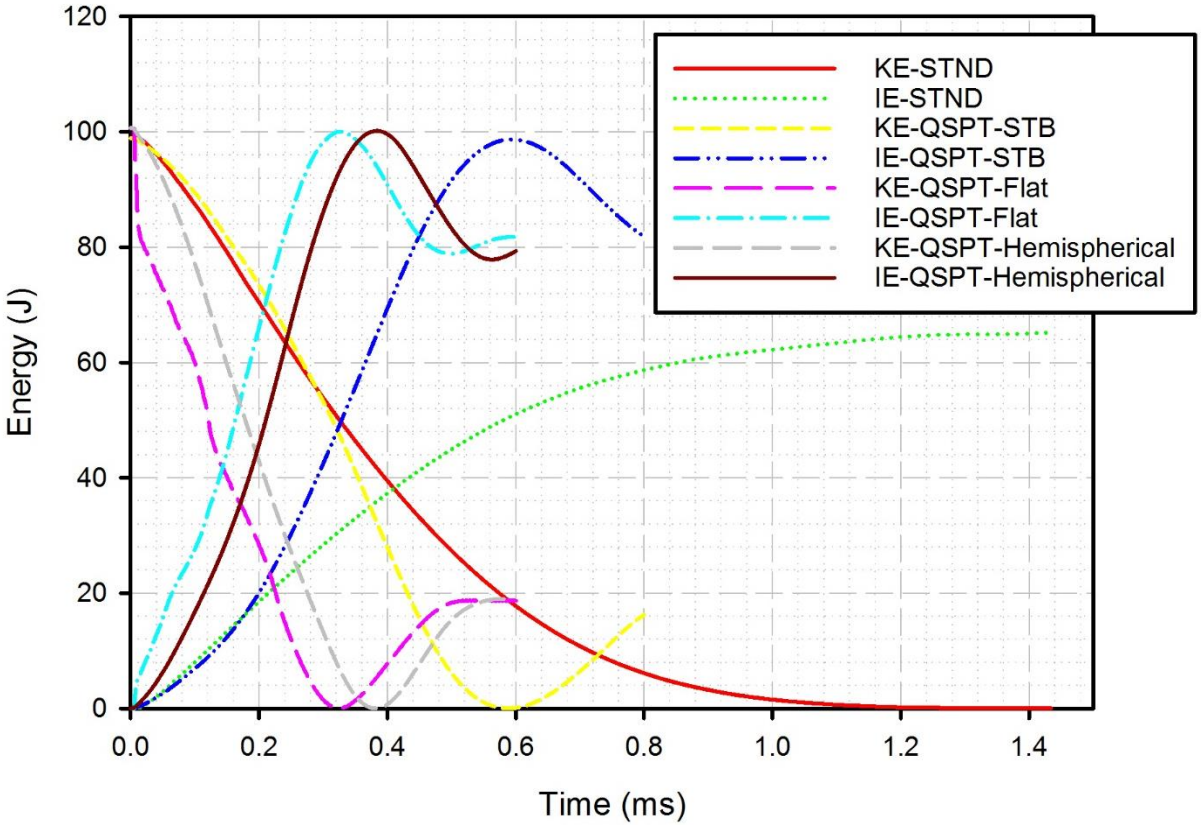

Figure 138 Kinetic energy (KE) and internal energy (IE) change of E-glass/polyester laminates in GM/RT2100 setup (STND) and in QSPT setups with steel ball (STB), flat, and

hemispherical ended projectiles. The offset between STB and flat/hemispherical projectiles is due to the relative size of the projectiles, and the distinctive character of STND case is due to the larger size of the sample.

It is apparent from the Figure 138 that steel ball (STB), flat and hemispherical projectiles exhibited almost the same characteristics in terms of energy loss. The offset between each case is due to the size and shape of each projectile. Given the huge difference between the specimen sizes ((1100x900 mm) vs (200x200 mm)) in this scenario, a local stiffness difference exists between the STND and QSPT setups at the vicinity of the impact, which can be seen from the contact response in Figure 139. Since local stiffness was higher in QSPT setup, loading and unloading of the structure happens more rapidly (in a shorter time scale) than the standard setup, in which the through-thickness deflection (bending) was higher. This relative stiffness difference caused by the boundary conditions has a significant influence over the penetration resistance Figure 139. Maximum contact force recorded in QSTP setup triples the maximum force obtained from the standard setup. As a result, the velocity of the projectiles in QSPT setup display a sharper decrease compared to STND case as shown in Figure 140.

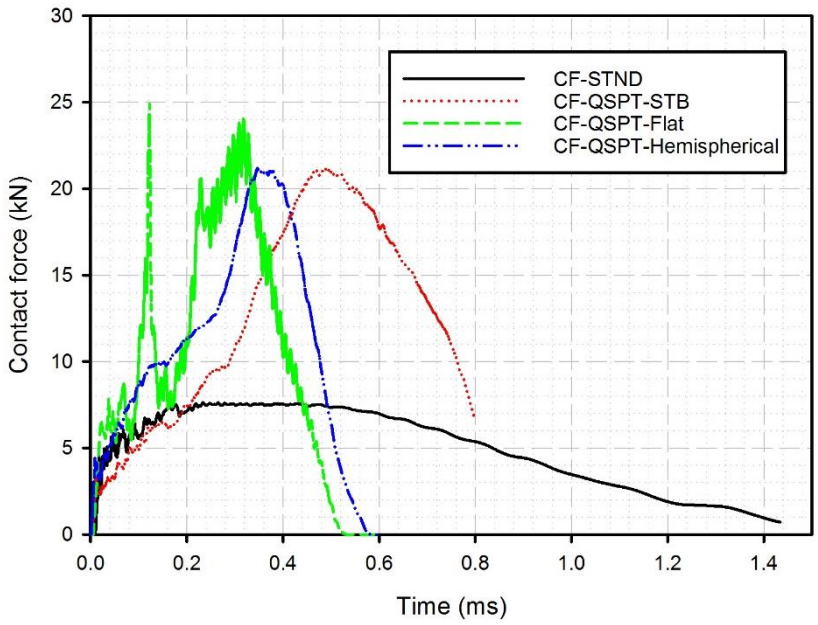

Figure 139 Contact force vs time output from the simulation cases: GM/RT2100 setup (STND), QSPT setups with steel ball (STB), flat, and hemispherical ended projectiles

Nonetheless, this is not influencing the overall structural response in both impact cases. No fibre failure was observed in either cases (Figure 141), and similar delamination response (slightly larger in QSPT setup) was recorded for each impact and these can be seen in Figure

142, Figure 143, and Figure 144. The delamination response of the laminates against flat and hemispherical impact was consistent with the standard case results as well (Figure 144).

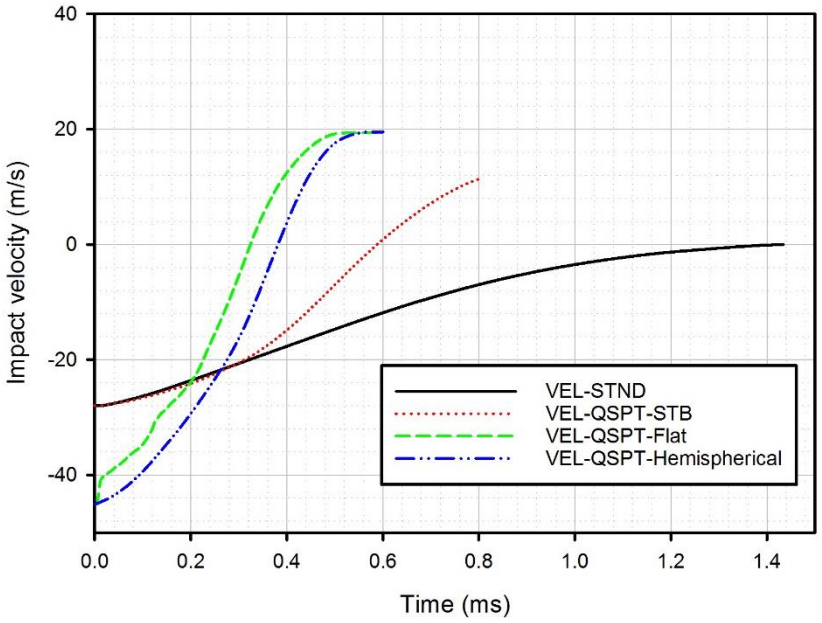

Figure 140 Impact velocity (VEL) change of steel ball (STB) and other projectiles with respect to time in bodyside window impact risk scenario. The sharper velocity decrease of the projectiles in QSPT setup is due to the relatively stiff status of the samples caused by the boundary condition

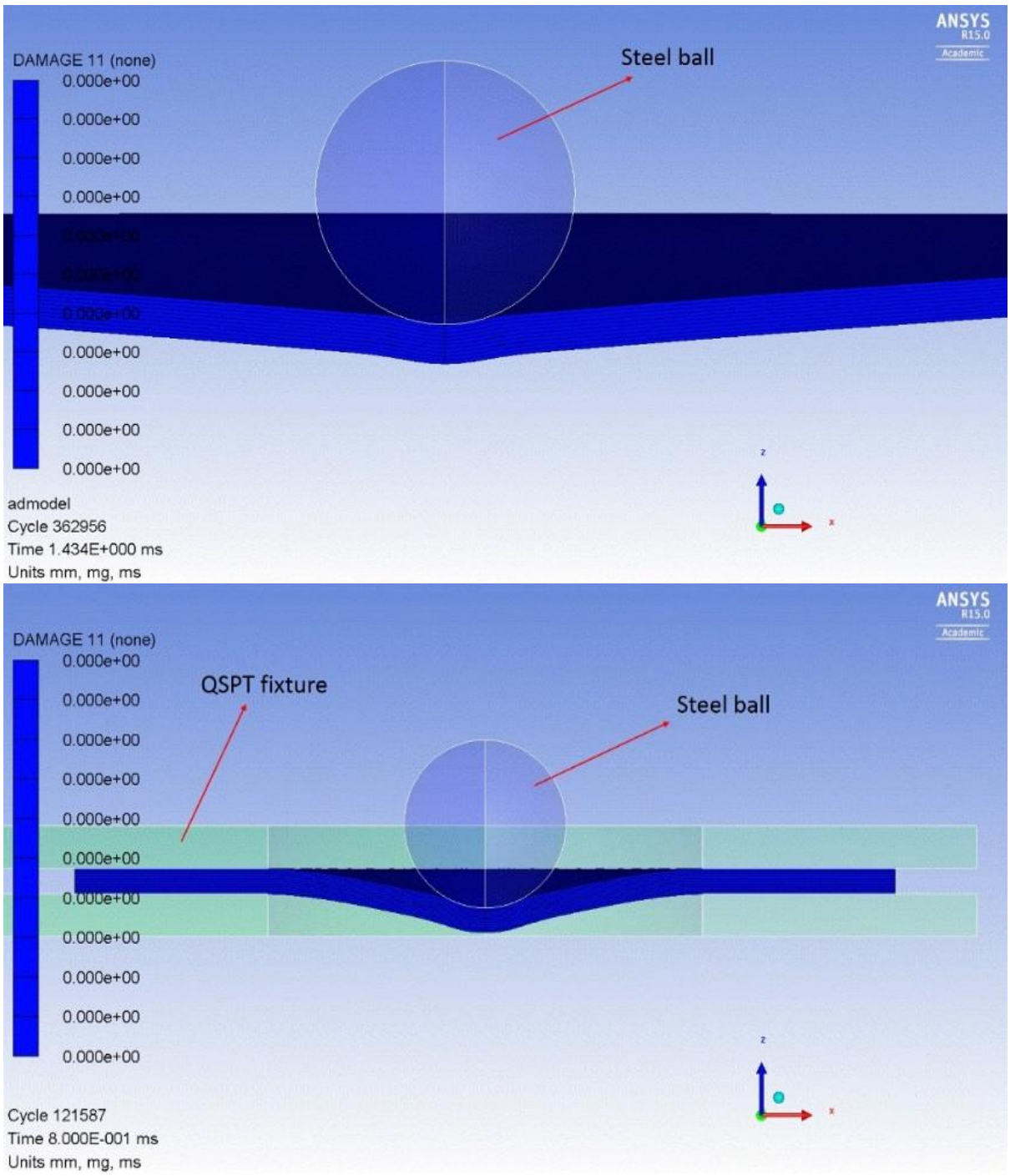

Figure 141 DAMAGE 11 contour plot showing no fibre failure in STND and QSPT setup with STB after 28 m/s impact

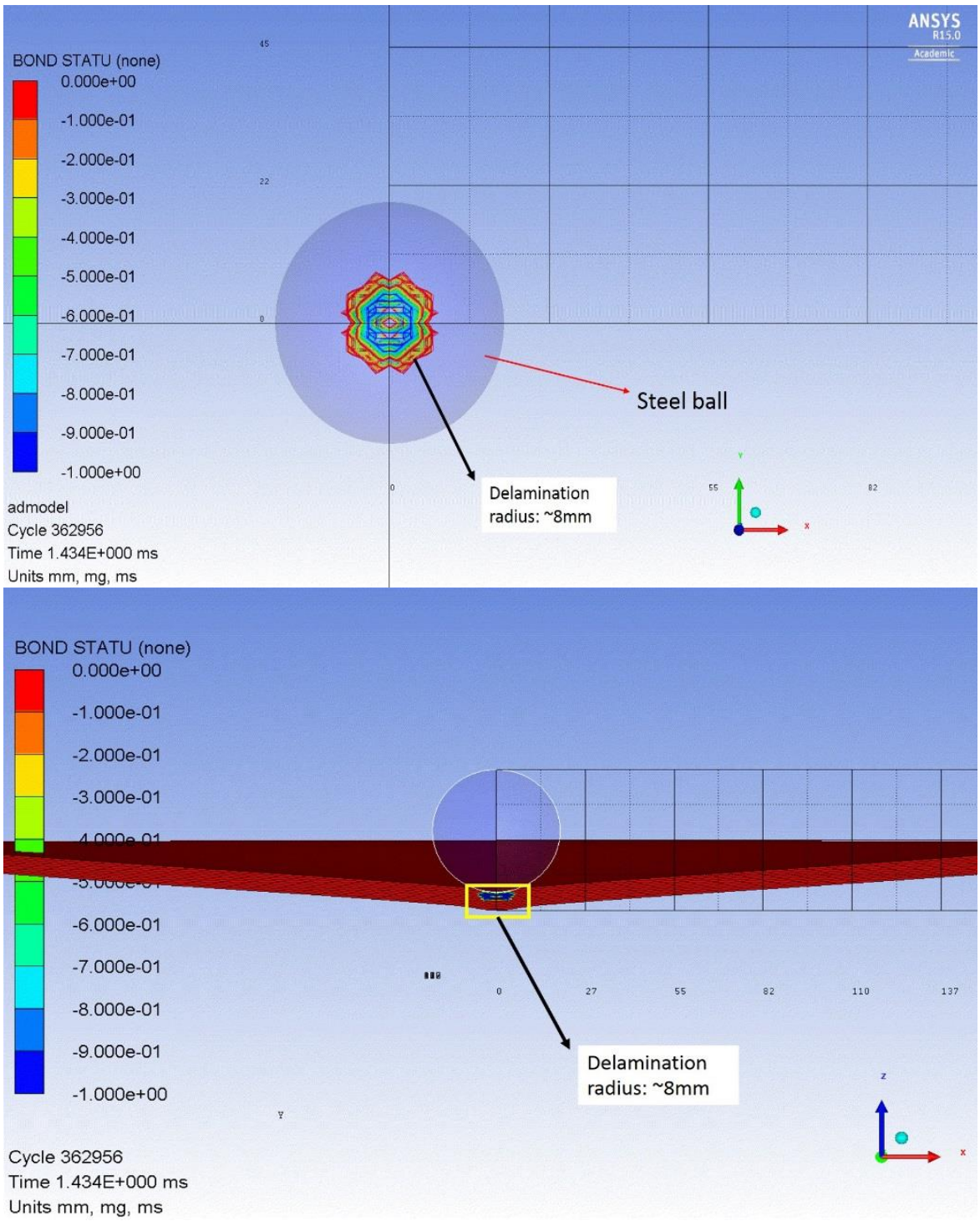

Figure 142 BOND STATU contour plot sowing the extent of delamination failure in GM/RT2100 setup after 28 m/s impact.

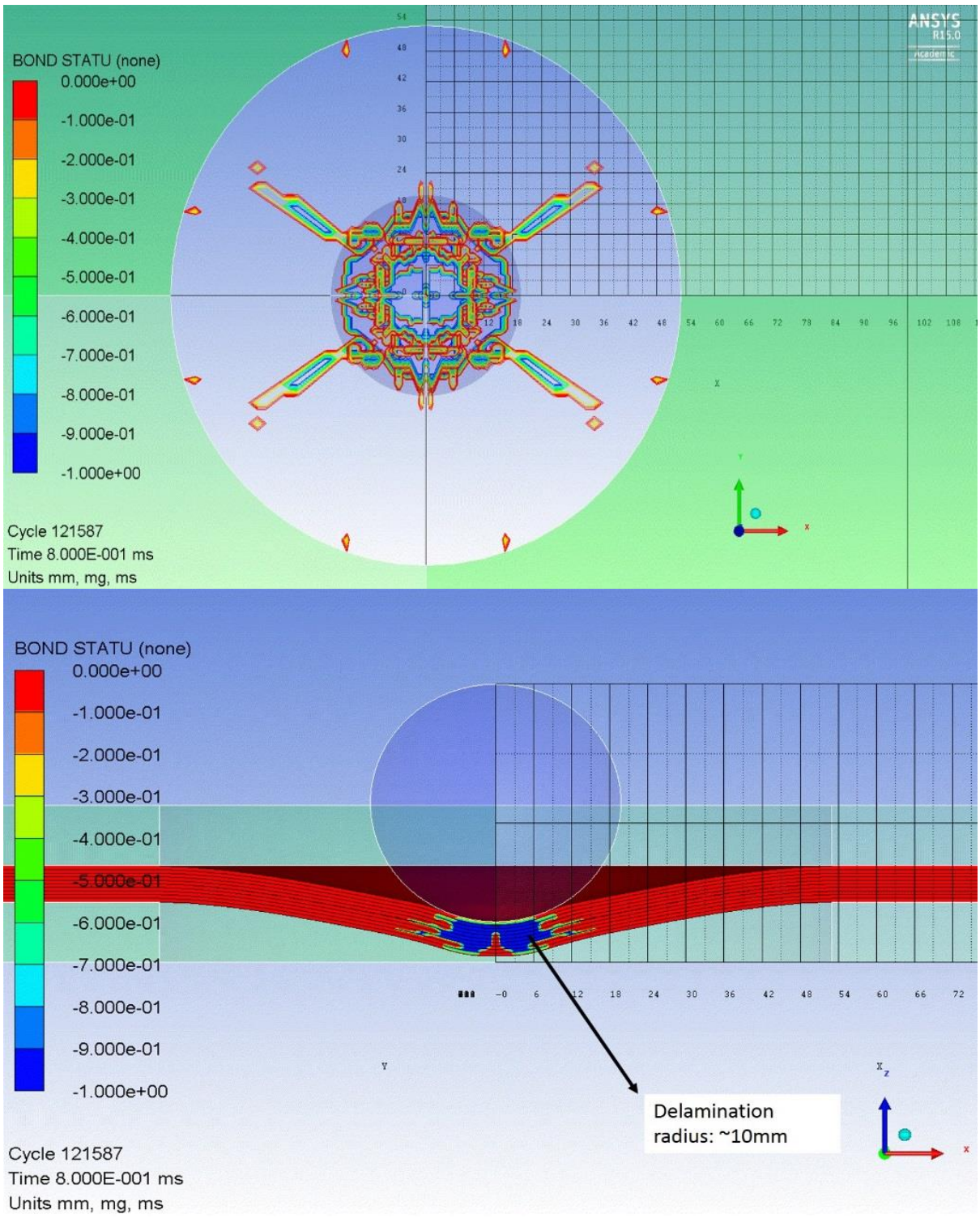

Figure 143 BOND STATU contour plot sowing the extent of delamination failure in QSPT setup with STB after 28 m/s impact

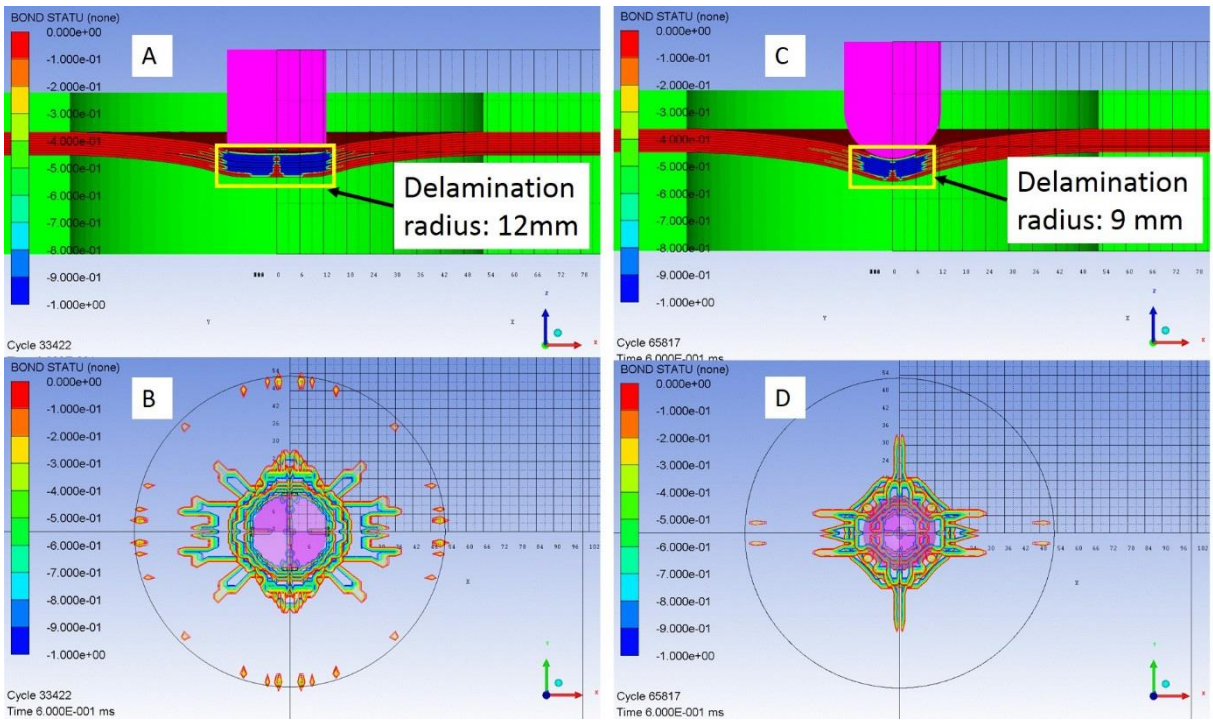

Figure 144 Delamination failure at the end of the impact in QSPT setup with flat (A, B) and hemispherical (C, D) projectile showing that similar delamination response was predicted. This outcome is consistent with the result of the standard case as well

6.2.2 Results & discussion – sandwich composite

The response of the foam core sandwich structure to the considered impact cases was illustrated in Figure 145 for energy transfer, Figure 146 for penetration resistance, and Figure 147 for projectile velocity change. What stands out in Figure 145 is the KE of flat projectile displays a difference compared to the others. This was an expected outcome considering that both the standard specific steel ball impactor (denoted as STB in graphs) and hemispherical projectile causes point contact whereas it is line contact in the flat projectile impact. Correspondingly, the contact force is much higher for the flat ended projectile (Figure 146) which in turn leads to a higher deceleration level (Figure 147). The surprising result from the flat ended projectile simulation was, despite the sandwich skins were thinner compared to monolithic laminates in the previous section, the impact didn't cause any fibre failure. Similar result was observed in the gravelling impact of sandwich plate. Delamination appeared to be the only failure mode, with a diameter equivalent to the projectile diameter (Figure 148).

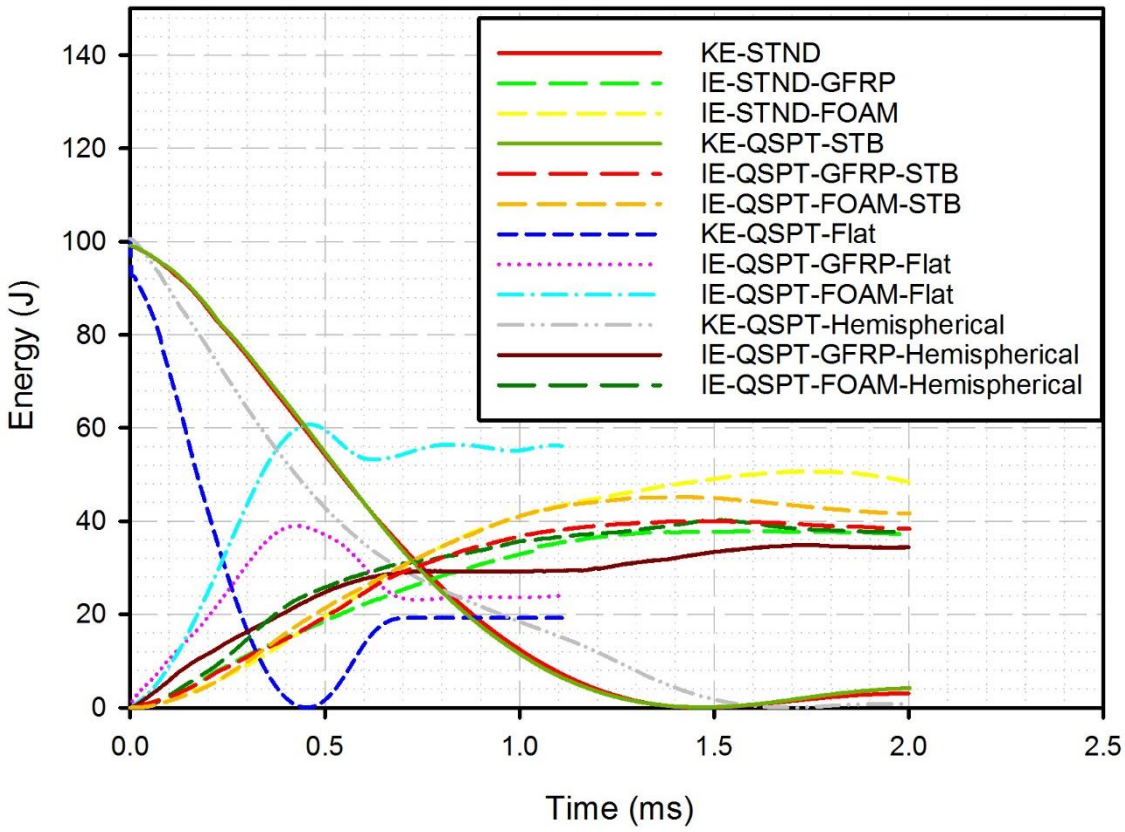

Figure 145 Kinetic energy (KE) change of the projectiles and internal energy (IE) change of the E-glass/epoxy foam core sandwich specimens in GM/RT2100 (STND) and QSPT setups with steel ball (STB), flat and hemispherical projectiles. The contribution of GFRP skins and FOAM core to the IE change was shown separately

The similarity of the energy transfer characteristics is clear between the standard scenario and the QSPT setups with steel ball and hemispherical projectile. In each case, the KE decreases steadily while the IE of the sandwich increases. A detail to point out in Figure 145 is that the foam core absorbed more energy than the GFRP skins in STB and hemispherical projectile impact. This is because the projectiles were embedded in the foam core at the end of the simulations (Figure 149) and failed to reach to the lower skin. The difference in specimen sizes (1100x900 mm vs 200x200 mm) and the change in boundary conditions evidently didn't cause any significant change in both the structures' and the projectiles' behaviour, revealing a potential materials saving. The only difference was the penetration level between the steel ball and hemispherical impactor in QSPT setup (Figure 146). On the other, hand both projectiles caused similar fibre failure (Figure 150).

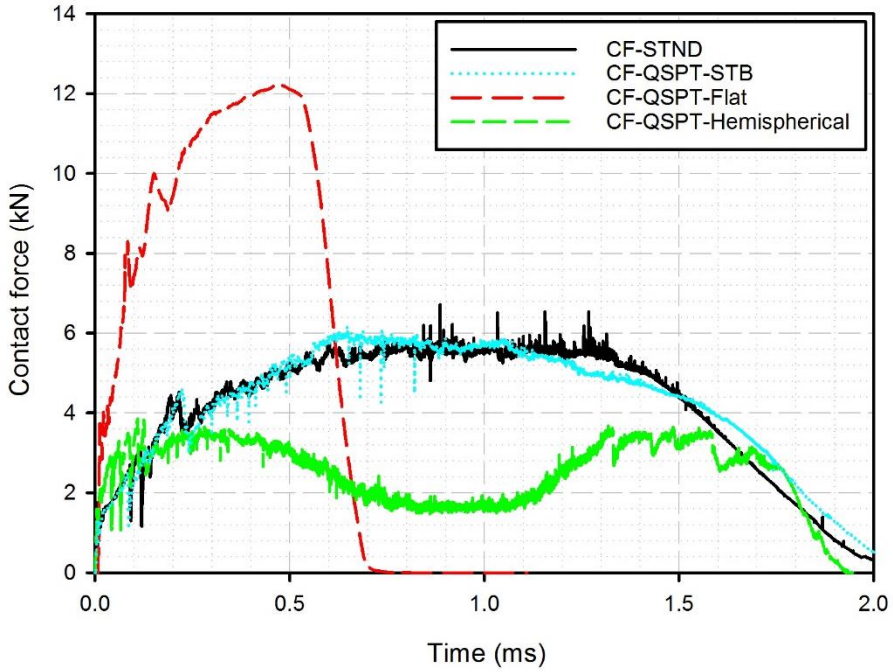

Figure 146 Penetration resistance of E-glass/epoxy foam core sandwich specimens in GM/RT2100 (STND) and QSPT setups with steel ball (STB), flat and hemispherical projectiles

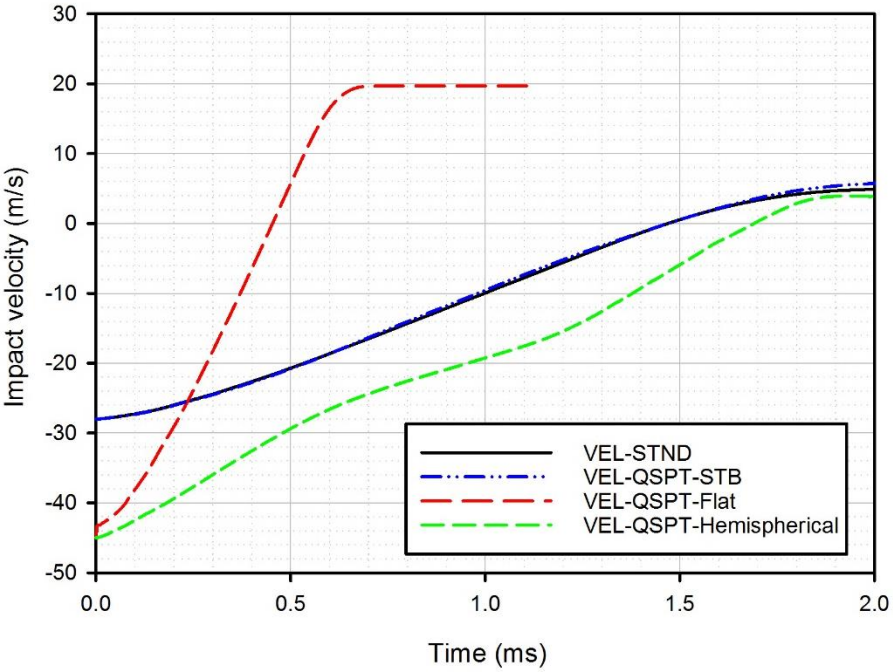

Figure 147 Velocity change with respect to time of projectiles in GM/RT2100 (STND) and QSPT setups

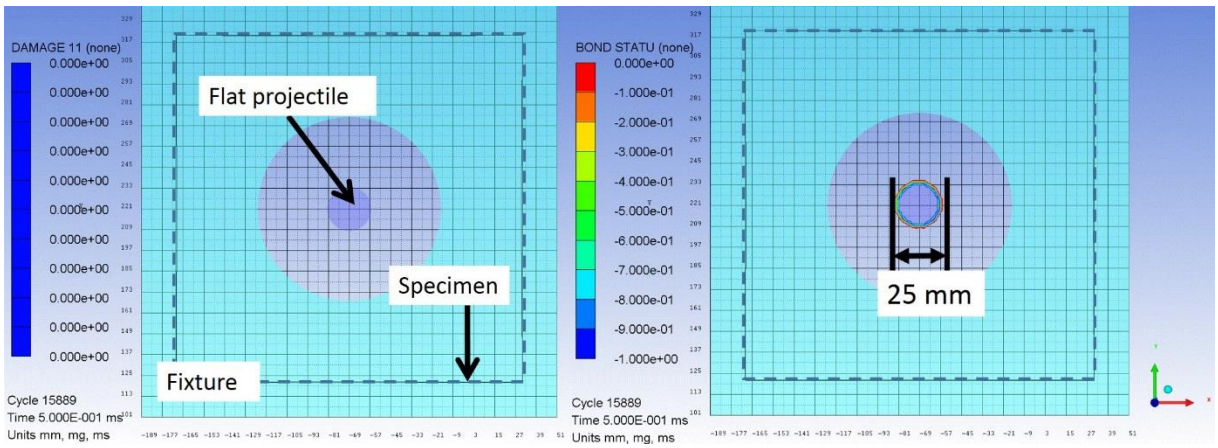

Figure 148 No fibre failure (DAMAGE 11=0) occurred after flat projectile impact (left), but 25 mm circular delamination was captured (right)

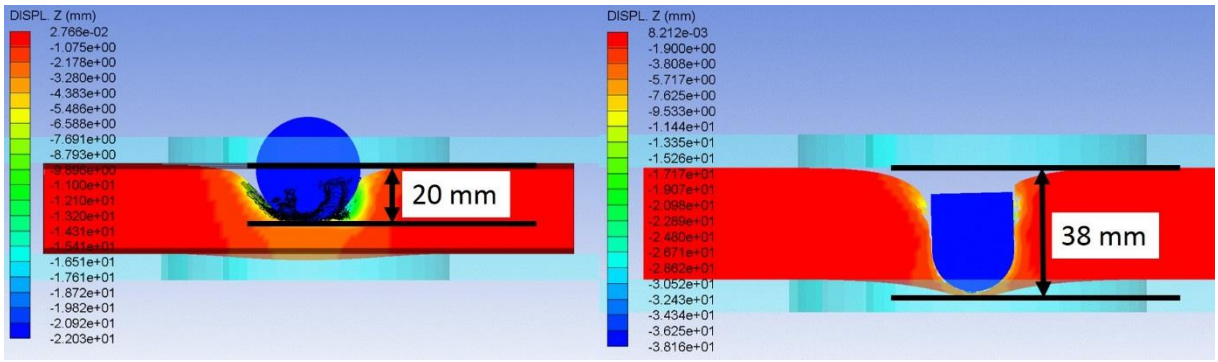

Figure 149 Difference of indentation levels between steel ball (left) and hemispherical (right) projectile

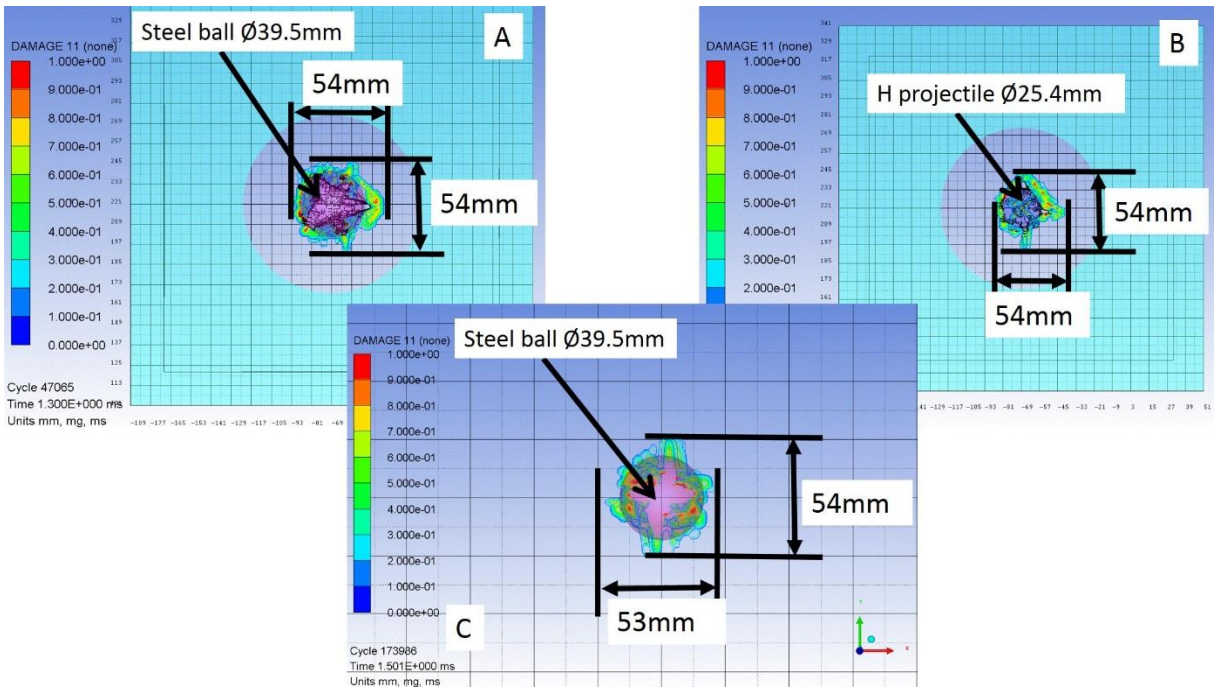

Figure 150 DAMAGE 11 contour plot showing fibre damage extent in: (A) QSPT-steel ball, (B) QSPT-Hemispherical, (C) GM/RT2100 standard simulations showing very similar failure responses

6.3 NF-F07-101 – Simulation of ballast strike

French national standard NF F07–101: "Railway applications - shock test by throwing up ballast simulation" was designed specifically for simulating a ballast impact against foam-based sandwich structures in rail vehicles (AFNOR 2002). An impactor (Figure 151) with a conical tip and of mass of 60±1 g impacts the structure for which minimum four shots is recommended, as well as carrying out additional tests in three different temperatures, i.e. -25°C, +20°C, +70°C, and impact at two different angles (0° and 35° relative to the surface normal). After the impact, the structure is classified in one of the eleven categories: K1 to K11, depending on the energy absorption (Figure 151). Since this standard was used as a means of comparison, single impact case was considered and other aspects such as repeated impact, temperature, and oblique impact was ignored. Thus, maximum energy class (K11 – 285 J, 97.5 m/s) was selected for evaluation. Numerical model of each case can be seen in (Figure 152).

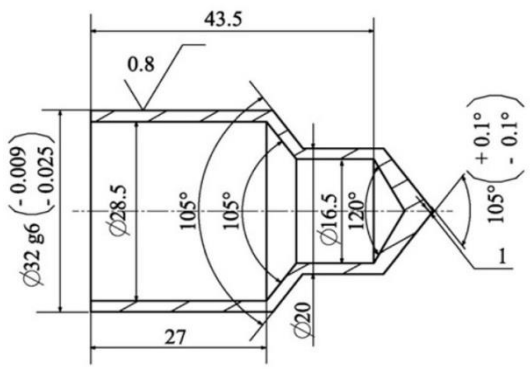

Class	Impact energy (J)	Impactor mass (kg)	Impact velocity (m/s)
K1	12	0.06	20
K2	15	0.06	22.4
K3	25	0.06	28.9
K4	35	0.06	34.2
K5	60	0.06	44.7
K6	95	0.06	56.3
K7	115	0.06	61.9
K8	170	0.06	75.3
K9	210	0.06	83.7
K10	240	0.06	89.4
K11	285	0.06	97.5

Figure 151 Geometry of the projectile (left) of NF-F07-101 standard (Sakly et al. 2016), and the energy categories with respect to the impactor mass and velocity (right).

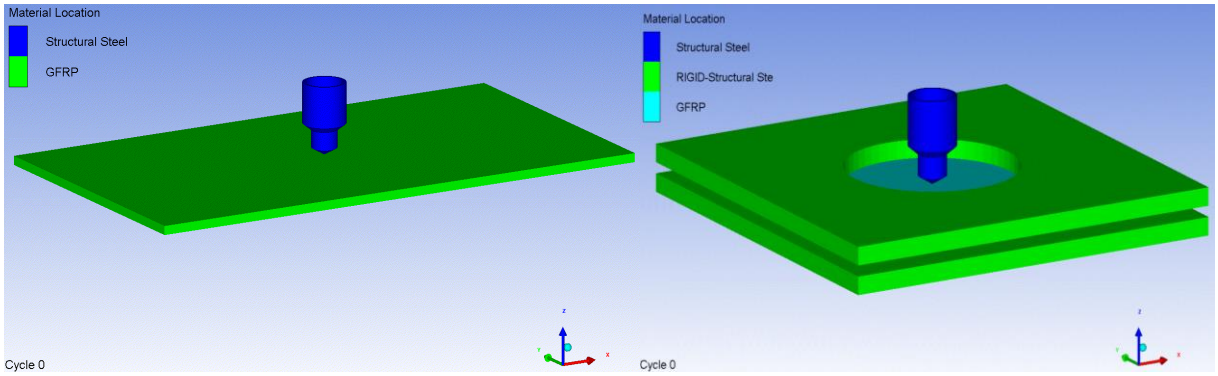

Figure 152 FE model of: NF-F07-101 setup (left), and QSPT setup (right)

6.3.1 Results & discussion – monolithic laminate

Figure 153 shows the energy transfer from the projectile to the laminate in four different numerical models: NF-F07 standard (denoted as STND), QSPT setup with conical projectile of the standard, flat, and hemispherical ended projectiles. Although similar responses were obtained from the laminates, first thing to notice is that the kinetic energy of the conical projectile of QSPT setup failed to reach zero, hence this indicates a complete penetration case, whereas in standard setup partial penetration was observed as well as it was in flat and hemispherical ended impact. This finding suggests that the boundary condition generated by QSPT setup is not sufficient for the representation of the impact with conical projectile. However, hemispherical projectile resulted in reasonable prediction compared to standard scenario for the same incident energy. Figure 154 and Figure 155 support this by illustrating the contact force and velocity change behaviour of the hemispherical projectile, respectively.

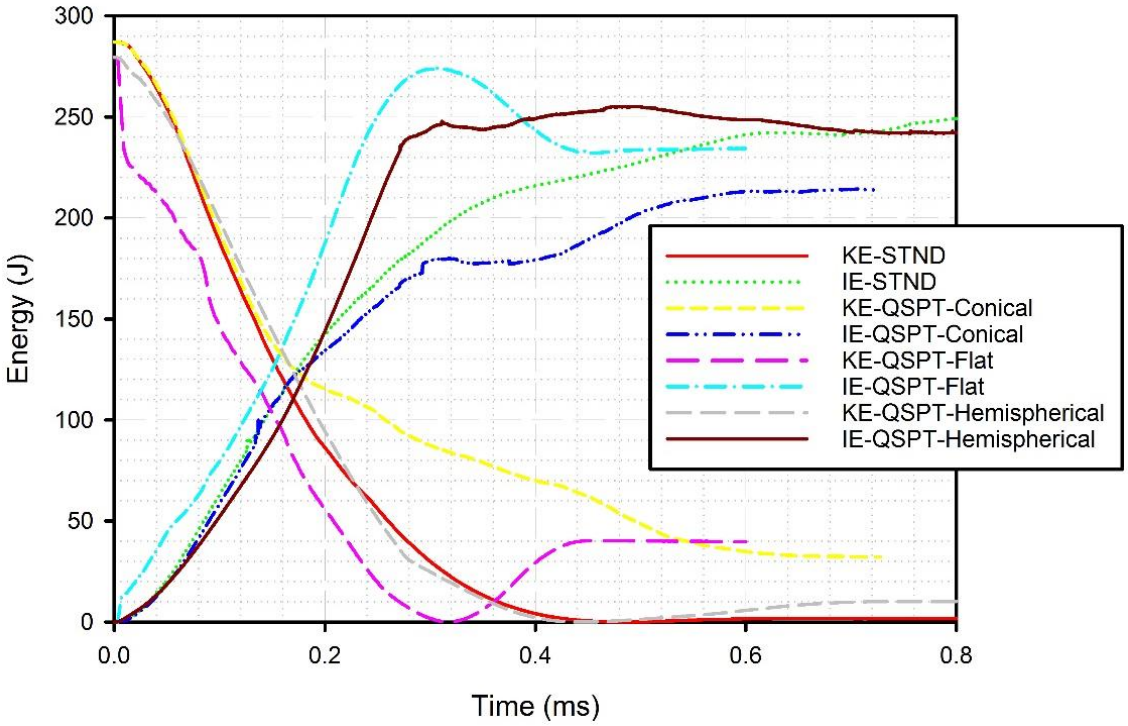

Figure 153 Kinetic energy (KE) and internal energy (IE) change of E-glass/polyester specimens in NF-F07-101 setup (STND), and in QSPT setups with conical, flat, and hemispherical ended projectiles.

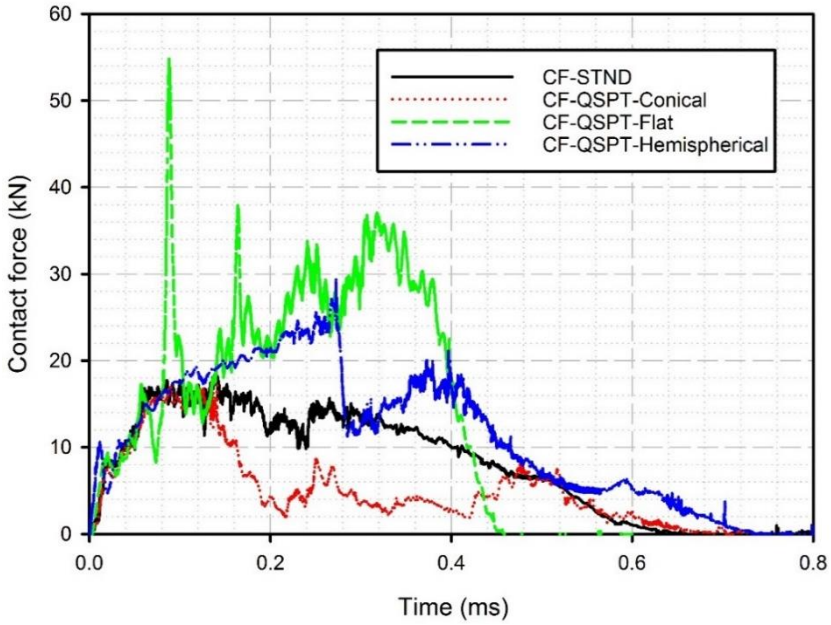

Figure 154 Penetration resistance of laminates against conical, flat, and hemispherical projectiles in ballast strike simulations in accordance with NF-F07-101 standard (STND) and QSPT setup. The sharp peak at 0.1 ms is due to the first layer failure of the laminate in flat projectile impact

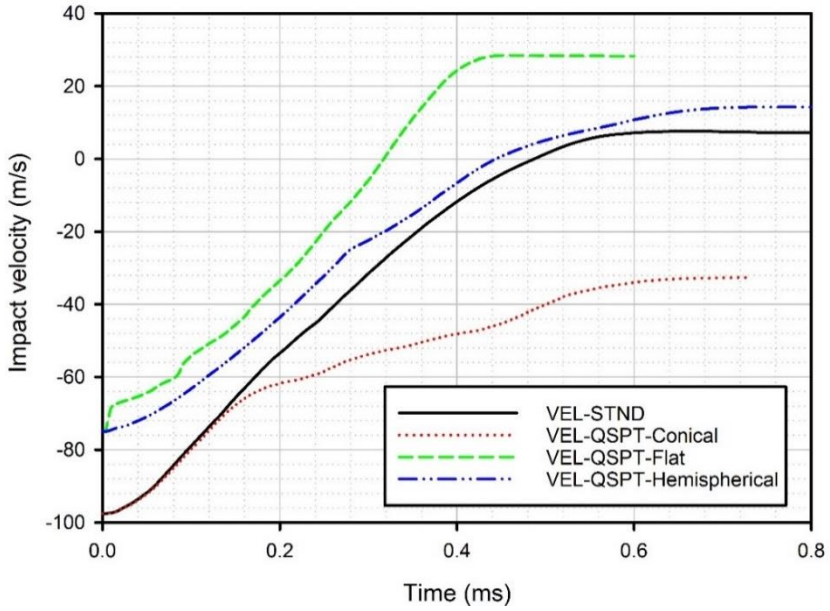

Figure 155 Change in projectile impact velocity for NF-F07-101 ballast strike scenarios. Hemispherical projectile can be preferred over conical projectile

Expectedly, penetration resistance of the laminate was higher against the flat ended impactor because of the line contact, and the flat projectile generated a higher sharp peak in Figure 154 at an earlier stage which was due to the top ply failure. As can be seen in Figure 155, deceleration of hemispherical and flat ended projectiles are similar to the conical projectile in STND setup. For QSPT-conical projectile pair, the change in the deceleration can be explained by the sensitivity of the laminates against point contact combined with the boundary conditions. Even though hemispherical and conical projectiles result in point contact, the penetration efficiency of the conical tip was greater as Figure 154 shows with a sharper decrease just before 0.2 ms. This leads to greater fibre failure at the contact location and ultimately complete penetration of the laminate which can be seen in Figure 156. Supporting this, Figure 157 illustrates the differences in delamination progression for STND and QSPT simulations with conical projectile. For STND setup, the extent of delamination is greater because of the relative flexibility of the laminate: the impact energy was dissipated by the inter-laminar shear failure instead of fibre failure. But in QSPT setup, the relative stiffness of the laminate leads to a more focused fibre failure, thus the delamination couldn't spread as much as in STND setup. Figure 158 shows the failure response of the laminate against hemispherical impact. It is clear that the failure response is similar to that of STND-conical impact: partial penetration with a cross-shaped fibre failure which is slightly greater because of the larger projectile size. The in-plane

delamination extent was less compared to the standard case, but similar through-thickness delamination was captured.

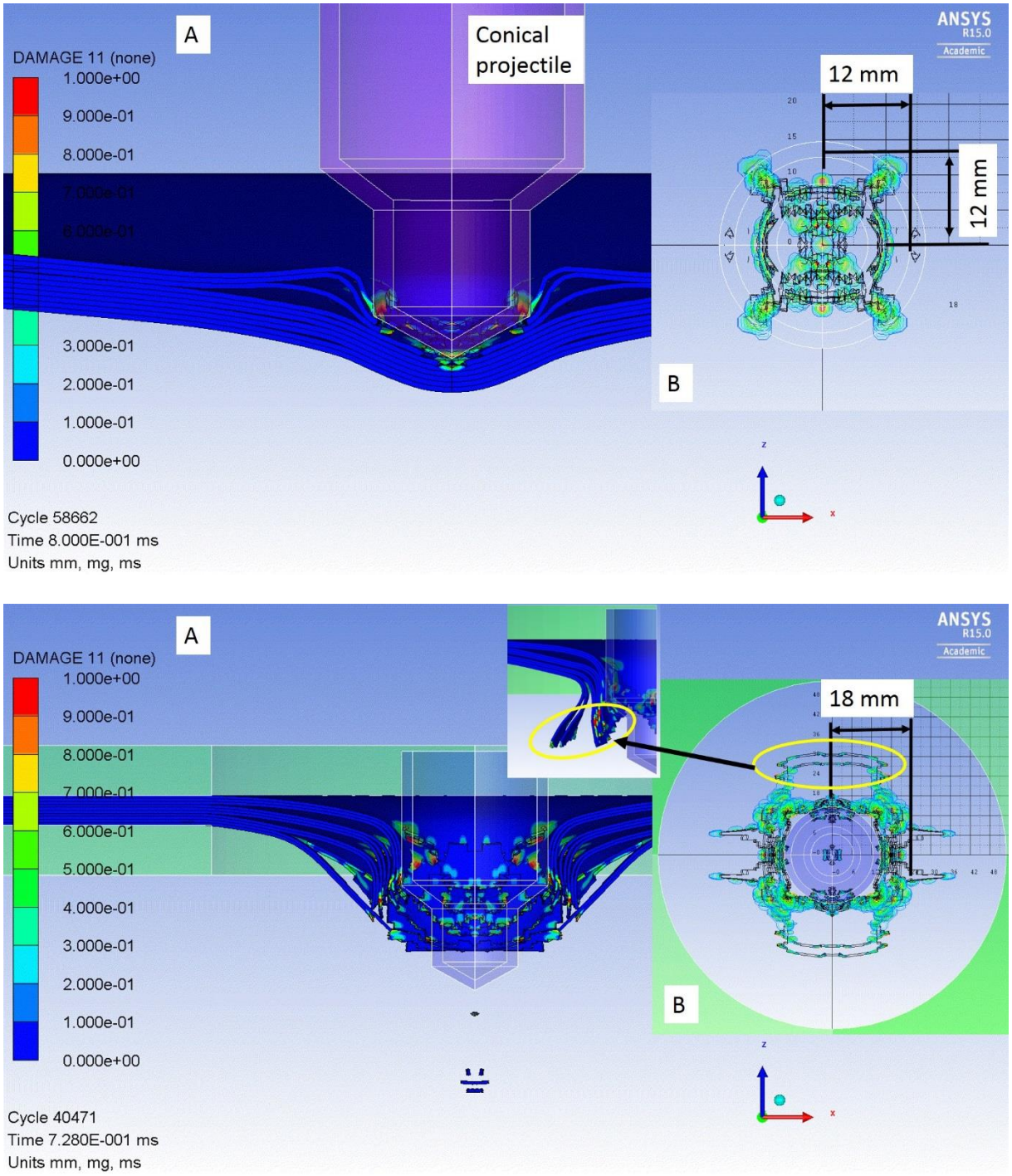

Figure 156 DAMAGE 11 contour plot illustrating the fibre failure extent in NF-F07 standard simulation (top) and QSPT setup with conical projectile (bottom). (A) of each figure shows the sectioned detail of the laminates, while (B) shows the top view and measured details of the inner (invisible) fibre failure of each case

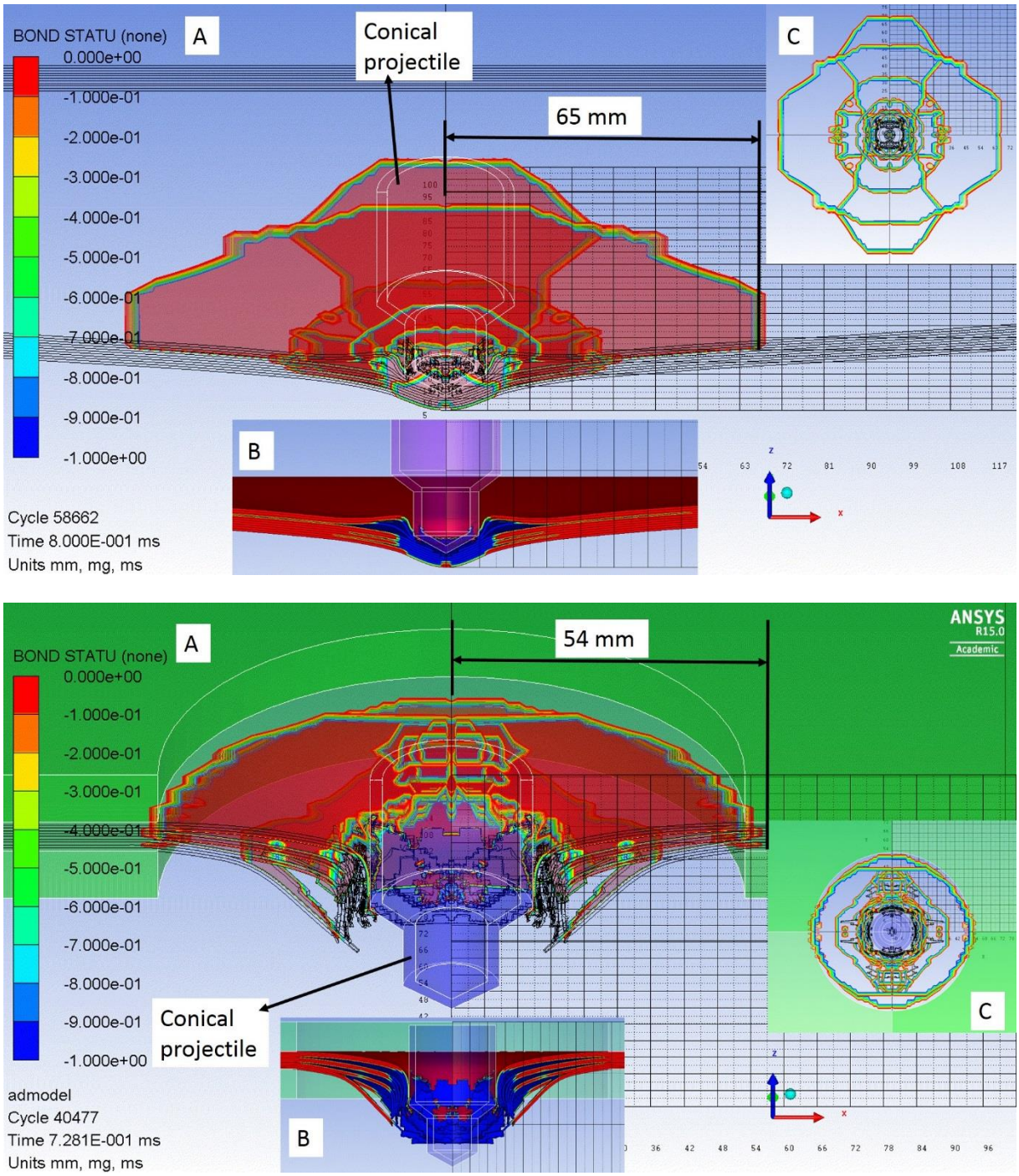

Figure 157 BOND STATU contour plot showing the delamination extent in: (top) NF-F07 standard, and (bottom) QSPT-conical projectile pair. (A) of each figure represents the sectioned 3D view of the delamination with the measured maximum, (B) shows the sectioned 2D view of delamination, and (C) illustrates the shape of delamination from the top view

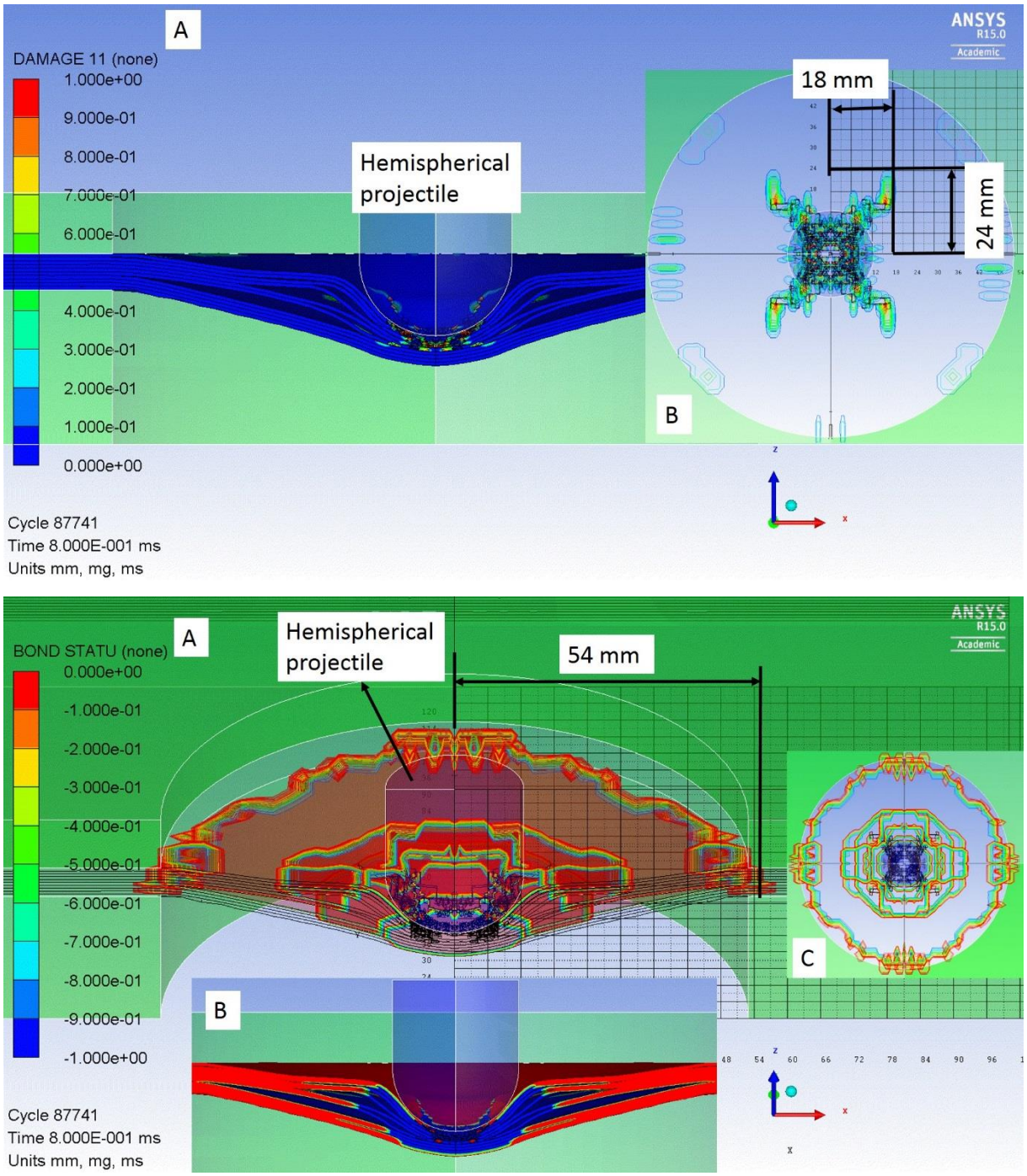

Figure 158 (Top) DAMAGE 11 contour showing the fibre failure extent for QSPT-hemispherical projectile pair: (A) overall sectioned view, (B) inner fibre failure from top view. (Bottom) BOND STATU contour showing the delamination extent in the same simulation: (A) 3D sectioned view with measured maximum, (B) sectioned 2D view, (C) overall delamination shape from top view

Based on the energy transfer, velocity change of the projectile, and material failure, it is reasonable to say that QSPT setup with hemispherical impactor can be an accurate alternative to the standard for the assessment of laminates.

6.3.2 Results & discussion – sandwich composite

The same conditions and analysis parameters given in the previous section apply except the use of foam core/GFRP skin sandwich composite instead of monolithic GFRP laminate. Figure 159 compares the breakdown of energy transfer from the projectile to sandwich composite during the impact in each simulation case. The contribution from the foam core and GFRP layers were illustrated separately. What stands out in the graph is the kinetic energy response of the flat ended projectile which appeared as the only rebounded projectile, while others concluded in full penetration.

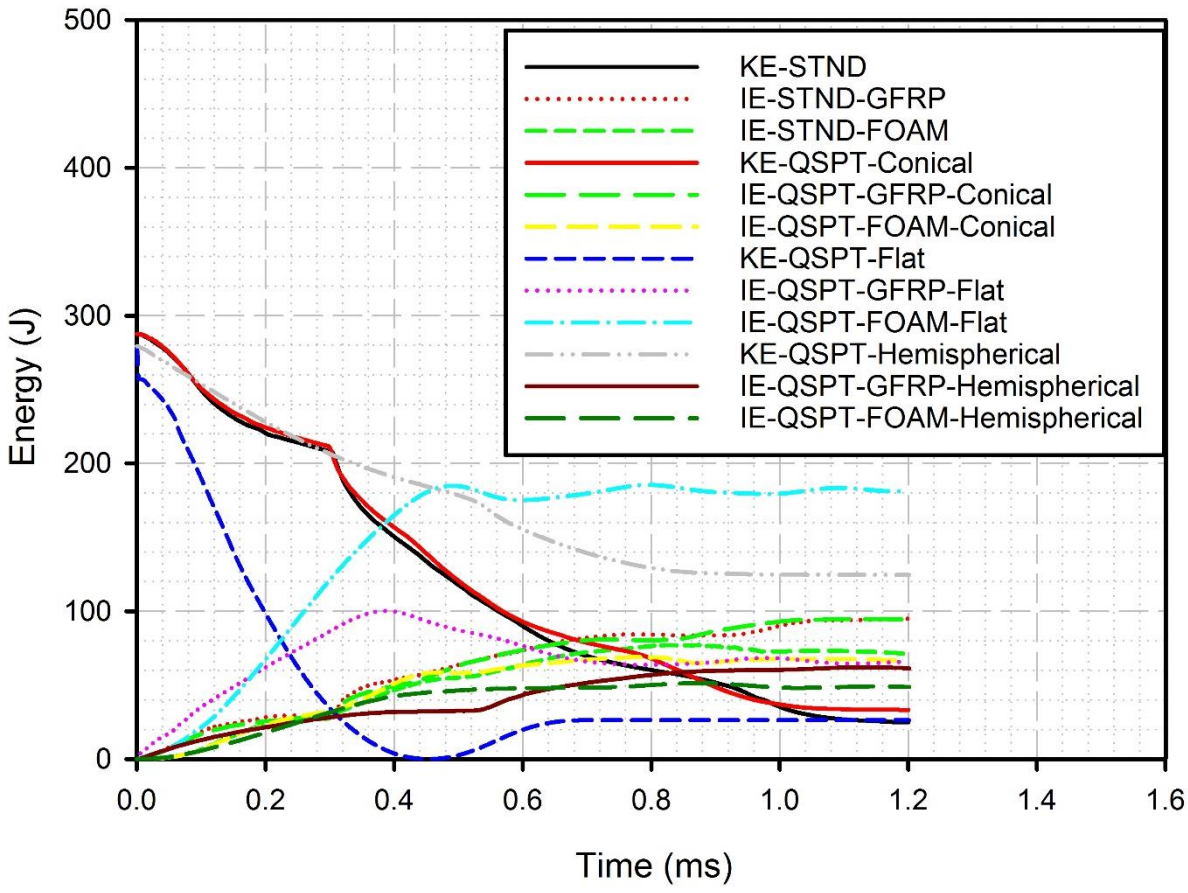

Figure 159 Energy transfer profiles of each impact scenario: NF-F07-101 standard (STND), and QSPT simulation setup with conical, flat ended, and hemispherical projectiles. The outcome from the flat ended projectile impact was different compared to others

In connection, the energy absorption by the foam core almost doubled the amount absorbed by the GFRP skins. The difference was significant if not surprising, given the fact that penetration didn't occur and only the top skin contributed to the energy absorption. Similarly to what has been explained in gravelling impact of sandwich plate, a likely explanation of this result is the resistance provided by the GFRP resulted in increased bending displacement of the skin which in turn was reacted by a larger foam area. The performance of the sandwich composite against the flat ended projectile can be clarified in Figure 160 which represents the penetration resistance of the sandwich against each projectile. Higher contact force was achieved between 0-0.6 ms interval for the flat end which has not been observed for the others. This in turn causes the projectile to slow down with a much higher deceleration compared to other cases (Figure 161). From Figure 159, significant positive correlation can be seen between the STND case and the QSPT-conical projectile impact setup. The sharp change of KEs at 0.3 ms was due to the two-step geometry of the conical projectile as Figure 162 illustrates. Both the KE and the IE profiles were almost the same. This is a remarkable outcome which is contrary to what has been found for monolithic laminates, and it clearly shows that it is possible to reduce the required specimen dimensions for this case. Figure 160 and Figure 161 also support this claim by demonstrating the positive correlation between penetration resistance and projectile velocity profiles.

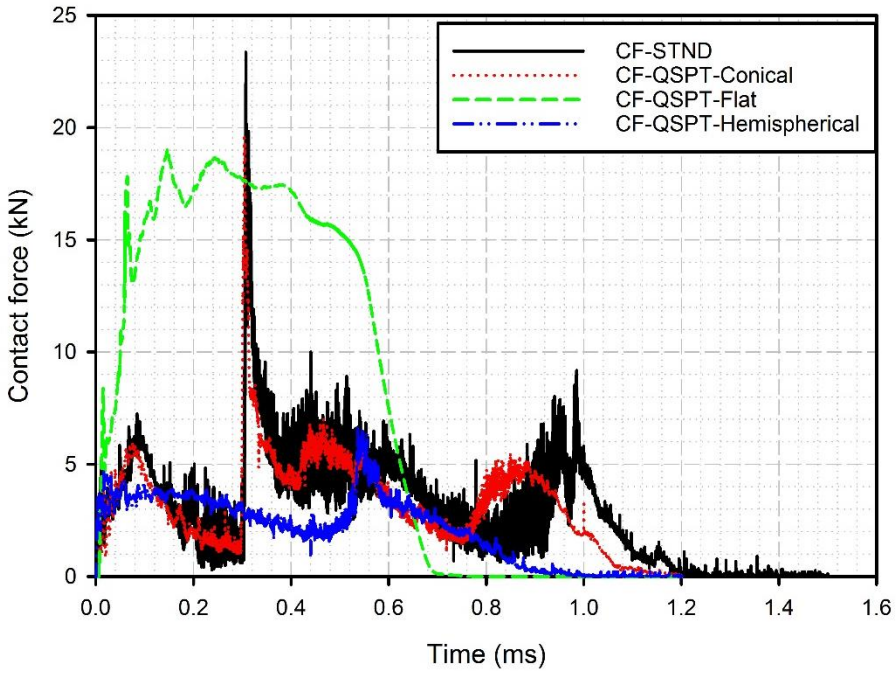

Figure 160 Penetration resistance of the sandwich structure in NF-F07-101 (STND) and QSPT setup with three different projectile profiles

It can be understood from Figure 159 that, among all the cases, hemispherical projectile appears as the most effective penetrator. The KE of hemispherical projectile was affected less when compared to others, leading to a higher residual KE and velocity at the end of the impact. In addition, the resistance of the sandwich structure was lowest as Figure 160 indicates. Closer inspection of the Figure 159 reveals that in full penetration cases the IE of foam is lower than that of GFRP. This indicates that the resistance of the sandwich skins should be maximised in order to have a required level of energy absorption which was reported in literature by many others (Gellert et al. 2000).

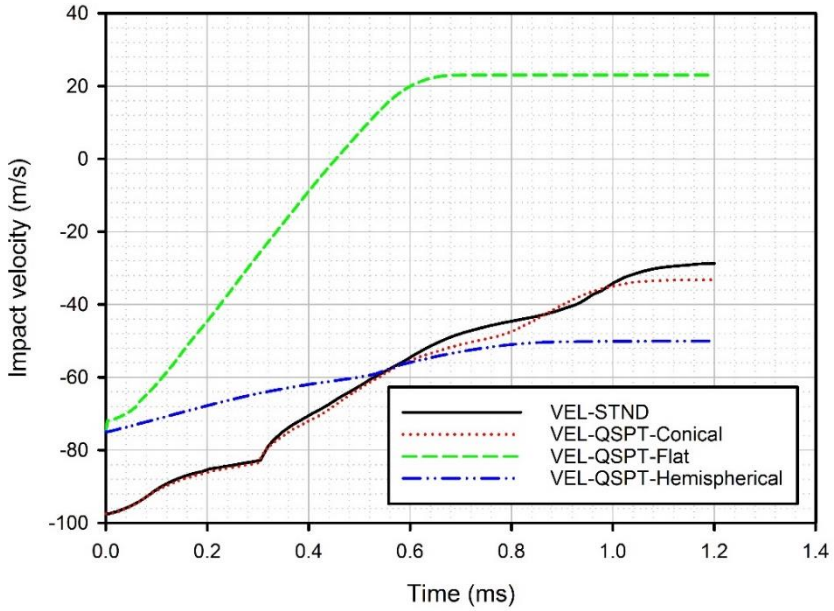

Figure 161 Impact velocity change of the projectiles in NF-F07-101 (STND) and QSPT simulation setup

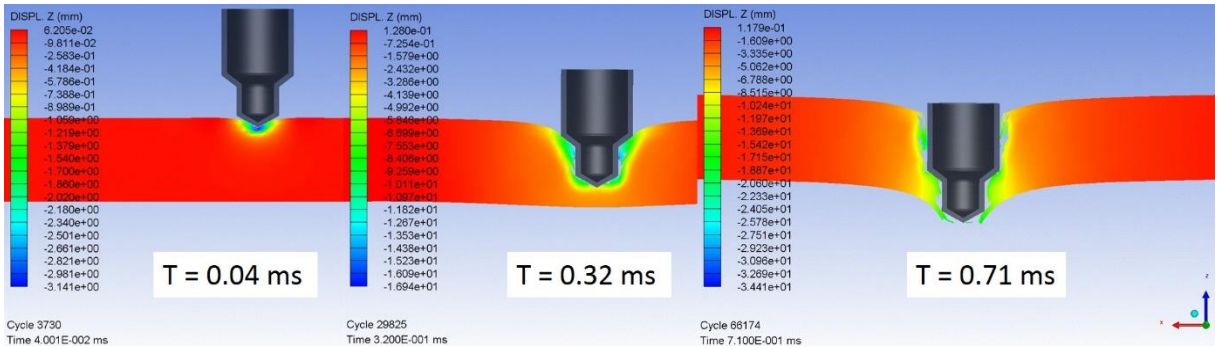

Figure 162 Penetration stages of the NF-F07-101 standard projectile illustrating the corresponding sharp changes in energy, contact force, and velocity graphs at 0.04 ms, 0.32 ms, and 0.71 ms. The jump at the contact force graph at 0.32 ms is due to the contact of the larger part of the projectile

Failure response of the sandwich plates against conical projectile is illustrated in Figure 163 and Figure 164. Very similar overall fibre failure was obtained in both cases with a wider damaged area at the reverse side of the sandwich, displaying a typical petal failure caused by the shape of the projectile as shown in Figure 163.

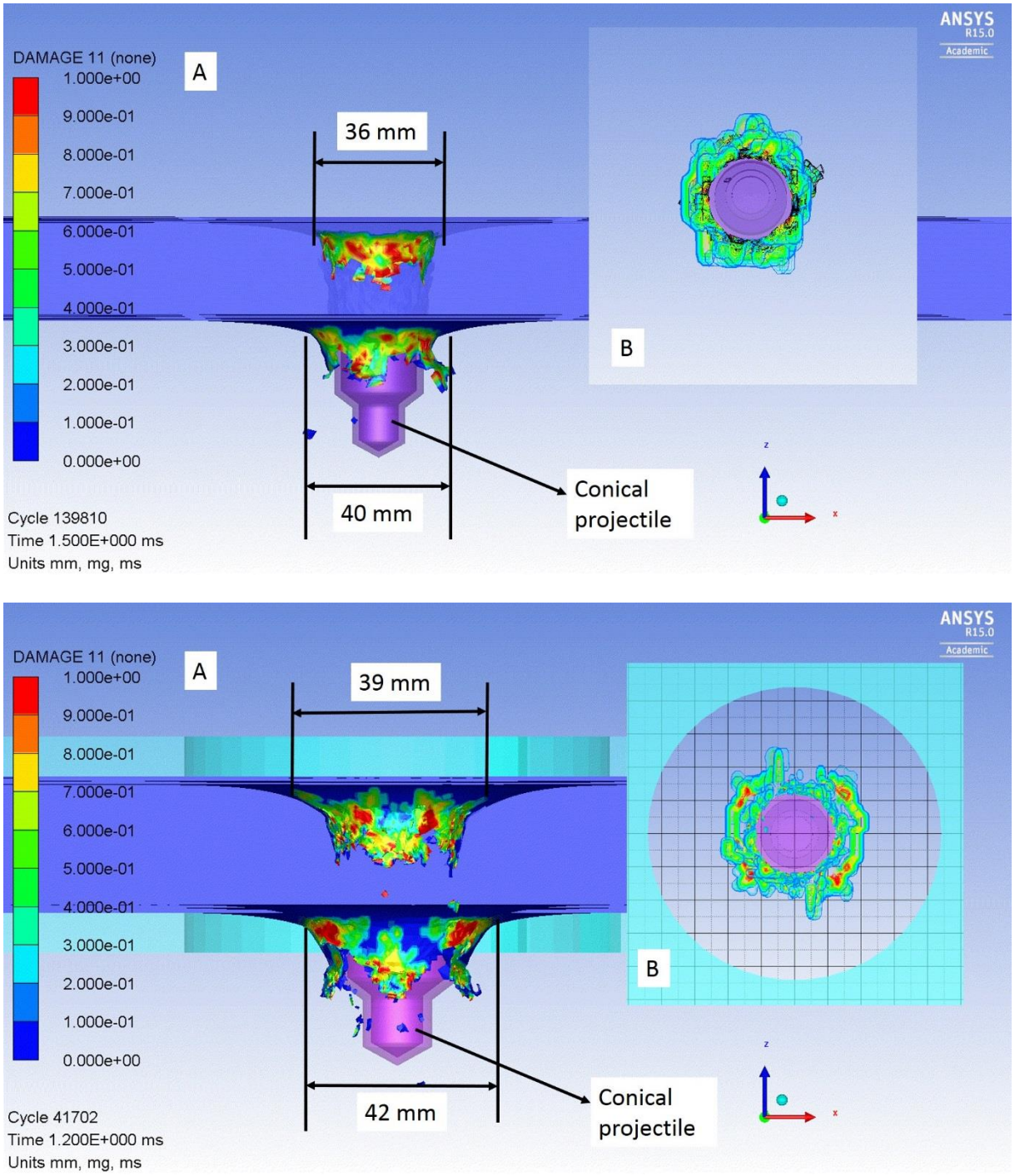

Figure 163 DAMAGE 11 contour plot showing the fibre damage extent in: (top) NF-F07 standard scenario, (bottom) QSPT setup with conical projectile. (A) of each figure depicts the side view of the sandwich, while (B) depicts the top view of the damage shape.

Delamination damage however, was very negligible and very confined. One of the reasons for this outcome is that the relatively thin facesheets of the sandwich are more susceptible to the impact of conical projectile, therefore fibre failure precedes delamination failure. Another reason for the confined delamination in all the HVI of sandwich plates considered in this chapter is that the modelling of the layer between the foam core and the facesheets was considered as a bonded contact without any stress failure criteria. The rationale was the absence of delamination between the core and the facesheets of sandwich plates in quasi-static punch tests, and the fact that shear strength of the epoxy resin was much higher than the shear strength of the foam core (42 MPa vs 0.8 MPa). Therefore, foam shear failure would precede the delamination at the core-facesheet interlayer.

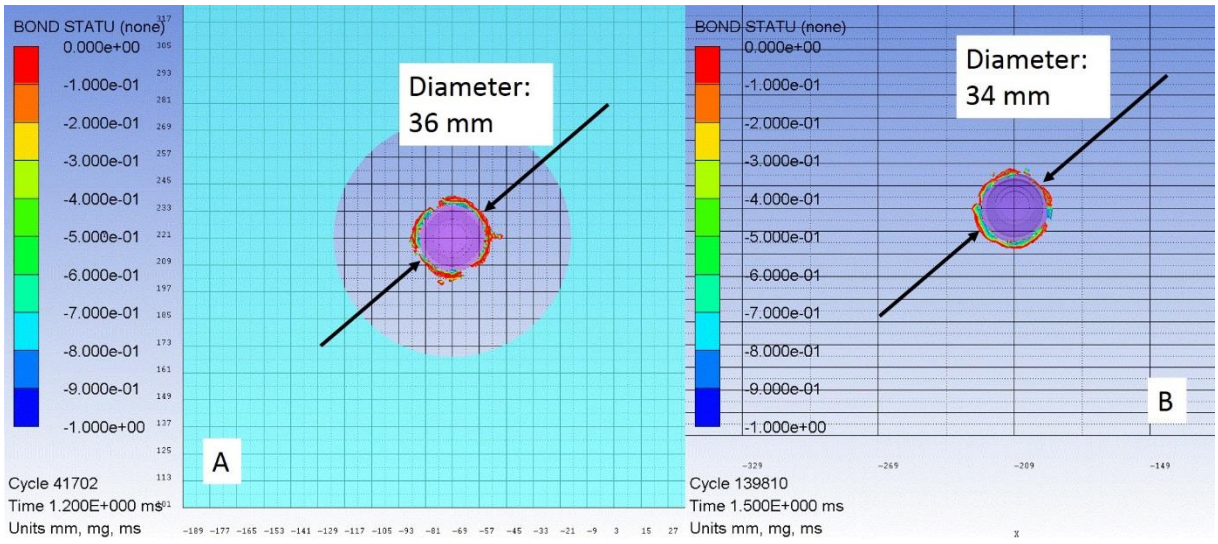

Figure 164 BOND STATU contour plot showing the delamination failure of (A) QSPT-conical setup, and (B) NF-F07 standard setup. No significant delamination was observed in these cases similarly to previous sandwich impact simulations

6.4 General discussion and conclusion

The essential objective of this research was to develop a prediction method that can be used alone instead of various existing railway standards for the impact resistance of composite railway carbodies. Since the railway industry recently made an effort towards promoting the use of composites as main load bearing structures (REFRESCO Project 2013), composites in railway vehicles is an active research field even though the impact on composites was very well understood by the scientific and engineering communities. Very few studies were found in the literature which attempted to address railway specific performance of composite materials, and no research was found that was similar to the work presented here, i.e. harmonising impact

related standards into one method. That is to say, it has been sought in Chapter 6 to analyse the performance of the composite structures under the circumstances defined by the railway standards together with the prediction method described in Chapter 4, then to compare their responses to decide whether the proposed method could be promoted. More clearly, the aim was to identify the closest structural response to what was obtained from the standard simulation.

There were challenging as well as helpful topics while making this determination. The first and important challenge arisen was the effect of projectile profile on penetration resistance of composites. The results of the simulations presented in this chapter, in addition to what has been found in Section 5.3, indicates that the penetration resistance of the composite targets is influenced by the end profile of the projectiles, which is in line with those of previous studies (Jordan & Naito 2014). In gravelling impact scenario (EN15152) of GFRP laminates, all four impact generated similar energy dissipation behaviour and projectile velocity history independent of the projectile end profile (Figure 127). However, even though the invisible failure (delamination) patterns were similar, the visible damage of the laminates was represented better while using the conical projectile with QSPT setup. On the contrary, in flying ballast impact (NF-F07101) of monolithic laminates, it has been shown that hemispherical projectile can provide accurate prediction as well when compared with the conical counterpart (Figure 153). For bodyside window impact scenario (GM/RT2100) the situation was simpler since only two type end profiles were considered, i.e. flat and hemispherical, and both projectiles resulted in similar response. These findings suggest that an uncertainty exists on the effect of projectile profile depending on the considered case.

To remove this uncertainty, it was shown in the Chapter 5 that the numerical model successfully predicted the ballistic response of the materials for both the flat and the hemispherical ended impactors. Therefore, in cases where, for example hemispherical or conical impactors give a better representation of a given standard, the methodology still applies because testing could be done with flat impactor while numerical investigation can be done with hemispherical impactor. A note of caution is due here since the observations from the validation of hemispherical impactor suggests that there may be a link between failure of the material and the numerical softening or erosion parameters (Nguyen et al. 2016), thus further investigation of relevant parameters might be required. Since through-thickness shear strength was one of the failure controlling parameters, obtaining shear strength is not viable using a hemispherical punch as it was done with a flat punch to determine the contact area and its relation to failure force. In

addition, there exists a considerable amount of through-thickness crush failure as well with the hemispherical punch, in other words, the failure was not purely shear.

It can be argued that, in Chapter 6, the masses, the velocities, and the sizes of the projectiles were different, and thus a comparison might be misleading. What this research attempted to accomplish was exactly influenced from this detail. This research considers the possible impact scenarios against a composite passenger railway vehicle. In a real-time rail operation, there is no clear probability for a predefined scenario. Therefore, the specification of projectiles does not necessarily need to be exactly the same. The methodology thus depends on the investigation of energy absorption behaviour which was demonstrated by considering the same impact energies. Generally speaking, in contact force and projectile velocity change figures, the differences between each impact case appears to be larger or their characteristics with respect to time emerge as varying, influenced by the projectile properties. However, the energy transfer figures shows a much better correlation between each case, despite the flat ended projectile displays a different behaviour at the beginning of the impact. Based on these influences, and the fact that distinctive projectiles can provide similar structural responses and failure patterns, the impact energy transfer emerged as a more reliable evaluation parameter. This is the answer to one of the research questions asked in Section 1.2: Which parameter is the most reliable for assessment?

It is also worth mentioning that the material failure influences the response of the structure. The impact simulations carried out in this chapter considered the uppermost limits of the standards except the bodyside window impact which has a single predefined specification. For gravelling impact and flying ballast strike, the impact parameters - such as the velocity and the energy - change with respect to the operation speed of the railway vehicle. In addition, the projectiles were modelled as rigid and was assumed that they experience zero deformation. In reality, particles can be stone and such, so it automatically creates a safety factor (so to speak) since a deformable object loses its penetration efficiency throughout the impact. It is therefore likely that a connection exists between a destructive impact and the accuracy of the prediction method. That is to say, there is a potential for lower impact energy scenarios that the similarity of the structural response might increase against different type of projectiles.

Another research question asked in Section 1.2 was the challenges of the proposed method. It was concluded in Section 5.5 that the enhancement level parameter (*ENL*) is the most important impact parameter based on the fact that it reveals the true response of the structure in absence of physical dynamic testing. In this respect, the investigation and determination of the *ENL* can

be addressed as the main challenge of this method. Generally speaking, under ballistic loading, the increase in performance of glass fibre reinforced composites is more noticeable compared to carbon fibre reinforced counterparts (Ochola et al. 2004). This can be attributed to the more brittle nature of the carbon fibres. However, as mentioned in the literature review there is no such universal rule for the enhancement of the material properties. Therefore, the determination of the enhancement of material properties requires some investigation and insight into strain rate effects depending on the specific material used.

One of the uncertainties faced during the validation of the prediction method was about the general concerns about the scaling issues of composites. There are concerns that using coupons or elements instead of actual structure/sub-structure might lead to a misconception or misinterpretation of results, creating inconsistency between the intended use of elements and structures. However, following the evidence and the general assumption that the damage would be localised in high-velocity impact (HVI), the area dimension of the target is less important in HVI compared to the importance of thickness of that section. It has been shown and proven that for the impact cases considered in this work, specimen size did not influence the outcome of the simulation. The findings suggests that it is possible to reduce the specimen size in all three standards. This is very encouraging and it is one of the most significant improvement of the proposed method over the existing standards. For example, in EN15152 – gravelling impact risk, the specimen dimensions was described as 500x500 mm, while in QSPT setup 200x200 mm samples were used. With no apparent influence to the results, 200x200 mm dimension was found enough to carry out such tests, consequently achieving 84% materials cost saving. Therefore, scaling was found to be insignificant in this study. These findings support the recent work of Zhou et al. (Zhou et al. 2016) in which the authors observed no significant scaling effects in four scaled sizes of corrugated composite sandwich structures subjected to through-thickness compression loading.

Taken together, the findings of this chapter provide answers to one of the research questions asked in Section 1.2: “To what extent is the new methodology a reliable representation of the assessment of object strike?” Naturally, it was expected (and found reasonable) to face some inconsistencies among various impact scenarios given the circumstances such as projectile profile or boundary conditions. Notwithstanding these variables, this study found significant correlation between considered scenarios. Generally speaking, for most of the cases, a high level of reliability was ascertained in terms of overall material failure and response, the energy absorption character, and the velocity change of the projectiles. These parameters were found

more important in determining the reliability of the method. The reliability was higher for monolithic laminates compared to sandwich plates. The penetration resistance of the materials were found more varying compared to the aforementioned parameters. It is therefore concluded that the proposed prediction method is more reliable if the energy absorption or material failure levels could be established for the needs.

Chapter 7. Conclusions

In the past years, railway passenger vehicles have included elements such as vehicle doors, seats, tables and inner panels made of composite materials. Recent studies by the industrial and institutional organisations exposed the clear advantages of composites for the railway system in terms of life cycle cost, manufacture, and efficiency. The implementation of these lightweight materials as main load bearing structures in railway vehicles is an active research area, but remains a challenge because of the lack of structural standards and certification procedures.

To accelerate the transition into the use of new lightweight materials, structural vehicle standards should be revised accordingly as they currently consider metallic materials. This necessity arises from the distinctive material structure and behaviour of composites. Unlike metallic counterparts, composites have direction dependent properties and various failure modes which make them challenging in vehicle carbody designs. One of the requirements of a passenger rail vehicle is to withstand the strike from a flying solid object. With the introduction of high-speed rail lines, small-sized object strike such as flying ballast has become an important issue which can affect the high-speed train operation and performance. The implementation of load bearing composites to railway carbodies is therefore likely to require an assessment of the railway specific impact events as these types of materials are sensitive to impact loading.

This thesis was therefore undertaken to present a method to predict the flying object strike response of composite carbodies, which can be used alone instead of various other impact related standards for rail vehicles. One of the goals of this research was to create a cost effective and time saving method for impact risk assessment of railway carbodies. This method is based on the similarities between the dynamic and static ballistic penetration impact. Benefiting from these similarities, a static destructive test method was combined with finite element modelling to replace expensive and hardly accessible high-velocity impact experiments. A step-by-step description of the method is given in Appendix – A.

The experimental program carried out has shown that the quasi-static punch test (QSPT) performed with the custom-made fixture (span-to-punch ratio: SPR4.1 setup) can indeed mimic the ballistic impact response of laminated and sandwich composites by displaying similar failure modes and damage sequences. It was found that the through-thickness shear strength obtained by further tests (SPR1.2 setup), together with the in-plane tensile strength, was able to control the major failure of the structure. Supported by the findings of the experimental program, the developed numerical model successfully simulated the QSPT experiments,

providing excellent correlation of visible and invisible damage, penetration resistance, and energy absorption capability.

To overcome the limitations in ballistic testing, high-velocity impact simulations were supported by the analytical models available in the literature. The results of the investigation with two types of GFRP laminates (E-glass/polyester and E-glass/epoxy) has shown that the enhancement level caused by high strain rate loading was similar. A 50% increase of the material properties provided accurate dynamic response.

The validation of the proposed method in Chapter 6 has shown that the importance of standard-specific projectile use was unclear. In some scenarios, all the projectiles gave reasonable and similar prediction, whereas in others a specific projectile would provide more accurate representation of, for example, visible damage, even though other aspects emerge similar. It was highlighted that there was greater agreement between the results from different projectiles when the impact didn't cause significant damage. Therefore, these findings suggest that standard specific projectiles should be taken into account to be more precise.

The key strengths of this study are its simplicity, practicality, and its cost effectiveness compared to the conventional ballistic testing. It requires a simple inexpensive fixture, a conventional tensile test rig which is easily accessible by any institution, and a numerical modelling software, which has become relatively cheap in recent years. Therefore, this study allows to avoid expensive and time consuming testing procedures. In addition, advantageously, the product of the method – thanks to the numerical modelling – is much more detailed as opposed to ballistic testing outcome which can be a key element in design phase. One of the most significant finding to emerge from this study was the potential minimization of the physical dimensions of the test sample. The evaluation of the railway impact standards with the proposed prediction method revealed that in all the considered cases the affected area of impact was localised around the projectile contact area. The dimensions of the test samples specified in each standard were found to be a lot more than sufficient. Therefore, significant materials (hence cost) savings can be achieved by using 200 x 200 mm samples. However, this outcome should be approached with caution as the HVI analysis is based on simulations even though they are sufficiently accurate, and physical experimentation might be required for enhancing the reliability this outcome.

From the railway industry perspective, the main product of this thesis: the proposed method, can be placed between the "sub-component" and "elements" level in the building block strategy

for the railway industry vehicle design (Figure 64 - Page 82). However, in some cases where critical parts such as joints are involved in the analysis, it can be extended to include “details” level.

As well as being a helpful tool in the design process of composite railway carbodies, the other potential practical use of the proposed method can be the application by the stakeholders responsible for vehicle repair and maintenance. As this method produces information about the failure patterns of the structures, it would be helpful to identify the extent and the type of the failures during regular inspections, which then can be used to generate a database of failures and corresponding repairs.

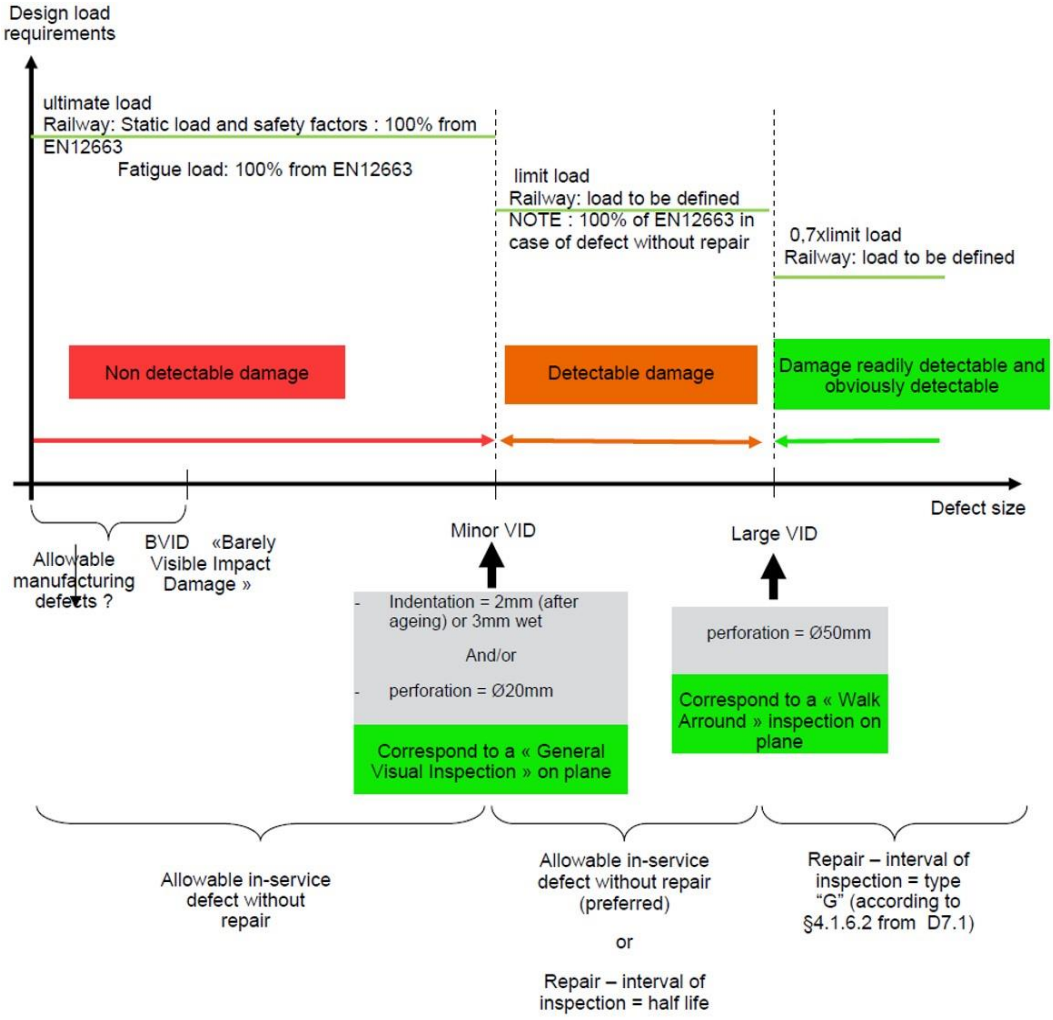

Figure 165 Recommendations by REFRESCO project on the consideration of impact damage levels for repair purposes (REFRESCO WP7-D7.3 2016)

This research supports the recommendations of the REFRESCO project. The project emphasized that, for the composite carbodies, the consideration of the large visible impact

damage (LVID) over barely visible impact damage (BVID) is more adequate for the railway industry (REFRESCO WP7-D7.3 2016) (Figure 165). The methodology therefore is consistent with this recommendation as it can demonstrate the visible failure analysis in addition to the delamination analysis which was one of the objectives of this research.

The proposed method was aimed to bring a practical assessment to railway sector on composite bodyshell resistance. However, as the test samples are ordinary and bear no railway specific requirements, the method has the potential to be used by other industries as well should a similar impact to the structures observed, for example debris impact to road or aviation vehicles. Although the railway industry is underdeveloped compared to the other industries in terms of composite material applications, and it is possible that there might be other methods developed in other industries, the method still can be used as long as the potential impact energy level is known, or at least can be used for benchmarking the methods.

7.1 Further research

This thesis presented an early and practical assessment method for a specific requirement of composite railway carbodies. Being a pioneering research with promising outcomes, it is believed that there is a substantial amount of future work for further improvements.

With a well-established methodology at hand, a natural progression of this work is to repeat the procedure by using carbon fibre based composites (CFRP) as they exhibit slightly different failure mode/progression. It would also be important to see the strain rate dependency of CFRPs in this specific loading and its correlation to the available analytical models. In parallel to this, further research should explore different sandwich cores like honeycomb. New information might be obtained as these type of core materials has different through-thickness crush mechanisms, intrinsic failure modes and interface bond strength caused by the geometry and structure of the core cells. In addition, different laminate lay-up and layer-orientated configurations could be investigated to explore optimized structural designs.

In a future study, when the conditions are suitable, it is highly desirable to access experimental ballistic testing and obtain the ballistic results to investigate the accuracy of the methodology as well as the analytical models used in this thesis. Positive results would greatly strengthen the validity of the proposed method, while variations to the results would allow the methodology to be refined and improved.

It would be interesting to further conduct an optimization study for the fixture span-to-punch diameter (SPR) ratio by changing the impactor diameter. There might exist a ratio which provides closer values of the static and the dynamic penetration energies at the same time. The outcome from that study (which are relevant to the properties of the punch/projectile) can then further be combined with other impactor properties such as the type of steel (considering the repeated nature of the test, failure of the impactor should be avoided) to generalise the criteria for the impactor, should the method becomes a standard.

Beside the projectile specifications, the other element to implement to the possible future standard is the analysis of a well-defined result parameter. As it was mentioned in the previous section, energy transfer figures emerged as a more reliable parameter to represent the structure's penetration resistance performance. However, it might be case-specific to this study, and therefore, a parameter or set of parameters should be decided after the analysis of the method while considering a wide range of material configurations as stated above. This parameter can be the ones analysed in this thesis, or it can be a unique parameter that incorporates the combination of many affecting parameters.

It might be possible that the prediction method could be extended to cover the rest of the standard requirements shown in Table 2 such as GM/RT2100 / UIC missile protection or NF-F15-818 standards. Although in this case, the fixture and the sample sizes would be larger, affected by the larger dimensions of the relevant projectiles. However, alternatively, the material properties used in prediction method can be used to separately simulate the standard cases since the dynamic properties and the responses have already been validated by the proposed method.

The implications drawn from this research could potentially feed a vehicle body structural integrity study such as residual strength investigation. Even though the industrial recommendations favour the large visible impact damage (LVID) for major repairs, residual strength measurements can further clarify if that really is the case. Likewise, the influence of vehicle life-cycle (ageing) effects such as hygrothermal (moisture and temperature), weather conditions, and ultraviolet radiation should be taken into account as these effects are known to degrade composite material performance over time.

Speaking of structural integrity, the protection performance (energy absorption) of the composites used in this research assumed the near perfect condition of the structures, and did not considered the many factors affecting the life-cycle performance (which is a vast field in

itself). One of the most important strength/integrity degradation factor is the fatigue loading. The effect of fatigue on polymer composites appears as the multiple crack formations which then leads to other major strength degrading failure modes such as delamination or de-bonding of layers/constituents. These mechanisms are similar to the ones observed after an impact loading and they contribute an important amount to the energy absorption if not the most. It is likely that the long term protection performance against object strike will be influenced by in-service fatigue loading. Therefore this should also be considered as a future study.

APPENDIX – A: PROPOSED METHOD TO PREDICT THE IMPACT RESISTANCE PERFORMANCE OF COMPOSITE CARBODIES

A step-by-step execution of the proposed method is given below:

1) *Determination of fibre tensile and through-thickness shear strength*: Determine the fibre direction tensile properties of composite laminates by ISO/ASTM standard (Table 1). Following, perform the quasi-static punch test (QSPT) with SPR1.2–circular flat ended punch (Section 4.3) to obtain the force-displacement graph. Using the maximum failure force (F_{max}) from the graph, calculate the shear strength with Eqn. 17:

$$S_{23} = S_{13} = \frac{F_{max}}{2\pi rt} \qquad \text{Eqn. 17}$$

2) *Determination of failure modes and sequences*: Perform QSPT with SPR4.1 setup with circular flat and hemispherical ended impactors, and analyse the failure modes. Usually very thin laminates fail by in-plane tensile failure, and thicker laminates fail by through-thickness shear followed by in-plane tensile failure. Conduct step-wise testing if required (Section 5.1.3).
3) *Validation of QSPT*: Create the finite element model for SPR4.1 setup and validate it with the quasi-static punch loading experiments in terms of contact force-displacement response and failure modes. It is important to observe the same failure sequence in simulations compared to the experiments. Attention should be given to the numerical parameters such as erosion strain of the material against varying impactors. For modelling details, refer to Sections 4.3.1.
4) *High-velocity impact simulations for desired application*: Use the FE model in Step 3 for the high-velocity impact simulations while using a 25.4 mm diameter 100 g non-deforming steel projectile (preferably hemispherical ended) with the desired impact velocity.
    - In case of GFRP use, increase the material strengths and moduli by 50%.
    - In case of FRP use other than glass fibre, determine the strain rate effect by using the method presented in Section 4.4, 4.4.1, and 4.4.2.
    - Analyse the contact force, energy absorption of the structure, and velocity change of the projectile.
    - For gravelling impact and flying ballast concerns, simulations with conical projectiles (defined in the standards) should also be taken into account in order to have a more accurate material response.

APPENDIX – B: PUBLICATIONS, CONFERENCES, SEMINARS, AND VISITS

Publications	[1] Onder A, O'Neill C, Robinson M. Flying Ballast Resistance for Composite Materials in Railway Vehicle Carbody Shells. Transport Research Procedia 2016; 14:595–604. doi:10.1016/j.trpro.2016.05.301. [2] Asim Onder, Conor O'Neill, Mark Robinson, "Flying Ballast Resistance for Composite Materials in Railway Vehicle Carbody Shells", Proceedings of 6th Transport Research Arena, April 18-21, 2016, Warsaw, Poland
Conferences	Next Generation Rail 2014, 11-13 June 2014, Manchester, UK Transport Research Arena - TRA2016, 18th April 2016, Warszawa, Poland
Presentations	*Podium presentation*: Enabling the implementation of composite materials in railway rolling stock - Next Generation Rail 2014, 11-13 June 2014, Manchester, UK *Podium presentation*: Flying ballast resistance for composite materials in railway vehicle carbody shells - TRA2016, 18th April 2016, Warszawa, Poland *Poster Presentation*: Missile protection requirement for composite materials in railway vehicles, Annual Postgraduate Conference, 4th May 2016, MSE, Newcastle University
Seminars	Impact resistance of composite materials for railway vehicle applications, 8th June 2016, MSE, Stephenson Building, F1, Newcastle University
Visits	*Exhibitor*: Newrail stand at UK Pavilion, InnoTrans 2014 – 23-26 September 2014, Berlin, Germany

REFERENCES

3A Composites, 2016. AIREX ® T90 Easy Processing Structural FST Foam. Available at: www.3ACCorematerials.com.

Abrate, S., 2011. *Impact Engineering of Composite Structures* S. Abrate, ed., SpringerWienNewYork.

Abrate, S., 1991. Impact on Laminated Composite Materials. *Appl Mech Rev*, 44(4).

Abrate, S., 1994. Impact on Laminated Composites: Recent Advances. *Applied Mechanics Reviews*, 47(JANUARY 1994), p.517.

AFNOR, 2002. *AFNOR NF F07–101: Railway applications — shock test by throwing up ballast simulation*,

Agretti, M., 2012. Sollevamento del Ballast sulla linea AV Roma-Napoli. *Interviewer: F. Bedini Jacobini*.

AI-Salehi, F., AI-Hassani, S. & Huston, M., 1989. Experimental investigation into the strength of angle ply grp tubes under high rate of loading. *J Comp Mat*, 23, pp.288–305.

Aktay, L., Johnson, A.F. & Holzapfel, M., 2005. Prediction of impact damage on sandwich composite panels. *Computational Materials Science*, 32(3–4), pp.252–260.

ANSYS Help Viewer, 2013. ANSYS, Help Viewer, v.15.0.0, 2013.

ANSYS Inc., 2013. AUTODYN Composite Modeling. In *ANSYS Help Viewer, Release 15*. p. 65.

Antonucci, V. et al., 2014. Strain monitoring of composite elements by fibre Bragg grating sensors during a quasi-static indentation. *Composites Part B: Engineering*, 56, pp.34–41. Available at: http://dx.doi.org/10.1016/j.compositesb.2013.07.020.

Arezoo, S. et al., 2013. Compressive deformation of Rohacell foams: Effects of strain rate and temperature. *International Journal of Impact Engineering*.

Armenakas, A.E., Sciammarella, C. a. & Armenàkas, a. E., 1973. Response of glass-fiber-reinforced epoxy specimens to high rates of tensile loading. *Experimental Mechanics*, 13(10), pp.433–440. Available at: http://link.springer.com/10.1007/BF02324887.

Ashby, M.F., 2011. *Materials Selection in Mechanical Design*, Oxford, UK: Elsevier Ltd.

Barré, S., Chotard, T. & Benzeggagh, M.L., 1996. Comparative study of strain rate effects on

mechanical properties of glass fibre-reinforced thermoset matrix composite. *Composites Part A*, 27, pp.1169–1181.

Batchelor, J. & Wilson, J.E., 1984. Applications of Fibre Reinforced Plastic Composites in the Railway Industry. *Proceedings of the Institution of Mechanical Engineers, Part D: Journal of Automobile Engineering*, V 43(N 198), pp.43–49.

Bedini-Jacobini, F., Tutumluer, E. & Saat, M.R., 2013. Identification of High-Speed Rail Ballast Flight Risk Factors and Risk Mitigation Strategies. In *World Congress on Railway Research*. pp. 1–8.

Belingardi, G., Cavatorta, M.P. & Duella, R., 2003. Material characterization of a composite-foam sandwich for the front structure of a high speed train. *Composite Structures*, 61(1–2), pp.13–25.

Boukhili, R., Hubert, P. & Gauvin, R., 1991. Loading rate effect as a function of the span-to-depth ratio in three-point bend testing of unidirectional pultruded composites. *Composites*, 22(1), pp.39–45. Available at: http://cat.inist.fr/?aModele=afficheN&cpsidt=19497322 [Accessed November 24, 2016].

Brevik, F.A., 1997. Sandwich panel for the high speed Gardermoen Airport Shuttle. In *Proc of the Euromech 360 Conference: Mechanics of Sandwich Structures*. France, pp. 369–377.

Broutman, L. & Rotem, A., 1975. *Impact strength and toughness of fiber composite materials*,

Buitrago, B.L. et al., 2010. Modelling of composite sandwich structures with honeycomb core subjected to high-velocity impact. *Composite Structures*, 92(9), pp.2090–2096. Available at: http://dx.doi.org/10.1016/j.compstruct.2009.10.013.

Buitrago, B.L., García-Castillo, S.K. & Barbero, E., 2010. Experimental analysis of perforation of glass/polyester structures subjected to high-velocity impact. *Materials Letters*, 64(9), pp.1052–1054. Available at: http://dx.doi.org/10.1016/j.matlet.2010.02.007.

Bulut, M., Erkliğ, A. & Yeter, E., 2016. Hybridization effects on charpy impact behavior of basalt/aramid fiber reinforced hybrid composite laminates. *Polymer Composites*, 98.

Camanho, P.P. & Lambert, M., 2006. A design methodology for mechanically fastened joints in laminated composite materials. *Composites Science and Technology*, 66(15), pp.3004–3020. Available at: http://www.sciencedirect.com/science/article/pii/S0266353806000546 [Accessed May 4, 2017].

Cantwell, W.J. & Morton, A., 1989. Comp.arison of the low and high velocity mpact response of CFRP. *Composites*, 20(6), pp.545–551.

Cantwell, W.J. & Morton, J., 1991. The impact resistance of composite materials - a review. *Composites*, 22(5), pp.347–362.

Carruthers, J., 1995. *Applications of Energy Absorbing Composite Materials for Crashworthy Rail Vehicle Design*, Sheffield.

Carruthers, J.J., Robinson, A.M. & Smith, R.A., 1998. Energy absorbing sandwich panels for crashwothy composite structures. In I.M. Allison, ed. *Proceedings of the 11th International Conference on Experimental Mechanics*. Oxford: A.A. Balkema / ROtterdam / Brookfield, pp. 307–312.

Cartié, D.D.R. & Irving, P.E., 2002. Effect of resin and fibre properties on impact and compression after impact performance of CFRP. *Composites - Part A: Applied Science and Manufacturing*.

Catalanotti, G. et al., 2011. An efficient design method for multi-material bolted joints used in the railway industry. *Composite Structures*, 94(1), pp.246–252. Available at: http://www.sciencedirect.com/science/article/pii/S0263822311002388 [Accessed March 31, 2017].

Chan, S. et al., 2007. Ballistic limit prediction using a numerical model with progressive damage capability. *Composite Structures*, 77(4), pp.466–474.

Cheeseman, B.A. & Bogetti, T.A., 2003. Ballistic impact into fabric and compliant composite laminates. *Composite Structures*, 61(1–2), pp.161–173.

Chen, J.K., Allahdadi, F.A. & Sun, C.T., 1997. A Quadratic Yield Function for Fiber-Reinforced Composites. *Journal of Composite Materials*, 31(8).

Choe, G., Finch, W.J. & Vinson, J., 1988. Compression testing of composite materials at high strain-rates. In *Proc of 4th Japan-US Conf Comp Mats*. Washington DC, pp. 82–91.

Choi, H.Y. & Chang, F.K., 1991. Impact damage resistance of graphite/epoxy laminated composites. *Polymer Engineering Science*, 31, pp.1294–1300.

Clegg, R.A. et al., 2006. Hypervelocity impact damage prediction in composites: Part I-material model and characterisation. *International Journal of Impact Engineering*, 33(1–12), pp.190–200.

Cortesi, A., Issenmann, T. & Kalbermatten, T., 1991. Light nose for fast locomotives. *Schweizer Eisenbahn Revue*, (12), pp.435–442.

Daniel, I., Hamilton, W. & LaBedz, R., 1982. Strain-rate characterization of unidirectional graphite/epoxy composites. *ASTM STP*, (787), pp.393–443.

Daniel, I., Hsiao, H. & Cordes, R., 1995. Dynamic response of carbon/epoxy composites. *ASME AD*, 48, pp.167–171.

Daniel, I. & LaBedz, R., 1983. Method for compression testing of composite materials at high strain-rates. *ASTM STP*, (808), pp.121–139.

Daniel, I., LaBedz, R. & Liber, T., 1980. New method for testing composites at very high strain-rates. In *Proc of 9th lnt Congress Exp Mech*. Boston MA, pp. 75–81.

DLR, 2012. Next Generation Train (NGT) Modular Railway Car Body Structure Sandwich Car Body Passenger Section.

Erkendirci, Ö.F., 2016. Investigation of the quasi static penetration resistance behavior of carbon fiber reinforced laminate HDPE composites. *Composites Part B: Engineering*, 93, pp.344–351. Available at: http://www.sciencedirect.com/science/article/pii/S1359836816300385.

Erkendirci, Ö.F. & (Gama) Haque, B.Z., 2012. Quasi-static penetration resistance behavior of glass fiber reinforced thermoplastic composites. *Composites Part B: Engineering*, 43, pp.3391–3405.

Feli, S. & Namdari Pour, M.H., 2012. An analytical model for composite sandwich panels with honeycomb core subjected to high-velocity impact. *Composites Part B: Engineering*, 43(5), pp.2439–2447. Available at: http://dx.doi.org/10.1016/j.compositesb.2011.11.028.

Fibermax composites, 2016. Weaving. Available at: http://www.fibermaxcomposites.com/shop/index_files/weavingstylesandpatterns.html [Accessed June 20, 2010].

Flores-Johnson, E.A. & Li, Q.M., 2011. Experimental study of the indentation of sandwich panels with carbon fibre-reinforced polymer face sheets and polymeric foam core. *Composites Part B: Engineering*, 42(5), pp.1212–1219.

Flores-Johnson, E.A. & Li, Q.M., 2010. Indentation into polymeric foams. *International Journal of Solids and Structures*, 47(16), pp.1987–1995. Available at:

http://dx.doi.org/10.1016/j.ijsolstr.2010.03.025.

Flores-Johnson, E.A., Li, Q.M. & Mines, R.A.W., 2008. Degradation of Elastic Modulus of Progressively Crushable Foams in Uniaxial Compression. *Journal of Cellular Plastics*, 44, pp.415–434.

Frey, T., Vinson, J. & Hall, I., 1991. High strain-rate effects on mechanical properties of glass/polyester and carbon/aluminum composite materials. In *Proc of 32nd SDM Conf*. pp. 19–29.

Frey, T., Vinson, J. & Prewo, K., 1991. High Strain-rate effects on mechanical properties of carbon/glass and graphite/epoxy composite materials. In *Proc of 8th ICCM Conf*. p. 32L/1-32L/11.

Gama, B.A. & Gabrys, J.W., 2007. Modeling the Ballistic Penetration of Thick- Section Composites and Sandwich Structures. In *22nd Annual AMERICAN SOCIETY FOR COMPOSITES TECHNICAL CONFERENCE*. University of Washington, Seattle, WA.

Gama, B.A. & Gillespie, J.W., 2011. Finite element modeling of impact, damage evolution and penetration of thick-section composites. *International Journal of Impact Engineering*, 38(4), pp.181–197. Available at: http://dx.doi.org/10.1016/j.ijimpeng.2010.11.001.

Gama, B.A. & Gillespie, J.W., 2008. Punch shear based penetration model of ballistic impact of thick-section composites. *Composite Structures*, 86(4), pp.356–369.

Gama, B. a et al., 2004. Experimental and Numerical Investigations on Damage and Delamination in Thick Plain Weave S-2 Glass Composites Under Quasi-Static Punch Shear Loading.

Gellert, E.P., Cimpoeru, S.J. & Woodward, R.L., 2000. A study of the effect of target thickness on the ballistic perforation of glass fibre-reinforced plastic composites. *International Journal of Impact Engineering*, 24, pp.445–456.

Ghalami-Choobar, M. & Sadighi, M., 2014. Investigation of high velocity impact of cylindrical projectile on sandwich panels with fiber-metal laminates skins and polyurethane core. *Aerospace Science and Technology*, 32(1), pp.142–152. Available at: http://dx.doi.org/10.1016/j.ast.2013.12.005.

Gibson, A.G., 2003. The cost effective use of fibre reinforced composites offshore. , pp.1–43.

Giere, A.C., 1964. Some energy and momentum considerations in the perforation of plates.

AIAA Journal, 2(8), pp.1471–1472. Available at: http://dx.doi.org/10.2514/3.2610.

Goldsmith, W., Dharan, C.K.H. & Chang, H., 1995. Quasi-static and ballistic perforation of carbon fiber laminates. *International Journal of Solids and Structures*, 32(1), pp.89–103. Available at: http://dx.doi.org/10.1016/0020-7683(94)00109-A.

Green Mechanic, 2017. Charpy and izod tests. Available at: http://www.green-mechanic.com/2014/04/difference-between-izod-and-charpy.html.

Guoqi, Z., Goldsmith, W. & Dharan, C.K.H., 1992. Penetration of laminated Kevlar by projectiles-II. Analytical model. *International Journal of Solids and Structures*, 29(4), pp.421–436.

Haque, B.Z.G. & Gillespie, J.W., 2015. A new penetration equation for ballistic limit analysis. *Journal of Thermoplastic Composite Materials*, 28(7), pp.950–972.

Harding, J., 1993. Effect of strain-rate and specimen geometry on the compressive strength of woven glass-reinforced epoxy laminates. *Composites*, 24, pp.323–332.

Harris, B., 1999. Engineering Composite Materials. , p.344.

Harte, A.M., McNamara, J.F. & Roddy, I.D., 2004. A multilevel approach to the optimisation of a composite light rail vehicle bodyshell. *Composite Structures*, 63(3–4), pp.447–453.

Hassan, M.Z. & Cantwell, W.J., 2012. The influence of core properties on the perforation resistance of sandwich structures - An experimental study. *Composites Part B: Engineering*, 43(8), pp.3231–3238. Available at: http://dx.doi.org/10.1016/j.compositesb.2012.03.012.

He, T., Wen, H.M. & Qin, Y., 2008. Finite element analysis to predict penetration and perforation of thick FRP laminates struck by projectiles. *International Journal of Impact Engineering*, 35, pp.27–36.

Hildebrand, M., 1996. *A comparison of FRP-sandwich penetrating impact test methods*,

Holmes, M., 2014a. Continued growth for European GRP market. *Reinforced Plastics*, 58(6), pp.28–30. Available at: http://dx.doi.org/10.1016/S0034-3617(14)70247-4.

Holmes, M., 2014b. Global carbon fibre market remains on upward trend. *Reinforced Plastics*, 58(6), pp.38–45. Available at: http://dx.doi.org/10.1016/S0034-3617(14)70251-6.

Hoo Fatt, M.S. et al., 2003. Ballistic impact of GLARE??? fiber-metal laminates. *Composite Structures*, 61(1–2), pp.73–88.

Hoo Fatt, M.S. & Sirivolu, D., 2010. A wave propagation model for the high velocity impact response of a composite sandwich panel. *International Journal of Impact Engineering*, 37(2), pp.117–130. Available at: http://dx.doi.org/10.1016/j.ijimpeng.2009.09.002.

Hosur, M. V. et al., 2004. Performance of stitched/unstitched woven carbon/epoxy composites under high velocity impact loading. *Composite Structures*.

Hou, J.P. et al., 2000. Prediction of impact damage in composite plates. *Composites Science and Technology*, 60(2), pp.273–281.

Hudson, C.W., Carruthers, J.J. & Robinson, A.M., 2010. Multiple objective optimisation of composite sandwich structures for rail vehicle floor panels. *Composite Structures*, 92(9), pp.2077–2082. Available at: http://dx.doi.org/10.1016/j.compstruct.2009.10.018.

Ido, A. et al., 2008. Study on under-floor flow to reduce ballast flying phenomena. *World Congress on Rail Research, Seoul, Paper*, (1). Available at: http://scholar.google.com/scholar?hl=en&btnG=Search&q=intitle:Study+on+under-floor+flow+to+reduce+ballast+flying+phenomena#0.

Ingleton, S., 2005. *Design of Composite Cabs for Structural Applications in UK Passenger Rolling Stock*. The University of Shefield.

Ipson, T.W. & Recht, R.F., 1975. Ballistic-penetration resistance and its measurement. *Experimental Mechanics*, 15(7), pp.249–257. Available at: http://link.springer.com/10.1007/BF02318057.

Ipson, T.W. & Recht, R.F., 1963. Ballistic perforation dynamics. *J Appl Mech*, 30(3), pp.385–391.

Ivañez, I. et al., 2011. Numerical modelling of foam-cored sandwich plates under high-velocity impact. *Composite Structures*, 93(9), pp.2392–2399.

Jaiswal, A., 2011. ANSYS Explicit Dynamics Seminar. , p.57.

Jeng, S.T., Jing, H.S. & Chung, C., 1994. Predicting the ballistic limit for plain woven glass/ epoxy composite laminate. *International Journal of Impact Engineering*, 15(4), pp.451–464.

Jenq, S. & Sheu, S., 1993. High strain-rate compressional behaviuor of unstitched composite laminates with radial constraint. *Comput Struct*, 25, pp.427–438.

Jing, G.Q. et al., 2014. Aerodynamic Characteristics of Individual Ballast Particle by Wind

Tunnel Tests. *Journal of Engineering Science and Technology Review*, 7(2), pp.137–142.

Jing, G.Q. et al., 2012. Ballast flying mechanism and sensitivity factors analysis. *International Journal on Smart Sensing and Intelligent Systems*, 5(4), pp.928–939.

Jones, R.M., 1999. Mechanics of composite materials. *Mechanics of Composite Materials*, (2), p.519.

Jordan, J.B., Naito, C. & Haque, B.Z., 2013. Quasi-static, low-velocity impact and ballistic impact behavior of plain weave E-glass/phenolic composites. *Journal of Composite Materials*, (June 2015). Available at: http://jcm.sagepub.com/cgi/doi/10.1177/0021998313499952.

Jordan, J.B. & Naito, C.J., 2014. An experimental investigation of the effect of nose shape on fragments penetrating GFRP. *International Journal of Impact Engineering*, 63, pp.63–71. Available at: http://dx.doi.org/10.1016/j.ijimpeng.2013.08.002.

Jordan, J.B., Naito, C.J. & Haque, B.Z., 2014. Progressive damage modeling of plain weave E-glass/phenolic composites. *Composites Part B: Engineering*, 61(MAY 2014), pp.315–323.

Jover, N., Shafiq, B. & Vaidya, U., 2014. Ballistic impact analysis of balsa core sandwich composites. *Composites Part B: Engineering*, 67, pp.160–169. Available at: http://dx.doi.org/10.1016/j.compositesb.2014.07.002.

Kawasaki, 2015. efWING Leaf spring.

Kim, J.K. & Sham, M.L., 2000. Impact and delamination failure of woven-fabric composites. *Composites Science and Technology*, 60, pp.745–761.

Kim, J.S. & Chung, S.K., 2007. A study on the low-velocity impact response of laminates for composite railway bodyshells. *Composite Structures*, 77(4), pp.484–492.

Kim, J.S., Jeong, J.C. & Lee, S.J., 2007. Numerical and experimental studies on the deformational behavior a composite train carbody of the Korean tilting train. *Composite Structures*, 81(2), pp.168–175.

Kim, J.S., Lee, S.J. & Shin, K.B., 2007. Manufacturing and structural safety evaluation of a composite train carbody. *Composite Structures*, 78(4), pp.468–476.

König, J. et al., 2009. Methodology for force flow optimised car body structures and implementation. , pp.1–13.

Kwon, H.B. & Park, C.S., 2006. An Experimental Study on the Relationship between Ballast-flying Phenomenon and Strong Wind under High-speed Train. *Proceedings of the World Congress on Rail Research*.

Lambert, J.P. & Jonas, G.H., 1976. Towards standardization in terminal ballistics testing: Velocity representation. , (January), pp.1–46.

Larsson, F., 1997. Damage tolerance of a stitched carbon/epoxy laminate. , pp.923–934.

Lassig, T. et al., 2015. A non-linear orthotropic hydrocode model for ultra-high molecular weight polyethylene in impact simulations. *International Journal of Impact Engineering*, 75, pp.110–122.

Lataillade, J.L. et al., 1996. Effects of the intralaminar shear loading rate on the damage of multi-ply composites. *International Journal of Impact Engineering*, 18(6), pp.679–699.

Lazaro, B.J. et al., 2011. Characterization and Modeling of Flying Ballast Phenomena in High-speed Train Lines. In *9th World Congress on Railway Research - May 22-26*.

Lee, S.W.R. & Sun, C.T., 1993. Dynamic penetration of graphite/epoxy laminates impacted by a blunt-ended projectile. , 49, pp.369–380.

Liang, Y. et al., 2015. Progressive damage in satin weave carbon/epoxy composites under quasi-static punch-shear loading. *Polymer Testing*, 41, pp.82–91. Available at: http://dx.doi.org/10.1016/j.polymertesting.2014.10.013.

Lifshitz, J., 1976. Impact strength of angle ply fiber-reinforced materials. *J Comput Mat*, 10, pp.92–101.

Luo, Y., Yin, H. & Hua, C., 1996. The dynamic response of railway ballast to the action of trains moving at different speeds. *Journal of Rail and Rapid Transit*, pp.95–101.

Manzella, A.F., Gama, B.A. & Gillespie, J.W., 2011. Effect of punch and specimen dimensions on the confined compression behavior of S-2 glass/epoxy composites. *Composite Structures*.

Marchetti, A., Vismara, A. & Palmeieri, D., 1999. Design and manufacturing of the front cab for the New Italian Locomotive E464. In *Proc 20th International SAMPE Europe Conference of the Society for the Advancement of Material and Process Engineering*. Paris, pp. 3–13.

Matzenmiller, A., Lubliner, J. & Taylor, R.L., 1995. A Constitutive Model for Anisotropic

Damage in Fiber Composites. *Mechanics of Materials*, 20, pp.125–152.

Mines, R.A.W., Roach, A.M. & Jones, N., 1999. High velocity perforation behaviour of polymer composite laminates. *International Journal of Impact Engineering*, 22(6), pp.561–588.

Mines, R. a. W., Worralls, C.M. & Gibson, a G., 1998. Low velocity perforation behaviour of polymer composite sandwich panels. *International Journal of Impact Engineering*, 21(10), pp.855–879.

Monti, M. et al., 2011. Carbon nanofibers for strain and impact damage sensing in glass fiber reinforced composites based on an unsaturated polyester resin. *Polymer Composites*.

Montiel, D. & Williams, C., 1992. Method for evaluating the high strain rate compressive properties of composite materials. *ASTM STP*, (1120), pp.54–65.

Morton-Jones, D.H. & Ellis, J.W., 1986. High speed train cab for British Rail. *Polymer Products Design, Materials and Processing*, pp.184–195.

de Moura, M.F.S.F. & Marques, A.T., 2002. Prediction of low velocity impact damage in carbon–epoxy laminates. *Composites Part A: Applied Science and Manufacturing*, 33(3), pp.361–368. Available at: http://www.sciencedirect.com/science/article/pii/S1359835X01001191 [Accessed May 4, 2017].

Naik, N.K. et al., 2007. Interlaminar shear properties of polymer matrix composites: Strain rate effect. *Mechanics of Materials*, 39(12), pp.1043–1052.

Naik, N.K. & Doshi, A. V., 2008. Ballistic impact behaviour of thick composites: Parametric studies. *Composite Structures*, 82(3), pp.447–464.

Naik, N.K. & Shrirao, P., 2004. Composite structures under ballistic impact. *Composite Structures*, 66(1–4), pp.579–590.

Naik, N.K., Shrirao, P. & Reddy, B.C.K., 2006. Ballistic impact behaviour of woven fabric composites: Formulation. *International Journal of Impact Engineering*, 32(9), pp.1521–1552.

Nasirzadeh, R. & Sabet, A.R., 2014. Study of foam density variations in composite sandwich panels under high velocity impact loading. *International Journal of Impact Engineering*, 63, pp.129–139. Available at: http://dx.doi.org/10.1016/j.ijimpeng.2013.08.009.

Newill, J. & Vinson, J., 1993. High Strain-rate Effects on Composite Materials. In *Proc of 9th ICCM V*. pp. 269–277.

Nguyen, L.H. et al., 2016. A methodology for hydrocode analysis of ultra-high molecular weight polyethylene composite under ballistic impact. *Composites Part A: Applied Science and Manufacturing*, 84, pp.224–235.

Nguyen, M.Q. et al., 2005. Simulation of impact on sandwich structures. *Composite Structures*, 67(2 SPEC. ISS.), pp.217–227.

Ochola, R.O. et al., 2004. Mechanical behaviour of glass and carbon fibre reinforced composites at varying strain rates. *Composite Structures*, 63(3–4), pp.455–467.

Onder, A., ONeill, C. & Robinson, M., 2016. Flying Ballast Resistance for Composite Materials in Railway Vehicle Carbody Shells. *Transportation Research Procedia*, 14, pp.595–604. Available at: http://linkinghub.elsevier.com/retrieve/pii/S2352146516303076.

Ou, Y. & Zhu, D., 2015. Tensile behavior of glass fiber reinforced composite at different strain rates and temperatures. *Construction and Building Materials*, 96, pp.648–656. Available at: http://dx.doi.org/10.1016/j.conbuildmat.2015.08.044.

Petras, A. & Sutcliff, M.P.F., 1999. Failure mode maps for honeycomb sandwich panels. *Composite Structures*, 44, pp.237–252.

Pintado, P. et al., 1993. Dynamic response of raphite-epoxy composite laminates under compression. In *Proc of 9th ICCM*. Madrid, Spain, pp. 438–494.

Potti, S.V. & Sun, C.T., 1996. A simple Model to Predict Residual Velocities of Thick Composite laminates Subjected to High Velocity Impact. *Science*, 18(3), pp.339–353.

Potti, S.V. & Sun, C.T., 1997. Prediction of impact induced penetration and delamination in thick composite laminates. *International Journal of Impact Engineering*, 19(1), pp.31–48.

Powers, B. et al., 1995. High strain-rate effects on two AS4 graphite fiber polymer matrix composites. *ASME AD*, 48, pp.179–189.

PRF Composite Materials, 2013. *RS-L135 Epoxy resin data sheet*, England. Available at: www.prfcomposites.com.

Quinn, A.D. et al., 2010. A full-scale experimental and modelling study of ballast flight under high-speed trains. *Proceedings of the Institution of Mechanical Engineers, Part F: Journal of Rail and Rapid Transit*, 224(2), pp.61–74.

Quinn, A.D. & Hayward, M., 2008. Full-Scale Aerodynamic Measurements Underneath a. *Civil Engineering*, 1(January 2008), pp.20–24.

Rajaneesh, A., Sridhar, I. & Rajendran, S., 2014a. Failure mode maps for circular composites sandwich plates under bending. *International Journal of Mechanical Sciences*, 83, pp.184–195. Available at: http://linkinghub.elsevier.com/retrieve/pii/S0020740314001167.

Rajaneesh, A., Sridhar, I. & Rajendran, S., 2014b. Relative performance of metal and polymeric foam sandwich plates under low velocity impact. *International Journal of Impact Engineering*, 65, pp.126–136. Available at: http://dx.doi.org/10.1016/j.ijimpeng.2013.11.012.

REFRESCO Project, 2013. REFRESCO Project. Available at: http://www.refresco-project.eu/ [Accessed June 1, 2016].

REFRESCO WP7-D7.2, 2014. *Deliverable 7.2 - Damage Scenarios*,

REFRESCO WP7-D7.2, 2016. *REFRESCO Deliverable 7.2*,

REFRESCO WP7-D7.3, 2016. *Deliverable 7.3 - Prognostic and Health Management - Methodological Guideline*,

Reid, S.R., Wen, H.M. & Zhou, G., 2000. *Perforation of FRP Laminates and Sandwich Panels Subjected to Missile Impact*, Woodhead Publishing Ltd. Available at: http://dx.doi.org/10.1533/9781855738904.239.

Reid, S.R., Zhou, G. & HANCOX, N.L., 2000. 1 – An overview of the impact behaviour of fibre-reinforced composites. In *Impact Behaviour of Fibre-Reinforced Composite Materials and Structures*. pp. 1–32.

Riedel, W. et al., 2006. Hypervelocity impact damage prediction in composites: Part II-experimental investigations and simulations. *International Journal of Impact Engineering*, 33(1–12), pp.670–680.

Rizov, V., Shipsha, A. & Zenkert, D., 2005. Indentation study of foam core sandwich composite panels. *Composite Structures*, 69(1), pp.95–102.

Robinson, M., 2000. Applications in trains and railways. In *Comprehensive Composite Materials*. Oxford, UK: Elsevier Science Ltd., pp. 395–428.

Robinson, M. et al., 2012. Transport of DE-LIGHT: The Design and Prototyping of a

Lightweight Crashworthy Rail Vehicle Driver's Cab. *Procedia - Social and Behavioral Sciences*, 48, pp.672–681. Available at: http://linkinghub.elsevier.com/retrieve/pii/S1877042812027814.

Roth, S. & Oudry, J., 2009. Influence of mesh density on a finite element model under dynamic loading. In *3rd European Hyperworks Technology Conference*. Ludwigsburg, Germany, p. 23.

RSSB, 2012. *GM/RT2100 - Requirements for Rail Vehicle Structures Issue 5*, London.

Saat, M.R. et al., 2015. *Identification of High-Speed Rail Ballast Flight Risk Factors and Risk Mitigation Strategies - Final Report*, Washington. Available at: http://www.fra.dot.gov.

Sabet, A., Fagih, N. & Beheshty, M.H., 2011. Effect of reinforcement type on high velocity impact response of GRP plates using a sharp tip projectile. *International Journal of Impact Engineering*, 38(8–9), pp.715–722. Available at: http://dx.doi.org/10.1016/j.ijimpeng.2011.03.004.

Saka, K. & Harding, J., 1990. Simple laminate theory approach to the prediction of the tensile impact strength of woven hybrid composites. *Composites*, 21, pp.439–447.

Sakly, A. et al., 2016. Experimental and modelling study of low velocity impacts on composite sandwich structures for railway applications. *Engineering Failure Analysis*, 68, pp.22–31. Available at: http://www.sciencedirect.com/science/article/pii/S1350630716300619.

Saussine, G. et al., 2011. Ballast flying risk assessment method for high speed line. *9th World Congress on Railway Research - May 22-26*.

Seo, S.I., Kim, J.S. & Cho, S.H., 2008. Development of a hybrid composite bodyshell for tilting trains. *Proceedings of the Institution of Mechanical Engineers, Part F: Journal of Rail and Rapid Transit*, 222(1), pp.1–14. Available at: http://pif.sagepub.com/lookup/doi/10.1243/09544097JRRT96.

Shin, K.B. & Hahn, S.H., 2005. Evaluation of the structural integrity of hybrid railway carriage structures including the ageing effects of composite materials. *Composite Structures*, 68(2), pp.129–137.

Sistema Compositi, 2016. Front cab of High Speed Trains for ETR 460 for Italian Railways. Available at: http://www.sistemacompositi.com/products/trains/front: [Accessed January 1, 2016].

Starlinger, A., 2013. Sandwich Structures : Sandwich Design Applications in Mass Transportation Regional Trains.

Sutherland, L.S. & Guedes Soares, C., 2012. The use of quasi-static testing to obtain the low-velocity impact damage resistance of marine GRP laminates. *Composites Part B: Engineering*, 43(3), pp.1459–1467. Available at: http://dx.doi.org/10.1016/j.compositesb.2012.01.002.

Tsai, S.W. & Melo, J.D.D., 2015. *Composite Materials Design and Testing*, Composites Design Group.

UIC, 2016. *Rail High Speed Network - Security Handbook*, Paris.

URL-1, 2016. URL-1. Available at: http://tinyurl.com/lzv2tbu [Accessed January 1, 2016].

URL-2, 2016. URL-2. Available at: http://www.kerfkore.com/Balsakore.html.

Wang, J., Waas, A.M. & Wang, H., 2013. Experimental and numerical study on the low-velocity impact behavior of foam-core sandwich panels. *Composite Structures*, 96, pp.298–311. Available at: http://dx.doi.org/10.1016/j.compstruct.2012.09.002.

Wang, Z., 1995. Experimental evaluation of the strength distribution of E-glass fibres at high strain rates. *Appl Comp Mat*, 2, pp.257–264.

Wen, H.M., 2001. Penetration and perforation of thick FRP laminates. *Composites Science and Technology*, 61(8), pp.1163–1172.

Wen, H.M., 2000. Predicting the penetration and perforation of FRP laminates struck normally by projectiles with different nose shapes. *Composite Structures*, 49(3), pp.321–329.

Wennberg, D., 2013. *Multi-Functional Composite Design Concepts for Rail Vehicle Car Bodies*. KTH Royal Institute of Technology.

Werne, D. V., 1997. Structural GRP front for metro car. In *Composites in the Rail Industry Conference*. Railview Ltd.

Wicklein, M. et al., 2008. Hypervelocity impact on CFRP: Testing, material modelling, and numerical simulation. *International Journal of Impact Engineering*, 35(12), pp.1861–1869. Available at: http://dx.doi.org/10.1016/j.ijimpeng.2008.07.015.

Xiao, J.R., Gama, B.A. & Gillespie, J.W., 2007. Progressive damage and delamination in plain weave S-2 glass/SC-15 composites under quasi-static punch-shear loading. *Composite Structures*, 78(2), pp.182–196.

Xin, S.H. & Wen, H.M., 2015. A progressive damage model for fiber reinforced plastic composites subjected to impact loading. *International Journal of Impact Engineering*, 75, pp.40–52. Available at: http://dx.doi.org/10.1016/j.ijimpeng.2014.07.014.

Yahaya, R. et al., 2014. Quasi-static penetration and ballistic properties of kenaf-aramid hybrid composites. *Materials and Design*, 63, pp.775–782. Available at: http://dx.doi.org/10.1016/j.matdes.2014.07.010.

Yen, C.-F., 2002. Ballistic impact modelling of composite materials. *Proceedings of the 7th International LS-DYNA Users Conference*, pp.15–26.

Yen, C.F., 2012. A ballistic material model for continuous-fiber reinforced composites. *International Journal of Impact Engineering*, 46, pp.11–22. Available at: http://dx.doi.org/10.1016/j.ijimpeng.2011.12.007.

Zangani, D., Robinson, M. & Gibson, A.G., 2007. Evaluation of stiffness terms for Z-cored sandwich panels. *Applied Composite Materials*, 14(3), pp.159–175.

Zeng, X.S., Shim, V.P.W. & Tan, V.B.C., 2005. Influence of boundary conditions on the ballistic performance of high-strength fabric targets. *International Journal of Impact Engineering*, 32(1–4), pp.631–642. Available at: http://linkinghub.elsevier.com/retrieve/pii/S0734743X05000977 [Accessed March 13, 2017].

Zhou, G. & Davies, G.A.O., 1994. Impact response of thick glass fibre reinforced polyester laminates. *International journal of impact engineering*, 16(3), pp.357–374.

Zhou, J., Guan, Z.W. & Cantwell, W.J., 2016. Scaling effects in the mechanical response of sandwich structures based on corrugated composite cores. *Composites Part B*, 93, pp.88–96.

Zinno, A. et al., 2010. Multiscale approach for the design of composite sandwich structures for train application. *Composite Structures*, 92(9), pp.2208–2219. Available at: http://dx.doi.org/10.1016/j.compstruct.2009.08.044.